FOREWORD

The present report on FLNP activity covers a two-year period from 1992 to 1993. (Earlier, the 1992 annual report was released in Russian). This was a time of radical economic and political changes in JINR member states which posed a series of difficult problems for Institute and Laboratory authorities connected with supporting and developing the research program. The main achievement of this difficult period is that the efficiency and stability of the Laboratory staff was preserved and we succeeded in solving large-scale scientific and technical problems within the framework of the FLNP programme.

With the aid of neutron scattering new results have been achieved into investigations in the physics of condensed matter. Using the method of inelastic cold neutron scattering the complex structure of the elementary excitation spectrum in superfluid helium was revealed. In bismuth HTSC compounds studied by neutron diffraction, the existance of an additional superstructure in the crystalline lattice was proven. By measuring the depolarization of a polarized neutron flux in superconducting YBaCuO ceramics the manifestation of the depinning line was observed in the magnetic field distribution of the sample. With the aid of reflectrometry using polarized neutrons, an investigation was carried out with latent film structures of Co/Cu/Co in which a very weak antiferromagnetic coupling between magnetic and non-magnetic layers was observed.

The experimental facilities for studies in the physics of condensed matter have been considerably developed and perfected. In 1992 for the first time at a pulsed neutron source, a Fourier diffractometer was put into operation. The achieved resolution and luminosity put this new HRFD diffractometer in the ranks of the best spectrometers in the world. The group of diffractometers at the IBR-2 reactor was also enhanced with a new specialized DN-12 setup designed for investigations under very high pressures. The first stage of up-dating the MURN small-angle diffractometer has been completed, bringing it up to the level of the best set-up of this type, located at ILL (Grenoble). The realization of the second stage (commissioning of a new position-sensitive detector, in particular) will make it possible to obtain record parameters at the MURN spectrometer with the installed cold moderator.

In another main field of research foreseen in the FLNP scientific programme - neutron nuclear physics - a number of experiments with a unique monoisotopic ^{113}Cd sample should be noted. Earlier a series of p-wave neutron resonances was observed by FLNP physicists. Their spins were determined in a joint Dubna-Geel experiment. At the LANSCE pulsed neutron source a joint group of scientists from Dubna and Los Alamos measured p-odd effects in these resonances. An analysis of all data has not confirmed the sign coherence of p-effects observed earlier for thorium and uranium nuclei. The technique developed at FLNP to investigate the cascade γ-decay of a compound nucleus

caused by thermal neutron capture, was applied to the measurement of cascade γ-radiation for the ^{170}Yb radioactive isotope produced after the β-decay of ^{170}Lu. The known scheme of levels has been considerably corrected and supplemented, thus revealing the existence of good prospects for combining this technique with traditional methods of nuclear spectroscopy. New measurements of the fission cross-section for the ^{237}Np isotope were performed, which eliminated discrepancies between the reported data.

Among the methodical developments, implementation of which is now under way, two major projects, UGRA and ISPIN, take a noticeable place. The first project aims at determining the neutron electric polarizability by a precision measurement of the angular distributions of scattered neutrons of intermediate energies. The purpose of the second project is to create a set-up for measuring the neutron lifetime using ultracold neutron gas from the BIGR pulsed reactor at Arzamas.

Among the applied studies, we can note the completion of the development and the first broad application of the method of biomonitoring atmospheric deposition with the aid of neutron activation analysis of moss and pine needles, the successful testing of methods of dynamic radiography, and neutron doping of silicon at the IBR-2 reactor.

The stable operation of the FLNP base installations, the pulsed IBR-2 reactor and the IBR-30 + LUE-40 pulsed booster, has contributed to the fulfilment of the FLNP research program. The IBR-2 reactor is still the most intense neutron source in the world. In 1994 it will be 10 years since it was put into service. In connection with the partial burn-up of fuel in 1993, the first renewal of the active core was carried out, and permitting the reactor to run for 6 more years, in the previous working mode. The physical start-up of a cold moderator based on solid methane has become a great achievement of 1992. An enhancement of the cold neutron flux by approximately a factor of 5 was obtained as compared with the regular water moderator. The program to prepare the moderator for regular operation at the reactor was completed in 1993.

In the near future another base installation, the IBR-30, will be replaced by a new high resolution pulsed neutron source. In March 1993 the Plenipotentiary Committee of JINR member-states arrived at the decision to construct a specialized source of resonance neutrons (IREN). The rate the project development has been carried out in collaboration with the Institute of Nuclear Physics of the Siberian Branch of the RAS (Novosibirsk) and some other Russian research institutes, allows us to hope that the installation will be put into service at the planned time - in 1996.

The data acquisition and processing complex of FLNP has received a large development effort. The computing complex distributed according to territories is based on seven SUN Work Stations and VAX Microcomputers which have been substituted for the central FLNP processor, with the PDP-11/70 computer forming its basis for many years. This work has been implemented within the framework of the CAS project - Computer-Aided Systems - for the IBR-2 spectrometers. In 1993 the project was carried to completion. Practically all neutron spectrometers at the base installations of the Laboratory are equipped with the new generation PC/AT computers. At the present time the laboratory computer network unites more than 100 personal computers and the computers of the physical installations.

The scientific achievements of FLNP were commended with JINR awards. In 1992 first prize in the scientific and technical research section was given to the series of investigations on "Small-angle neutron scattering as a method to investigate the submolecular structure of matter". The "P-odd correlation investigation in reactions with light nuclei following the capture of thermal polarized neutrons with the emission of charged particles" research was awarded the encouraging prize. In 1993 first prize in the scientific and technical applied studies section was granted to the work "Textural analysis by the method of neutron diffraction and problems of geophysics".

An extensive program of collaboration with foreign scientific centers within the agreements and minutes adopted by JINR, or directly by the Laboratory, undoubtedly contributed to obtaining high scientific results. Contacts with German research institutes within the framework of the JINR-BMFT agreement and with Hungarian institutes were especially diverse.

During the period covered by the report the structure of the Laboratory underwent some changes. The Department of Electronics and Computing Techniques was dissolved and a number of sectors and research groups were organized within the scientific Department of the Physics of Condensed Matter headed by A.M.Balagurov. The low temperature sector became part of the Institute of Technical Physics Problems of the Russian Ministry of Atomic Energy.

The number of employees has been reduced from 580 people for 1.01.92 to 492 people by the beginning of 1994.

The creation of a large group of neutron spectrometers at the FLNP base installations and, a broad level of cooperation with other institutes gave rise to the creation of a new user policy. Committees of users for every research direction have been established comprizing the most well-qualified members of the Laboratory Staff.

The budget financing of FLNP during these years was only enough to maintain normal functioning of the personnel and infrastructure of the Laboratory. The resources for supporting and developing scientific research to a considerable extent were provided by external investments granted by the Russian program of high-temperature superconductivity, the Russian fund for fundamental research and other programs.

In 1992 the Laboratory of Neutron Physics suffered a heavy loss. On the 1st of August Yu.M.Ostanevich (born 25.07.1936) died. He was a Doctor of physics and mathematics head of the scientific Department of Physics of Condensed Matter. Yu.M.Ostanevich was a recognized leader in the team of experimenters working in the field of fundamental and applied physics of condensed matter. He was a prominent scientist and a well-known specialist in the world community of neutron physicists for investigations in the field of solid matter with the aid of small-angle neutron scattering. The name of Yu.M.Ostanevich will undoubtedly remain in the history of the Frank Laboratory of Neutron Physics of JINR.

V.L.Aksenov,
Director

1. SCIENTIFIC RESEARCH

This chapter deals with reviews and original communications on the results of scientific research carried out in 1992-93 at FLNP in the three principal fields of research foreseen in the FLNP scientific program: the physics of condensed matter, neutron nuclear physics, and applied research.

1.1. EXPERIMENTAL EQUIPMENT

The base installations of the Laboratory used for implementing this research were the IBR-2 fast pulsed reactor and the IBR-30 pulsed booster. The experimental equipment for studies in the physics of condensed matter is located at the IBR-2 reactor (Table 1), and for studies in neutron nuclear physics, mainly at the IBR-30 booster (Table 2).

Table 1

Neutron spectrometers at the IBR-2 pulsed reactor

Spectrometer	Object of investigation	Collaboration
	I. Neutron diffraction	
1. Time-of-flight diffractometer, DN-2	Crystal structure, phase transitions, transition processes	Russia, France, Germany, et.al.
2. High resolution Fourier diffractometer, HRFD	Precise structure analysis	Russia, Finland, GB, Germany
3. Time-of-flight diffractometer, DN-12	Crystal structure at high pressure (to 200 Kbar)	Russia, Germany, Hungary, Uzbek Repub.
4. Texture diffractometer, HRNS	Textures of industrial products and rocks	Russia, Germany
5. Diffractometer with a pulsed magnetic field, SNIM	Magnetic structure in a magnetic field of up to 15 T	Russia, Bulgaria, Czech
6. Diffractometer of ideal crystals, DIFRAN	Dynamic diffraction of neutrons	Russia, Latvia
	II. Small-angle neutron scattering	
7. MURN spectrometer	Subatomic structure of matter: glasses, solutions, polymers	Russia, France, GB, Germany, Hungary, Ukraine
	III. Inelastic scattering of neutrons	
8. Direct geometry spectrometer, DIN	Hydrogen in metals, liquid helium	Russia
9. Inverted geometry spectrometer, KDSOG	Crystal fields, phonon spectra	Russia, Poland
10 High resolution spectrometer, NERA-PR	Molecular spectroscopy	Russia, GB, Poland
	IV. Neutron optics	
11. Spectrometer of polarized neutrons, SPN-1	Magnetic inhomogeneities, domains	Russia, France, Germany, Poland
12. Neutron reflectometer, REFLEX	Surface phenomena, internal fields	Russia, Germany, Hungary, Poland

Table 2

Neutron spectrometers at the IBR-30 booster

No Beam	Spectrometer	Object of investigation	Collaboration
1	**PARCS**	*Rare reactions (neutron, charged particles) on stable and radio-active nuclei in the resonance energy range*	Russia: PINP; USA
1A	**CASCADE**	*Two quanta decay of compound states*	Latvia
3	**DRENIS**	*Sub-barrier fission*	Bulgaria
4	**POLYANA**	*Polarized neutron and nuclei*	USA
5	**DELRENE**	*γ - spectra of fission fragments, fission of aligned nuclei*	Russia: PEI; Slovakia
7	**UGRA**	*Neutron elastic scattering angular distributions*	Germany
7	**ROMASHKA**	*γ - multiplicity in capture and fission*	Russia: RNC KI; Bulgaria

The reported investigations were partly carried out at external neutron sources. For example, the entire program of research with ultracold neutrons is implemented at the reactors of the St.Petersburg Institute of Nuclear Physics (Gatchina) and All-Russian Research Institute of Experimental Physics (Arzamas). On the other hand, the interest of external users in the neutron sources of the Laboratory is rising. During the past two years the number of users has, in particular, increased in the field of the condensed matter physics, which can be seen from Table 3.

Table 3

Experiments on the IBR-2 spectrometers

November 1992 - June 1993

Spectrometer	Number of experiments (samples)	Users			Comments
		FLNP	Others	Total	
1	2	3	4	5	6
Diffraction:					
DN-2	14(20)	10	12	22	*Structure and real-time*
HRFD	4(6)	4	6	10	*Structure*
DN-12	2(2)	1	3	4	*High pressure*
HRNS	3(72)	2	8	10	*Texture analysis*
DIFRAN	1(1)	3	4	7	*Dynamic diffraction*
SNIM	2(1)	2	3	5	*Pulsed magnetic field*
SANS:					
MURN	17(280)	7	13	20	*Small angle scattering*
INS:					
DIN-2	5	2	12	14	*Direct geometry*
KDSOG	14(23)	5	7	12	*Inverted geometry*
NERA	10(38)	5	6	11	*Quasi elastic scattering*
Neutron Optics:					
SPN-2	13(9)	8	3	11	*Depolarization and reflectometry*
Total	**85(>450)**	**49**	**77**	**126**	

1.2. THE PHYSICS OF CONDENSED MATTER

1.2.1. EXPERIMENTAL STUDIES

Experiments in the physics of condensed matter are mainly conducted with the spectrometers at the IBR-2 reactor. The EG-5 electrostatic generator and the DRON-4 X-ray diffractometer have also been utilized during the past two years for the certification of samples and for solving certain special problems.

At present, 10 spectrometers have been put into operation on eight beams of the IBR-2: HRFD, DN-2, HRNS, SNIM, DIFRAN, MURN, DIN, KDSOG-M, NERA-PR, SPN-1. During the period dealt with in the report new results have been obtained in all sections of PCM research under development at FLNP.

Diffraction. Studies of HTSC materials occupy a noticeable place among the investigations of structure.

A series of studies of the magnetic phase diagram of the HTSC $YBa_2(Cu_{1-x})Fe_x)_3O_{6+y}$ compound versus the concentration of iron, x, and the oxygen content, y, has been completed within a range of temperatures from 8 to 450 K. Experiments were carried out with the diffractometers of FLNP and LLB, Saclay, and, making use of the Moessbauer effect, at the IC RAS with samples enriched with the ^{57}Fe isotope. The high contrast achieved has permitted one the unambiguous determination of the probability of iron to substitute for copper atoms (Fig. 1), and to reveal the nature of the changes occurring at the interatomic distances (Fig. 2).

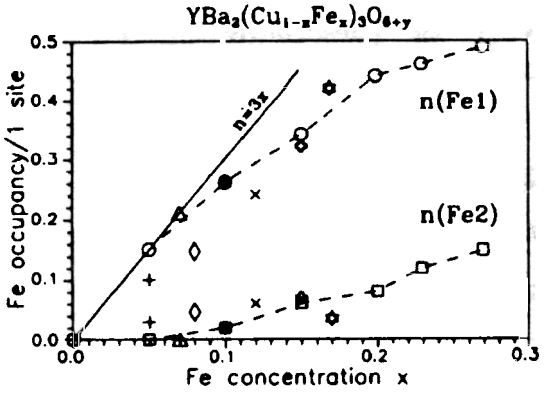

Fig. 1. Occupation factors of Cu1 and Cu2 positions in Y123-Cu/Fe by atoms of iron versus their concentration and in samples saturated with oxygen. Shown are the data of A.M.Balagurov et. al. (points O, □) and data in literature (the remaining points).

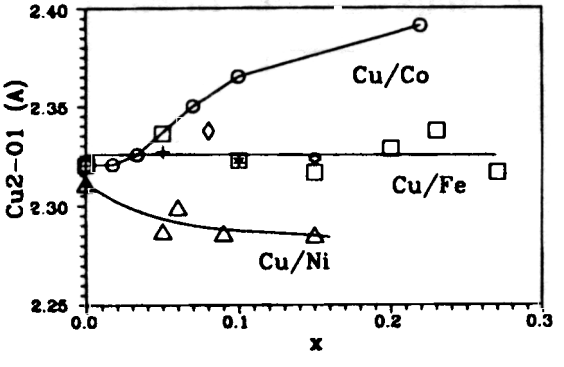

Fig. 2. Dependence of Cu2-O1 interatomic distance in Y123 on the concentration of impurity atoms: Fe, Ni, and Co. For Y123-Cu/Fe, data from literature are also presented. The size of the points corresponds to the errors.

Unlike the Y123 system, involving the substitution of cobalt for copper, the absence of a correlation between the temperature of the super-conducting transition and the Cu2-O1 interatomic distance was established. This lack of correlation was almost constant throughout the entire range of concentrations of the dopant atoms. This effect is in contradiction with the universal mechanism of

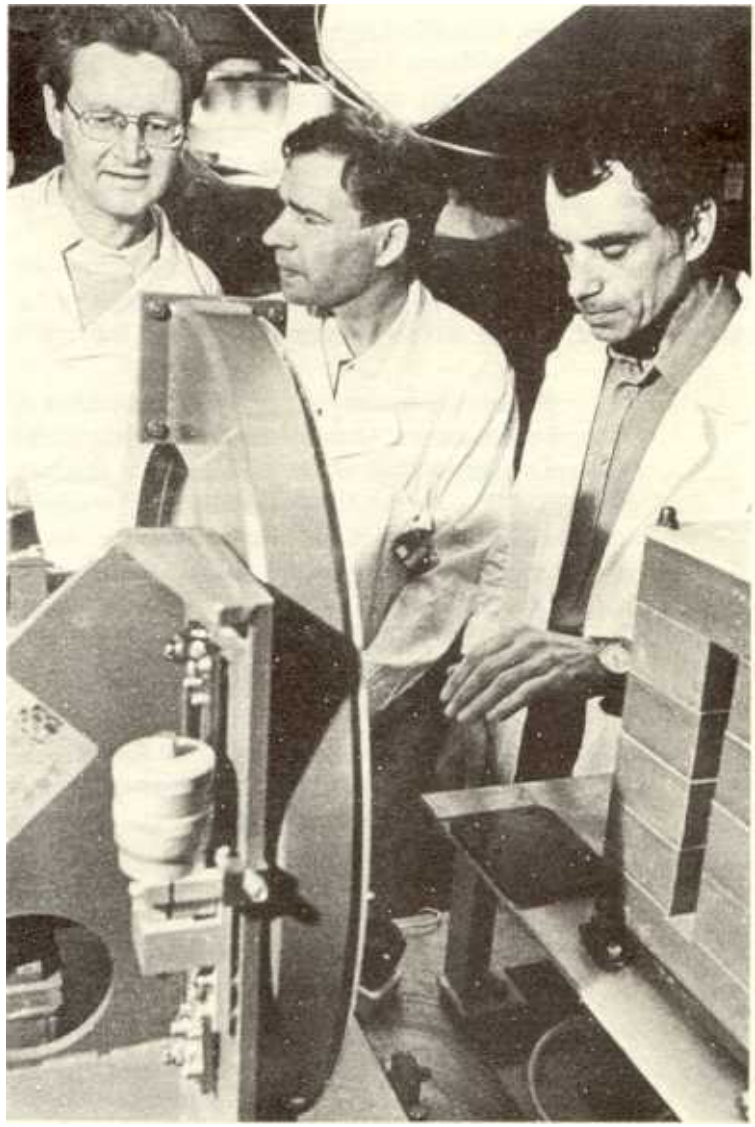

HRFD Fourier diffractometer on beam 5 at the IBR-2 reactor

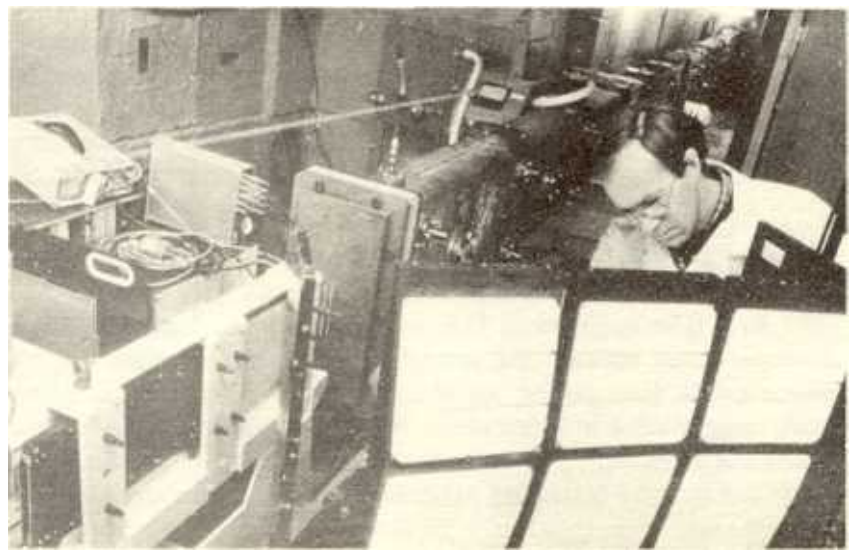

Neutron guide and Li-detector of HRFD

superconductivity loss in Y123 discussed in the literature. This effect is due to an enhancement of the interatomic distance and to the related transfer of negative charge from the chains in the plane, and points to processes taking place in the course of doping being more complicated than originally assumed. The magnetic phase diagram has been determined for the compound, meaning that domains have been established for the coexistence of superconductivity and magnetic ordering of the type of spin glass moments present in Cu-O chains, as well as the domains in which long-range antiferromagnetic order arises. The collinear antiferromagnetic structure existing for Fe concentrations exceeding 5% has been confirmed, together with a recovery behavior at temperatures below 100 K. In the region of iron concentrations of 7-23%, an unexpectedly strong coupling has been revealed between the spins of iron and copper, as well as a large magnetic moment induced at the Cu1 nodes.

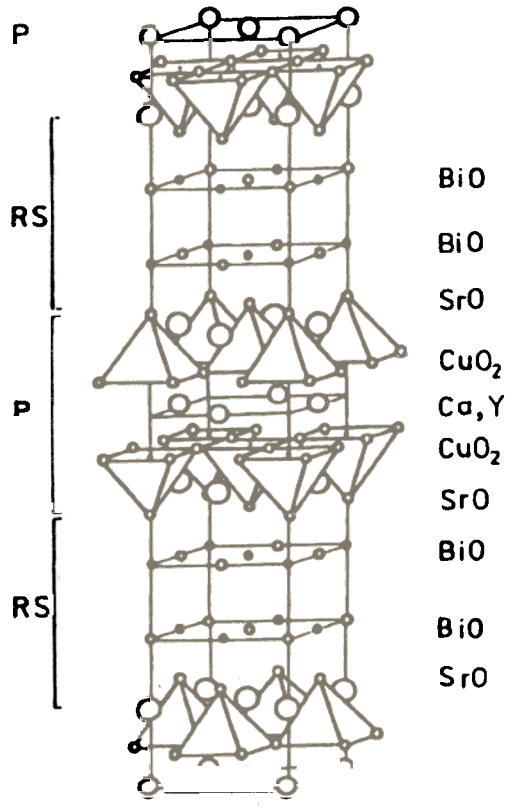

Fig.3. A simplified model of the $Bi_2Sr_2CaCu_2O_{8+\gamma}$ or $Bi_2Sr_2YCu_2O_{8+\gamma}$ structures.

Studies continued of modulated structures of Bi-superconductors. Owing to the complicated electronic configuration of the Bi^{3+} ion, it is precisely these HTSC compounds that exhibit a tendency towards the production of superstructures which might result in the formation of HTSC properties. The following systems were studied in experiments performed at the DN-2 diffractometer with mono- and polycrystals: $Bi_2(Sr, Ca)_3Cu_2O_{8+\gamma}$, $Bi_2Sr_{3-x}Y_xCu_2O_{8+\gamma}$ and $Bi_2Sr_2CuO_{6+\gamma}$. All these compounds were shown to exhibit structural modulation along the *a*-axis of an elementary cell. For concrete compositions of the systems indicated above, modulation was observed with periods of 4.25*a*, 4.75*a* and 5.0*a*, respectively. The structures of these compounds were determined (Fig. 3), and it was shown that the superperiod is due to the formation of $Bi_nO_{n+\gamma}$ chains along the *a*-axis (Fig. 4). Insertion of an additional oxygen atom (γ) into these chains leads to the appearance of wavelike displacements of the planes of atoms with amplitudes of 0.2-0.4 Å along the c-axis. Investigation of the temperature dependence of the modulation period and amplitude reveals no direct relationship with the superconducting properties of Bi compounds, but they determine, to a large extent, the balance of charge in an elementary cell. Thus, an extremely complicated structural problem found its solution in these experiments, which made possible an essential clarification of the situation with Bi compounds.

Of the numerous experiments performed by the method of diffraction in real-time mode, we note the work on phase states in titanium deuteride, TiD, carried out together with physicists of the SSPI, RAS (Chernogolovka). This work was the continuation of studies initiated in 1991 performed at temperatures between the temperature of liquid nitrogen and room temperature. This time, measurements were carried out at temperatures from room temperature up to 870 K. Thus, the entire range studied included about 700 K. Measurements showed that there were seven different phases and intermediate states with hcp, fcc, fco or bcc lattices of metal with deuterium atoms distributed over the octahedral or tetrahedral sites of the structure.

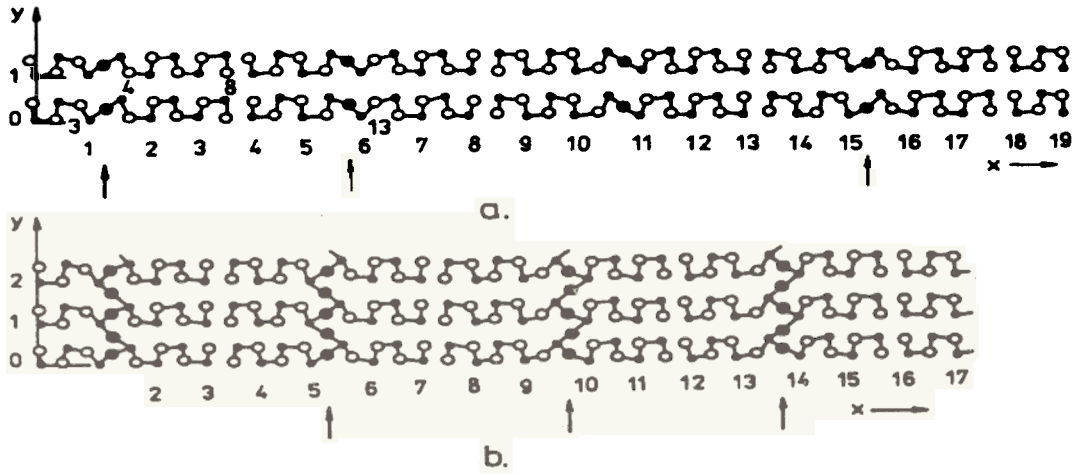

Fig. 4. Structure of $BiO_{1+0.5\gamma}$ planes in the 19a·b·c supercell of the $Bi_2Sr_{2.14}CaO_{0.72}Cu_2O_{8.21}$ compound (a) and 17a·b·c of the $Bi_2Sr_{2.4}Y_{0.6}Cu_2O_{8.5}$ compound (b) (Bi cations are indicated by black circles, the arrows point to the positions of the additionally inserted oxygen).

Formation of the Bi(Pb)-Sr-Ca-Cu-O HTSC compound was studied. For the first time it became possible to observe the formation and decomposition processes of the main phases of this system: 2201 and 2212 (Fig. 5). It has been shown that the intermediate $Sr_{1-x}Ca_xCuO_2$ phase plays an important part in these processes. At temperatures above 850°C the decomposition mechanism involves a process of partial melting. The stoichiometry that appears when the phase undergoes partial melting, determines the stoichiometry of the HTSC phase which forms when partial melting of the phase occurs. This, in turn, determines the stoichiometry of the HTSC phase which forms when the mixture cools slowly. The short annealing times of the produced phases permit formation of the 2212 phase. For formation of the 2223 phase, which exhibits a higher T_c, a more prolonged annealing is required. The work was carried out together with scientists from the Institute of Physics and Technology, Bucharest.

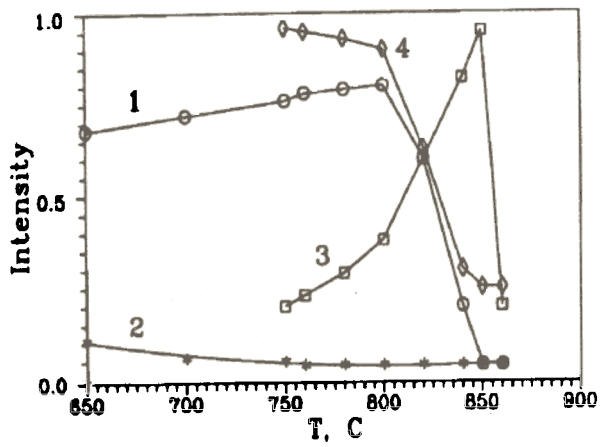

Fig. 5. Temperature dependence of the integral intensity of peak (002) for phases 2201 and 2212 in case of heating (curves 1 and 3) and cooling (curves 2 and 4), respectively.

Experiments are still under way for investigating structural phase transitions in ferroelectric and ferroelastic materials. A structural ferroelastic phase transition was observed in $RbLiH_3(SO_4)_4$ and the symmetry of the ferrophase was determined in a joint investigation carried out with the Institutes of Physics UAM (Poznan) and IPTM (Bucharest). Studies of the strontium-barium niobate ferroelectric were continued in collaboration with the MC, Rossendorf. In addition to the two high-temperature phase transitions studied previously, the existence of two low-temperature transitions was revealed, one of which is related to the rotation of the of which is related to the rotation of the ferroelectric axis through an angle of 90°.

Studies in the kinetics of the spin-flop transition in the antiferromagnetics Cr_2O_3 and α-Fe_2O_3 were continued with the SNIM-2 diffractometer equipped with a pulsed magnet. A hysteresis was observed in the dependence of the sublattice magnetization rotation angle upon the acting magnetic field (Fig. 6), in which the behavior of the antiferromagnetic when the the magnetic pulse field increases is found to differ from its behavior when the field decreases. The hysteresis phenomena are due to the following:

1) when the field variation is sufficiently rapid (~ $2x10^8$ Oe/s), the spin-flop transition proceeds adiabatically, i.e., the exchange of energy between the spin and phonon systems has no time to occur;

2) in the experiment, relaxation processes are observed that are related to the finite time (~10^{-5} s) required for establishment of an equilibrium state in the magnetic system, due to relativistic magnetic interactions.

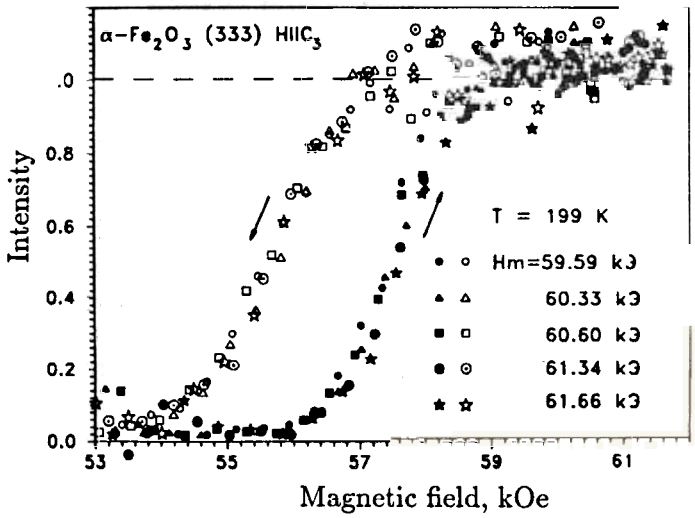

Fig. 6. Dependence of the diffraction peak (333) intensity of the α-Fe_2O_3 monocrystal on the pulsed magnetic field strength at a temperature of 199 K. The black dots correspond to the leading edge of the magnetic pulse, the light dots to the trailing edge.

Diffraction investigations have been made of a $HoFeO_3$ sample subjected to an external magnetic field. Antiferromagnetic ordering has been found in this rare-earth sublattice, which in the absence of the field is in a paramagnetic state. Studies were performed of this antiferromagnetic state. The sensitivity of the magnetic moment measurements amounted to 0.1 μ_B per cation. Temperature dependence of the "antiferromagnetic susceptibility" in the range from 79 to 220 K was measured. The noncolinearity of antiferromagnetic ordering in the iron sublattice was also determined and turned out to be 2%.

The HRNS textural diffractometer was used to obtain total pole figures from 42 samples of quartzites, gneisses, amphibolites and xenolites, including 12 samples from the Kola and German super-deep boreholes. Textures of artificially deformed quartzites and vanadium-titanium alloys were studied. This work was carried out in collaboration with scientists from Germany (from the Research Centre in Rossendorf, the Gottingen University, the Higher Technical School in Aachen and the Technical University of Klaustal) and Russian scientific centers (IEP RAS, GEOSYSTEM, MPII, UPI in Ekaterinburg, TTSU in Tula). Besides the above, measurements were performed of the form factors of liquid alkali metals (together with scientists of the Romanian IAP in Bucharest). Investigations were carried out of the distribution of atomic pairs in electric alloys (together with the Technical University in Kemnitz (Germany)) and the short-range ordering in oxide glasses (together with the University of Rostok (Germany)).

HRNS texture neutron diffractometer on beam 7a at the IBR-2 reactor

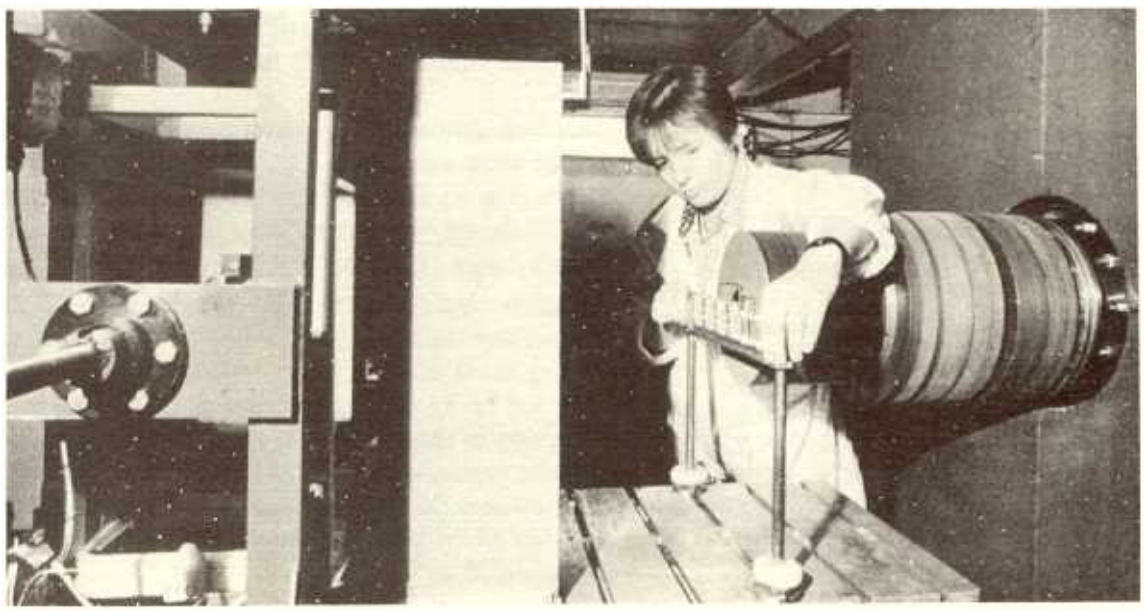

MURN small-scattering diffractometer on beam 4 at the IBR-2 reactor

Small-angle scattering. Intense studies were carried out with the MURN small-angle scattering spectrometer,.

A straightforward experimental comparison of MURN with one of the best spectrometers of this type, D-11 at ILL (Grenoble) was performed. Parallel measurements were carried out with samples composed of particles exhibiting an extremely wide spectrum of sizes. The following conclusions were made on the basis of a joint analysis of the measurement results: 1) the absolute intensities and inertia radii of both installations coincide within the errors; 2) the range of momentum transfers with MURN is 2 times wider than with D-11; 3) measurements of weakly scattering samples (with cross sections $\mu < 0.05$ cm^{-1}) take the same time with both instruments; 4) measurements of strongly scattering samples ($\mu > 0.1$ cm^{-1}) require significantly more time with MURN, than with D-11. The D-11 diffractometer, however, is about at its level of technical perfectness, while the commissioning of a cryogenic moderator at the IBR-2 reactor, as well as the nearly completed installation of a new position-sensitive detector at beam N 4 will essentially broaden the facilities of MURN by increasing in the spectral range and allowing better spatial resolution in the detection of scattered neutrons.

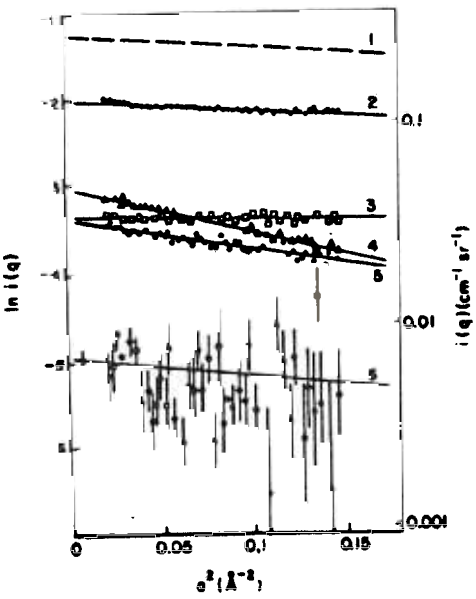

Fig. 7. Guignet curves obtained from measurements of neutron small-angular scattering on the MURN spectrometer: 1 - H_2O:D_2O solution = 1:1 (the experimental points are not presented); 2 - H_2O:D_2O = 1:4; 3 - vanadium sample 3 mm thick; 4 - solution (1M) H-TMU in D_2O; 5 - solution (1b) of mixture H- and D-TMU in H_2O-D_2O at 30 mol.% H_2O; 6 - solution (1M) H-TMU in H_2O-D_2O at 60 mol.% H_2O.

Various types of Portland cement were investigated, as well as their hydration in compounds. Dry cement was found to follow the Porod potential law, while compounds did not yield, in the measured Q-range, a similar behavior of small-angle scattering curves. Investigation of nuclear tracks in solid-state detectors by the method of small-angle neutron scattering was carried out in collaboration with FLNR JINR. RERT type foils of the were also studied. The irradiated foils displayed a Guignet-like behavior of the scattering curves. The measured radius of inertia turned out to be about 8 nm. Annealing (160°) lead to a decrease of the radius.

Searches continued for perturbation effects of the structure of a solvent in the vicinity of a dissolved molecule (Fig. 7). In collaboration with staff members of CIPR, Budapest, experiments were carried out with tetramethylurine (TMU), and the temperature and temperature and concentration dependences of the scattering law were obtained. Despite the fact that the scattering cross sections to be measured were small, it turned out to be possible to reveal the orientational perturbation of the structure of a solution in the vicinity of a TMU molecule and, also, to establish the existence of an attractive potential between the molecules, which arises due to hydrophobic interactions in accordance with assumptions.

For the first time studies were performed of micelle systems at high hydrostatic pressures. In solutions of tetradecildimethylaminoxide (C_{14}-DMAO) at pressures in ranges up to 8 kbar, a phase transition was found in which cylindrical micelles with radii of 18.5 Å and lengths of 160 Å undergo

transition to states with a 52 Å radius. The experiments were carried out together with physicists from Baireuth (Germany).

Inelastic scattering. New results in the molecular dynamics of condensed matter were obtained by the method of inelastic neutron scattering.

The DIN-2PR and DIN-2PI direct geometry spectrometers (monochromatization of the neutrons incident upon the sample) were, used for continued investigations of the dynamics of liquid helium, liquid metals and molecular liquids, as well as the dynamics of alloys and local oscillations of dopant hydrogen, nitrogen and oxygen atoms in metals and alloys.

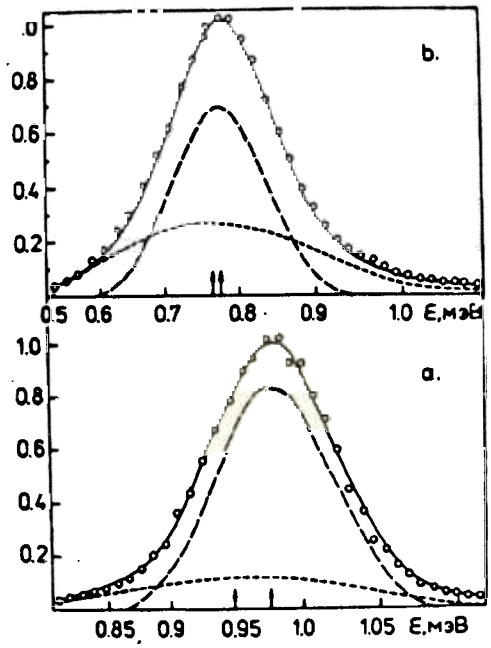

Fig. 8. Spectrum of neutrons back-scattered on He II: a - T = 1.4 K; E_0 = 2.05 meV; q = 1.6 Å^{-1}; b - T = 1.72 K; E_0 = 2.45 meV; q = 1.83 Å^{-1}. The solid line is a fit to the experimental data; the dashed lines indicate a decomposition into two Gaussians. The arrows point to the positions of the Gausssians.

The main accent in the investigation of the quantum properties of liquid helium-4 has shifted from studies of the momentum distribution of atoms by analysis of the spectra of neutrons scattered with large momentum transfers (the impulse approximation) to a detailed investigation of the dispersion curve of excitations in liquid helium at various temperatures. To perform the indicated research, the DIN-2 spectrometer operated at initial neutron energies below 2 meV. The low initial energies made possible an essential reduction of the influence of multiphonon and multiple scattering of neutrons and improvement of the resolution from 50 up to 100 meV depending on the energy transfer. A manifestation of the high sensitivity achieved was the observation of peaks related to neutron scattering in liquid helium involving acquirement of energy, i.e. of excitations present in the liquid. An analysis of the experimental spectra of inelastically scattered neutrons revealed that the phonon-maxon-roton peak has a complex multicomponent structure (Fig. 8).

At temperatures above the λ-point in the phonon region, excitations were observed that can be associated with long wave excitations such as the first or zeroth sound (Fig. 9, indicated by triangles).

At all wave vectors a broad peak is seen, the physical nature of which is not quite clear at present. It may be due to the quasicrystalline structure of the liquid or to neutron scattering on thermal excitations or to other mechanisms (full circles in Fig. 9). At temperatures below the λ-point, an additional branch is observed, besides the indicated branches,, which is the dispersion curve for quasiparticles and is related to the canonized Landau curve (open circles in Fig. 9). The temperature dependence of the relative intensity of scattering on quasiparticles repeats the behavior of the order parameter curve in liquid helium II.

The results show that, most likely, three different excitations exist in liquid helium-4, which manifest themselves in different ways, depending on the temperature and the wave vector. Here two characteristic regions of significant restructuring of the excitation energy spectra may be distinguished. First, strong qualitative and quantitative changes in the nature of neutron scattering occur within a very narrow temperature interval or actually at the point of transition to super-fluidity, T_λ. Second, explicit changes in the nature of excitations both in superfluid and in normal helium take place in a narrow range of wave vectors (0.5-0.65) Å^{-1} in the transition from phonons to maxons.

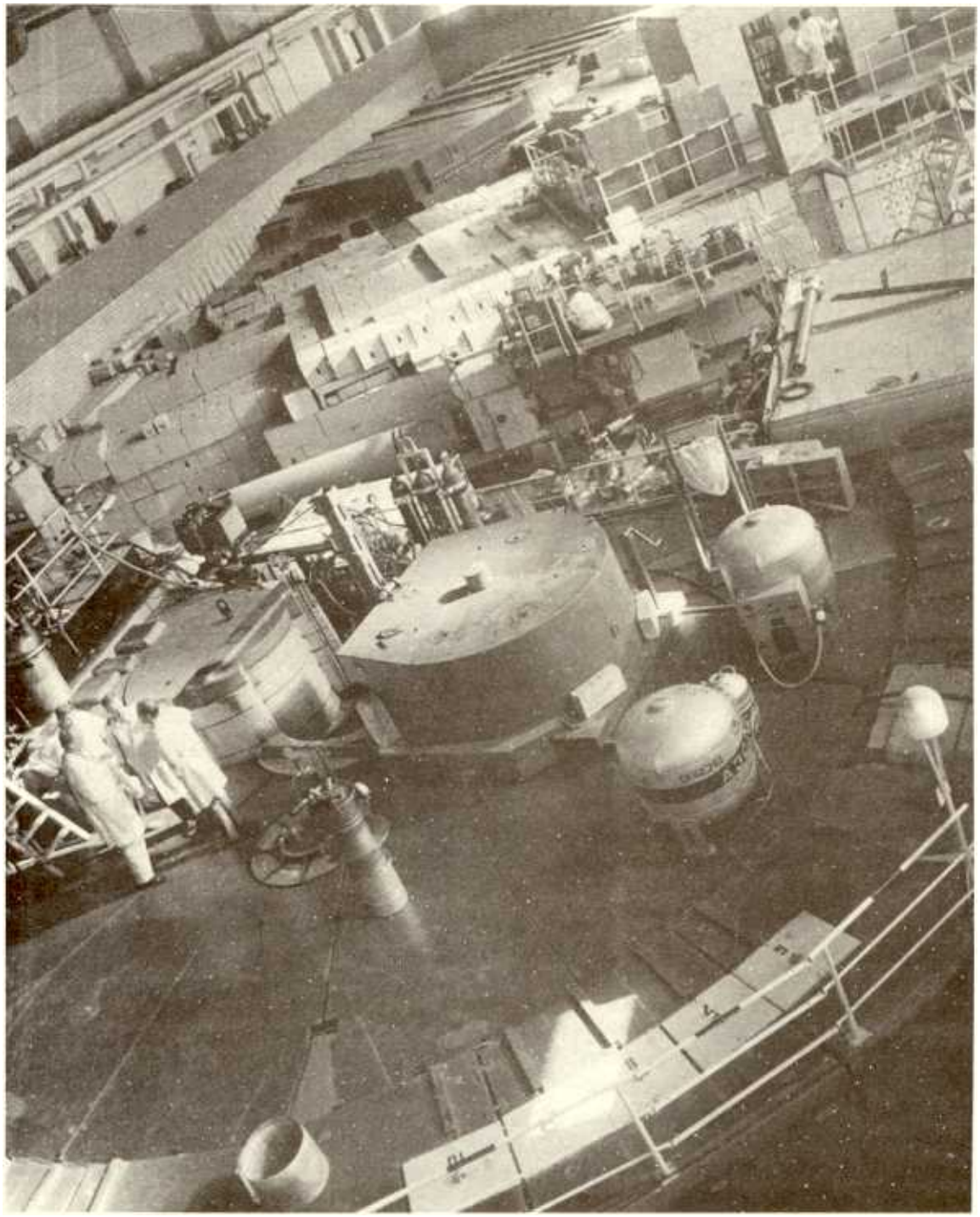

DIN-2PI inelastic scattering spectrometer of the direct geometry on beam 2 at the IBR-2 reactor

The issue of the amount of Bose-condensate in super-fluid helium-II is still under discussion, initiated by the works of F.London, N.N.Bogolubov and S.T.Belyaev. According to the Glide-Griffins concept, the intensity of the peak of quasiparticles is determined by the density of Bose condensate. Therefore, the experiments made it possible to apply an independent method for determining the density of Bose condensate.

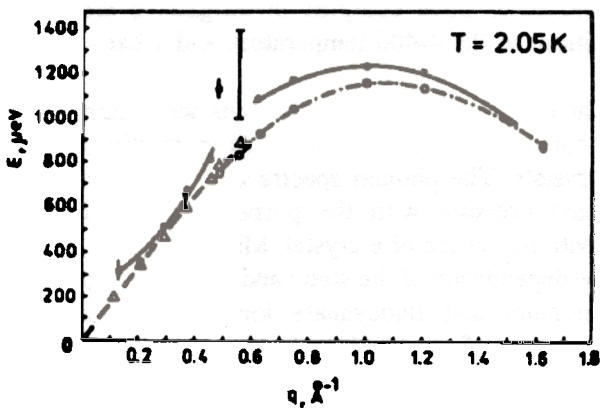

Fig.9. Dispersion curves for liquid helium-4 at a temperature of 2.05 K.

Studies of nitrous austenitic steels are under way to determine the force constants of interatomic interactions. Admixtures of nitrogen strongly influence the hardness of austentitic steels. The frequency spectra have been investigated for austenitic alloys Fe-Cr-Mn-Ni (f.c.c) with nitrogen contents in the range of 0.06-0.5 weight %. It was found that, unlike the nitrous chrome-manganic steels investigated previously, theaddition of nitrogen does not lead to a change in the Me-Me and Me-N force interaction, in the case of a Fe-18Cr-10Mn-16Ni compound. Studies were also performed of alloys of the $TaN_{0.45}$ and $NaN_{0.45}H_{0.1}$ β-phase intrusions. Data were obtained on the oscillation energies of nitrogen and hydrogen atoms and on constants of the force interaction of interstitial metal-atom interaction. Investigation has continued of double and triple hard interstitial solutions. The phenomenon of interstitial nitrogen atoms being "captured" by Ta-V substitution admixtures has been studied using the example of a $TaV_{0.03}N_{0.03}$ solution. Besides local nitrogen peaks in the frequency spectrum of the solution investigated, peculiarities were observed that were due to oscillations of vanadium atoms associated with the "captured" nitrogen atoms. Investigation of the structure of the admixture zone in the $YO_{0.03}H_{0.03}$ alloy revealed that the oscillations of interstitial hydrogen and oxygen atoms do not correspond to the location of these atoms at the centre of the octahedral inter-nodal position of the yttrium cubic lattice.

Spectra have been measured for inelastic neutron scattering on PbF_2 in the 293-773 K temperature interval with the aim of determining the density of phonon states at temperatures higher and lower than the super-ionic transition, $T_c \sim 700$ K.

Two-dimensional liquids have been studied, taking advantage of the example of water adsorbed on the surface of pyrogenous silica and porous silicon dioxide. Simulation of the quasielastic scattering law and analysis of the angular dependence yielded the self-diffusion coefficients of water molecules, the hydration shell of silica and of aerosil hydrogel, and the average square deviations of hydrogen atoms from equilibrium positions.

Studies were performed of the scattering of slow neutrons by liquid potassium in the 340-550 K temperature interval. A technique for taking coherent effects into account was elaborated on the basis of the Lovsee viscous-elastic model. Analysis of experimental spectra with the aid of the developed technique resulted in our obtaining the hitherto unavailable temperature dependence for the frequency spectrum of oscillations of atoms of the melt and for other microdynamic characteristics related to this spectrum: autocorrelation speed function, root-mean-square oscillation amplitude of atoms averaged over the direction of the force constant of interatomic interactions, and, also, the calculated isochronic heat capacity taking into account anharmonic effects. The characteristics were obtained for diffusion processes in liquid potassium in the indicated temperature

range together with an idea of the mechanism governing these processes. The correspondence of the experimental results with the theory of interaction between modes was investigated. Collective modes in liquid helium were investigated, and these data were used to calculate the lifetime and non-Markovian behavior criteria characteristics of relaxation processes in a melt:.

The KDSOG and NERA-PR inverted geometry spectrometers make simultaneous studies of inelastic scattering and diffraction of neutrons possible. Such complex investigations are being successfully implemented for studying phase transitions in the 4-400 temperature and 1 bar - 1 kbar pressure ranges.

Investigations of the dynamics of molecular crystals and phase transitions were carried out with the NERA-PR spectrometer. Studies were continued of phase transitions in plastic crystals, such as camphor, and other types of molecular crystals. The phonon spectra of meta-, ortho- and paraxylene were measured versus temperature and pressure with the purpose of studying the dynamics of methyl groups and their interactions with the lattice of a crystal. Mixed $K_{1-x}(NH_4)_xSCN$ crystals were used for investigating the temperature dependence of the static and dynamic disorder of ammonium and thiocyanate ions in the range of temperatures from 10 K up to room temperature and in a broad range of ammonium concentrations. Several phase transitions were revealed that are related to the dynamics of ammonium ions: a structural phase transition of the order-disorder type at low temperatures for x = 0.75, a transition from dynamic reorientation to the phase of proton glass for $0.3 < x < 0.75$ and to the phase of nearly free quantum rotation at helium temperatures for $x < 0.1$.

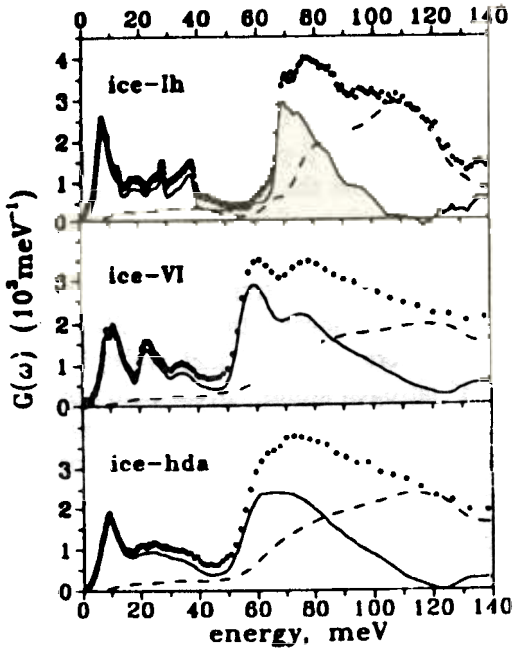

Fig. 10. Plots of generalized vibrational density of states G(ω) for hexagonal H_2O-ice Ih, the quenched high pressure phase VI, and amorphous ice of high density (hda). The points indicate the overall experimental spectrum, the dashed lines show theoretically calculated contributions of multiphonon neutron scattering; the solid lines are one phonon spectra.

The good resolution that can be achieved with the NERA-PR spectrometer was used for investigations of both lattice dynamics and internal molecular oscillations of a series of amino acids with the purpose of determining the characteristic oscillation frequencies of the CH_3 and NH_3 molecular groups. Owing to the large scattering cross sections of neutrons on protons, the dynamics of these groups is manifested clearly in neutron spectroscopy.

The vibrational spectrum of quenched amorphous ice of high density (hda), obtained by compressing hexagonal Ih ice up to 13 Kbar at 77 K, was studied with the aid of inelastic incoherent neutron scattering in the energy region from 1 to 120 meV at 80 K (Fig. 10). The spectra of Ih ice and of the quenched high-pressure phase IV ice were also measured for comparison. In the translational zone of the hda ice phase spectrum, the first peak in the region of acoustic modes is shifted by 2 meV towards higher energies, as compared to Ih ice, while in the tortional zone the spectrum reveals that the low-energy cutoff of this zone is shifted by 13 meV toward low energy transfers. The principal characteristics peculiar to the spectra of hda ice and of ice IV were observed to be similar, thus indicating that the dynamics of these phases must depend on the same atomic correlations and force constants.

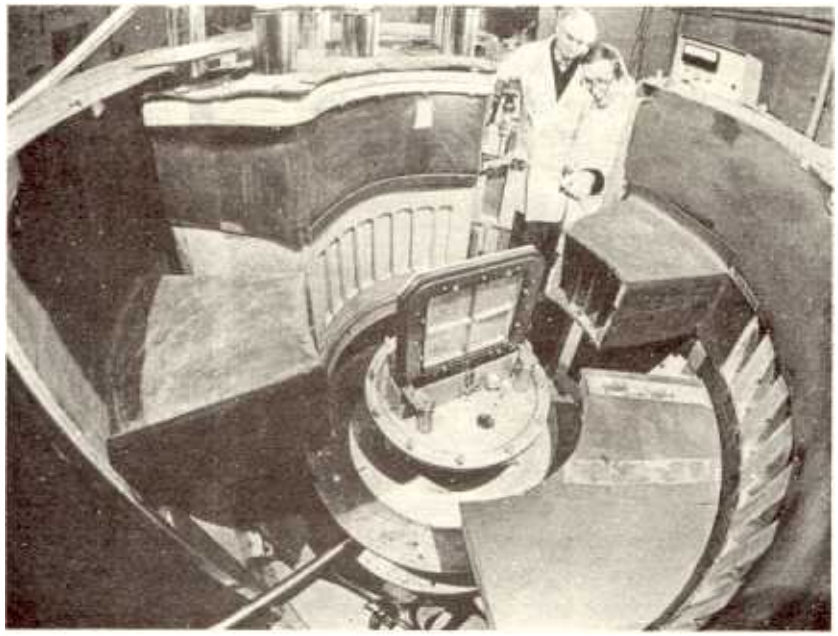

NERA-PR inelastic scattering spectrometer of inverted geometry on beam 7b at the IBR-2 reactor

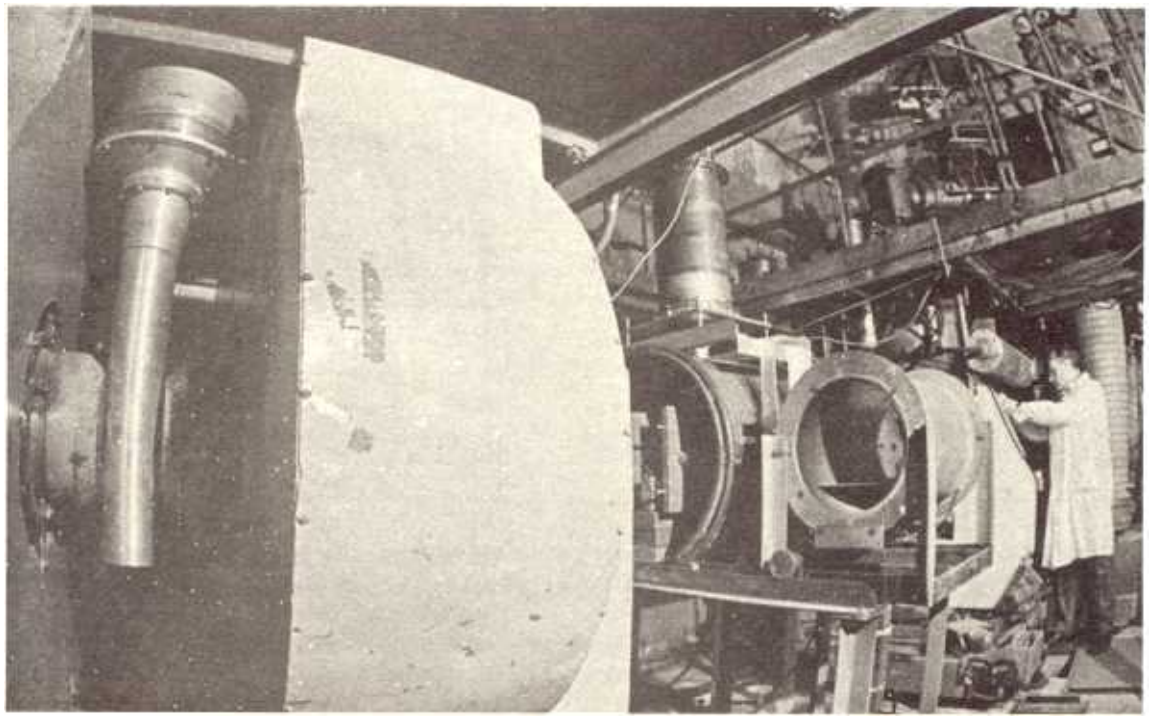

POLYANA spectrometer for experiments with polarized neutrons and nuclei on beam 4 of the IBR-30 booster

Vibrational spectra of finely granulated silicates and of water adsorbed on them were studied with the KDSOG spectrometer. The results are used for clarifying the microscopic mechanisms of water adsorption on the surface of silicates. Generally, this spectrometer is used for studies of crystalline fields in alloys and compounds of rare-earth elements. A series of experiments has been carried out to studyi the crystal electric field (CEF) in $ReCu_2Si_2$ compounds (Re = Ce, Nd, Pr, Er, Tb, Ho, Yb). The dependence of the parameters on Re was determined. The spectra of magnetic excitations in systems with intermediate valence (IV), CeNi, Ce(La, Y)Ni and PrCe(La, Y)Ni, were studied with the purpose of investigating the CEF transformation in transition from IV to the Condo mode of the 4f-electron shell.

Polarized neutrons. The SPN-1 polarized neutron spectrometer was used for continuing studies of the magnetic properties of thin and multilayer films by the method of specular reflection.

The profile of the constant magnetic field penetrating into superconducting niobium films (Fig. 11) was measured. At a temperature of 4.9 K, a 500 Gauss field within the limits of ξ = 28 nm penetrated the superconductor at the boundary with vacuum practically without damping, which is related to the near-surface suppression of the order parameter of the superconductor. Deeper in the film the damping follows the London law with a constant Λ = 45 nm. By the improved method of inverse resonance scattering of accelerated helium ions on oxygen it turned out to be possible to establish the existence of a natural 5 nm thick NbO oxide at the surface of the niobium superconductor film being studied with the aid of neutrons. Observation of the oxide confirms the existence of a hitherto unknown mechanism for the origination of the normal phase at a real microcoarse boundary with a vacuum.

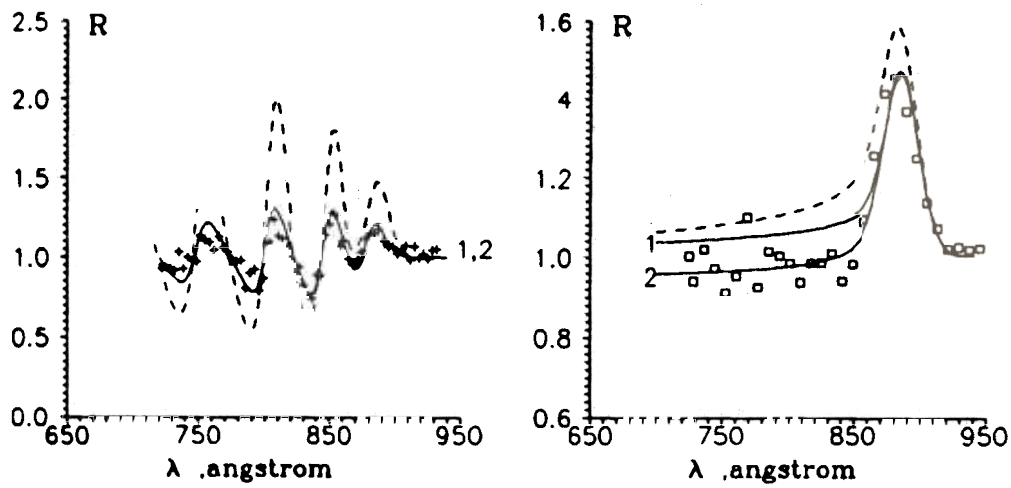

Fig. 11. Experimental ratio R of the reflection coefficients of neutrons with opposite polarizations versus the normal to the film plane component of the neutron wavelength λ: the crosses indicate a thin film, the squares a thick film. The dashed line is calculated within the London model for Λ = 43 nm. The solid line indicates: 1 - calculation within the London model for the best fit and Λ = 95 and 90 nm for the thin and thick films, respectively; 2 - calculation by the model with inclusion of a dead layer at the boundary of the film (a solution consistent for both films has been obtained with ξ = 28 nm and Λ = 45 nm).

It has been demonstrated and experimentally proven that single-axis anisotropic magnetic films exhibit a sufficiently large coercive force to create neutron beams of differing polarizations, depending on the orientation of a weak external magnetic field relative to the magnetization vector of the film (Fig. 12). This makes it possible to use them as wide-spectrum neutron polarizers in neutron polarization spectrometers without applying spin-flippers.

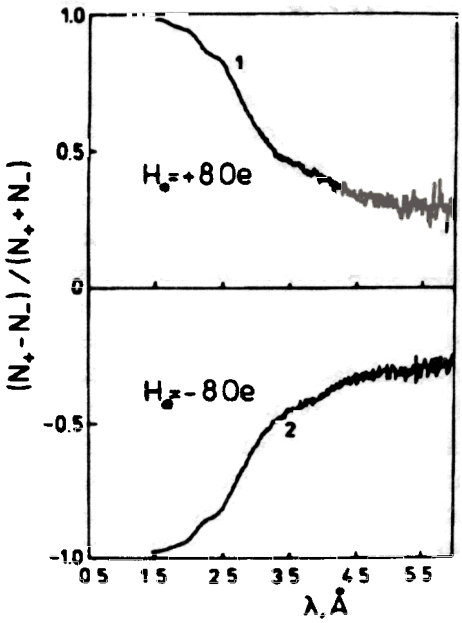

Fig. 12. Experimental dependence of the quantity $P_0P = (N_+-N)/(N_++N)$, where P_0 is the incident beam polarization, P is the polarizing power of the film, upon the neutron wavelength λ for a FeCo film with a rectangular hysteresis loop: 1 - orientation of external magnetic field parallel to the film magnetization; 2 - antiparallel.

The first experiments have been performed in search of an induced magnetic moment in a non-magnetic medium adjacent to the magnetized medium. Measurements were performed with a series of Pd/Co (20 Å)/Pd samples (Fig. 13). The magnetic moment in the Co layer turned out to be 1.7 μ_B. No moment was found to appear in the Pd layer, the upper limit imposed on its value was $\mu < 0.4\ \mu_B$. The aim of another investigation was to study ferro- and antiferromagnetic exchange interactions in coupled films. These investigations are of great interest for clarifying the nature of the giant magnetoresistance in such films. Unlike optical and magnetometric methods, the method of neutron reflection permits a determination of the value and orientation of the magnetization vector in each individual layer. The first experiments were carried out with Co/Cu/Co samples with Cu thicknesses of 9 and 13 Å. An unusual behavior of these epitaxial structures was observed, which demonstrate a very weak or practically zero antiferromagnetic pairing between the magnetic and non-magnetic layers. Ferromagnetic interaction had already been observed in the case of weak external magnetic fields: at 30 Gauss the magnetic moment per 1 Co atom amounted to 1.1 μ_B. When the external field was increased up to 1.4 kGauss, only a weak enhancement of the magnetization in these films was observed (up to 1.3 μ_B per 1 Co atom). The issue of the relationship between this increase in magnetization and the giant magnetoresistance observed in this range of magnetic fields remains unclear.

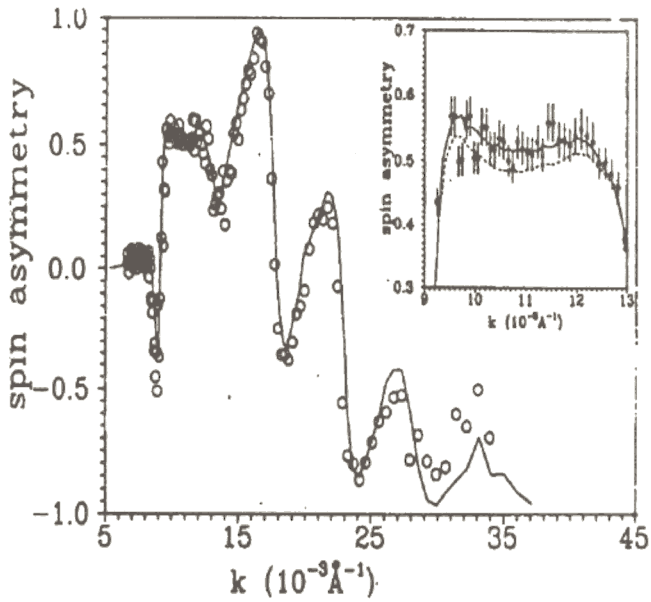

Fig. 13. Dependence of spin asymmetry $SA = (R_+-R)/(R_++R)$ in reflection of polarized neutrons on the normal component of the neutron wavevector K for a Pd/Co/Pd film, deposited on the surface of silicon with a sublayer of gold: the dots represent the experiment, the line - calculations of $\mu_{Co} = 1.73\ \mu_B$ and $\mu_{Pd} = 0.4\ \mu_B$ in a layer 5 Å thick at each Co/Pd boundary. Both lines in the insertion are computed; solid line - $\mu_{Co} = 1.8\ \mu_B$; dashed line - $\mu_{Co} = 1.73\ \mu_B$ (corresponds to a massive sample).

The SPN-1 spectrometer provides good possibilities for applying the method of neutron depolarization to the study of magneto-inhomogeneous media. The spectral function of depolarization contains information both on the parameters of magnetic inhomogeneities (size, spread of magnetization orientations) and on the nature of pair correlations between local magnetization vectors in adjacent microregions. Manifestations of the information on correlations should depend on the depolarization function $D(\lambda)$, and on the neutron path length d in the sample, which can be altered by rotating the sample through an angle θ about the axis coinciding with the direction of the magnetic field. In the Halpern-Holstein theory there exists a constant, $f = D_1(\lambda)^{d2(\theta 2)/d1(\theta 1)}/D_2(\lambda)$, independent of the neutron wavelength. However, in the case of samples exhibiting a correlation between mutual orientations of the micromagnetization, or in the case of samples with micromagnetic elongated inhomogeneities packed anisotropically, the value of f depends on the neutron wavelength. Fig. 14 presents experimental data for a thin laminated steel ribbon. The form of function $f(\lambda)$ points to the packing of the magnetic particles elongated in a direction perpendicular to the rolling. The function $f(\lambda)$ obtained for annealed Permalloy (Fig. 15) confirms the absence of pair correlations between the orientations of local magnetizations and, also, of any priority orientation in the packing of magnetic particles. Inclination of the plane of a thin sample relative to the external field allows the defining of an initial polarization, P_0, at the entrance to the sample, that differs in orientation from the induction vector within the sample. In this case the depolarization process is complemented by rotation of the vector, P, about the induction vector, as in the technique of three-dimensional polarization analysis. An example of a depolarization curve obtained by transmission through an inclined sample of transformer iron is presented in Fig. 16. In this case the function $P(\lambda)$ is most informative since it allows spectral analysis to be performed simultaneously with the three polarization vector components at the exit from the sample.

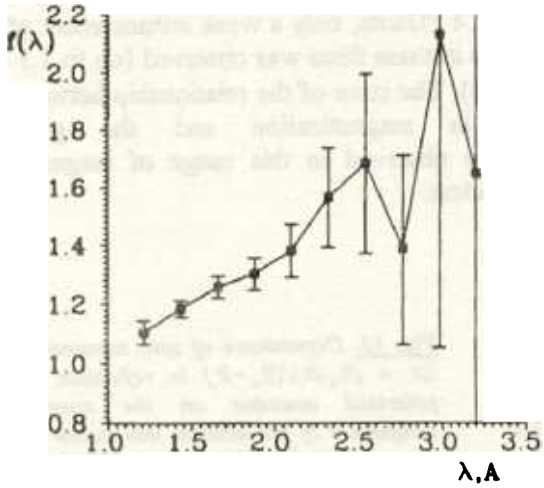

Fig. 14. Shape of function f(λ), measured for a thin rolled steel ribbon 300 μm thick in an external field of 160 Oe.

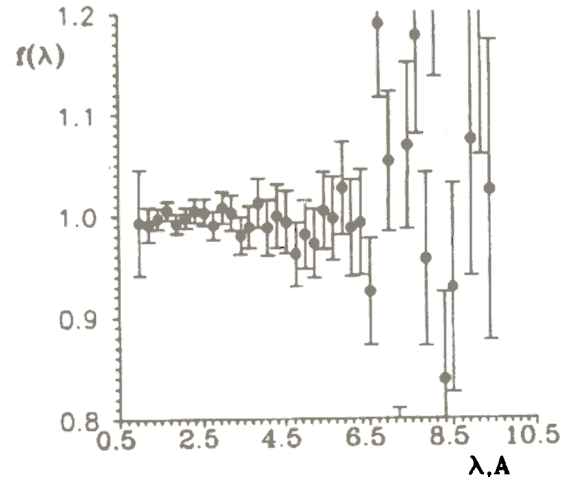

Fig. 15. Shape of function f(λ) for an annealed Permalloy ribbon 160 μm thick.

Systematic investigation was performed of the dependence of neutron depolarization in samples of HTSC ceramics Y123 (T_c = 91 K) upon temperature (77-250 K) and the external magnetic field. The most interesting temperature region is found around T_c, where theory predicted new magnetic phenomena such as: transition of the vortex lattice into the spin-glass state, melting of the vortex lattice and others, which may be manifested in specific behavior of the neutron

depolarization when the temperature and external field undergo variations. New information has been obtained on the magnetic field distribution in a sample. Thus, for example, a possible manifestation was found of the so-called depinning line, which separates captured and freely moving vortexes.

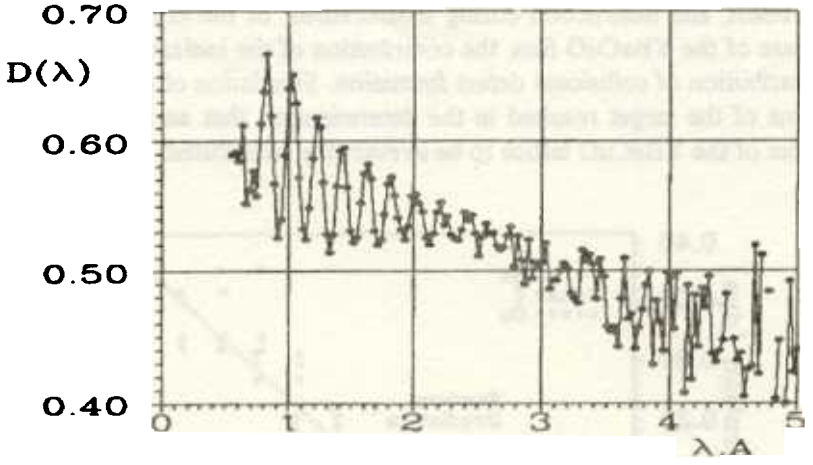

Fig. 16. *Depolarization function D(λ) measured with the aid of neutron transmission through an inclined sample of transformer iron 300 μm thick. The angle between the axis of the sample and the external field (460 Oe) equals 10 °.*

Scattering of accelerated helium ions. New possibilities for investigating the structure of HTSC materials opened up with the application of a combination of channeling and inverse-scattering methods at the EG-5 accelerator. The method of channeling charged particles occupies an intermediate position in between atomic microscopy and diffraction spectroscopy. Because this method exhibits the precision of diffraction methods, it yields direct information in real space (naturally, for periodic structures) and, unlike atomic spectroscopy, it allows the visualization of large lattice volumes. Moreover, the high energy resolution of electrostatic accelerators provides the possibility of independent investigation of the sublattices of various (including light) elements and their depth profiles by measuring the energy of the detected scattered particles.

Experiments were performed involving inverse scattering of 3.6 MeV helium ions from a monocrystalline Y123 film 1400 Å thick on a support of strontium titanate in the channeling position along the <001> direction. Since the wave function of helium ions, in the case of channeling, is concentrated inside the crystallographic channel, free from nuclei, the intensity of nuclear scattering drops drastically. Here the observed scattering is mainly related to the presence of defects and displacements of nuclei from regular crystallographic positions. It turned out that the distribution of defects is inhomogeneous through the thickness of the film. The quantity of defects is maximal at the surface of the film and on its inverse side adjacent to the support. Extension of defective layers is quite significant and amounts to 400-600 Å. The resonance nature of the scattering of helium ions on oxygen ($E_{res.}$ = 3.045 MeV) permitted clear identification of scattering on the oxygen sublattice, in spite of the high background of scattering from the support. For the first time, the angular width of the oxygen sublattice channeling entrance crater was measured. It turned out that this width is significantly smaller than the crater width of the barium, copper, and yttrium sublattices, which can be explained by the significant dynamic (or static) instability of oxygen in the lattice. Similar investigations will be carried out in the vicinity of the critical temperature of superconductive transition.

The mechanism of radiative formation of defects in YBaCuO monocrystalline films irradiated with helium-4 ions was studied. The influence was determined of the dose accumulated in the course of measurement on the properties of the object being studied. Two aspects were considered: variation of the depth distribution of elements in the film (profiles of elements) under the action of the analyzing ion beam, and destruction during measurement of the crystal lattice being irradiated (Fig. 17). In the case of the YBaCuO film, the contribution of the ionization mechanism amounts to 30-60% of the contribution of collisional defect formation. Simulation of the interaction processes of ions with the atoms of the target resulted in the determination that an average energy of 5 eV is required for an atom of the YBaCuO lattice to be irreversibly substituted.

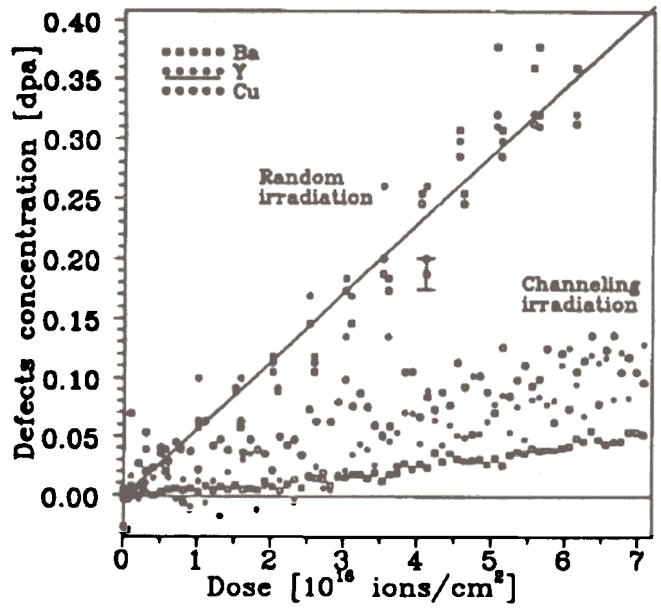

Fig. 17. Dependence of concentration of defects in $YBa_2Cu_3O_7$ film 90 nm thick on the irradiation dose by ^4He ions of 1 MeV energy for chaotic and tunnelled irradiation.

2.2.2. DEVELOPMENT OF THE EXPERIMENTAL BASE

The main event of 1992 turned out to be the beginning of operations of the high resolution Fourier diffractometer (HRFD). It took four years to construct the HRFD in accordance with a joint project of JINR, PINP (Gatchina) and the Centre of Technical Research (Finland). The first run of measurements with the HRFD was carried out in June 1992, just before the summer intermission of the IBR-2 reactor. The idea of realizing the Fourier technique at a pulsed neutron source like the IBR-2 was confirmed to be correct, namely, record parameters of the diffractometer for resolution and luminosity can be obtained with its aid. Routine operation of the Fourier diffractometer started in 1993. Experiments with standard samples (Ge, Al_2O_3) revealed its parameters to be close to the computed ones. Resolution amounted to about 0.0015, which is close to the resolution of the HRFD of RAL (Fig. 18).

The processing of measured diffraction spectra has been organized by using the Rithvield method (Fig. 19) and the first physical experiments were carried out in which HTSC compounds (Y124, Hg-1212) and superproton conductors etc. were studied. A program of applied research has

been initiated with the HRFD. Joint experiments were performed with physicists from the FRG on internal strains in massive objects. A technical base is being created for simultaneous measurement of deformations in two directions perpendicular to each other (the NIDA project).

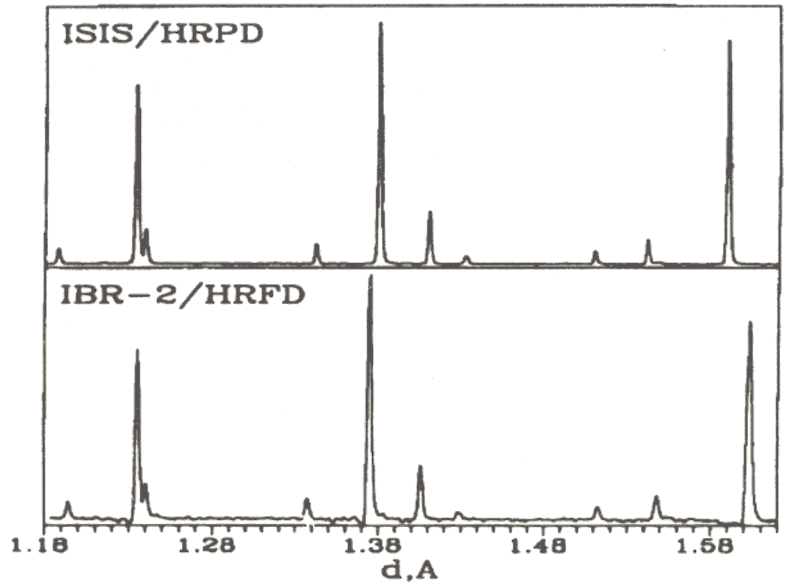

Fig.18. A small section of the Al_2O_3 diffraction patterns measured on the HRPD diffractometer at ISIS (top) and on the HRFD one at IBR-2 (bottom). The horizontal scale is slightly different for the patterns.

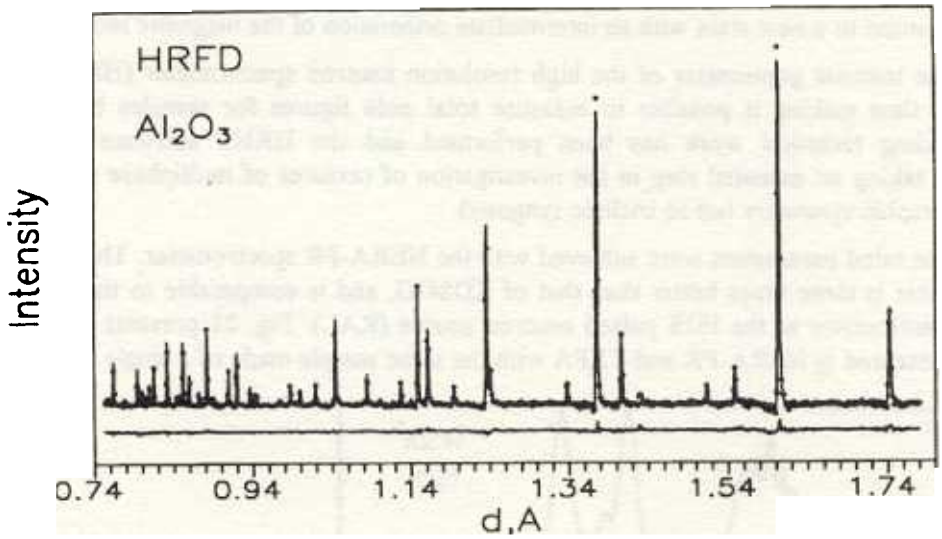

Fig.19. A section of Rietveld refinement pattern for Al_2O_3 measured on the HRFD. As experimental points only every fourth is shown.

A very interesting new study "Investigations at very high pressures" has been initiated at the IBR-2 reactor. The first results have been obtained with the DN-12 diffractometer put into operation in 1993. The idea of DN-12 is based on the peculiarities of observing diffraction by the time-of-flight method at a pulsed neutron source, namely, in the case of an experiment with fixed geometry, there

exists a possibility of detecting diffraction spectra from a polycrystalline sample at a very wide solid angle without significant loss of resolution. To this end it is necessary to use a multidetector detection system with counters located along Debye-Sherer rings.

The first realization of the idea occurred at the beginning of the 1960's, when a diffractometer was constructed at the IBR-1 reactor with a wide-aperture 90° detector (V.V.Nietz, et. al.). The detector of the DN-12 diffractometer represents a circular (360°) set of ^{3}He counters, situated in the vertical plane, and the scattering angle can vary from 45° to 135°. In such geometry effective use of high pressure chambers based on sapphire or diamond anvils is possible, with the primary beam passing through the anvil. Measurements showed the luminosity of DN-12 to exceed by about two times that of the DISK diffractometer at the RNC KI (Moscow) exhibiting a close resolution. In its turn, the luminosity of DISK is several times higher than that of the diffractometers of LLB (Saclay), with which studies are carried out at high pressures, and it approximately corresponds to the POLARIS diffractometer at RAL (England). In principle, this level already permits conducting experiments at pressures of about 100 kbar and to accumulate statistics in reasonable time. The time required for data accumulation from a DyD_3 sample 0.03 mm^3 in volume at a pressure of 80 kbar amounts to about 24 hours (Fig. 20). Experiments with hematite α-Fe_2O_3 at a pressure of 45 kbar confirmed the phase transition to a new state with an intermediate orientation of the magnetic moments.

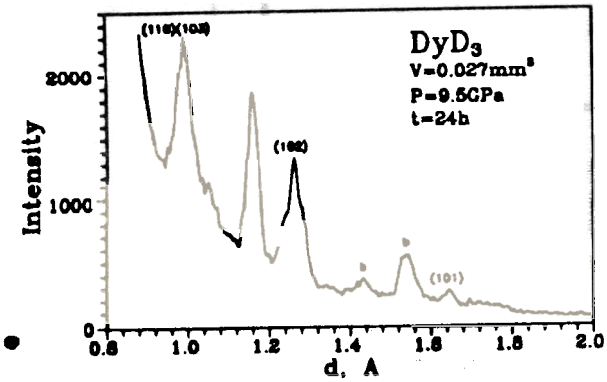

Fig. 20. Diffraction spectrum from DyD_3 measured at a pressure of 9.5 GPa during 24 hours. The sample volume was 0.027 mm^3.

The textural goniometer of the high resolution neutron spectrometer (HRNS) has been re-equipped, thus making it possible to measure total pole figures for samples being studied. The corresponding technical work has been performed and the HRNS software improved, which permitted taking an essential step in the investigation of textures of multiphase materials with low crystallographic symmetry (up to triclinic syngony).

The rated parameters were achieved with the NERA-PR spectrometer. The resolution of this spectrometer is three times better than that of KDSOG, and is comparable to the resolution of the TXFA spectrometer at the ISIS pulsed neutron source (RAL). Fig. 21 presents inelastic scattering spectra measured at NERA-PR and TXFA with the same sample made of a single molecular crystal.

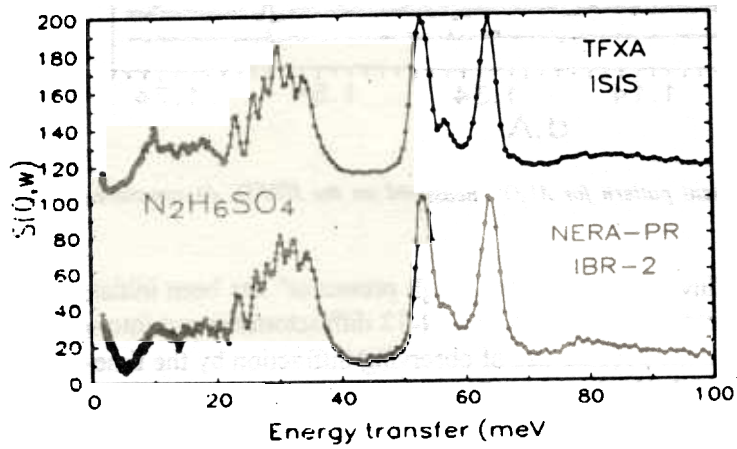

Fig. 21. The high resolution IINS spectra of hydratine sulfate measured on the TXFA (ISIS) and NERA-PR (IBR-2) spectrometers.

Construction of the "Reflex" reflectometric complex at channel 9 of IBR-2 is close to completion. The main mechanical parts of the reflectometer and the storage and measurement electronics have been assembled. The helium cryostat and the magnetic system are close to being completed. Test measurements have estimated fluxes at the sample to be approximately twice the fluxes at the SPN-1 spectrometer operating in the reflectometric mode. Putting the reflectometric complex Reflex-1 (for polarized neutrons) plus Reflex-2 (non-polarized neutrons) into operation will allow essential enhancement of the experimental program for studies of surfaces and thin magnetic and non-magnetic films.

2.2.3. THEORETICAL STUDIES

New theoretical results have been obtained on phase transitions. The freezing temperature $T^*_c > T_c$ for the scalar lattice φ-model of structural phase transitions has been found within the theory of coupled modes. The frequency and temperature dependences of the linear and square susceptibilities have been obtained by self-consistent solution of the equations of coupled modes used for studying the critical behavior of this transition. Two cases have been analyzed: 1) a perfect crystal lattice with a characteristic B-transition at T^*_c, and 2) a system with randomly distributed defects and an A- transition at T^*_c. The experimental aspects of the presented theory are under discussion.

Analysis of the multicomponent order parameter in the $CsHSO_4$ superionic conductor has been carried out. The symmetry of the observed superionic and non-conducting phases was determined and a symmetry of high-pressure phases was predicted.

A number of studies have been conducted in HTSC physics. The spectral density of a hole moving along the AP ground state has been computed within the framework of the Emery model. It has been shown that eigenenergy is nondiagonal in the vicinity of the quasiparticle pole. The mixing of a singlet and triplet depends on the wavevector. Estimation of the optical conductivity has been performed. The results are in good agreement with experimental data and numerical calculations.

The possibility of a self-localized state to form has been examined within the Holstein model. It has been shown that unlike the continual limit, the solution of the Schrodinger equation on a 2D lattice in the adiabatic approximation leads to the formation of a barrier separating self-localized and de-localized states.

The nature of many unusual properties of high-temperature superconductors is due to the existence of a disordered set of weak Josephson links inside them. Within the framework of the model of superconducting granules with randomly distributed phases, it has been shown by renormalizable group methods in replica space that the recurrent Kosterlitz-Tauless transition occurs only for order parameters in the $\pi/8 < A < 1.2\pi/8$ range.

Analysis has been performed of the upper critical field of superconducting super-lattices based on vanadium and copper. It was shown that, owing to a decrease of the magnetic length in strong magnetic fields, a normal metal does not affect the distribution of the superconducting nucleus in the super-lattice. Numerical computation of the Ginzburg-Landau equation is in good agreement with experimental data. Analysis has been performed of the temperature dependence of the line width for transitions between f-levels of Tm ions split by a crystalline field in YBCO. It has been shown

that the main contribution to the broadening is due to antiferromagnetic fluctuations in the vicinity of the G-point of the Brillouin zone, while the temperature dependence is determined by the static susceptibility. Numerical analysis has been performed of the strongly interacting phonon-electron system. It was shown that the exact solution coincides with the adiabatic Holstein polaron. Exact diagonalization was applied to calculations of an optical polaron of small radius, which can be done only in the limit of strong coupling.

The problem of reconstructing the distribution of internal magnetic fields from the depolarization function observed for a polarized neutron beam on its passage through a magnetic medium is very important. A new approach, based on the model of strong interaction, has been developed for computation of the depolarization function. The results of the Halpern-Holstein theory are reproduced for the limit of small wavelengths. Investigation of the specular reflection of neutrons from various types of multilayers is one of the important practical issues of constructing mirrors for neutron guides. Numerical analysis has been performed of the neutron reflection coefficient from multilayer structures, forming a sequence of so-called Fibonacci layers. It has been shown that disorder of the quasicrystalline type in how the materials of the mirrors are arranged may result in a shift of the neutron backscattering region toward either longer or shorter wavelengths.

1.3. NEUTRON NUCLEAR PHYSICS

1.3.1. TECHNICAL PROJECTS

The decision to create a new pulsed source of resonance neutrons, IREN, and the startup of realization of this project, stimulated the active work of nuclear physicists to update the existing and to develope novel techniques for experiments in sectors traditional for FLNP.

After a prolonged delay due to insufficient financial support, full-scale realization of the UGRA project began for measurement of the neutron electric polarizability. Implementation of the UGRA project is under way in collaboration with the Institutes of Nuclear Research in Kiev (Ukraine) and Rez (Chekhia), and with the Technical University of Munich (FRG). A large-scale vacuum multidetector chamber is under construction for measurement of neutron angular distributions in elastic scattering. Two new types of neutron detectors have been created and tested for this chamber. At the same time a series of technical issues has been investigated with a prototype of the UGRA setup. For example, new data have been obtained on the contribution of p-wave neutron scattering on heavy nuclei. Assembly of the chamber in the experimental hall and its tests are scheduled for the end of 1994. The setup should be ready by the startup of the new pulsed neutron source, IREN.

Good facilities for studying short-lived fissioning isomers and delayed fission neutrons in the millisecond region are provided by a new device installed on beam N 11 of IBR-2, that was commissioned in 1992. Test experiments revealed the necessity of modifying the device, which was done in 1993. For instance a new chopper was constructed and installed on the neutron beam. On-beam adjustment of the device was performed. In 1994 measurements will be carried out with samples prepared at NIIAR.

Preparation has been started in collaboration with Physics-Power Engineering Institute (Obninsk) for measurements of the energy and angular dependences of emissions from fission fragments at resonances with an aligned ^{235}U nuclear target. The first version of the target was installed on beam N 5 of the IBR-30 booster. Tests of the target permitted the choice of the final target construction. In 1993 it was realized, and complex adjustment of the setup was performed. The first measurements were carried out for the (n, f)-reaction with the ^{235}U nucleus. The setup is ready for data taking in 1994.

An experimental setup is being created for measuring the p-odd asymmetry of γ-quanta emission from the reaction $^{10}B(n, \alpha)^{7}Li^{*} \rightarrow {}^{7}Li+\gamma$ in the high intensity beam of polarized thermal neutrons at the St.Petersburg Institute of Nuclear Physics (Gatchina). Measurements are scheduled for the second half of 1994.

The ROMASHKA setup has been updated for the investigation of γ-quanta multiplicities in decays of neutron resonances. It comprises neutron detectors with a 2π-geometry, which will permit significant improvement of the accuracy in extracting the parameters of neutron resonances.

Much work has been carried out for mathematical simulation of the experiment and of a series of parts of the setup intended for the first straightforward measurement of the neutron-neutron scattering amplitude at the BIGR reactor (All-Russian Research Institute of Experimental Physics, Arzamas).

1.3.2. EXPERIMENTAL STUDIES

During the period covered by the report, implementation continued of the program fixed earlier of experimental studies of the fundamental properties of the neutron, of parity violation in the interaction of slow neutrons with nuclei, neutron resonance decay channels, etc. Studies were performed at the FLNP JINR pulsed neutron sources, IBR-2 and IBR-30, and also at neutron sources of a number of other world nuclear centers (PINP, Gatchina; INR, Kiev; Oak Ridge and Los Alamos, USA; Garching, FRG; Beiging, China, Geel, Belgium).

The FLNP-PINP-VNIIEF-TU (Munich)-INR (Ukraine) collaboration continued, examining the issues of electric polarizability within the framework of the research program for investigating the electromagnetic properties of the neutron. Measurements were performed of the energy dependence of the total neutron interaction cross section with the nucleus of the lead isotope ^{208}Pb. Their analysis revealed that the neutron coefficient of electric polarizability strongly (up to a change in sign) depends on the neutron-electron interaction amplitude chosen for the calculations. Since the values of this amplitude derived from various experiments differ by several standard deviations, new approaches are necessary to this problem. One such approach involves precise measurement of the total cross section for the lead isotope indicated in filtered neutron beams. These measurements were initiated at the reactor of the INR of the Ukrainian Academy of Sciences in 1993. The first experiments demonstrated the feasibility of achieving the required precision. Great difficulties are encountered, unfortunately, in providing the resources required for operation of the reactor in Kiev.

Another fundamental characteristic of the neutron is its lifetime τ_n, relative to β-decay. In the FLNP report covering 1991, joint measurements of τ_n at the KOVSH setup were announced by the Dubna-Gatchina collaboration. The precision achieved in measuring τ_n amounted to about 0.3%. Here an anomalous leakage of UCN was observed, which exceeded by a factor of over 100 the theoretical estimate derived from experimental data obtained with very cold neutrons (VCN). To investigate the reasons for such leakage, an activation technique was developed for measuring the spectra of neutrons produced in inelastic interactions of UCN with the surface material of the vessel. The technique was tested at the UCN channel in Gatchina with materials exhibiting record low absorption coefficients (10^{-5}-10^{-6} per collision). At the same time, modernization of the KOVSH-2 setup was completed. It was ready for the experiment, but it was not possible to start experiments in 1993, because of difficulties in putting the new UCN channel in operation at the VVR-M reactor in Gatchina.

Precise measurement of τ_n is one of the purposes of the new project that is being developed jointly by FLNP and VNIIEF (Arzamas). Design and construction have been completed of the ISPIN setup, which will permit realization of a new method for obtaining, extracting and utilization of superdense (about 10^5 cm^{-3}) UCN gas from the BIGR aperiodic pulsed reactor. Estimates show that when the expected parameters of the setup are achieved, it will be possible to measure τ_n with an accuracy higher than 0.3%. However, since the safety requirements at BIGR have become more stringent, the construction of the setup must be modified. This will result in a delay of the first experiments until 1995.

Essential development took place of the program for studying parity violation and time invariance in neutron induced reactions. New results have been obtained on violation of space parity. The Dubna monoisotopic ^{113}Cd sample was used in a joint Dubna-Geel experiment, in which measurements were performed of the spins of p-wave neutron resonances observed earlier by FLNP physicists. Then, the same sample was used for measuring p-odd effects in neutron transmission with the wide aperture spectrometer of resonance neutrons, LANSCE, at Los Alamos. A preliminary analysis of the first series of joint measurements, that relied heavily on data relevant to the spins of p-

wave resonances, seems to indicate an absence of the sign coherence of p-odd effects observed earlier for thorium and uranium nuclei. Experiments with the ^{113}Cd sample will be continued considering the sign anomaly to be essential for understanding the nature of space parity violation in nuclei.

The obtained information turned out to be very useful in planning future experiments for studying the effects of p- and t-parity violation. A special monocrystalline ^{165}Ho sample was made at Duke University for investigating the violation of t-invariance. The depolarization of neutrons in the sample must be known with a high accuracy before the main measurements can be initiated. To this end the POLYANA spectrometer of polarized neutrons and nuclei has been modernized, and a new cryostat has been created for alligning the nuclei in the ^{165}Ho sample. The first stage of measurements were performed at the IBR-30 booster by the FLNP-Duke University-LANL collaboration. Analysis of the results points to a significant (up to 300%) angular dependence of the depolarization effect (Fig. 22), which requires correction of the technique for the planned measurement of the t-odd five-vector correlation between the spins of the neutron and nucleus and the neutron momentum.

Also with the POLYANA setup, and using a record-breaking (1.5 kg) polarized ^{139}La sample, a measurement was made of the transmission cross section for polarized neutrons (Fig. 23). The energy dependence, necessary for analyzing p- and t-odd effects to be studied at Dubna and Gatchina, was obtained for the polarization cross section.

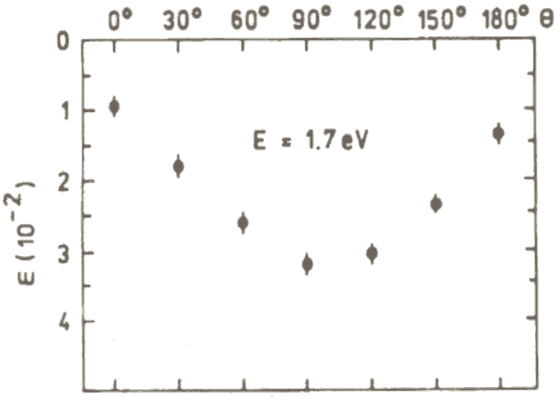

Fig. 22. Angular dependence of the transmission effect ε due to depolarization of neutrons in a holmium monocrystal for various orientations of its c- axis.

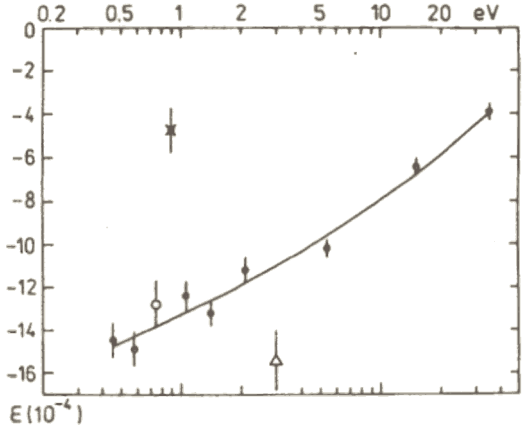

Fig. 23. Transmission effect ε of polarized neutrons through a polarized lanthanum target. The open circle represents the 0.74 eV resonance (^{139}La), the triangle - the 3.0 eV resonance (^{138}La), the cross - the 0.87 eV resonance (mixture of ^{149}Sm in La target), black dots indicate the region of smooth dependence of the ^{139}La cross section, due to a strong negative resonance.

Closely related to the above topic are the joint studies carried out by the Dubna-Gatchina collaboration at the PINP high-intensity beam of polarized thermal neutrons for observing parity violation in reactions involving emission of charged particles. The p-odd asymmetry a_{pnc} was measured in the $^{10}B(n, \alpha)^7Li$ reaction. The upper limit of the effect, significant from the point of view of theory, was derived from experimental data for α_0-lines - $a_{pnc} = (3.4\pm6.7)\cdot10^{-7}$ and the α_1-line - $a_{pnc} = (-2.4\pm1.6)\cdot10^{-7}$.

A series of interesting new results was obtained in traditional neutron spectroscopy. Studies of amplified (by factors of up to ten) electromagnetic transitions between highly excited states, which are most likely related to the fragmentation of single-particle 4S- and 4P-neutron shells into states participating in gamma transitions, were continued with a number of even-even nuclei in the vicinity of ^{158}Gd using the CASCAD setup. A joint analysis of experimental data on (n, γ)- and (n, 2γ)-reactions for the ^{187}W nucleus resulted in obtaining a record-breaking, from the point of view of completeness, scheme of levels including the 1.5-3.5 MeV excitation energy interval, not previously studied. The radiation strength functions of primary dipole γ-transitions of the discharge cascade of the capture state were obtained for $^{137, 139}$Ba and ^{181}Hf nuclei. For these nuclei, like for the nuclei studied previously, the radiation strength function was established to depend on the temperature of the excited nucleus.

Measurements of the cascade γ-radiation were performed for the ^{170}Yb nucleus produced after the β-decay of ^{170}Lu. This allowed an essential correction of the known scheme of levels (Fig. 24) obtained by traditional methods of precision nuclear spectroscopy. This experiment revealed the existence of new possibilities in this field.

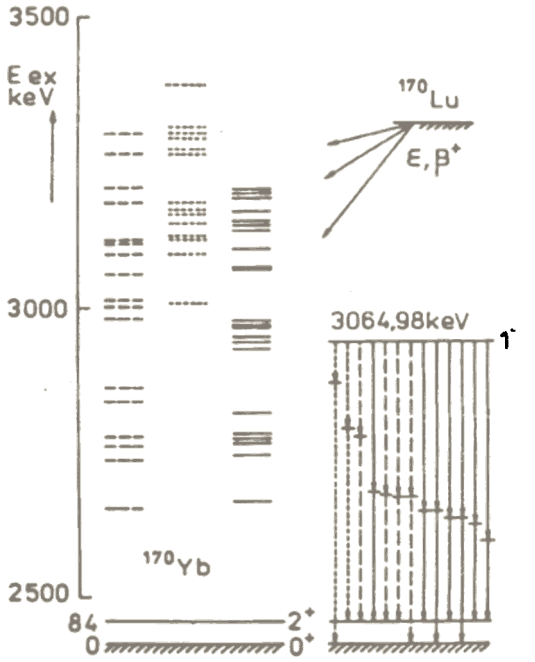

Fig. 24. Scheme of the levels of ^{170}Yb: ------ - previously known levels confirmed by this work; - - - - not confirmed levels; — — — - newly discovered levels. At the right - example of analysis of two-quantum gamma-transitions from the 3064.98 keV level of the ^{170}Yb nucleus. The notation is the same.

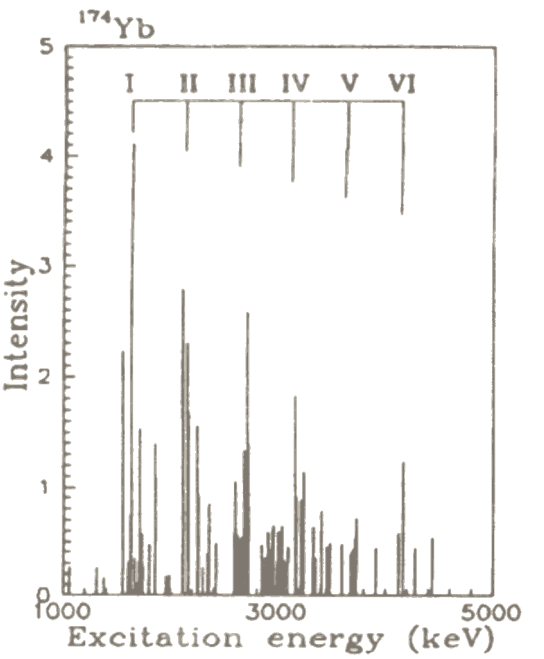

Fig. 25. Dependence of absolute intensity of two-quantum cascades to the first excited state of ^{174}Yb on excitation energy. The Roman numbers indicate probable groups of equidistant states.

The two-step γ-cascades measured earlier at FLNP for twenty target nuclei in the 114 < A < 187 mass interval were analyzed with the aim of revealing intense γ-transitions between approximately equidistant excited levels (Fig. 25). A conclusion was made concerning the possible existence in heavy nuclei of groups of excitations of the vibrational type with a characteristic energy interval E = 500-800 MeV. For confirmation of this conclusion measurements must be performed at a number of neutron resonances, which requires a significant (and expensive) enhancement of the

luminosity of the existing spectrometer. Certain progress is expected in 1994, should the new gamma spectrometers ordered in Krakow arrive.

Measurements of the multiplicity distribution of γ-quanta after radioactive capture of neutrons by $^{147, 148, 149}$Sm nuclei, that were started earlier with the aid of the ROMASHKA setup (a 4π-detector based on NaJ(Tl) crystals), have been completed. New data have been obtained on resonance parameters. For example, a unique set of data on the total radioactive widths has been determined for ^{149}Sm (Fig. 26). Similar measurements have been carried out for the $^{176, 177, 178}$Hf isotopes, but have not been processed yet.

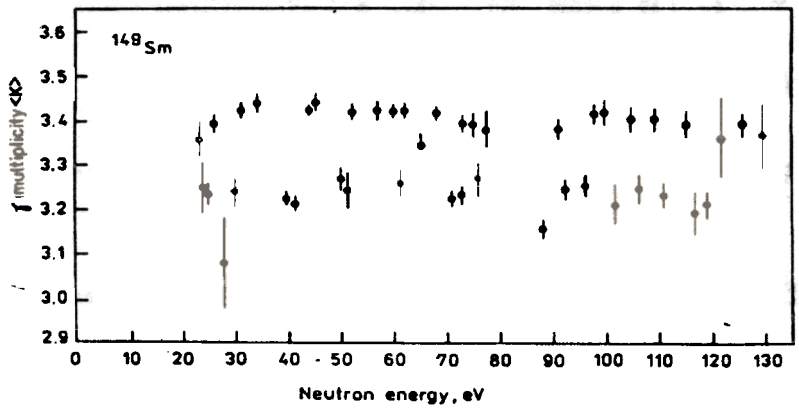

Fig. 26. Dependence of average multiplicity on neutron energyin the radiative capture of neutrons by ^{149}Sm

Studies have continued of reactions induced by neutrons on stable and radioactive isotopes and involving the emission of charged particles. Results were obtained in measurements of (n, p)-reactions on the radioactive target nuclei ^{36}Cl and ^{49}V, carried out by the Dubna-Gatchina group and by the Dubna-Los Alamos collaboration with the aid of the technique developed at FLNP.

Processing has been completed of measurements of the ^{36}Cl(n, p)^{36}S reaction that plays a key part in the production of the ^{36}S isotope, which, in turn, essentially affects the branching of the fast and slow processes of nucleosynthesis in stars. Analysis of the energy dependence of the cross section (Fig. 27) within a wide range of neutron energies (up to 800 keV) has required the application of multilevel multichannel formalism. The calculated ^{36}S production reaction rate turned out to be two times lower than the rate utilized previously in calculations, which permits significant difficulties in the theoretical description of the S-process of nucleosynthesis to be overcome.

Earlier, measurements were reported of the spectra of prompt γ-quanta from fragments produced in the fission of the ^{240}Pu compound nucleus. Processing of these measurements has been completed. Data have been obtained on the variation of independent yields of fragments produced at a level >-1% in the neutron resonances of ^{239}Pu, and the yields and lifetimes of the isomer fragments have been determined. Within a 5% precision, the conclusion has been made that fission from the compound state of spin 1^+ is single-channeled. Indications have been obtained that the integrated yield of fragments is dependent upon the fission resonance width. Multiplicity measurements have been carried out of prompt γ-quanta from ^{233}U, ^{235}U, ^{237}Np and ^{239}Pu fission resonances.

Measurements have been completed and analyzed of the neutron induced fission cross section for the ^{237}Np isotope, which is important in the problem of transmutation of the minor actinides. The results permitted the removal of a previous contradiction between the data of different groups (Fig. 28).

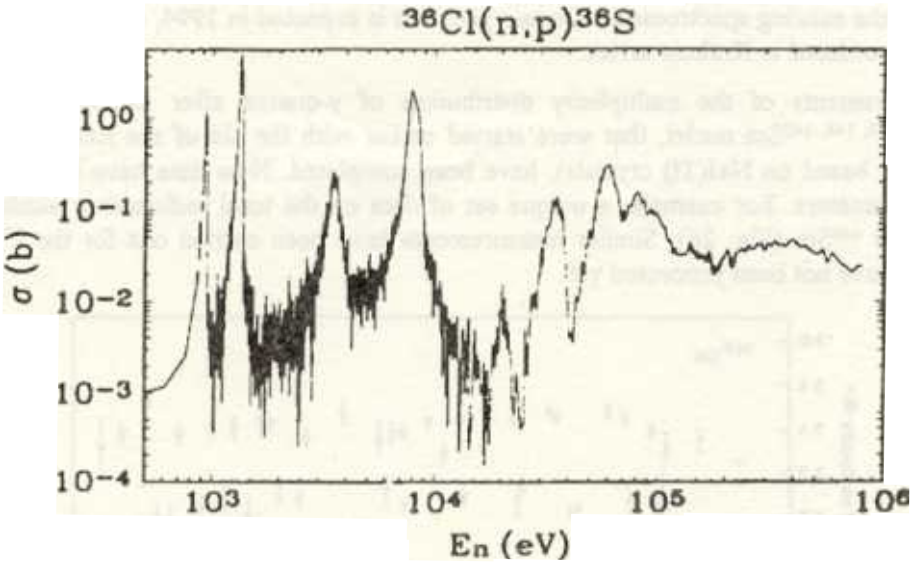

Fig. 27. Dependence of $^{36}Cl(n, p)^{36}S$ reaction cross section on neutron energy.

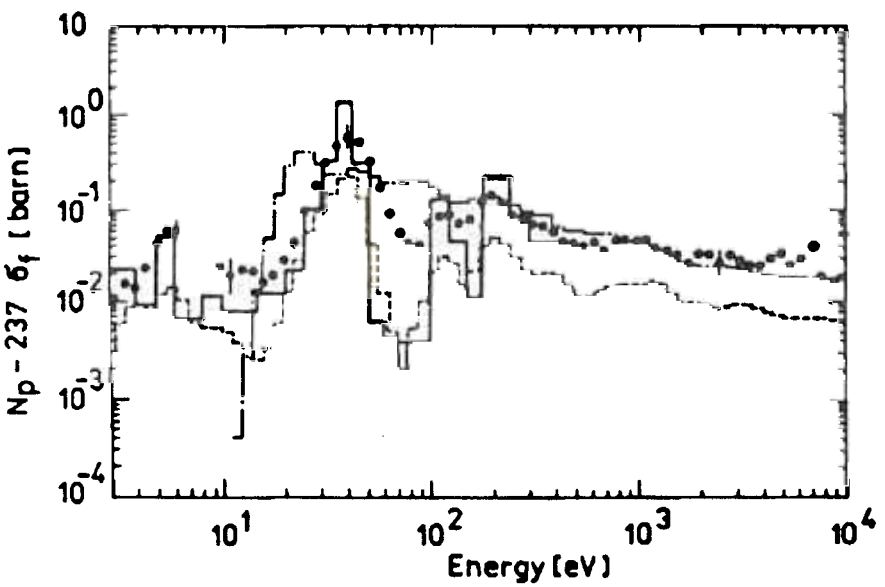

Fig. 28. Comparison of fission cross sections σ_f for ^{237}Np measured in Saclay (dashed line), for neutrons from an underground nuclear explosion (dot-dashed line), on the lead cube of the Kyoto university (black dots) and at FLNP (solid line)

Completion of the above indicated studies turned out to be possible due to RFFI grants, and to the contribution of collaborants from Poland, Chekhia, Slovakia, USA, and the Netherlands.

1.3.3. THEORETICAL INVESTIGATIONS

Theoretical work in fundamental nuclear physics continued in a number of sectors.

Calculations were performed of the electric polarizability α_n of a free neutron and of a neutron bound in nuclear matter. The resulting values of α_n are in quantitative agreement with existing experimental estimates. Meson (π, ρ and ω) degrees of freedom have been shown to be essential for describing nuclear matter, especially in the case of high densities and temperatures. Dense nuclear matter has been investigated at a temperature $T \sim (1\text{-}2)\ m_\pi$. The change in the pion spectrum of such a gas, as compared with the spectrum of free pions, consists in substitution of the effective mass $m_\pi(T)$, that increases with temperature for the mass m_π. The main thermodynamic quantities of the system decrease, as compared with an ideal pion gas.

An original method of solving the multiparticle problem has been applied in studying a system of three neutrons. The phenomenon of the appearance of artificial resonances has been observed and explained as non-physical solutions, as the area considered was limited. This gives rise to doubt concerning the previous conclusion on the existence of a three-neutron resonance.

An original microscopic method of describing cluster radioactivity has been applied in making detailed calculations of the probability of emission of carbon, oxygen and neon nuclei for the region of daughter nuclei in the vicinity of the doubly magic $^{100}Sn^{50}$ nucleus. The theoretical predictions differed from previous ones by six and more orders of magnitude and were confirmed by measurements performed at FLNR JINR. Theoretical investigation of effects due to the structure of the initial and final nuclei in cluster decay points to their being of a more complex nature than the similar mechanism of α-decay. Thus, for example, the hindrance factors of cluster radioactivity cannot be explained if only singlet nucleon-nucleon pairing is taken into account.

An experimental method for measuring UCN reflections from powders has been developed at FLNP for studies of anomalous losses of UCN. Owing to the diffusion of a neutron between grains and to multiple scattering from the surface of individual grains, the sensitivity to small losses of a single reflection increases. For interpreting the results of measurements, a model was proposed that takes into account the influence of the packing density of grains on the albedo. It turned out to be possible to achieve qualitative agreement with experimental data with the aid of this model.

The theory of multiple scattering of waves was analyzed in detail to establish the applicability of the optical potential in describing UCN reflection from a boundary surface. With its aid corrections were found to the reflection from the surface of a monocrystal with a precision up to $(d/\lambda)^2$, where d is the lattice parameter, and λ is the neutron wavelength.

1.4. APPLIED STUDIES

Nuclear data for nuclear energetics. Within the program for creating a new generation of power reactors, measurements were performed at the IBR-30 booster of the total transmission and self-indication functions in the fission cross sections for ^{232}Th, ^{238}U, and ^{239}Pu nuclei within a wide range of neutron energies up to 200 keV. An analysis has been completed of the results of measurements with the ^{238}U isotope in the range of energies from 0.465 to 200 keV. The resonance self-screening factors in cross sections were found which are used in practical calculations of nuclear reactors and of radiation shielding. The coincidence, within standard deviations, of the total and partial transmissions at energies above 20 keV points to the absence of resonance self-screening in the radiative capture cross section. The non-exponential behavior of the total transmission points to resonance blocking of the total cross section throughout the entire energy range. The results of the measurements were used for estimating the average resonance parameters: scattering radii and neutron force functions.

Modernization of the DIN-1 installation located at IBR-30 beam N 7 was carried out for measuring thermal cross sections of reactor materials. Implementation of the program of measurements has started.

Activation analysis. The preceding report announced the development of devices such as "AZOT" for express analysis of the nitrogen content in food grains, combined fodder and nitrogen-containing organic compounds. During the period covered by the report, modification and correction of the techniques and schematic solutions on the basis of industrial tests were performed. The final documentation has been given to the Institute of Technical Physics (Chelyabinsk-70) for serial production of instruments. Technical support was also given in adjusting the devices. The technical facilities of the instruments, obtained in the course of multi-year tests, were reported at a scientific conference held in the USA.

Methodological work has been completed on the utilization of moss and of pine-tree needles for biomonitoring atmospheric deposition with the aid of instrumental neutron activation analysis (INAA). Utilization of the record-breaking flux of resonance neutrons from the IBR-2 reactor made it possible to extend the number of identified elements up to 40 (for comparison, in Norway 20 elements were identified). Metals from vanadium to uranium, including REE, are reliably identified, as are a number of non-metal elements. During the years covered by the report this technique was applied in studies of the distribution of atmospheric deposition at a series of sites in Norway and at 20 points on the Kola peninsula. In the latter case, the depositions, including those of nickel, were traced from nickel factories to distances of up to 300-500 km. The work was carried out jointly with the University of Tronheim and the RAS Institute of Ecology of the North.

Complex studies of pollution by heavy metals and REE of the basins of the Upper Volga and Oka have been carried out in collaboration with the RAS Institute of the Lithosphere of the Earth. Water, residues, etc., were used for monitoring. A number of anomalies in the pollution were revealed. For example, one of the tributaries of the Oka river is strongly polluted with zirconium.

Neutron radiography. Studies were carried out of the transportation of gadolinium ions along micro cracks in concrete. The results permitted the conclusion that the technique of dynamic radiography can be used at neutron beam N11 of the IBR-2 reactor for studying the transportation of ions of gadolinium and cadmium, of analogs of calcium, potassium and sodium, and of chlorine also.

Experiments have revealed that, unlike H_2O, ions and their complexes are transported deep into concrete not in the course of diffusion through the main matrix of the material, but only along micro cracks with dimensions from 30 to 1000 μm. Knowledge of such non-stationary transport processes is extremely important for studies of the aging of concrete, especially of concrete under stress in a water medium with admixtures of heavy metal ions and organic compounds. This work was carried out jointly with the Institute of Non-Destructive Methods of Control (Saarbrucken). The project of a device for dynamic radiography is scheduled to be prepared jointly in 1994.

Radiation studies. In accordance with the proposal of physicists from LSHE JINR, CERN and FRG, studies have been initiated at the IBR-2 reactor of the radiation resistance of various detectors and electronic devices developed for experiments at the new powerful hadron colliders. A series of studies of the radiation resistance of Si-detectors in beams of fast neutrons has been carried out. For the first time have data been obtained on the possibility of using the chosen type of detector in the case of fast neutron fluences up to 10^{14} n/cm^2. The results of studies have shown that such detectors can be applied both in experiments at accelerator complexes and in constructing rapid mosaics for detecting thermal neutrons from pulsed neutron sources.

Irradiation of electronic equipment based on GaAs comprising 20 low-noise preamplifiers and shapers has revealed that the parameters of the equipment start changing when a fluence of 10^{14} n/cm^2 is accumulated, and that the equipment becomes totally inoperative after receiving a fluence of 10^{15} n/cm^2.

Neutron doping of silicon. The possibility of neutron doping of silicon was studied in 1992 at beam N 3 of the IBR-2 reactor. A monocrystal silicon ingot 61 mm in diameter and 242 mm long was irradiated using an experimental setup. Measurement of the electric parameters of the doped ingot showed that its average specific resistance of 61 Ohm·cm was in accordance with the requirements of the customer, within a spread not exceeding 3%.

The design, construction and assembly of a setup for commercial production (up to 1500 kg) of neutron doped silicon monocrystals (with maximum dimensions of ϕ127 mm x 370 mm) were completed in 1993. Work has started to put it in operation and for adjustment. Test runs have been carried out for irradiation of silicon samples at a reactor power of 100 kW with the aim of determining the operational parameters of the setup.

2. NEUTRON SOURCES

2.1. THE PULSED IBR-2 REACTOR

In 1992-93 the high-flux pulsed reactor IBR-2 was in operation for 4910 hours, as compared with the scheduled 5000 hours, which provided for completion of the program of physics experiments on 12 neutron beams. More detailed information on the operation of the reactor is presented in Table 4.

Table 4

Operation of IBR-2 reactor in 1992-93

Cycle	Cycle time	$T_{p.e.}$	$T_{m.r.}$	EPR
1	06.01-17.01.92	263	269	1
2	27.01-08.02.92	248	209	3
3	17.02-29.02.92	265	299	2
4	17.03-29.03.92	268	321	3
5	13.04-25.04.92	265	277	2
6	12.05-24.05.92	278	284	1
7	08.06-24.06.92	325	408	7
8	16.11-29.11.92	244	287	7
9	07.12-25.12.92	406	443	4
	Total for 1992	***2562***	***2797***	***30***
1	11.01-22.01.93	243	273	3
2	01.02-13.02.93	249	280	2
3	22.02-05.03.93	254	270	3
4	22.03-02.04.93	250	281	5
5	12.04-22.04.93	236	248	3
6	17.05-29.05.93	216	279	8
7	07.06-19.06.93	257	295	6
8	25.10-01.11.93	154	176	0
9	15.11-26.11.93	252	272	4
10	06.12-17.12.93	237	267	3
	Total for 1993	***2348***	***2641***	***37***
	Overall total	**4910**	**5438**	**67**

Comment: $T_{p.e.}$ is the time of operation for physical experiments; $T_{m.r.}$ is the operation time of the moving reflector; EPR is the number of emergency power shutdowns.

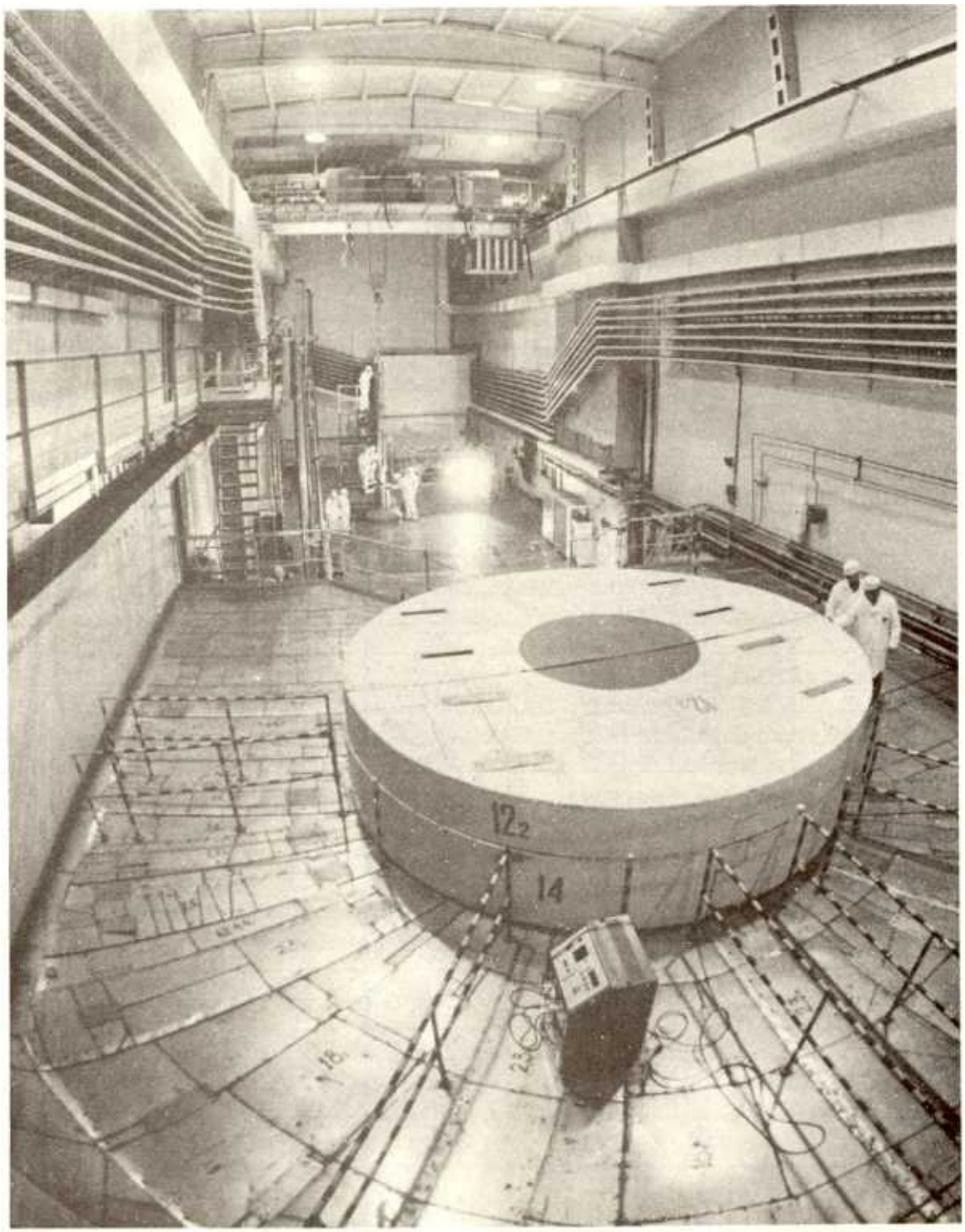

IBR-2 reactor hall

Short-term shutdowns of the reactor were initiated by unexpected actuation of the emergency safety system, caused by events classified as zero level events, in accordance with the international scale of events.

Since the start-up of power production by the reactor (the end of 1980) up to 01.01.1994 it has run for 26038 hours. The total number of emergency shut-downs during this period was 318, of which 307 were unexpected. The flux density of neutrons with energies > 0.1 MeV incident on the wall of the reactor casing amounts to $1.3 \cdot 10^{14}$ n/cm^2 s, when the power is 2 Mw. For the above figures the neutron fluence on the reactor casing amounted to $1.22 \cdot 10^{22}$ n/cm^2 by 01.01.94.

The active core. Long-term operation of the reactor resulted in a partial burn-up of the fuel and to a corresponding reduction of the operational supply of reactivity. The first renewal of the active core of the reactor was performed between July 19 and 23, 1993. The decoy cassette (without fuel) was extracted from the core and put away for long-term storage in the reactor storage pit. It was substituted by a heat-generating assembly (HGA) with fresh plutonium dioxide fuel (Fig. 29).

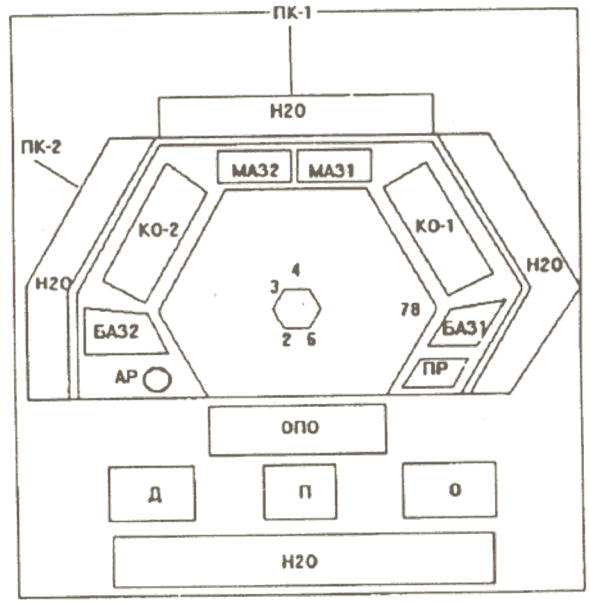

Fig. 29. Active core of the IBR-2 reactor. The figures indicate the numbers of cells filled with simulators of fuel element assemblies. Renewal of the active core consisted in substitution of a fresh energy releasing assembly (ERA) for the simulator of cell 3. The total number of ERAs in the active core became 74. KO-1, KO-2 are reactivity compensaters, MA31, MA32 are emergency safety blocks, БА31, БА32 - rapid emergency safety blocks, ПР - intermediate regulator, AP - automatic regulator, ОПО and ДПО - main and additional reflectors, respectively, H2O - neutron moderators, ПК-1, ПК-2 - trigger channels.

Measurements carried out after the renewal showed the supply of reactivity was enhanced by a quantity sufficient for implementation of the scheduled energy production for 6 years of reactor operation in the previous mode. The resource parameters of the core after renewal are presented in Table 5.

The renewal of the core, being a task classified as nuclear-dangerous, was carried out together with all necessary organizational and technical measures required for nuclear and radiation safety. A routine test of the state of nuclear, radiation, and technical safety was made by a Gosatomhadzor (Russian State Atomic Inspection) commission upon completion of the renewal

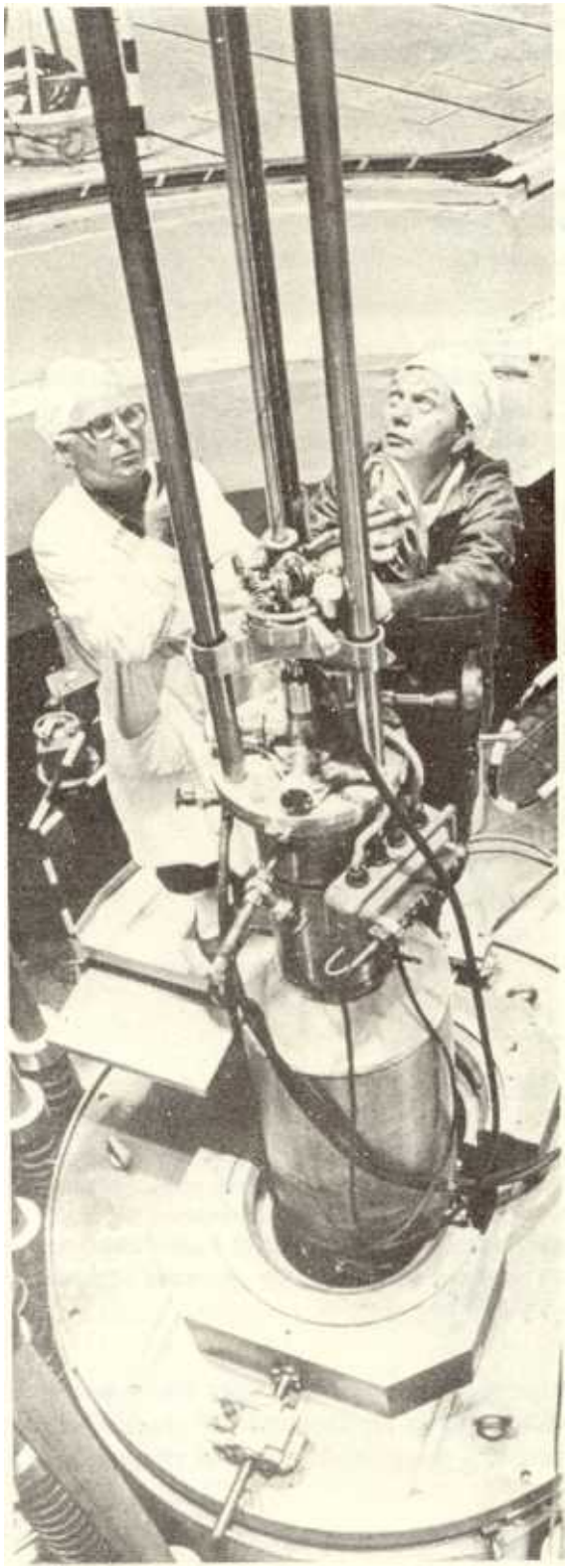

New movable reflector
of the IBR-2 reactor

Renewal of the IBR-2 reactor core

activities at the reactor, and no deviations from or violations of the established safety restrictions of the reactor operation were observed.

Table 5

Service characteristics of the IBR-2 core after renewal

Characteristic	For 01.01.94	By the end of the scheduled service time (May 2003)
Burn-out of plutonium - average - maximum	2050 MW·day 2.7% 4.1%	4000 MW·day 5.2% 7.8%
Reserve of reactivity	1.55±0.05%	0±0.05%
Fluence of fast neutrons (n/cm^2) - at the centre of the core - at the reactor vessel (maximum)	 $2.05 \cdot 10^{22}$ $1.17 \cdot 10^{22}$	 $4.0 \cdot 10^{22}$ $2.28 \cdot 10^{22}$
Volume coefficient of inhomogeneous energy release	1.53	1.50
Number of loaded fuel element assemblies	74	74

Comment: The burn-out of plutonium due to fission is assumed to be equal to 1.1 g/MW·day, which corresponds to an energy release of 192 MeV/fis. The reactivity coefficient with respect to the burn-out of fuel is $dK/dQ = -8 \cdot 10^{-6}$ k/MW·day. The specific fluence of fast neutrons (E > 0.1 MeV) was used at values of $d\Phi/dQ = 1.0 \cdot 10^{19}$ neutr./cm^2·MW·day in the central channel and $0.57 \cdot 10^{19}$ at the reactor vessel in a median cross section of the core.

The moveable reflector. A second moveable reflector, PO-2, has been in operation at the reactor since October 1987, having been substituted for the first moveable reflector, PO-1, the first reflector had been in operation for 13211 hours from the reactor startup. The permitted service time for PO-2 is 19000 hours. By 01.01.94 the running time of PO-2 amounted to 18791 hours. When the resources of PO-2 are exhausted in 1994, it will be replaced by a new moveable reflector, PO-2R. The new PO-2R reflector is fully analogous to the existing one, except that the control system for positioning the rotators is more developed. The construction of PO-2R was mainly completed in 1993, and now part-by-part assembly is under way together with some additional machining. Balancing of the rotors was completed. The tempo of work on PO-2R has been hindered both in 1992 and 1993 by insufficient financial support.

The control system for fuel elements. Work has been completed on the construction of an automated control system for the hermetic cases of the fuel elements in the core zone. The system controls the activity of the gas in the argon cavity of the expansion tank of contour I with a Ge(Li) detector. When leakage of gaseous fission products occurs, relevant information will appear automatically on the control panel of the reactor.

The IBR-2 automated measurement and monitoring system (AMMS). During the period covered by the report work continued on developing the reactor AMMS. Detailed information on the system is presented in the 1991 report. The AMMS consists of three subsystems: 1) technical control (T); 2) control of the reactor and of the reflector (R); and 3) the logical system for processing and forming control and emergency signals (L).

The measuring equipment for subsystem T was provided and assembled in 1991. The subsystem has been in service for two years. Periodic control of its characteristics revealed its

operation to be stable. The equipment for subsystem R was obtained and installed at its working place in 1992 and tested with real signals. In 1993 improvement of the software was performed for reducing the time delays in the formation of signals for resetting the emergency safety control system. At present the parameters of the system correspond to the technical assignment. The measurement channels of subsystem R are to be tested, when the new moving reflector is put in operation in 1994. As to subsystem L, development work and the construction of equipment was to be completed in 1993. Adjustment work should be completed in 1994. To a significant degree all the necessary work was delayed by insufficient financial support.

The cryogenic moderator. In 1992 work was completed on the construction of a cryogenic moderator (CM) based on solid methane. A detailed description of the design was presented in the report for 1991. The moderator was established at its regular place near the core, transport operations for its installation and removal from the active zone were worked out, and the control and diagnostics systems were assembled and adjusted. Complex technological tests of the CM, involving cooling the methane down to 12 K, were carried out in October 1992. A CM test program was worked out for the reactor in operation, the safety of these tests was substantiated for certain restrictions (for powers not exceeding 5 MW·hour).

30.10.92-5.11.92 the CM was put in physical operation while the IBR-2 was operating at a power up to 1 MW. Measurements of the thermal and neutron-physical parameters were performed. The following results were obtained at 1 MW: temperature of solid methane was 20 K; power consumed by the moderator was 490 W as compared with 300 W at zero power; the admissible rise of reactor power cannot be greater than 0.3 MW/hour; and enhancement of the cold neutron flux ($\lambda > 4$ Å) was by a factor of 4.2-5.2 as compared with the regular comb-like water moderator.

In Fig. 30 the variation of the moderator parameters is presented for cooling without power, when the reactor is operating with power and when the moderator being heated. Fig. 31 presents experimental spectra of neutrons from the comb-like and from the cryogenic moderators, and in Fig. 32 the respective gain factor for the CM is shown. On the whole, the assignment parameters of the moderator were achieved.

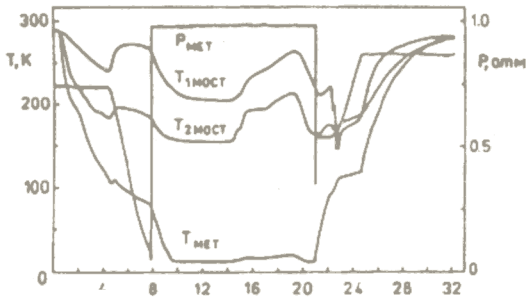

Fig. 30. Change in pressure $P_{met.}$ and temperature $T_{met.}$ in the moderator and temperatures $T_{1bridge}$ and $T_{2bridge}$ at two points of the thermal bridge of the moderator: t ~ 8 h - the moderator is filled with helium up to 1 atm; t ~ 14 h - the IBR-2 power is enhanced up to 1 MW; t ~ 19.5 h - the reactor is shut down; t ~ 21 h - the moderator is connected to the receiver, the cooling is switched off.

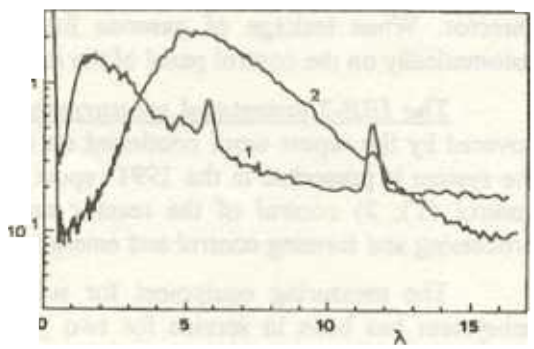

Fig. 31. Neutron spectra measured in beam N 4 of IBR-2 reactor: 1 - comblike moderator, 2 - cryogenic moderator. The x-axis - λ(Å), the y-axis represents the count intensities in arbitrary units for each spectrum.

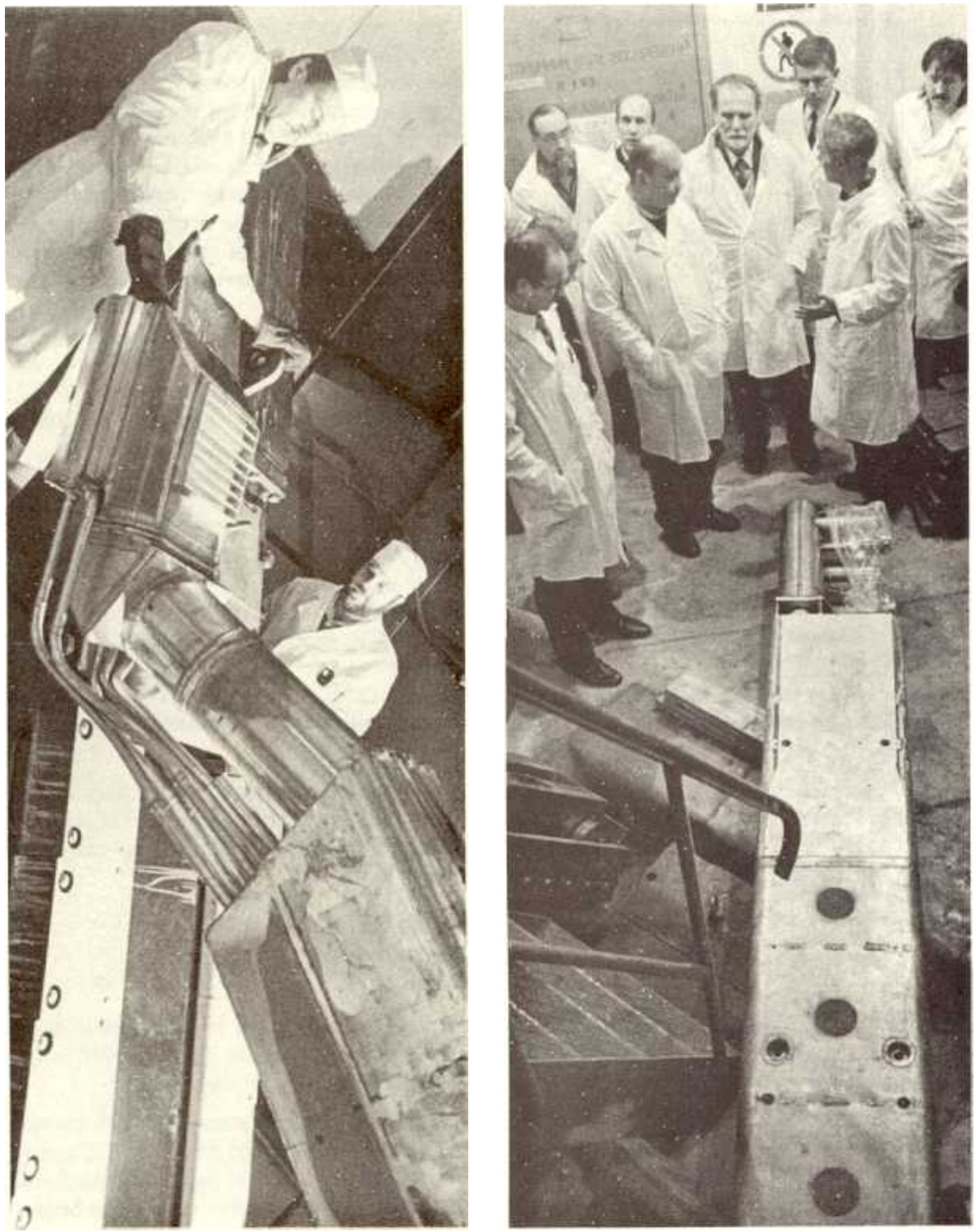

Cold moderator of the IBR-2 reactor

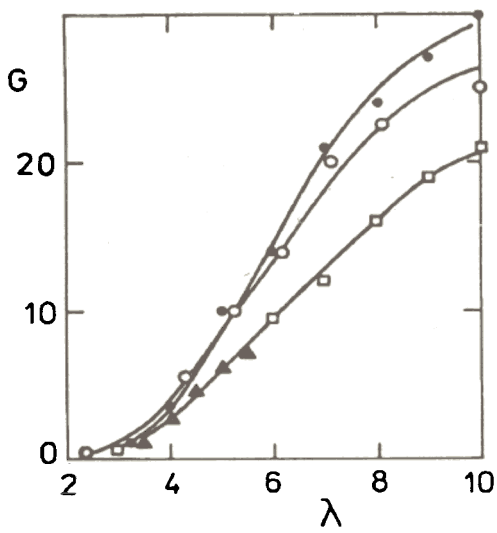

Fig. 32. Dependence of gain factor G on the neutron wave length λ (Å): • - measurement of spectra with a semiconductor Si(Li) detector in beam N 4 with a flight base L = 18 m; O - measurement on small-angular scattering diffractometer SANS with carbon, L = 18 m; □ - current ^{235}U fission chamber in beam N 6, L = 5.5 m; Δ - measurements on DN-2 diffractometer with zirconium dioxide ZrO_2, L = 25 m.

In 1993 work continued for mastering the moderator. The main work was the investigation of solid methane irradiated in conditions close to the operating conditions of the cryogenic methane moderator at a power of 2 MW over a prolonged period of time. The purpose of the work was to obtain the following quantitative characteristics: the degree of swelling of methane exposed to radiation, the rate of accumulation and disposal of radiolytic hydrogen, and the reaction rates for radicals.

The following results were obtained with the specially made URAM installation:

1. No radiation swelling of the methane in the 20-60 K temperature interval was observed under irradiation during periods up to 4 days.

2. A strong temperature dependence has been observed for kinetics of the hydrogen yield from methane. At T > 50 K, hydrogen diffusion was insignificant. At T > 55 K the diffusion rate was so high, that when the methane was submitted to heating for periods of about 10 min, the radiolytic hydrogen had time to leave the methane before the methane started to melt.

3. No spontaneous fast recombination reaction of radicals (RRR) was observed in the conditions of the URAM experiment. RRR were initiated in the case of sufficiently rapid heating of the cooling helium by 3-5 K, if the preceding irradiation continued for at least 4 hours.

A CM test program for reactor powers up to 2 MW has been elaborated on the basis of data analysis of the physical startup and studies at the URAM installation. The results of the CM tests will be used in choosing its optimum operation modes. Implementation of the program is scheduled for the first half of 1994.

2.2. THE IBR-30 + LUE-40 BOOSTER

In 1992-93 the IBR-30 pulsed fast booster, with its injector based on the LUE-40 linear electron accelerator, was in regular operation for 20 cycles of total duration equal to 5030 hours, which provided for implementation of the nuclear physics program on 6 neutron beams.

In the 1991 report, the development of a new tantalum target was announced. The purpose of this project was an enhancement of the efficiency using photo-neutrons and the creation of a more uniform thermal field about the target channel. To the latter end the target has been surrounded with a tantalum screen. The target was installed at its regular place inside the active zone of the booster and prepared for working tests in October 1992. During tests at nominal power the temperature of the fuel elements around the target was two times lower than when the target was without a screen. However, week-long tests of the target turned out to be unsuccessful, on the whole. The tantalum target, cooled by liquid helium, started to disintegrate under the influence of the electron beam, which resulted in pieces of tantalum jamming the target channel, in a drop of helium consumption and in a corresponding increase in the target temperature. The tests were stopped. The target was

replaced by the regular tungsten target, with which the 1992-93 campaign continued. A new target has been improved taking into account the results of the tests; for instance, tungsten has been substituted for tantalum, while the tantalum screen of the target has been retained.

At the end of 1992 control of IBR-30 installation became the responsibility of Gosatomnadzor (State Atomic Supervision) of Russia. In connection with the introduction of new documentation regulating technical standards, much work was performed in 1993 to bring the booster into accordance with the new requirements for safe operation.

Financial support of IBR-30 is based on non-budgetary funds allocated to the scientific self-supporting section "The IBR-30 reactor".

2.3. THE SOURCE OF RESONANCE NEUTRON (IREN)

The 1991 report announced the start of work on the design of a new high resolution neutron source (the old name of the project was HRNS), which is to replace the source actually in service, the IBR-30 booster. In the course of work on the project in 1992 it became clear that it was possible to create a relatively cheap pulsed source of resonance neutrons with parameters at a world level in its class. In March 1993 the JINR Plenipotentiaries, upon completion of a large preparatory work for choosing the most promising source, made the decision to create a new pulsed source of resonance neutrons (IREN) at FLNP.

The rated parameters were defined for the two main systems of the installation: for the electron accelerator and the multiplying target. The principal part of the installation is the powerful linear electron accelerator LUE-200. The parameters of the IREN setup and of the LUE-100 accelerator are presented in Table 6, while the location of IREN in the building where the IBR-30 is situated, is shown in Fig. 33.

Table 6

Rated parameters of the IREN installation

Electron energy, MeV	200
Peak current, A	1.5
Pulse frequency, Hz	150
Pulse duration, mcs	0.2
Average power of electron beam, kW	10
Duration of neutron pulse, mcs	0.4
Average fission power, kW	30
Peak fission power, MW	540
Average flux n/s	$1{,}5 \cdot 10^{15}$
Peak flux, n/s	$2{,}7 \cdot 10^{19}$
The background in between pulses, %	5.6
Multiplication	28
Average lifetime of prompt neutrons, mcs	0.01
Volume of active zone, dm^3	2.5

Comment: The neutron yield is calculated for e-γ-n-converter made from stainless steel, uranium-235 and uranium-235 mononitride, and for an active zone of plutonium.

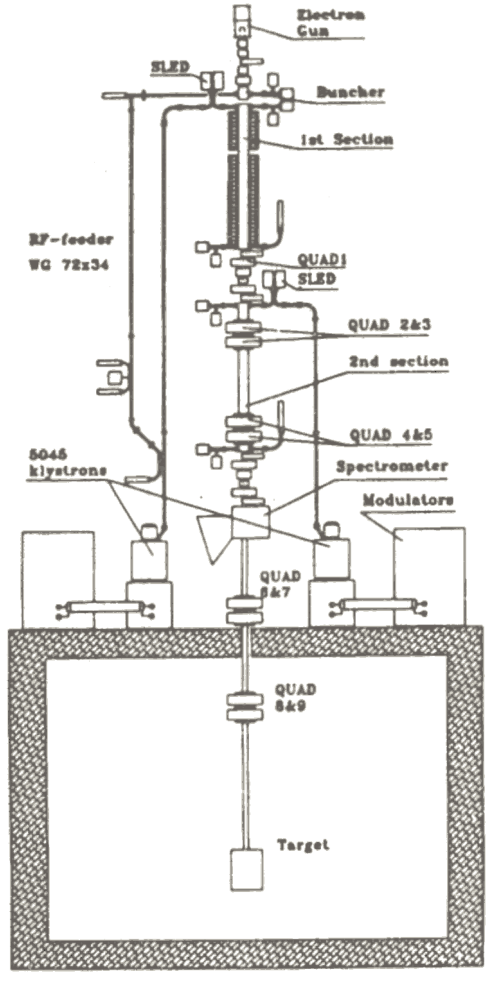

Fig. 33. Layout of IREN installation in building 43 of JINR FLNP (vertical section).

In 1992 an agreement was concluded for designing and constructing the LUE-200 at the Institute of Nuclear Physics of the RAS Siberian Branch (Novosibirsk). For two years the INP carried out a large volume of work in creating the working design of the electron accelerator. International expertise of the design was carried out. In connection with the close completion of the design work a detailed division of responsibilities for constructing the linac was performed between INP and JINR: about 20% of high technology norm-hours are to be consumed in Novosibirsk and the rest in Dubna. Preparation is under way for signing a financial Agreement for implementing the work in INP.

Close collaboration has been established with Stanford University (USA) concerning the issues of the linac construction. For the IREN project the most modern and most powerful clystrons in the world, constructed at Stanford, will be used as sources of SHF power. A corresponding agreement has been prepared and signed between the Department of Energy (USDOE) and JINR. Permission has been obtained and a program has been worked out concerning the supply and transport of the clystrons and the equipment for them. The first clystron and its equipment have been paid by JINR and will be delivered to FLNP in the summer of 1994.

A new scientific experimental department was formed in FLNP, and its task is realization of the IREN project. In order to reduce the design and construction time and realization expenses a cooperation has been established between FLNP and some other JINR laboratories. The linac focusing system and the channel for transporting the beam to the target are under development at the Laboratory of Nuclear Problems. Here, also, the general layout of the linac in the appropriate building is being worked on. The electron source is being designed together with staff members of the Laboratory of High Energies and the Laboratory of Nuclear Problems. At present a version of the vertical arrangement of the electron source and of the high-voltage supply for it has been completed. Work is under way in the new department on modulators for the American clystrons. At the same time the department has begun working on design and experimental work for a choice for elements of the linac beam diagnostics system.

An agreement has been concluded with NIKIET (Moscow) for preparation of the technical design for the target complex of the IREN installation. The project involves development of the active zone with plutonium fuel elements such as the elements for IBR-30, of an electron-neutron converter, of cooling systems, of an emergency safety system, of a biological safety system, and of neutron reflectors and moderators. The layout of the multiplying target together with the tungsten reflector (a tungsten-nickel-iron alloy) and water neutron moderator is shown in Fig. 34.

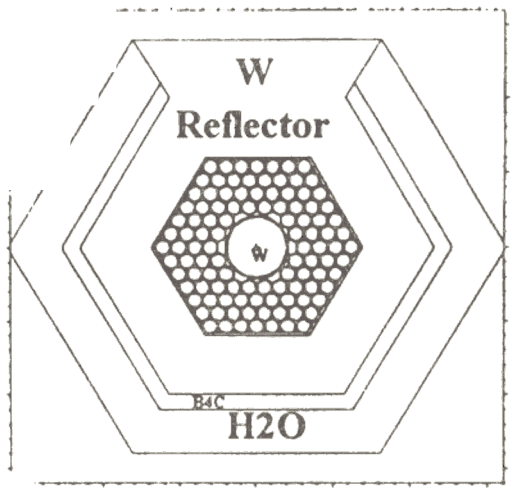

Fig. 34. Multiplying target of IREN setup.

The active zone of the target consists of 108 fuel elements 16 cm high. The amount of loaded plutonium is 17.6 kg for a neutron multiplication coefficient equal to 0.98. Utilization of plutonium, instead of uranium, as planned for the first version of the target, will permit a twofold enhancement of the neutron flux at the surface of the moderator. The spectrum of neutron leakage is presented in Fig. 35.

Practically all 10 kW of the electron beam power are released in the form of heat in the heavy material of the converter inside a volume of the order of magnitude of 1 cm^3. A beryllium beam scatterer is to be utilized in order to reduce the energy release density. The role of the scatterer is clearly demonstrated in Fig. 36, in which a comparison is made of electron-phonon showers, when a beryllium scatterer 10 cm high is present and when it is absent; 25 histories were simulated for electrons of initial energy equal to 150 MeV. The radial distribution of released power is shown in Fig. 37.

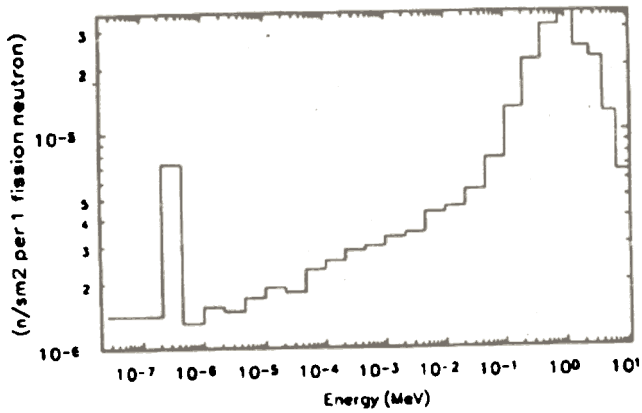

Fig. 35. Group spectrum of neutrons leaking from the surface of the moderator of the multiplying target of IREN. The moderator is 3 cm thick. The spectrum of decelerated neutrons $\varphi(E) \sim 1/E^{1-\alpha}$, *where* $\alpha = 0.11$.

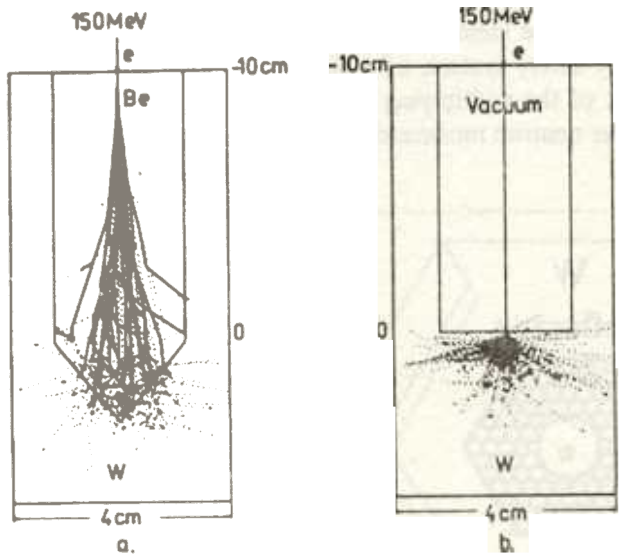

Fig. 36. Electron-photon shower in tungsten target with beryllium scatterer (a) and without scatterer (b). The scatterer reduces the maximum heat release density in tungsten by a factor of 2, when the beam is 1 cm in diameter.

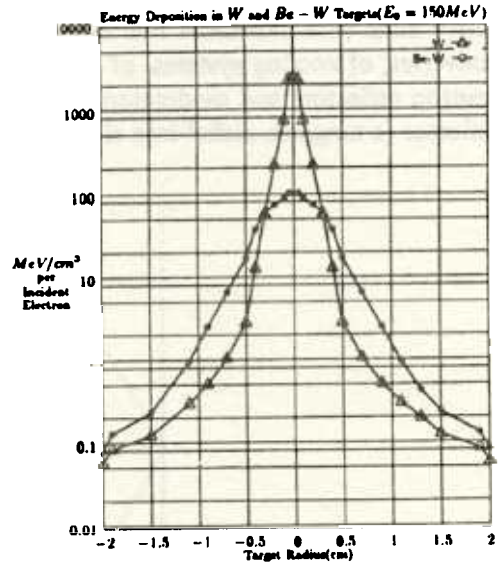

Fig. 37. Radial distribution of the heat release in a tungsten target at a depth of 3 radiation lengths (maximum heat release) in presence of beryllium scatterer (1) and without scatterer (2).

An agreement has been concluded with PKNTs "Reconstruction" for a computational technical substantiation of the multiplying target. However, owing to a delay of the preliminary payment by JINR, provided for in the agreement, implementation of the agreement has been delayed by half a year. This has shifted the performance of work in NIKIET. An agreement has been concluded with GSPI (Moscow) for preparation of the working design of IREN, that is to include disassembly of the IBR-30 booster and appropriate accommodation of the parts of the new electron accelerator and of the neutron multiplying target. At present all design work is being carried out in close collaboration with FLNP.

Besides creation of the IREN installation itself in 1994-96, plans are to reconstruct the experimental base for studies in neutron nuclear physics. This will not only make possible the utilization of a first-class neutron source, but also, to actually have a neutron factory providing the broadest experimental facilities possible for specialists from JINR member states and from other countries.

3. MEASUREMENT-AND-COMPUTATION COMPLEX

CENTRAL PROCESSOR COMPUTERS

1992 was the last year when the complex of three computers (PDP-11/70 and two microVAX-II computers), constituting the central FLNP processor, supported physical measurements at the FLNP reactors. One of the microVAX-II computers was incorporated into the Institute's common ETHERNET network and was used for archiving experimental information. In 1993 the PDP 11/70 that was in service for 12 years, was put out of operation. In its place, five SPARCstation-2 and two SPARCserver-2 computers were put in operation. Both microVAX-II computers were combined in a cluster with common disk space of about 1 Gbyte. On the whole, this made possible an essential enhancement of the computational facilities of the laboratory and development of a new archiving and experimental data processing system.

COMPUTER NETWORKS

Work performed in 1992-93 for development of the infrastructure of a local ETHERNET computational network and renewal of the stock of computers resulted in creation in the laboratory of a computational complex distributed according to territory (Fig. 38).

From a structural point of view, the laboratory network is a segment of the common network of the Institute, as one of its segments. This allows laboratory users to have access to the networks of different countries. It gives them the following possibilities: e-mail, Remote Job Entry, File Transfer, TCP/IP service, etc.

Inside the laboratory, the network consists of a series of segments located in the buildings of the IBR-2 reactor and in the laboratory buildings. These buildings are connected with the FLNP measurement-and-computation centre (Building N 119) by LVS optical cables. On the whole, besides the computers indicated above, the network combines over 100 personal computers and computers pertaining to physical installations.

MEASUREMENT SYSTEMS OF PHYSICAL SETUPS

In 1992-93 work was under way to create the hardware and software for the measurement systems of physical setups at the IBR-2 and IBR-30 reactors, and, moreover, in the VME standard.

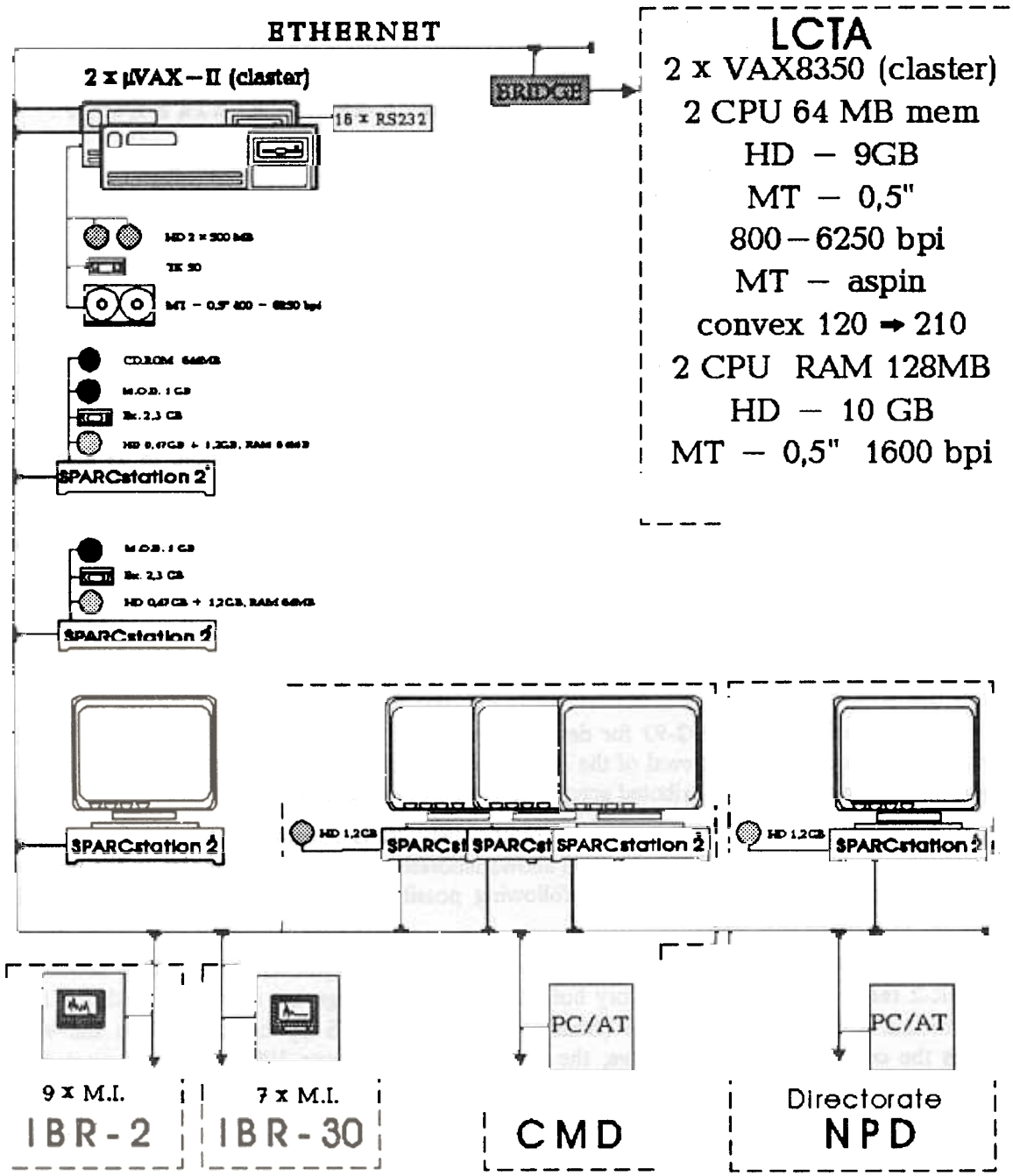

Fig. 38. The FLNP computation complex.

In 1992, in collaboration with specialists from the Technical Centre (Finland) and PINP (Gatchina), work was completed on the measurement module of the new powder diffractometer HRFD on beam N 5 of the IBR-2 reactor, and it was put in operation. The electronics of the multichannel Li-detector of the diffractometer were improved. Electronics were made for the 90° detector. Successful tests were carried out of the prototype of the RTOF correlator based on digital signal processors. The software for the accumulation system in the BITBUS standard was developed and put into service. The software for including a PC-controlled refrigerator in the FDVR system was updated.

The measurement module of the DN-12 diffractometer was created and put in operation. The first measurements with the measurement module, in the VME standard, were carried out at the NSVR installation. A multidimensional MMM (moving measurement module) system has been made and put in operation. The first line of the data acquisition system for the UGRA setup has been completed. The physical installations NERA-PR and KDSOG have been modernized and their equipment updated.

ELECTRONIC EQUIPMENT

New electronic blocks have been developed and constructed in the VME and CAMAC standards: a CAMAC-VME interface based on the KK 009 controller-crate and the software for the crate; a 2 Mb (24; 16) incremental memory block in the VME standard; a 5 kV high-voltage supply in the CAMAC standard; and a coding block for time spectra with 16 detector inputs in the CAMAC standard.

4. ORGANIZATION

4.1. LABORATORY STRUCTURE

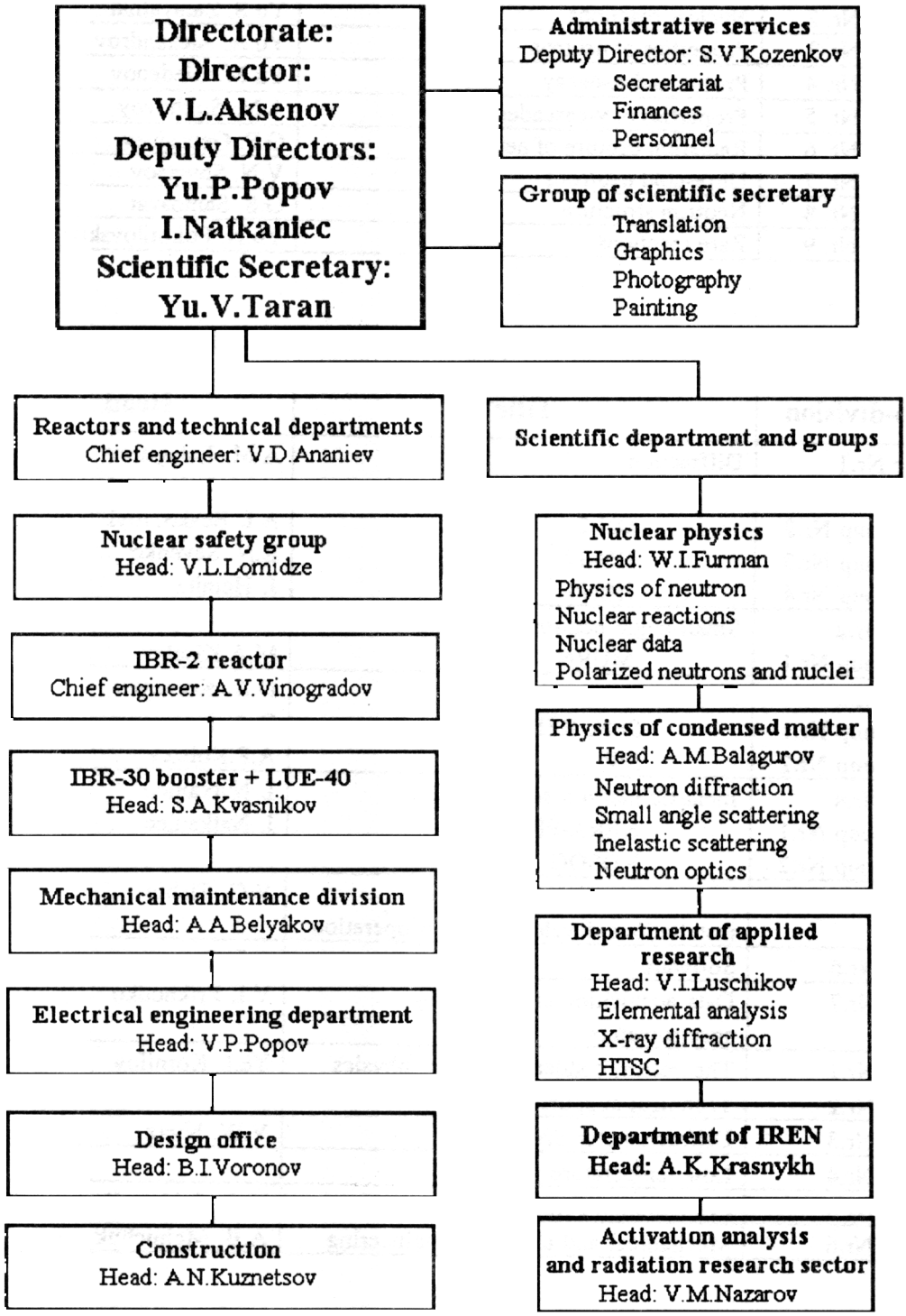

Table 7

THE NUCLEAR PHYSICS DEPARTMENT

Sub-division	Title	Head
Sector Nr. 1	Neutron spectroscopy	V.P. Alfimenkov
Group Nr. 1	Fission physics	A.B. Popov
Group Nr. 2	Nuclear reactions	Yu.S. Zamyatnin
Group Nr. 3	Properties of neutron	Yu.A. Alexandrov
Group Nr. 4	Proton and α-decay	Yu.M. Gledenov
Group Nr. 5	Properties of γ-cascades	A.M. Sukhovoy
Group Nr. 6	Radiation capture of neutrons	G.P. Georgiyev
Group Nr. 7	Ultra-cold neutrons	V.N. Shvetsov
Group Nr. 8	Neutron structure	G.S. Samosvat
Group Nr. 9	Rare reactions	Yu.N. Pokotilovskiy

Table 8

THE CONDENSED MATTER DEPARTMENT

Sub-division	Title	Head
Sector Nr.1	Diffraction	A.M. Balagurov
Group Nr.1	HRFD	A.M. Balagurov
Group Nr.2	DN-2	A.I. Beskrovnyi
Group Nr.3	DN-12	B.N. Savenko
Group Nr.4	HRNS	J. Heinitz
Sector Nr.2	Small-angle neutron scattering	I.N. Serdyuk
Group Nr.1	MURN	M.A.Kiselev
Sector Nr.3	Neutron optics	D.A. Korneyev
Group Nr.1	SPN, REFLEX	D.A. Korneyev
Group Nr.2	SIP	A.P.Kobzev
Sector Nr.4	Inelastic neutron scattering	I. Natkaniec
Group Nr.1	NERA-PR	I. Natkaniec
Group Nr.2	KDSOG	A.Yu. Muzychka
Sector Nr.5	Detector electronics; physics installations development and operation	V.G. Tishin
Sector Nr.6	Software	A.I. Ostrovnoy
Sector Nr.7	Data acquisition and handling spectrometers	V.I. Prikhodko
Group Nr.1	Theoretical condensed matter physics	Ye.I. Kornilov
Group Nr.2	Technical support	V.V. Zhuravlyov
Group Nr.3	Diffractometer SNIM-2	V.W. Nietz
Group Nr.4	Low temperature physics	
Group Nr.5	Computation center	G.A. Sukhomlinov
Group Nr.6	Mechanical and electrical engineering	A.B. Melnichuk

4.2. USER POLICY

At present, the experimental installations for condensed matter investigations and neutron nuclear physics are effectively used on all beams of the IBR-2 reactor and the IBR-30 booster, which form the FLNP base facilities. The number of performed experiments, including those carried out at the requests of the outside users, has grown considerably.

A new scheme of managing the experimental investigations proposed by the laboratory's own and outside users has been worked out. It demands that:

- *The head of the Condensed Matter Department is appointed the one responsible for carrying out the experiments (any activities using neutrons) at all the IBR-2 beams.*
- *The next cycle schedule is drawn up based on the "Application for an Experiment" for the laboratory's own scientists and the "Application for Beam Time" for the outside users.*
- *The applications for experiments are submitted to the head of the sector before drawing up the IBR-2 schedule, considered by the corresponding users' specialized committee, and adopted by the FLNP deputy director or by the head of the Condensed Matter Department.*
- *The IBR-2 beam schedules are drawn up by the head of the Condensed Matter Department with regard to the adopted experiments, checked with the one responsible for monitoring the radiation level, and adopted by the director or the deputy director for condensed matter physics.*
- *On performing an experiment, one fills out the "Experimental Report" form, which is then submitted to the head of the sector.*
- *For realizing the procedure of distributing the resources and time required for performing experiments at the IBR-2 spectrometers, users' committees have been set up for the following specializations: diffraction, small-angle scattering, inelastic neutron scattering, neutron optics, and nuclear physics. Also, the committee for beam experiments of applied or commercial character has been set up. These committees consider applications for experiments.*

Each of the specialized committees is comprised of:

- *the FLNP deputy director for specialization,*
- *head of the Condensed Matter Department or the Nuclear Physics Department,*
- *head of the corresponding sector,*
- *head of the group of physicists at the spectrometer.*

The committee on the applied works is comprised of:

- *the FLNP deputy director of the applied works,*
- *the FLNP chief engineer,*
- *head of the Heavy Ions Physics Department,*
- *head of the Condensed Matter Department,*
- *head of the Neutron Activation Analysis and Radiation Investigations.*

The temporary staff of the users' committees has been formed.

Diffraction	Small-angle scattering
1. I. Natkaniec	1. I. Natkaniec
2. A.M. Balagurov	2. A.M. Balagurov
3. A.I. Beskrovnyi	3. I.N. Serdyuk
4. V.W. Nietz	4. M.A. Kiselev
5. J. Heinitz	

Inelastic scattering	Neutron optics
1. I. Natkaniec	1. I. Natkaniec
2. A.M. Balagurov	2. A.M. Balagurov
3. A.Yu. Muzychka	3. D.A. Korneyev
4. A.V. Puchkov	4. L.P. Chernenko

Nuclear physics investigations	Applied investigations
1. Yu.P. Popov	1. Yu.P. Popov
2. I. Natkaniec	2. V.D. Ananyev
3. W.I. Furman	3. V.I. Lushchikov
4. A.M. Balagurov	4. A.M. Balagurov
5. Yu.A. Aleksandrov	5. V.M. Nazarov

In addition to the brief information on the FLNP spectrometers, which is given in Section 2.1 (Tables 1 and 2), their more detailed characteristics are presented in the "User Guide (Neutron Experimental Facilities at JINR)", issued by FLNP, Dubna, 1992.

4.3. SEMINARS

Date	Authors	Title
23.01.92	**V.O.Nesterenko** (BLTP JINR)	*Metal clusters as a new field for application of ideas and methods of nuclear physics*
26.03.92	**Prof. C.R.Gould** (TUNL and NSCU, USA)	*Tests of Time Reversal Invariance with Polarized Neutrons and Oriented Targets*
23.04.92	**G.N.Zorin, E.D.Vorobiov** (FLNR JINR)	*Chain reaction of nuclear synthesis*
14.05.92	**A.Bland** (Cambridge Univ., England)	*Spin Polarized Neutron Reflection Studies of Magnetic Ultra-Thin Film Structures*
21.05.92	**A.D.Yesyutin** (Committee for foreign trade relations of Russia)	*Goals and problems of marketing in conditions of transition of scientific institutions to the market*
9.06.92	**Prof. H.R.Wenk** (Univ. of Calif., Berkeley, USA)	*Some Geological Applications of Texture Analysis*
25.06.92	**Yu.N.Alexakhin, A.Yu.Molodozhontsev** (LSHE JINR), **V.L.Lomidze** (FLNP JINR)	*Strong current accelerator-recirculator RIU-100 as injector of electrons for general-purpose multiplying target*
13.08.92	**B.Dorner** (ILL, France)	*Inelastic Neutron Scattering in Lattice Dynamics*
10.09.92	**F.Fillaux** (Laboratoire de Spectrochimie Infrarouge et Raman, CNRS, France)	*Inelastic Neutron Scattering Studies of the Quantum Sine-Gordon Breather in 4-Methyl-Pyridine*

17.12.92	**V.K.Ignatovich** (FLNP JINR)	*Issues of quantum mechanics (conference in Trani, Italy)*
24.12.92	**B.N.Zakhariev** (BLTP JINR)	*1. Exotics of the motion of waves along grids of channels.* *2. Discrete and continuous quantum mechanics*
14.01.93	**P.Hiismaki** (VTT, Espoo, Finland)	*How to Implement the RTOF Method for Inelastic Scattering Studies on Single Crystals*
4.02.1993	**Yu.A.Bykovsky, A.S.Tsybin** (MIPE, Moscow)	*Laser neutron generator*
11.02.93	**A.I.Frank** (FLNP JINR), **V.G.Nosov** (RNC KI, Moscow)	*Quantum effects in the case of fast modulation of the neutron wave*
25.02.93	**S.Frankle** (LANL, Los Alamos, USA)	*LANSCE-2: Project of 1 MW Pulsed Spallation Neutron Source*
4.03.93	**B.V.Deryagin, A.G.Lipson, B.F.Lyakhov** (RAS Institute of Physical Chemistry, Moscow)	*Observation of the yield of products of nuclear D-D-synthesis (neutrons and tritium) from deuterium-containing ferroelectrics in transition through the Curie point*
20.05.93	**Ye.P.Shabalin** (FLNP JINR)	*Investigation of the behavior of solid methane (20-60 K) irradiated at the IBR-2 reactor (URAM experiments)*
21.09.93	**T.M.Holden** (Chalk River, Ontario, Canada)	*Industrial Application of Neutron Diffraction*

4.4. CONFERENCES and MEETINGS

1992

1. International seminar on studies of biological and lipid membranes, amphiphyls using neutrons (17-20 May 1992, Dubna)

At the seminar methods were considered for studying the structure and dynamics of membranes and molecules composing amphiphyls with the aid of neutron and γ-ray scattering. Issues were discussed of further improvement of experimental installations for studying these objects at IBR-2. Original works were heard on studies of biological and lipid membranes and of lipid monolayers.

2. International seminar on structural investigations at pulsed neutron sources (1-4 September 1992, Dubna)

At the seminar discussions were held of the latest achievements of scientific and methodological nature in investigations of the structure of condensed matter with the aid of diffraction and small-angular scattering of slow neutrons. The main goal of the seminar was to draw the attention of specialists to the possibilities opening up of diffraction investigations at a qualitatively new level and to hold discussions of the program of studies with the high-resolution Fourier diffractometer (HRFD). At the seminar, also, information was presented on the course of work on the construction of a new cold moderator at IBR-2, which will extend significantly, when put in operation, the possibilities of studying the structure of matter with the aid of small-angle scattering. The seminar was held in commemoration of Yu.M.Ostanevich.

3. International workshop on the application of activation analysis in the protection of the environment (15-18 September 1992, Dubna)

The workshop was held for determining the place and role of neutron activation analysis in solving the problem of environment monitoring. Issues were considered that were related to requirements of analytic quality control of environmental objects when relative and absolute methods of analysis are applied.

1993

1. International Workshop on Time Reversal Invariance and Parity Violation in Neutron Reactions (May 4-7, 1993, Dubna)

International Workshop was organized by JINR and sponsored by Triangle Universities Nuclear Laboratory (TUNL) and Los Alamos National Laboratory (LANL).

The workshop focused on the study of parity violation and time reversal invariance in neutron physics. Emphasis was placed on measurements with polarized neutron beams and polarized targets as well as on the implication of recent theoretical developments for future progress in this intensively developing field of research. A special session on experimental possibilities and new directions of research at the new Dubna intense resonance neutron pulsed source, IREN, took place for two last days of the workshop. The aim of the workshop was to discuss the results of theoretical and experimental investigations obtained since the 1st Workshop at Chapel Hill, USA, in 1987. Over 100 participants came to Dubna. In addition to scientists from Russia (30 participants) and JINR (39 participants) there were physicists from USA (13 participants), Germany (5 participants), Japan (3 participants), Israel (2 participants), as well as scientists from Australia, Belarus, Belgium, Canada, Poland, the Netherlands, South Africa and the Ukraine.

2. 3rd International Conference on Surface X-Ray and Neutron Scattering (SXNS-3) (June 24-29, 1993, Dubna)

This conference was organized by FLNP and sponsored by the Commission of European Communities.

Attending the Conference were 120 scientists from Bulgaria, UK, Germany, Denmark, the Netherlands, Poland, Russia, USA, the Ukraine and France. The main topics of the Conference were investigations of physical and chemical properties of thin films and multilayer structures, semiconductors, polymers and biological materials. These investigations had been carried out at the IBR-2 reactor by the method of polarized neutron reflection for several years.

3. International Seminar on Superprotonic Conductors (ISSPC) (September 7-11, 1993, Dubna)

Participants of the Seminar were physicists from the JINR, USA, UK, Germany, Italy, Poland, Russia, CIS members, Sweden and Yugoslavia. About 10 years ago, a new class of crystals was discovered at the Institute of Crystallography, Russian Academy of Sciences. A specific feature of these crystals is intrinsic superproton conduction, i.e., it is not caused by defects or impurities. Studying this type of crystal involves the most important fields of condensed matter physics: the physics of ferroelectric, ferroelastic and related phenomena, physics of structural phase transitions, superion state physics, hydrogen bond physics, etc. These issues were the subject of discussions at the seminar.

4. VI Trilateral German - Russian - Ukrainian Seminar on High-Temperature Superconductivity (September 14-18 1993, Dubna)

A wide scientific program of the Seminar embraced the issues of the theory of high temperature superconductivity, production of new materials, application of superconducting materials, growth mechanisms of films and crystals, application of nuclear physics methods to HTSC investigations, etc. More than 50 invited and 80 poster reports were contributed. The Seminar was attended by many well-known scientists, representatives of the Academy of Sciences, Ministry of Atomic Power and Ministry of Science of the Russian Federation as well as representatives of the Federal Ministry of Research and Technology of Germany.

PLANS FOR 1994

1. International Seminar "Neutron Spectroscopy, Nuclear Structure, Applications", Dubna, 26-28 April.

2. International Seminar "Present and Future of the IBR-2 High-Flux Pulsed Reactor", Dubna, 14-16 June.

3. 30th Russian Conference on Low Temperature Physics, Dubna, 6-9 September.

4. International Seminar "Neutron Scattering at High Pressures", Dubna, 4-8 October.

4.5. LIST OF VISITORS FROM NON-MEMBER STATES OF THE JINR IN 1992-1993

Name	Organization	Country	Dates of visit
H.J.Lauter	ILL, Grenoble	France	11.01-28.01
A.Shakil	Joint.Vent. Ltd., London	UK	26.01-28.01
T.H.Gneupel-Herold	Univ.Leipzig	FRG1	0.02-03.03
K.Ullemeier	Univ. Gottingen	FRG	17.02-02.03
D.Leppin	Univ. Leipzig	FRG	17.02-27.02
W.Birkholz	TU Leipzig	FRG	12.03-28.03
N.D.Glen	North Carolina Univ.	USA	13.03-21.03
C.R.Gould	North Carolina Univ.	USA	24.03-29.03
S.J.Seestrom-Morris	LANL, Los Alamos	USA	07.04-20.04
H.J.Lauter	ILL, Grenoble	France	14.04-19.05
J.A.Bland	Cambridge Univ.	UK	08.05-19.05
K.Walther	FZ Rossendorf	FRG	11.05-12.06
F.Prokert	FZ Rossendorf	FRG	11.05-23.05
W.Hinz	Univ. Chemnitz	FRG	18.05-26.06
R.Joedicke	Univ. Chemnitz	FRG	18.05-26.06
B.T.M.Willis	Oxford. Univ.	UK	01.06-08.06
J.Gladkikh	Hahn-Meitner Inst., Berlin	FRG	03.06-09.06
H.R.Wenk	Univ. of Calif., Berkeley	USA	05.06-09.06
A.T.Tiitta	TRCF, Espoo	Finland	08.06-14.06
W.Birkholz	TU Leipzig	FRG	11.06-14.06
H.Baumbach	IzfP, Saarbrucken	FRG	11.06-14.06
M.Kroening	IzfP, Saarbrucken	FRG	11.06-14.06
G.Dobman	IzfP, Saarbrucken	FRG	11.06-14.06
G.Operschall	TU Leipzig	FRG	11.06-14.06
M.H.Neumann	Max-Planck Inst., Munich	FRG	11.06-13.06
T.Hermann	Max-Planck Inst., Munich	FRG	11.06-14.06
A.Goertd	TU Leipzig	FRG	15.06-20.06
P.E.Hiismaki	TRCF, Espoo	Finland	24.06-27.07
B.M.M.Dorner	ILL, Grenoble	France	11.08-12.09
B.Irmer	Univ. Erlangen-Nurenberg	FRG	28.08-20.09
J.Schreiber	IzfP, Dresden	FRG	31.08-18.09
A.T.Tiitta	TRCF, Espoo	Finland	31.08-05.09
F.Fillaux	CRNS, Saclay	France	09.09-12.09
A.Sekveir	At.Res.Centre	India	17.09-17.09
H.Radjhopa	At.Res.Centre	India	17.09-17.09
M.Ono	Kyoto Univ.	Japan	28.09-03.10
R.M.A.Maayouf	Cairo Univ.	Egypt	01.10-05.10
M.Betzl	FZ Rossendorf	FRG	09.11-20.11

S.J.Kafala	Imperial Coll., Ascot	UK	12.11-03.12
H.Siemens	TH, Aachen	FRG	15.11-28.11
E.Niedergehlay	TH, Aachen	FRG	15.11-28.11
H.J.Lauter	ILL, Grenoble	France	21.11-29.12
U.Hoppe	Univ, Rostock	FRG	03.12-19.12
A.K.Kollmar	FZ Julich	FRG	07.12-15.12
F.Stallmach	Univ. Leipzig	FRG	07.12-18.12
W.W.Boede	FZ Rossendorf	FRG	25.01-05.02
J.Pepy	LLB, Saclay	France	27.01-30.01
L.B.Johannes	Univ. Gottingen	FRG	10.02-15.04
S.C.Frankle	LANL, Los Alamos	USA	14.02-28.02
C.M.Frankle	LANL, Los Alamos	USA	14.02-28.02
W.Birkholz	TU Leipzig	FRG	23.02-01.03
T.Streil	TU Leipzig	FRG	23.02-01.03
A.R.Kollmar	FZ Julich	FRG	26.02-12.03
J.Alkemper	TH Darmstadt	FRG	10.03-20.03
K.Walther	FZ Rossendorf	FRG	11.03-26.03
H.J.C.Lauter	ILL, Grenoble	France	13.03-01.05
G.Klose	Univ. Leipzig	FRG	23.03-30.03
A.Filip	Centre d'Etudes Nucleaire, Cadarache	France	03.04-14.04
M.A.Gradzielski	Univ. Bayreuth	FRG	13.04-23.04
R.Oberg	Univ. of Washington	USA	08.05-10.05
K.Walther	FZ Rossendorf	FRG	11.05-26.06
M.Hempel	IzfK, Saarbrucken	FRG	13.05-27.06
E.E.Niederschlag	Mineralogie In-t, Aachen	FRG	15.05-26.06
P.Nozar	ICTP, Trieste	Italy	16.05-21.05
A.T.Tiitta	ESPOO, Helsinki	Finland	16.05-20.05
A.Nathan	Univ. of Illinois	USA	03.06-05.06
B.H.Tietze-Jaensch	RAL, Chilton	UK	12.06-20.06
G.H.Lorenz	Univ. Gottingen	FRG	20.06-27.06
L.J.Bernd	Geol. Dynam. Lyt. Inst., Gottingen	FRG	20.06-27.06
H.J.C.Lauter	ILL, Grenoble	France	20.06-15.07
S.K.Sinha	CRSL, New Jersey	USA	21.06-24.06
R.Wedel	Decor Design. Inc.	USA	24.06-26.06
T.Staut	Decor Design. Inc.	USA	24.06-26.06
W.Voitus	FZ Rossendorf	FRG	28.06-17.07
M.Maaza	LLB, Saclay	France	29.06-09.09
J.J.Huentelmann	Hart Crowser Inc.	USA	3.07-07.07
A.Ke-Li Shen	Hart Crowser Inc.	USA	03.07-07.07
K.P.Michel	SIEMENS, Erlangen	FRG	05.07-08.07
H.Operschall	SIEMENS, Erlangen	FRG	05.07-08.07
K.Helming	TU Clausthal	FRG	18.07-31.07
M.A.Ali	AEA, Cairo	Egypt	20.07-17.12

G.A.Loew	SLAC, Stanford	USA	26.07-29.07
E.Steinnes	Trondheim Univ.	Norway	09.08-19.08
Zhu Bin	MSL, Stockholm	Sweden	29.08-06.09
T.M.Holden	Chalk River. Lab.	Canada	20.09-23.09
F.-J.Hambsch	IRMM	Belgium	21.09-27.09
J.H.Schreiber	IzfP, Dresden	FRG	30.09-14.10
J.-P.Theobald	TU Darmstadt	FRG	30.09-02.10
R.M.A.Maayouf	AEA, Cairo	Egypt	07.10-26.10
E.W.Pridoehl	IzfP, Saarbrucken	FRG	11.10-14.11
T.Staut	Decor Des. Inc.	USA	17.10-19.10
R.Kruse	Univ. Gottingen	FRG	21.10-10.11
J.R.E.Hester	Univ. of West. Austr.	Australia	27.10-28.10
V.H.Urbanus	Delft Univ.	Netherlands	02.11-02.11
A.B.Sterk	Delft Univ.	Netherlands	02.11-02.11
K.Walther	FZ Rossendorf	FRG	06.11-27.11
E.E.Niederschlag	Mineralogie In-t, Aachen	FRG	06.11-27.11
J.Keuter	GKSS, Geesthacht	FRG	17.11-26.11
G.Klose	Univ. Leipzig	FRG	19.11-25.11
O.McGrath	ESRF, Grenoble	France	05.12-15.12
H.J.Lauter	ILL, Grenoble	France	06.12-28.12
K.Helming	TU Clausthal	FRG	06.12-17.12
T.Staut	Decor Des. Inc.	USA	07.12-09.12
J.H.Schreiber	IzfP, Dresden	FRG	08.12-15.12
E.Steinnes	Trondheim Univ.	Norway	09.12-14.12
R.K.Heenan	RAL, Chilton	UK	09.12-15.12
C.J.Clinch	RAL, Chilton	UK	09.12-15.12
T.Staut	Decor.Des. Inc.	USA	18.12-19.12
M.Rudalics	J.Kepler Univ.	Austria	30.12-30.01

4.6. THE CENTRE OF EDUCATION AND SCIENCE

The Centre of Education and Science (CES) affiliated with the Joint Institute for Nuclear Research and based on the departments of the Moscow State University and of the Moscow Physics Technics Institute admits, for continuation of studies, undergraduate students of the last two years of study at higher education institutions who have attended introductory specialized courses of lectures in the following topics: particle physics, nuclear physics, investigation of condensed matter at nuclear reactors and accelerators, radiation biology. The second and third specializations are quite in line with research performed at FLNP, which has at its disposal, for both sectors, a good experimental base comprising pulsed neutron sources - the IBR-2 reactor and the IBR-30 booster.

The education courses and practical training for the students affiliated with FLNP have been organized, to a large extent, for preparing specialists in neutron physics both for the Laboratory and for other Russian neutron centers. As an example illustrating this claim we present the list of courses in the physics of condensed matter:

- *theoretical methods in condensed matter physics;*
- *methods of investigation of condensed matter at nuclear reactors and accelerators;*
- *the fundamentals of neutron physics and neutron sources;*
- *experimental physics and low-temperature techniques;*
- *physics of high-temperature superconductors;*
- *the influence of radiation on solid-state properties;*
- *methods of experimental data processing.*

A number of leading FLNP scientists take part in delivering these courses. Each student is allowed access to the computer Laboratory network. For example, an obligatory condition for successful completion of the 4th year is the capability of using modern personal computers. Earlier, students were included in the research groups led by their instructors which made it possible for undergraduate students working on their theses, to take part in preparing or performing experiments.

In 1993 the first group of nine students graduated from the Centre of Education and Science in FLNP topics: seven in the physics of condensed matter and two in nuclear physics. FLNP has concluded contracts for work with three of the former students. The experience accumulated during the relatively short functioning time of the CES reveals that a group of 8-10 persons is just the optimum size.

4.7. PERSONNEL

The personnel of the laboratory includes permanent and temporary staff members. The latter are employed in accordance with contracts (temporary employment agreements). Until 1992 most of the staff members from the Commonwealth of Independent States (CIS) were permanent members of the personnel. In 1992 the situation underwent a drastic change: most of the staff members of the laboratory concluded contracts. The total number of personnel has decreased noticeably: 492 on 31.12.93 against 580 in 1991. More detailed information related to the end of 1992 is presented for various Departments in Table 9.

Table 9

Distribution of Personnel for Various Departments as of 31.12.93

Department	Permanent personnel			Contracts		
	R. P.	E.	S.	R. P.	E.	S.
1. Neutron Sources and Nuclear Safety Department	2	1	4	9	39	9
2. Nuclear Physics Department	2	-	2	29	9	4
3. Department of Physics of Condensed Matter	8	-	7	21	16	6
4. Department of Physical and Technical Research and Department of Activation Analysis	6	6	3	6	7	4
5. Department of Radioelectronics and Computation Techniques	5	24	8	12	17	5
6. Technical and Administrative Services	2	13	5	1	58	142
Total	**25**	**51**	**22**	**78**	**146**	**170**
Total	**98 (20%)**			**394 (80%)**		
Total	**492 (100%)**					

Comment: **R.P.** - Research personnel, **E.** - Engineers, **S.** - Support staff.

Serious changes occurred during the past two years regarding the personnel from JINR member states and other countries (the so-called personnel of the Directorate). In 1992 the number of specialists from the "old" member states decreased. CIS republics, including Russia, joining the Joint Institute for Nuclear Research as members with full rights has led to the appearance in the personnel of the Directorate of specialists from these countries, which has resulted in its increasing in number in 1993 (Table 10).

Table 10

Personnel of the Directorate

Country	on 31.12.91	on 31.12.92	on 31.12.93
"Old" member states			
Bulgaria	6	8	8
Chekhia, Slovakia	12	3	2
Korea	9	-	-
Hungary	3	1	Departed from JINR
Mongolia	8	4	3
Poland	15	5	5
Romania	1	1	-
Vietnam	8	3	2
"New" member states			
Armenia	-	-	1
Russia	-	-	11
Ukraine	-	-	3
Other countries			
Germany	9	8	6
USA	-	-	1
Total	**71**	**33**	**42**

4.8. FINANCES

The serious changes in the economic situation of the host state, Russia, that occurred during the past two years have influenced formation of the JINR budget, and consequently, that of the Laboratory.

Starting from 1993 the budget is expressed in dollars. This circumstance, as well as the high inflation rate in Russia, makes it difficult to make a straightforward comparison of the FLNP budgets of 1992 and 1993 (Tables 11 and 12) from the point of view of dynamics of financial support of activities in the Laboratory. From an analysis of the structure of the budget during the period covered by the report one may make the following conclusions:

1) the positive balance of the budget in these years testifies that the minimum financing required for the laboratory was actually supplied;

2) a drastic drop occurred regarding the relative part of external investments from national programs (6% in 1992, 3% in 1993) as compared with 1991, when they amounted to 33%. Under the conditions of strong inflation, the actual introduced indexation of the grants of these programs was insufficient;

3) the actual share of FLNP of the JINR budget was lower than the control figures approved by the Committee of Plenipotentiaries: 13.3% against 21.7% in 1992, 14.7% against 16.75% in 1993.

Table 13 demonstrates in greater detail the disbursement of the "pure" (the part allotted for the JINR infrastructure has been subtracted) financial support coming from JINR in 1993. The resources for supporting and developing scientific research (expenditures for: materials and equipment for physical departments) after the decline down to 16% in 1992 exceeded the 1991 level and comprised 33% of the total expenditure.

Table 11

FLNP budget in 1992

Income		**Expenditure**	
Source	**thous. rbl.**	**Where to**	**thous. rbl.**
1. Income from JINR	123313.9	1 Scientific research and infrastructure. Amount returned to JINR	106108.4 17205.5
2. External investments: Program of high-temperature superconductivity Other programs	6613.2 248.6	2. Scientific research and infrastructure. Amount returned to JINR	5411.5 1370.7
Total	**130175.7**	**Total**	**130095.6**
Saldo: +50.1 thous. rbl.			

Table 12

FLNP budget in 1993

Income			Expenditure		
Source	thous. rbl.	K$	Where to	thous. rbl.	K$
1. Income from JINR	1514850.7	1537.3	1 Scientific research and infrastructure	1350557.1	1355.5
			Amount returned to JINR	42273.8	45.5
2. External investments:			2. Scientific research and infrastructure	164293.6	181.8
Russian fund for fundamental research	32950.0	35.5	Amount returned to JINR	588.9	0.63
Program of high-temperature superconductivity	8375.0	9.0			
Other programs	2409.1	2.6			
Total	**1558584.8**	**1584.4**	**Total**	**1557713.4**	**1583.4**
Saldo: +871.4 thous. rbl. (0.9 K$)					

Table 13

Expenditures for scientific research and FLNP infrastructure from the income supplied by JINR in 1993

Where to	thous.rbl.	K$
1. Neutron sources		
1.1. IBR-2		
Salary	92273.3	94.0
Other expenses	105348.4	99.3
1.2. IBR-30	extra-budget financial support	
2. Physics and Maintenance Departments		
Salary	369466.3	369.2
Materials and equipment	454080.7	465.6
Other expenses	329388.4	336.3
Total	**1350557.1**	**1355.5**

5. PUBLICATIONS
The Physics of Condensed Matter

Diffraction

1. Aldica A., Mironova G.M., Popa N.C., Stoica A.D., Stoica M.G. Time-Resolved Neutron Diffraction Study of the $Bi(Pb) - Sr - Ca - Cu - O$ System. Journal of Supercond., 1992, 6, 273.

2. Aksenov V.L., Balagurov A.M., Simkin V.G., Taran Yu.V., Trounov V.A., Kudrjashev V.A., Bulkin A.P., Muratov V.G., Hiismaki P., Tiitta A., Antson O. The New Fourier Diffractometer at the IBR-2 Reactor: Design and First Results. JINR Communications, E13-92-456, Dubna, 1992.

3. Balagurov A.M., Mironova G.M. Phase Transformation in Materials Studied by TOF Neutron Thermo-Diffractometry. Powder Diffraction II, Enshede, Netherlands, 1992.

4. Balagurov A.M. The Present-Day Structure Neutron Investigations at the Pulsed Neutron Sources. Particles and Nucleus, 1992, 23, 1088-1143 (in Russian).

5. Balagurov A.M., Lyubutin I.S. The Atomic and Magnetic Structure of $YBa_2(Cu_{1-x}Fe_x)_3O_{6+x}$ at $0.05 \leq x \leq 0.30, y \cong 1$ and$y \cong 0.5$. JINR, É14-92-579, Dubna, 1992 (in Russian).

6. Balagurov A.M., Bouree F., Lyubutin I.S., Mirebeau I. Atomic and Magnetic Structure of $YBa_2(Cu_{1-x}Fe_x)_3O_{6+y}$ Studied by Neutron Diffraction on Isotope Enriched Samples. Accepted in Physica C.

7. Balagurov A.M., Mironova G.M. Phase Transformations in Materials Studied by TOF Neutron Thermo-Diffractometry. Materials Science Forum, 1993, 133-136, 397-402.

8. Balagurov A.M., Simkin V.G., Taran Yu.V., Trounov V.A., Kudrjashev V.A., Bulkin A.P. Possible Utilization of High Resolution Fourier Diffractometer at Reactor IBR-2 for Strain Measurements. JINR Communications, E14-93-333, Dubna, 1993.

9. Balagurov A.M., Piechota J. Neutron Powder Diffraction Studies of $YBa_2(Cu_{1-x}M_x)_3O_{7-\delta}$ with $M = {}^{57}Fe, {}^{58}Ni$. Ed. by R.Kossowsky, B.Raveau, Wohlleben D., Patapis S.K. Kluwer Academic Publishers, 1992.

10. Beskrovnyi A.I., Jirak Z., Nevrila M., Shelkova I.G. Neutron Diffraction Study of the Modulated Structure of $Bi_2Sr_{3-x}Y_xCu_2O_{8+\gamma}(x \approx 0.6)$. Physica C, 1993, 206, 27-32.

11. Georgiev D., Nietz V.V., Yakovlev A.A. The "Coherent" Spin-Flop Transition in a Single Antiferromagnetic. JINR Comm., P14-92-399, Dubna, 1992 (in Russian).

12. Georgiev D., Nietz V.V., Sirotin A.P., Yakovlev A.A. The Neutron Scattering Intensity Dependence on the Field and Temperature at the Coherent Spin-Flop Transition in Cr_2O_3. JINR Comm., P14-92-400, Dubna, 1992 (in Russian).

13. Georgiev D., Nietz V.V., Sirotin A.P. Hysteresis Phenomena at the Spin-Flop Transition Induced by the Pulsed Magnetic Field. JINR Comm., P14-92-401, Dubna, 1992 (in Russian).

14. Gordeliy V.I., Islamov A.Kh., Syrykh A.G. Determining the Fluctuations of the Lipid and Biological Membranes Repeting Period by the Neutron Diffraction Method. Biol. membr., 1992, 9, 193 (in Russian).

15. Gordeliy V.I. The Study of Lateral Structure of Biological and Model Membranes by Neutron Scattering. Physica B, 1992, 180-181, 750-752.

16. Gordeliy V.I., Golubchikova L.V., Kuklin A., Syrykh A.G., Watts A. The Study of Single Biological and Model Membranes via Small-Angle Neutron Scattering. Progress in Colloid & Polymer Science, 1993, 93, 38-43.

17. Helming K., Voitus W., Walther K. Progress in Texture Investigation at the Pulsed Reactor IBR-2. Physica B, 1992 180-181, 1025-1028.

18. Ivankina T.I., Kovalyov L.A., Kovalyova Ye.V., Nikitin A.N. The Influence of the Texture Transitions within an Inclusion on the Stressed Elastic Medium. Fiz. Zemli, 1993, 6, 95-103 (in Russian).

19. Ivankina T.I., Nikitin A.N., Heinitz J., Kovalev L.A. Influence of Texture Transformations within Inclusions on the Stress State of an Elastic Medium. Materials of the XXIII General Assembly of the European Seismological Commission, 7.9-12.9, 1992, Prague, Czechoslovakia.

20. Lyubutin I.S., Terziev V.G., Dmitrieva T.V., Balagurov A.M., Nasu S. Magnetic Ordering of Fe Atoms in Oxygen-Saturated and Oxygen-Reduced $YBa_2(Cu_{1-x}Fe_x)_3O_y$. Physica C, 1992, 195, 383-389.

21. Lyubutin I.S., Terziev V.G., Luchko S.V., Shapiro A.Ya., Balagurov A.M., Bonch-Osmolovsky G.A. Magnetic Ordered States in the Oxygen Deficient $YBa_2(Cu_{1-x}Fe_x)_3O_{y<6.5}$ System. Physica C, 1992, 199, 296-304.

22. Lyubutin I.S., Terziyev V.G., Balagurov A.M., Luchko S.V., Shapiro A.Ya., Bonch-Osmolovskiy G.A. Transformation of the Mössbauer Spectra in the $YBa_2(Cu_{1-x}Fe_x)_3O_y$ System at the Oxygen Distillation and the Magnetically Ordered States of the Iron Ions. Superconductivity: Phys., Chem., Techn., 1992, 5, 1842-1854 (in Russian).

23. Lyubutin I.S., Terziyev V.G., Dmitriyeva T.V., Balagurov A.M. Structure Positions and Magnetic Order of the Fe Atoms in the $YBa_2(Cu_{1-x}Fe_x)_3O_y$ System Enriched by and Depleted of Oxygen. Fiz. Tv. Tela, 1992, 34, 3212-3219 (in Russian).

24. Mironova G.M. Time-Resolved Diffraction and SANS Study of Thermal Behaviour of $YBa_2Cu_3O_{7-x}$ Compound over a Temperature Range 900-1470 K. Materials Science Forum, 1993, 133-136, 847-852.

25. Mironova G.M. New Scope for the Condensed Matters Offered by the Single and Combined Pulsed Neutron Source and the Projection Geometry of an Experiment. In: Proc. of the Int. Workshop on Advanced Pulsed Neutron Sources. JINR, D3-92-76, Dubna, 1992, p.25 (in Russian).

26. Nikitin A.N., Archipov I.K., Kurtasov S.F., Walther K. The Model of Induced Anisotropy in Crystalline Rocks. Materials of the XXIII General Assembly of the European Seismological Commission, 7.9-12.9, 1992, Prague, Czechoslovakia.

27. Nikitin A.N., Arkhipov I.K. Modeling the Texture Formation in the Quartz-Containing Rocks at the Phase Transitoins. Fiz. Zemli, 1992, 12, 29-40 (in Russian). .

28. Nikitin A.N. Piezoelectric Textures of the Mountain Rocks and Mechanisms of their Formation in the Earth. Theses of the Report to the XVIII General Assembly of the European Geophysics Society. Wiesbaden, Germany.

29. Nikitin A.N. Texture Analysis of the Geological Matters and Geophysics Problems. Theses of the Report to the X international conference on texture of materials (ICOTOM 10). Clausthal-Zellerfeld, Germany.

30. Nikolayev D.I. Computational Optimization of the Bunge-Row Method. Fiz. Zemli, 1993, 6, 68-72 (in Russian).

31. Nietz V.V. Kinetics of the "Coherent" Spin-Flop Transition in the Antiferromagnetic with the Single-Axis Anisotropy. JINR Comm., P14-92-402, Dubna, 1992 (in Russian).

32. Prokert F., Savenko B.N., Balagurov A.M. Accurate Determination of IC Modulation Parameter in $Sr_xBa_{1-x}Nb_2O_6$ from Second-Order Satellites of Neutron Diffraction TOF Spectra. JINR Communication E14-93-279, Dubna, 1993.

33. Savenko B.N., Keen D.A., Mroz B., Sangaa D., Wilson C.C. Neutron Diffraction Study of the Low Temperature Domain Structure in $LiKSO_4$. Physica B, 1992, 180-181, 309-311.

34. Stark P., Nikolayev D.I. Toward Tabular Tomography. J.Geophysical Research, 1993, 98, 8095-8106.

35. Tatulian S.A., Ermakov Yu.A., Gordeliy V.I., Sokolova A.B., Syrykh A.G. The Influence of Ca^{2+} and Some Chaotropic Ions on Inter Membrane Interaction. Biological Membranes, 1993, 6, 983-1008.

36. Trounov V.A., Kaganovich T.Yu., Kurbakov A.I., Matveev A.V., Balagurov A.M., Hewat A.W., Fischer P., Antson O., Maayouf R.M. Neutron Diffraction Studies of Isotope-Substituted Tetragonal Superconductors $RBa_{2.76}Cu_{2.76}Fe_{0.24}O_{7+y}(R = Sm, Y)$. Physica C, 1992, 197, 123-130.

37. Uhrikova D., Cherezov V., Yaradaikin S., Balgavy P. Mathematical Model of the Cut-Off Effect in the Homologous Series of Tertiary Amine Local Anestetics. Pharmazie, 1993, 48, 450-466.

38. Ullemeier K., Weber K. Preferable Orientation of the Sheet Silicates in the Milonite Rocks and their Significance for the Kinetic Interpretation. Fiz. Zemli, 1993, 6, 104-112 (in Russian).

39. Voitus W., Heinitz J., Walther K., Isakov N.N. Neutronographische Bestimmung von Polfiguren am Diffraktometer NSWR in VIK Dubna. Materialien zum Arbeitstreffen des Verbundes Forschung mit Neutronen, 29.3-1.4., 1992, Bad Schandau, BRD.

40. Vladimirov V.A., Georgiyev D. et al. Handling Some Final-Control Mechanisms of the TEXT and DVR Experimental Facilities at the IBR-2 and IBR-30 Reactors. JINR Comm., 13-92-123, Dubna, 1992 (in Russian).

41. Walther K., Isakov N.N., Nikitin A.N., Ullemeier K., Heinitz J. Investigation of the Texture Structure of the Geological Materials by the Diffraction Method with the Help of the High-Resolution Neutron Spectrometer at the Frank Laboratory of Neutron Physics of the Joint Institute for Nuclear Research. Fiz. Zemli, 1993, 6, 37-44 (in Russian).

42. Walther K., Kurtasov S.F., Nikitin A.N., Torina Ye.G. Modeling the Deformation Textures in the High-Temperature Quartz. Fiz. Zemli, 1993, 6, 45-48 (in Russian).

43. Walther K., Nikitin A.N., Shermergor T.D., Yakovlev V.B. Determining the Effective Electroelastic Constants of the Polycrystalline Textured Mountain Rocks. Fiz. Zemli, 1993, 6, 83-88 (in Russian).

Small-Angle Scattering

1. Bezzabotnov V.Yu., Cher L., Grosz T., Jancso G., Ostanevich Yu.M. Small-Angle Neutron Scattering in Aqueous Solutions of Tetramethylurea. Journ.Phys.Chem., 1992, 96, 976-982.

2. Birkholz W., Häußler F., Stetsenko S.G. Proc. II Int. Workshop "Solid State Nuclear Track Detectors and their Applications". JINR, E7-93-61, Dubna, 1993, p.29.

3. Cher L., Farago B., Grosz T., Jancso G., Ostanevich Yu.M. Structure and Dynamics of Aqueous Solutions of Tetramethylurea. Physica B, 1992, 180-181, 848-850.

4. Eichhorn F., Häußler F., Baumbach H. Development of Structures in Hydrating Cement Paste. Annual Report 1991 of the Research Centre Rossendorf Inc., FZR 92-06, p.64.

5. Eichhorn F., Häußler F., Baumbach H. Study of Hardening of Portland Cement Paste by Small-Angle Neutron Scattering. Annual Report 1992 of the Research Centre Rossendorf Inc., FZR 93-06, 1993, p.72.

6. Eichhorn F., Häußler F., Baumbach H. Structural Studies on Hydrating Cement Pastes. Accepted for publication in Journal de Physique (Proc. of the IX Int. Conf. on Small-Angle Scattering).

7. Gorsky N., Pstanevich Yu.M., Klose G. From und grosse von C12E4-D20-losung an hand der SANS-untersuchungen. Forschung mit Neutronen. Bad Schandau, 29.3-1.4.92, Conf. Proceedings.

8. Häußler F., Eichhorn F., Baumbach H., Birkholz W. Strukturbildung in hydratisierendem Zementstein. Forschung mit Neutronen, Bad Schandau, 29.3-1.4.92, Conf. Proceedings.

9. Häußler F., Eichhorn, Baumbach H., Röhling S. Untersuchungen zur Mikrostruktur ausgewählter Zementklinkerphasen und deren Hydrationsprodukten mittels Neutronenkleinwinkelstreuung. Wiss. Z. Hochsch. Archit. Bauwes. B, Weimar, 1991. 3, 123-126.

10. Häußler F., Eichhorn F., Baumbach H. Small-Angle Neutron Scattering on Hardened Cement Paste and Various Substances for Hydration. Submitted to Cement & Concrete Research, 1993.

11. Häußler F., Eichhorn F., Birkholz W., Baumbach H. SANS Study of Hardening Cement Pastes and Solid State Nuclear Track Detectors. Int. Seminar on Structural Investigations at Pulsed Neutron Sources. Dubna, Sept. 1-4, 1992. Conf.Proc., Dubna, 1993, p.315.

12. Häußler F., Eichhorn F., Baumbach H. SANS Studies of Hydrating Cement Pastes. Accepted for publication in Progress in Colloid and Polymer Science (Proc. of the VI.ECIS Conference).

13. Häußler F., Eichhorn F., Baumbach H. Description of the Structural Evolution of a Hydrating Portland Cement Paste by Small-Angle Neutron Scattering (SANS). Accepted for publication in Physica Scripta (Proc. of the Euroconference 1993, Studsvik, Sweden).

14. Hempel M., Häußler F., Eichhorn F. Vom ungebundenen zum gebundenen Wasser - Hydrationsfortschritt beim Zementstein, gemessen mittels Neutronenkleinwinkelstreuung. Submitted for publication in Proceedings des Feuchtetages der BAM am 21.09.1993, Berlin, P11.

15. Nikitenko Yu.V., Ostanevich Yu.M. Proposal of a Wide-Band Mirror Polarizer of Slow Neutrons at a Pulsed Neutron Source. JINR, E13-92-316, Dubna, 1992.

16. Plestil J., Ilavsky M., Pospisil H., Hlavata D., Ostanevich Yu.M., Degovics G., Laggner P. SAXS, SANS and Photoelasticity of Poly (N,N-diethylacrylamide) Networks. 1. Structure Changes after Temperature Jumps. Polymer, 1992.

Inelastic Neutron Scattering

Alekseev P.A., Clementyev E.S., Lazukov V.N., Sadikov I.P., Goremychkin E.A., Sashin I.L. Neutron Scattering and X-Ray Diffraction Study of the Valence-Unstable System $Ce_{1-x}La_xNiSn$. Physica B, 1993, 186-188, 416-418.

2. Alenitcheva T.V., Danilkin S.A., Novikov A.G., Pavlov A.F., Puchkov A.V., Semenov V.A., Yadrovskii E.L. Modernization of DIN-2PI, DIN-2Pr-Spectrometers and theirs Parameters. IPPE-2216 Preprint, Obninsk, 1992.

3. Belushkin A.V., Vagov A.V., Zemlyanov M.G., Parshin P.P. Computer Simulation and Neutron Scattering Studies of Lattice Dynamics of $Ba_{1-x}K_xBiO_3$. Physica C, 1992, 199, 103-111.

4. Blagoveshchenskii N.M., Bogoyavlenskii I.V., Karnatsevich L.V., Kozlov Zh.A., Puchkov A.V. Bose-Condensate Temperature Dependence and the First Measurements on DIN-22PR Spectrometer. IPPE-2241 preprint, Obninsk, 1992.

5. Blagoveshchenskii N.M., Bogoyavlenskii I.V., Karnatsevich L.V., Kozlov Zh.A., Puchkov A.V. Elementary Excitations Spectrum of He II Investigation by 2 meV Incident Neutron Scattering. IPPE-2259 preprint, Obninsk, 1992.

6. Blagoveshchenskii N.M., Bogoyavlenskii I.V., Karnatsevich L.V., Kozlov Zh.A., Kolobrodov V.G., Puchkov A.V., Skomorokhov A.N. The Structure of the Liquid Helium-4 Elementary Excitations Spectrum. Pisma v zhurn. eksp. i teor. fiz., 1993, 57, 414-417 (in Russian).

7. Bobrowicz L., Kartusiak A., Nawrocik W., Wasicki J., Natkaniec I. Neutron Scattering in 1,3-Cyclohexanadione. Int. Seminar on Structural Investigations at Pulsed Neutron Sources, Dubna, Sept.1-4, 1992. JINR, E3-93-65, Dubna, 1993, p.307-314.

8. Bogoyavlenski I.V., Karnatsevich L.V., Kozlov Zh.A., Puchkov A.V. Neutron Scattering Determination of Condensate in Liquid ^4He. Physica B, 1992, 176, 151.

9. Danilkin S.A., Minaev V.P., Sumin V.V., Chimit G. The Scope for the Inelastic Neutron Scattering Method in Investigations of the Hydrogen State in the Austenite Steels. Preprint PhEI-2334, Obninsk, 1993, 10 (in Russian).

10. Fedotov V.K., Kolesnikov A.I., Synitsyn V.V., Ponyatovsky E.G., Natkaniec I., Mayer J., Brankovski E., Belushkin A.V. Investigation of Hydrogen in the Superconducting Ceramics by the Inelastic Neutron Scattering Method. Fiz. tv. tela, 1993, 35, 189-197 (in Russian).

11. Fedotov V.K., Kolesnikov A.I., Kulakov V.I., Ponyatovsky E.G., Natkaniec I., Mayer J., Kravchik G. Investigation of the Anharmonism of the Copper and Oxygen Atoms Vibrations in the Yttrium Ceramics by the Inelastic Neutron Scattering Method. Fiz. tv. tela, 1993, 35, 310-319 (in Russian).

12. Gavriluk V.G., Danilkin S.A., Efimenko S.P., Minaev V.P., Sumin V.V. Slow-Neutron Scattering Study of the Nitrogen Fe-18Cr-10Mn216Ni Austenic Steel. PhEI-2266 preprint, Obninsk, 1992.

13. Gomankov V.I., Sumin V.V., Fedorov V.G. The Atomic Ordering Energy Increase at the $L1_2$ Structure Doping. Fizika metallov i metalloved., 1992, 5, 158-160 (in Russian).

14. Gomankov V.I., Gezalyan A., Sosnin V.V., Sumin V.V., Tretyakov B.N., Fedotov V.G. The Structure Transformations and Metastable States in the Alloys of the $Ni_3Mn - Ni_3Ti$ System. Fiz. metallov i metalloved., 1992, 8, 105-109 (in Russian).

15. Gomankov V.I., Fedotov V.G., Sosnin V.V., Sumin V.V., Zhigalina O.M., Makarov V.A. The Atomic Ordering in the Micro- and Nanocrystal Alloys. Fiz. metallov i metalloved., 1993, 2, 75-79 (in Russian).

16. Goremychkin E.A., Muzychka A.Yu., Osborn R. Crystal Field Potential of $NdCu_2Si_2$: A Comparison with $CeCu_2Si_2$. Physica B, 1992, 179, 184.

17. Goremychkin E.A., Osborn R. Crystal Field Excitations in $CeCu_2Si_2$. Phys.Rev., B47, 1993, 14280.

18. Holderna-Natkaniec K., Natkaniec I. Study of Internal Vibrations of dl-camphene by IINS Method. XX International Conference on Low Temperature Physics. Eugene, Oregon, 1993, Physica B (in press).

19. Holderna-Natkaniec I., Habrylo S., Mayer J. Comparative Neutron Scattering Study of Molecular Ordering in d-Camphor and dl-Borneole. XX International Conf. on Low Temp.Phys. Eugene, Oregon, 1993, Physica B (in press).

20. Janik J.A., Mayer J., Habrylo S., Natkaniec I., Zajac W., Janik J.M., Stanck T. Phase Diagram of 4,4'-di-n-butyloxyazoxybenzene: Neutron Diffraction Measurements at Higher Pressures. Phase Transitions, 1992, 37, 239-251.

21. Kalus J., Wolfrum J., Worlen F., Holderna-Natkaniec K., Natkaniec I., Monkenbush M., Prager M. Internal Rotation-Phonon Coupling in Lattice Dynamics of p-Xylene. Phonon Scattering in Condensed Matter VII. Ed. by M.Meissner and R.O.Pohl. Springer Series in Solid State Sciences, vol.112, 1993, 521-523.

22. Kozlov Zh.A., Pedureanu I., Razhanu S., Rotarescu G., Semenov V.A. Functions of the Vibration Frequency Distribution of Atoms in ThO_2 UO_2. Fiz. tv. tela, 35, 1993, 1988-1995 (in Russian).

23. Markichev I.V., Natkaniec I., Sheka E.F. The Method of Constructing the Basis Spectra of the Multicomponent System: the Criterium of the Zero Correlation Coefficient. JINR Comm., P14-92-85, Dubna, 1992. Zhurn. strukt. khimii, 34(1), 1993, 44-53 (in Russian).

24. Markichev I.V., Natkaniec I., Sheka E.F. Constructing the Basis Spectra of the Multicomponent System Oscillations. 1. Aerosil. JINR Comm., P14-92-86, Dubna, 1992. Zhurn. strukt. khimii, 34, 1993, 54-63 (in Russian).

25. Markichev I.V., Natkaniec I., Sheka E.F. Constructing the Basis Spectra of the Multicomponent System Oscillations. 2. Silicagel. JINR Comm., P14-92-87, Dubna, 1992. Zhurn. strukt. khimii, 34(1), 1993, 64-76 (in Russian).

26. Markichev I.V., Muzychka A.Yu., Natkaniec I., Sheka E.F. Constructing the Basis Spectra of the Multicomponent System oscillations. 3. Aerogel. Zhurn. strukt. khimii, 34(4), 1993, 29-37.

27. Morozov S.I., Kazarnikov V.V., Sumin V.V. Impurity Vibrations in Interstitial Phases. PhEI-2273 preprint, Obninsk, 1992.

28. Muzychka A.Yu., Goremychkin E.A., Sashin I.L., Divis M., Nekvasil V., Nevrina M., Fillion G. Crystal Field in Nd_2CuO_4. Sol. St. Comm., 82, 1992, 461-464.

29. Muzychka A.Yu., Goremychkin E.A., Natkaniec I., Sashin I.L., Divis M. The crystal field in the Nd_2CuO_4 compound. SFKhT, 5, 1992, 1417-1422.

30. Natkaniec I., Fricke J., Khavryuchenko V., Markichev I., Muzychka A., Reichenaner G., Sheka E.F. Water on Amorphous Silicas: INS Study. Physica B, 180-181, 1992, 522-524.

31. Natkaniec I., Bragin S.I., Brankowski J., Mayer J. Multicrystal Inverted Geometry Spectrometer NERA-PR at the IBR-2 Pulsed Reactor. Proc. Int. Collaboration on Advanced Neutron Sources ICANS XII, RAL, Abingdon, 1993 (in press).

32. Natkaniec I., Smirnov L.S., Solov'ev A.I., Bragin S.I. Neutron Scattering Studies of Ammonium Dynamics and Phase Transition in $K(1-x)(NH4)(x)SCN$ at 10K. XX Int. Conf. on Low Temperature Physics. Eugene, Oregon, 1993, Physica B (in press).

33. Sheka E.F., Markichev I.V., Khavryutchenko V.D., Natkaniec I. Comparative Analysis of the Vibration Spectra of the Dispersed Silicas and their Components. Zhurn. strukt. khimii, v.34(4), 1993, 39-51 (in Russian).

34. Sheka E.F., Natkaniec I., Khavryutchenko V.D., Nechitaylov P.B., Muzychka A.Yu., Markichev I.V., Ogenko V.M. Vibration Spectroscopy of the Dispersed Silica: Inelastic Neutron Scattering. Zhurn. fiz. khimii, 67(1), 1993, 38-47 (in Russian).

35. Sheka E.F., Natkaniec E., Khavryutchenko V.D., Markichev I.V. Vibration of Disperse Silicas. Phonon Scattering in Condensed Matter VII. Ed. by M.Meissner and R.O.Pohl. Springer Series in Solid State Sciences, vol.112, 1993, 303-305.

36. Sheka E.F., Natkaniec I., Khavryutchenko V.D., Markichev I.V., Chuyko A., Ogenko V. Vibrations of Dispersed Silicas: A Comparative Study. React.Kinet. Catal. Lett., v.50, 1993, 221-226.

37. Sheka E.F., Natkaniec I., Khavryutchenko V.D., Markichev I.V., Muzychka A.Yu., WangY., Herron N. Density of Vibrational States of Thiol Capped CdS Particles. Inelastic Neutron Scattering. 3rd Int. Conf. on Surface X-Ray and Neutron Scattering, Dubna, 1993. Physica B (in press).

38. Sheka E.F., Natkaniec I., Khavryutchenko V.D., Markichev I.V., Muzychka A., Goncharova N., Chukalin V., Nikitina E. Density of Vibrational State of Silicone Nitride. 3rd Int. Conf. on Surface X-Ray and Neutron Scattering, Dubna, 1993. Physica B (in press).

39. Sheka E.F., Khavryutchenko V.D., Natkaniec I., Markichev V.I., Muzychka A.Yu., Nechitaylov P.B. Vibrational Spectroscopy of Dispersed Silica: Aerosol. Zh. Struct. Khimii, vol.33, No.4, 1992, 66-75 (in Russian).

40. Smirnov L.S., Gorchakova V.A., Gromnitskaya E.L., Il'ina G.G., Natkaniec I., Solov'ev A.I., Stal'gorova O.V. The Acoustic and Neutron Scattering Investigations of NH4SCN Phase Diagram. High Pressure Conf., Belfast, 1993 (in press).

41. Tumanov A.A., Zarko V.I. The Influence of Pyrogenic Silica Hydration on Water Diffusion in Surface Layers. In: Int. Conf. of Oxide Surface Chemistry and Reaction Mechanism. Kiev, Ukraine, 1992, v.1, p.139-143.

42. Wojcik G., Jakubowski B., Szostak M.M., Holderna-Natkaniec K., Mayer J., Natkaniec I. Neutron Diffraction and Direct Dilatometric Studies of Two Polymorphs of Meta-Nitrophenol Crystals. phys. stat. sol.(a), 134, 1992, 139-150.

43. Zaetz V.A., Nikitina E.A., Khavryutchenko V.D., Sheka E.F., Natkaniec I., Nechitaylov P.B., Muzychka A.Yu. Vibrational Spectrum of Water Absorbed on High Disperse *Ni* Particles. Poverhnost: fiz., khim., mekhanika, 9, 1992, 33-46 (In Russian).

44. Zaezzhev M.V., Ivanovskii M.N., Novikov A.G., Savostin V.V., Shimkevich A.L. The Elementary Excitation Spectrum of Liquid Potassium. PhEI-2245 preprint, Obninsk, 1992.

45. Zaezzhev M.V., Novikov A.G., Savostin V.V. The Isotopic Specific Heat and Anharmonic Effect in Liquid Potassium. PhEI-2276 preprint, Obninsk, 1992.

Reflectometry, Polarized Neutrons

1. Aksenov V.L., Korneev D.A., Chernenko L.P. Time-of-Flight Four-Beam Neutron Reflectometer (REFLEX) at the IBR-2 Pulsed Reactor of JINR, Dubna: Some Applications of Polarized Neutron Reflectometry. Proc. of SPIE's 1992 Int. Symp. on Optical Applied Science and Engineering, 19-24 July, 1992.

2. Aksenov V.L., Korneev D.A., Maayuf R.M.A., Chernenko L.P. Multi-Beam Neutron Reflectometer for a Steady State Reactor. JINR Communications E3-93-430, Dubna, 1993.

3. Aksenov V.L., Korneev D.A., Chernenko L.P. The Time-of-Flight Four-Beam Neutron Reflectometer REFLEX at the High Flux Pulsed Reactor IBR-2 and Some Possible Application. JINR Communications E3-93-215, Dubna, 1993.

4. Aksenov V.L., Dokukin E.B., Nikitenko Yu.V., Petrenko A.V., Sergeenkov S.A. Neutron Polarization Investigations of High Temperature Superconductors. Physica Scripta, 48, 1993.

5. Dokukin E.B., Nikitenko Yu.V. On Variants of the Neutron Adiabatic Spin Flipper. Nucl. Instr. and Meth., A330, 1993, 462-464.

6. Krezhov K., Lilkov L., Korneev D., Konstantinov P. On the Wavelength Dependent Neutron Depolarization Studies of the Domain Structure in Ferromagnetic Amorphous Alloys. Journal of Physics: Condensed Matter, 5, 1993, 9277-9287.

7. Korneev D.A. New Aspect in Employing Magnetic, Anisotropic *FeCo* Thin Film as Neutron Polarizers. Proc. of SPIE's 1992 Int. Symp. on Optical Applied Science and Engineering, 19-24 July, 1992.

8. Korneev D.A., Chernenko L.P., Petrenko A.V., Balalykin N.I., Skrypnik A.V. Measurement of Magnetic Field Depth Profile in Superconducting Niobium Films by Polarized Neutron. Proc. of SPIE's 1992 Int. Symp. on Optical Applied Science and Engineering, 19-24 July, 1992.

9. Korneev D.A., Chernenko L.P., Petrenko A.V., Balalykin N.I., Skrypnik A.V. Anomalous Behavior of the Diamagnetic Profile of the Superconducting Niobium at the Boundary with Vacuum. Pisma v zhurn. eksp. i teor. fiz., 55, 1992, 653-656 (in Russian).

10. Korneev D.A., Pasyuk V.V., Petrenko A.V., Jankovski H. Absorbing Sublayers and their Influence on the Polarizing Efficiency of Magnetic Neutron Mirrors. Nucl. Instr. and Meth., B63, 1992, 328-332.

11. Korneev D.A., Chernenko N.V., Chernenko L.P. A New Aspect in the Investigation of the Polarized Neutron Passing Through Ferromagnetics. JINR Comm., P3-92-533, Dubna, 1992.

12. Korneev D.A., Chernenko L.P., Petrenko A.V., Balalykin N.I., Skrypnik A.V. Anomalous Behaviour of the Diamagnetic Profile of Superconducting Niobium near a Vacuum Boundary. Pi'sma Zh. Eksp. Teor. Fiz., 44, No.11, 1992, 653-656 (in Russian).

13. Korneev D.A., Chernenko L.P., Petrenko A.V., Balalykin N.I., Skrypnik A.V. Measurement of Magnetic Field Depth Profile in Superconducting Niobium Film by Polarized Neutron Reflectometry. In: Neutron Optical Devices and Applications. Ed. by C.F.Majkrzak, J.L.Wood. Proc. SPIE 1738, 1992, 254.

14. Nagy D.L., Pasyuk V.V. Calculation of Mossbauer Reflectometry Spectra. Hyperfine Interactions, 71, 1992, 1349-1352.

15. Nikitenko Yu.V., Ostanevich Yu.M. Proposal of a Wide-Land Mirror Polarizer of Slow Neutrons at a Pulsed Neutron Source. Nucl. Instr. and Meth., A325, 1993, 485-488.

16. Pasyuk V.V., Lauter H.J., Bland J.A., Petrenko A.V., Johnson M.T., den Broeder F.J.A. Magnetic Moment in $CoPd$ Ultra-Thin Film Studied by Polarized Neutron Specular Reflection. Proc. of Symp. on Surface Science. La Plagne, Savoie, France, 15-21 March 1992.

Accelerated Ions

Borovik A.S., Epifanov A.A., Korneev D.A., Malyshevsky V.S. The Peculiarities of the Ion Channeling in the $YBa_2Cu_3O_7$ Single Crystal. JINR Communications P14-92-396, Dubna, 1992 (in Russian).

Borovik A.S., Epifanov A.A., Kobzev A.P., Korneev D.A., Malyshevsky V.S., Potapov C.N. Determining the Thickness of the Disordered Layers at the Twin and the Film/Base Boundaries. A Report to the XXIII International Workshop on the Physics of the Interactions of Charged Particles with Crystals. Moscow State University, May 31–June 2, 1993 (in Russian).

3. Borovik A.S., Kobzev A.P., Korneev D.A., Potapov A.S., Chernenko L.P., Shirokov D.M. Damaging the Crystal Lattice of the $Y-Ba-Cu-O$ Film Irradiated by the ^4He Ions with the Energy of 3.075 MeV. A Report to the XXIII International Workshop on the Physics of the Interactions of Charged Particles with Crystals. Moscow State University, May 31–June 2, 1993 (in Russian).

4. Borovik A.S., Kobzev A.P., Korneev D.A., Chernenko L.P., Shirokov D.M., Ivanov P.B. Channeling the ^4He Ions in the $Y-Ba-Cu-O$ Film on the $SrTiO_3$ Base. A Report to the XXIII International Workshop on the Physics of the Interactions of Charged Particles with Crystals. Moscow State University, May 31–June 2, 1993 (in Russian).

5. Chernenko L.P., Kobzev A.P., Korneev D.A., Shirokov D.M. Backscattering Method Possibilities for Precise Determination of the Oxygen Profile in Oxide Films by the Use of the Elastic Resonance in Reaction $^{16}O(^4He,^4He)^{16}O$ at 3.045 MeV of ^4He. Surface and Interface Analysis, 18, 1992, 585-588.

6. Chernenko L.P., Kobzev A.P., Korneev D.A., Shirokov D.M. Damage in $Y-Ba-Cu-O$ Films Produced by ^4He Ions. 3rd European Workshop on Modern Developments and Applications in Microbeam Analysis. Rimini, Italy, 9-13 May, 1993. Accepted in Microchimica Acta.

7. Chernenko L.P., Kobzev A.P., Korneev D.A., Shirokov D.M. On Mechanism of Damage Production in $YBaCuO$ Films by ^4He Ions. VI Trilateral German-Russian-Ukrainian Seminar on High-Temperature Superconductivity. Dubna, September 14-18, 1993. To be published in "Superconductivity: Physics, Chemistry, Mechanics".

8. Chernenko N.V., Chernenko L.P., Shirokov D.M. The Program for Calculating the Cross-Section of the $^{16}O(^4He,^4He)^{16}O$ Reaction in the Energy Interval of 2.4 to 4.0 MeV. JINR Communications P3-93-11, Dubna, 1993 (in Russian).

9. Duvanov S.M., Kobzev A.P., Tolopa A.M., Shirokov D.M. Investigation of the Metallized Intermingled Layers at the Surface of the Ion-Irradiation Modified Glass. A Report to the XXIII International Workshop on the Physics of the Interactions of Charged Particles with Crystals. Moscow State University, May 31–June 2, 1993 (in Russian).

10. Grubich L., Kobzev A.P., Shandrik R., Shafrankova Ya. Using the Proton Irradiation for Improving the Properties of the $GaAs$-based Semiconductor Structures with Shottky Barrier. JINR Communications P14-93-75, Dubna, 1993 (in Russian).

11. Klyuenkov E.B., Churin S.A., Chernenko L.P. Obtaining the Nb Ultrathin Layers from the Erosion Laser Plasma and Investigation of their Properties. JINR Communications P3-93-174, Dubna, 1993 (In Russian).

12. Kobzev A.P., Korneev D.A., Chernenko L.P., Shirokov D.M. Increasing the Accuracy of the Oxygen Concentration Profile Measurement in the Thin Film Samples. JINR Preprint, P14-93-161, Dubna, 1993 (in Russian).

Theory

1. Aksenov V.L., Kabanov V.V. On the Role of Antiferromagnetic Fluctuations in Temperature Dependence of Linewidth of the Transition Between the Crystal Field Levels in High-T_c Superconductors. JINR Communications E17-93-229, Dubna, 1993.

2. Aksenov V.L., Kabanov V.V. Inelastic Neutron Scattering and Antiferromagnetic Fluctuations in High Temperature Superconductors. JINR Communications E17-93-366, Dubna, 1993.

3. Aksenov V.L., Bugoslavsky Yu.V., Dokukin E.B., Ignatovich V.K., Minakov A.A., Nikitenko Yu.V., Petrenko A.V., Sergeenkov S.A. A Possible Observation of the Depinning Line in $YBaCo$ Ceramics from Neutron Polarization Studies. Proc. of the VI Trilateral Seminar on HTSC, Dubna, 14-18 September, 1993.

4. Chesca B. On the Theoretical Study of an RF-SQUID Operation Taking into Account the Noise Influence. Accepted in Journ. of Low Temp.Phys.

5. Chesca B. On the Theory of Symmetrical Double

6. Kornilov E.I. An Exact Enumeration of Self-Avoiding Loops on the Square Lattice. Communication ICTP, IC/93/382, Trieste, 1993. SQUID. Accepted in Physica C.

7. Kornilov E.I., Pomjakushin V.Yu. Strong Collision Approach to Calculation of Depolarization Function for Neutron Beam Passing Through Ferromagnetic Bulk Domains. Communication ICTP, IC/93/384, Trieste, 1993.

8. Kornilov E.I. Calculation of Reflectivity from Fractal Multilayers. Proc. of the VI Trilateral Seminar on HTSC, Dubna, 14-18 Sept., 1993. Accepted in Physica B.

The Neutron Nuclear Physics

Experiment

1. Alexandrov Yu.A. Comments on the paper by V.G.Nikolenko and A.B.Popov "On the Correctness of Estimates on (n,e)-Amplitude and Neutron Polarizability from Total Cross Sections of Bi and Pb. Z.Phys. A341, 1992, p.365.

2. Alexandrov Yu.A., Koester L., Samosvat G.S., Waschkowski W. ^{208}Pb and the Electric Polarizability of the Neutron. In: Abstracts of the International Seminar on the Interactions of Neutrons with Nuclei. Dubna, April 14-17, 1992. JINR, à3-92-128, Dubna, 1992, p.19.

3. Alexandrov Yu.A. What is the Mean Square Radius of the Neutron Actually Equal to? JINR Preprint, E3-92-441, Dubna, 1992.

4. Alexandrov Yu.A. The Mean Square Radius of Electric Charge Distribution Inside the Neutron. What is it Still Equal to? In: In: Abstracts of the International Seminar on the Interactions of Neutrons with Nuclei. Dubna, April 14-17, 1992. JINR, à3-92-128, Dubna, 1992, p.18.

5. Alexandrov Yu.A. Fundamental Properties of the Neutron. Clarendon Press, Oxford, London, 1992.

6. Alexandrov Yu.A. What is the Mean Square Charge Radius of the Neutron Actually Equal to? In: Abstract Booklet of 8th Int. Symp. on Capture Gamma-Ray Spectroscopy and Related Topics. Bribourg, Switzerland, 20-24 Sept., 1993, p.77.

7. Alexandrov Yu.A. On Discrepancy between the Garching and Dubna Results of Determination of the (ne)-Scattering Length on Bismuth. JINR, E3-93-35, Dubna, 1993.

8. Alfimenkov V.P., Mareev Yu.D., Novitsky V.V., Pikelner L.B., Skoy V.R. PNC Study with Polarized Target and Spin Property of La. In: Time Reversal Invariance and Parity Violation in Neutron Reactions. World Scientific, 1993, p.84.

9. Alfimenkov V.P., Mareev Yu.D., Pikelner L.B., Skoy V.R., Shvetsov V.N. Investigation of Parity Violation in Neutron Resonances of Rb and ^{113}Cs. In: Int. Nucl. Phys. Conf., July 26 - August 1, 1992, Wiesbaden, Germany. Book of Abstracts. Ed. by U.Grundinger, p.4.2.4.

10. Alfimenkov V.P. et al. Method for Calibration of Losses in Neutron Lifetime. Experiments with UCN. Nucl. Instr. and Meth in Phys. Res., 1993, v.A324, p.496-500.

11. Ali M.A., Vasilieva E.V., Vojnov A.V., Kulik V.D., Le Khong Khiem, Popov Yu.P., Sukhovoj A.M., Pham Dinh Khang, Khitrov V.A., Kholnov Yu.V., Shilin V.N. The Decay Scheme of the 7937 keV ^{158}Gd Compound State Induced in the (n,γ) Reaction. In: Nuclear Spectroscopy and atomic Nucleus Structure. Theses of the Reports to the 42nd International Workshop. St. Petersburg, Nauka, 1992, p.81 (in Russian).

12. Ali M.A., Khitrov V.A., Kholnov Yu.V., Kulik V.D., Khiem L.H., Khang P.D., Popov Yu.P., Shilin V.N., Sukhovoj A.M., Vasilieva E.V., Vojnov A.V. Intense Cascades Following ^{158}Gd Compound-State Decay. In: International Nucl.Phys. Conf., Wiesbaden, Germany, 1992. Book of Abstracts. Ed. by U.Grundinger, p.1.3.42.

13. Ananiev V.D., Voronov B.I., Gundorin N.A., Popov A.B. The Way of Measuring the Spatial Distribution of the Primary Neutrons in the Pulsed Booster. JINR, É3-92-350, Dubna, 1992 (in Russian).

14. Andrzejewski J., Gledenov Yu.M., Popov Yu.P., Salatski V.I., Sedyshev P.V., Li Ho Bom., Pshenichnyj V.A. Investigation of the $^{14}N(n,p)^{14}C$ Reaction by Neutron Filter Technique. In: "Nuclei in the Cosmos". Proc. of the Second Int.Symp. on Nuclear Astrophysics, Karlsruhe, Germany, 6-10 July, 1992. Ed. by F.Kappeler, K.Wisshak. Bristol and Philadelphia, 1993, p.239-242.

15. Barabanov A.L., Sharapov E.I., Skoy V.R. Measurements of T-Odd, P-Even Effects in $^{113}Cd(n,\gamma)^{114}Cd$ and $^{117}Sn(n,\gamma)^{118}Sn$ Reactions. In: Abstract Booklet of VIII Int. Symp. on Capture Gamma-Ray Spectroscopy and Related Topics, Fribourg, Switzerland, 20-24 Sept., 1993, p.78.

16. Barabanov A.L., Sharapov E.I., Skoy V.R., Frankle C.M. Testing T-Odd, P-Even Interactions with γ-Rays from Neutron p-Wave Resonances. Phys. Rev. Lett., 1993, v.70, p.1216-1219.

17. Beitins M.R., Bondarenko V.A., Kuvaga I.L., Prokofiev P.T., Le Khong Khiem, Popov Yu.P., Sukhovoj A.M., Pham Dinh Khang, Khitrov V.A., Kholnov Yu.V. Investigation of ^{177}Lu in the $(n, 2\gamma)$ Reaction. In: Nuclear Spectroscopy and Atomic Nucleus Structure. Theses of the Reports to the 42nd International Workshop. St. Petersburg, Nauka, 1992, p.93 (in Russian).

18. Beitins M.R., Bondarenko V.A., Kuvaga I.L., Le Hong Khiem, Popov Yu.P., Prokofiev P.T., Sukhovoj A.M., Pham Dinh Khang, Khitrov V.A., Kholnov Yu.V. Investigation Into the Decay of the ^{177}Lu Nucleus Compound State in the $(n, 2\gamma)$ Reaction. Izv. RAN, ser. fiz., 57, 1993, 36-46 (in Russian).

19. Beitins M.R., Boneva S.T., Khitrov V.A., Malov L.A., Popov Yu.P., Prokofiev P.T., Rezvaya G.L., Simonova L.I., Sukhovoj A.M., Vasilieva E.V. Study of the ^{187}W States Excited in the (n, γ) Reaction. Z.Phys. A - Hadrons and Nuclei, 1992, 341, p.155-170.

20. Bogdzel A.A., Gundorin N.A., Gohs U. et al. Peculiarity of the Fission of ^{239}Pu by Resonance Neutrons. In: Nuclear Data for Science and Technology. Proc. of Int. Cond. Jülich, FRG, 13-17 May, 1991. Springer Verlag, 1992, p.150-152.

21. Bogdzel A.A., Gundorin N.A., Popov A.B. et al. Prompt Gamma-Ray Emission from Fission of ^{239}Pu by Resonance Neutrons. In: Dynamical Aspects of Nuclear Fission. Proc. of Int. Workshop, Smolenice, Czechoslovakia, June 17-21, 1991. JINR E7-92-95, Dubna, 1992, p.305-311.

22. Bogdzel A.A., Gundorin N.A., Popov A.B. et al. Prompt Gamma-Rays Yields at Individual Fission Resonances of $239Pu$. In: Dynamical Aspects of Nuclear Fission. Proc. of Int. Workshop, Smolenice, Czechoslovakia, June 17-21, 1991. JINR, E7-92-95, Dubna, 1992, p.312-313.

23. Bondarenko V.A., Kuvaga I.L., Prokofiev P.T., Le Khong Khiem, Popov Yu.P., Sukhovoj A.M., Pham Dinh Khang, Khitrov V.A., Kholnov Yu.V. Gamma-Decay of the ^{135}Ba Compound State. In: Nuclear Spectroscopy and Atomic Nucleus Structure. Theses of the Reports to the 42nd International Workshop. St. Petersburg, Nauka, 1992, p.68 (in Russian).

24. Bondarenko V.A., Kuvaga I.L., Prokofjev P.T., Khitrov V.A., Kholnov Yu.V., Le Hong Khiem, Popov Yu.P., Sukhovoj A.M. Thermal-Neutron Capture Studies on Ba-135. Nucl.Phys., A551 (1993) 54-72.

25. Bondarenko V.A., Kuvaga I.L., Le Khong Khiem, Popov Yu.P., Prokofiev P.T., Sukhovoj A.M., Pham Dinh Khang, Khitrov V.A., Kholnov Yu.V. γ-Transition Cascades of the ^{143}Nd Compound State Decay. Izv. RAN, ser. fiz., 57, 1993, 47-55 (in Russian).

26. Bondarenko V.A., Kuvaga I.L., Le Khong Khiem, Popov Yu.P., Prokofiev P.T., Sukhovoj A.M., Pham Dinh Khang, Khitrov V.A., Kholnov Yu.V. γ-Decay of the ^{135}Ba Compound State. Izv. RAN, ser. fiz., 57, 1993, 56-60 (in Russian).

27. Boneva S.T., Khitrov V.A., Kholnov Yu.V., Le Hong Khiem, Pham Dinh Khang, Popov Yu.P., Sukhovoj A.M., Bondarenko V.A., Kuvaga I.L., Prokofiev P.T., Rezvaya G.L., Simonova L.I. Experimental Estimates on Radiative Strength Function of Low-Energy γ-Quanta Following Even-Odd Heavy Nuclei Decay. JINR E3-92-244, Dubna, 1992. Z.Phys. A - Hadrons and Nuclei, A346 (1993) 35-42.

28. Chelkov G.A., Ignatenko M.A., Kotov S.A., Kravchenko I.V., Krumstein Z.V., Samosvat G.S., Shvetsov V.N., Strelkov A.V., Fadeev V.A. Investigation of Spectral Efficiency of Pressurized Drift Tubes for Detection of Neutrons in the Energy Range between 5 eV and 200 keV. ATLAS Internal Note MUON-NO-031, Nov. 15, 1993.

29. Dermendjiev E., Goverdovski A.A., Furman W.I. et al. Fission Gamma-Ray Multiplicity Measurements in ^{233}U,^{235}U,^{237}Np and ^{239}Pu Low Energy Fission Resonances. Proc. of the Int. Conf. "Nucl. Data for Science and Technology", Jülich, 13-17 May, 1991, p.147-149, Springer-Verlag, Berlin, 1992.

30. Dermendjiev E. et al. An Experimental Facility for Studying Delayed Neutron-Emission. JINR, E13-93-6, Dubna, 1993.

31. Dermendjiev E., Furman W.I., Zamyatnin Yu.S. A Study of Delayed Neutrons and Nuclear Fission at the Dubna IBR-2 Pulsed Reactor. JINR, E3-93-7, Dubna, 1993.

32. Frank A.I. Microscopy with Ultracold Neutrons. In: Neutron Optical Devices and Applications. Ed. by C.F.Majkrzak, J.L.Wood. SPIE, 1993, v.1738, p.323-334.

33. Frank A.I., Nosov V.G. Quasi-Energy of Cold Neutrons and Neutron Time Interferometer. In: Quantum Interferometry. Ed. by F. de Martini, A.Zeilinger. World Scientific, Singapore, 1993.

34. Frank A.I., Amandzolova D.B. Neutron Quantum Reflection. JINR Communication E3-93-418, Dubna, 1993; In: New Horizons: A Workshop on the State of the Art in Neutron Reflectometry. Gaithersburg, Ma., USA, Dec. 9-10, 1993.

35. Frankle C.M., Bowman C.D., Bowman J.D., Seestrom S.J., Sharapov E.I., Popov Yu.P., Roberson N.B. P-Wave Resonance Spectroscopy in ^{113}Cd. Phys. Rev., 1992, C45, p.2143.

36. Georgiev G.P., Grigoriev Yu.V., Zamyatnin Yu.S. et al. Determining Parameters of the ^{149}Sm Neutron Resonances by Method of the γ-Quanta Multiplicity Spectroscopy. JINR Comm., P3-92-346, Dubna, 1992 (in Russian).

37. Georgiev G.P., Zamyatnin Yu.S., Pikelner L.B. et al. Determining Parameters of the $^{147,148}Sm$ Neutron Resonances. Vopr. atomn. nauki i tekhn. Series: Yad. konst., 1992, v.2, p.75-85 (in Russian).

38. Georgiev G.P. et al. Determining the Neutron Resonances Spin from the Shape of the Spectrum of the Capture Gamma-Quanta Multiplicity. PhEI-2277 preprint, Obninsk, 1992 (in Russian).

39. Georgiev G.P., Grigoriev Yu.V., Zamyatnin Yu.S. et al. On the Study of Neutron Resonances in ^{147}Sm. Proc. of Int.Conf. "Nuclear Data for Science and Technology", Jülich, Germany, 13-17 May, 1991, p.80. Springer Verlag, Berlin, 1992.

40. Georgiev G., Grigoryev Yu.V., Muradyan G.V., Yaneva N.B. Multiplicity of Gamma-Rays in Neutron Resonances of ^{176}Hf and ^{179}Hf. In: Abstract Booklet of Eight Int. Symp. on Capture Gamma-Ray Spectroscopy. Fribourg, Switzerland, Sept. 20-24, 1993, p.203.

41. Georgiev G., Grigoryev Yu.V., Faykov-Stanczyk H. et al. Multiplicity of Gamma-Rays Following Neutron Resonance Capture in Sm Isotopes and Determination of the Resonance parameters of $^{147,148,149}Sm$. In: Proc. of Second International Symposium on Nuclear Excited States. Lodz, June 1992. Ed. by L.Lason and M.Przytula. Lodz Univ., 1993, p.264-271.

42. Gledenov Yu.M., Khuukhenkhuu G., Popov Yu.P., Bao Shanglian, Tang Guoyou, Qu Decheng, Cao Wentian, Chen Zemin, Chen Yingtang, Qi Huiquan. Energy Spectra of Charged Particles Emission Induced by 3-4 Mev Neutrons. In: Int. Seminar on the Interactions of Neutrons with Nuclei. Dubna, 14-17 April, 1992. JINR, E3-92-128, Dubna, 1992, p.41.

43. Gledenov Yu.M., Salatski V.I., Sedyshev P.V., Sedysheva M.V., Pshenichnyj V.A., Andrejewski J. $^{14}N(n,p)^{14}C$ Reaction Cross Sections at Thermal, 24 keV, 54 keV and 144 keV Neutron Energy. In: "Abstract Booklet". 8th Int. Symp. on Capture Gamma-Ray Spectroscopy and Related Topics. Fribourg, Switzerland, 20-24 Sept., 1993, p.204.

44. Gledenov Yu.M., Khuukhenkhuu G., Popov Yu.P., Bao Shanglian, Tang Guoyou, Qu Decheng, Cao Wentian, Chen Zemin, Chen Yingtang, Qi Huiquan. Study of the $^{40}Ca(n,\alpha)^{37}Ar$ Reaction at Neutron Energies 4 and 5 MeV. In: "Abstract Booklet". 8th Int. Symp. on Capture Gamma-Ray Spectroscopy and Related Topics. Fribourg, Switzerland, 20-24 Sept., 1993, p.505.

45. Gledenov Yu.M., Khuukhenkhuu G., Popov Yu.P., Bao Shanglian, Tang Guoyou, Qu Decheng, Cao Wentian, Chen Zemin, Chen Yingtang, Qi Huiquan. Measurement of Cross Section at 5 MeV and Angular Distribution at 4 and 5 MeV for Reaction $^{40}Ca(n,\alpha)^{37}Ar$. Communication of Nuclear Data Progress, No.8, 1992, p.7-15. China Nuclear Information Center, Atomic Energy Press, Beijing.

46. Gohs U. Evaluation of Total Fission Characteristics for ^{239}Pu in the Low Energy Region. In: Dynamical Aspects of Nuclear Fission. Proc. of Int. Workshop, Smolenice, Czechoslovakia, June 17-21, 1991. JINR, E7-92-95, Dubna, 1992, p.314-319.

47. Gohs U. Evaluation of Total Fission Characteristics for ^{235}U in the Low Energy Region. In: Nuclear Data for Science and Technology. Proc. of Int. Conf. Jülich, FRG, 13-17 May, 1991. Springer Verlag, 1992, p.98-100.

48. Golikov V.V., Ignatovich V.K., Kulagin E.N. Measurement of the Ultracold Neutrons Loss Coefficient in the Beryllium Powder. Yad. Fiz., 1992, v.55, 3, p.608-616 (in Russian).

49. Grigoriev Yu.V., Gundorin N.A., Duka-Zolyomi A. Measurement of the Total Transmission and Self-Indication Functions in the ^{239}Pu Fission Cross-Section within the Energy Band of 4.65 eV to 200 keV. PhEI-2226 preprint, Obninsk, 1992 (in Russian).

50. Grigoriev Yu.V., Georgiev G.P., Zamyatnin Yu.S. et al. Measurement and Analysis of Resonance Structure for ^{238}U Total and Radiative Capture Cross Sections in Energy Range 0.465-200 keV. Proc. of Int. Conf. "Nuclear Data for Science and Technology", Jülich, FRG, 13-17 May 1991. Springer Verlag, Berlin, 1992, p.83-85.

51. Gundorin N.A., Popov A.B., Dao Ahn Minh, Michailov L.V., Kliman J., Polgorski V., Duka-Zolyomi A., Gohs U. On the Independent Fragment Yields in the Fission of ^{239}Pu Induced by Resonance Neutrons. In: Proc. of Second International Symposium on Nuclear Excited States. Lodz, June 1992. Ed. by L.Lason and M.Przytula. Lodz Univ., 1993, p.181-188.

52. Iolin E.M, Raitman E.A, Gavrilov V.N., Kuvaldin B.V., Alexandrov Yu.A., Sedlakova L.N, Loshkarev A.A. The Effect of High Frequency Ultra-Sound on the Diffraction of Thermal Neutrons in Bent Silicon Single Crystal. Bragg Case. Int. Seminar on Structural Investigations at Pulsed Neutron Sources. Dubna, 1-4 Sept., 1992. JINR, E14-93-65, Dubna, 1993, p.278.

53. Janeva N., Georgiev G., Sirakov I. et al. A Setup for Precise Measurement of Resonance Neutron Capture by Self-Indication. Nucl. Instr. and Meth. in Phys. Res., A313, 1992, p.266-272.

54. Khitrov V.A. Investigation of Main Parameters of Deformed Nuclei Compound State Gamma Decay. In: Proc. of the Second Int. Symp. on Nucl. Excited States. Lodz, June 22-26, 1992. Ed. by L.Lason and M.Przytula. Lodz Univ., 1993, p.190-195.

55. Khuukhenkhuu G., Gledenov Yu.M., Sedysheva M.V. Systematics of the (n,p) Cross Sections Averaged over ^{235}U Thermal Fission Neutron Spectrum. JINR Communication, E3-93-205, Dubna, 1993.

56. Klora J., Borner H.G., von Egidy T., Georgii R., Jolie J., Judge S., Khitrov V.A., Krusche B., Libman V.A., Lindner H., Litvinsky L.L., Mayerhofer U., Murzin V.A., Robinson S.J., Sukhovoj A.M., Treb H. Nuclear Structure of ^{156}Gd Studied with $(n,\gamma),(n,e^-),(d,p),(d,t)$ Reactions and Lifetime Measurements. Nucl. Phys., A561 (1993) 1-73.

57. Koehler P.E., Gledenov Yu.M., Graff S.M., Harvey J.A., Hill N.W., Kappeler F., Kavanagh R.W., O'Brien H.A., Popov Yu.P., Schatz H., Trautvetter H.P., Vogelaar R.B., Wiescher M. Recent Resulkts in Explosive and S-Process Nucleosynthesis from Measurements on Radioactive and Stable Targets. In: "Abstract

Booklet". 8th Int. Symp. on Capture Gamma-Ray Spectroscopy and Related Topics. Fribourg, Switzerland, 20-24 Sept., 1993, p.65.

58. Koehler P.E., Graff S.M., O'Brien H.A., Gledenov Yu.M., Popov Yu.P. $^{36}Cl(n,p)^{36}S$ Cross Section from 25 meV to 800 keV and the Nucleosynthesis of the Rare Isotope ^{36}S. Phys. Rev., C47, No.5, 1993, p.2107-2112.

59. Le Khong Khiem, Popov Yu.P., Sukhovoj A.M., Pham Dinh Khang, Khitrov V.A., Kholnov Yu.V., Bondarenko V.A., Kuvaga I.L., Prokofiev P.T. γ-Transition Cascades of the ^{143}Nd Compound State Decay. In: Nuclear Spectroscopy and Atomic Nucleus Structure. Theses of the Reports to the 42nd International Workshop. St. Petersburg, Nauka, 1992, p.71 (in Russian).

60. Lason L., Przytula M., Stanczyk H. Fluctuation of Total Radiation Widths of Neutron Resonances. In: Abstract Booklet of Eight Int. Symp. on Capture Gamma-Ray Spectroscopy. Fribourg, Switzerland, Sept. 20-24, 1993, p.74.

61. Mitsyna L.V., Samosvat G.S. On the Anomalous p-Neutron Scattering by the Tellurium Nuclei. JINR Comm., P3-92-230, Dubna, 1992 (in Russian).

62. Mitsyna L.V., Samosvat G.S. On the Anomalous p-Neutron Scattering by the Tellurium Nuclei. Yad. Fiz., 1993, v.56, 2, pp.23-28 (in Russian).

63. Nikolenko V.G., Popov A.B. On the Correctness of Estimates on n,e)-Amplitude and Neutron Polarizability from Total Cross Sections of Bi and Pb. Z.Phys. A - Hadrons and Nuclei, 1992, 341, p.365.

64. Nikolenko V.G., Popov A.B. n,e-Amplitude Estimate Independent of Nuclear Scattering Model. In: Contribution Papers of the Int. Conf. of the Structure of Baryons and Related Mesons. - "Baryons'92", New Haven, USA, 1-4 June, 1992, p.1; In: Proc. Workshop on Hadron Structure from Photo-Reactions at Intermediate Energies. Brookhaven Nat. Lab., BNL-47972, May 28-29, 1992, p.140.

65. Nikolenko V.G., Popov A.B. Reestimation of Neutron Polarizability from Cross Section of ^{208}Pb. JINR, E3-92-254, Dubna, 1992.

66. Nikolenko V.G., Popov A.B. n,e-Amplitude Estimate Independent of Nuclear Scattering Model. JINR, E3-92-255, Dubna, 1992.

67. Nikolenko V.G., Popov A.B. Unmodel $n-e$-Amplitude Estimate on Basis of Neutron Scattering Data. In: Abstract Booklet of VIII Int. Symp. on Capture Gamma-Ray Spectroscopy and Related Topics, Fribourg, Switzerland, 20-24 Sept., 1993, p.402.

68. Nikolenko V.G., Popov A.B. Comments on Neutron Polarizability Estimation from Scattering Cross-Section of ^{208}Pb. In: Abstract Booklet of VIII Int. Symp. on Capture Gamma-Ray Spectroscopy and Related Topics, Fribourg, Switzerland, 20-24 Sept., 1993, p.401.

69. Pikelner L.B. Weak Interaction in Neutron-Nucleus Reactions. In: Proc. of the Second Int. Symp. on Nuclear Excited States. Lodz, 1993. Ed. by L.Lason and M.Przytula. Lodz Univ., 1993, p.234-241.

70. Pokotilovski Yu.M., Takhtamyshev G.G. Experimental Verification of the Skobeltsyn–Bogdan Hypothesis on the Non-Stable Particles Emission in ^{214}Bi Decay. JINR Rapid Comm., No.2[53]-92, Dubna, 1992, p.29-34; Yad.Fiz., 1992, 55(9), p.2017-2022 (in Russian).

71. Pokotilobski Yu.N. Moving Converters as the Possible Tool for Producing Ultracold Neutrons on Pulsed Neutron Sources. NIM, 1992, A314, 561-2.

72. Pokotilovski Yu.N., Takhtamyshev G.G. Neutron – Neutron Scattering: a Possibility of the Beam Experiment. Yad. Fiz., 56(4), 1993, 184-9 (in Russian); JINR preprint, E3-92-417, Dubna, 1992.

73. Pokotilovski Yu.N. "Darmstadt Effect" and Related Issues. Particles and Nucleus, 1993, 24(1), 5-30 (in Russian).

74. Pokotilovski Yu.N. On Mössbauer Effect Experiments to Search for the New Light Bosons. Proc. of III Symp. on Weak and Electromagnetic Interactions in Nuclei. Dubna, June, 1992. World Scientific, p.878-880.

75. Popov Yu.P., Gledenov Yu.M. Neutron Induced Reactions Followed by Charged Particles Emission. In: "Nuclei in the Cosmos". Proc. of the Second Int.Symp. on Nuclear Astrophysics, Karlsruhe, Germany, 6-10 July, 1992. Ed. by F.Kappeler, K.Wisshak. Bristol and Philadelphia, 1993, p.233-238.

76. Pospisil S., Kubasta J., Telezhnikov S.A. Doppler-Broadened Lineshapes Produced at Isotropic Velocity Distribution. In: Abstract Booklet of VIII Int. Symp. on Capture Gamma-Ray Spectroscopy and Related Topics, Fribourg, Switzerland, 20-24 Sept., 1993, p.517.

77. Stoica A.D., Strelkov A.V., Shvetsov V.N. Proposal of Experiments with Ultracold Neutrons (UCN) at BIGR Reactor (Arzamas-16). Programme and Abstracts of 6th Int. Conf. on Nuclei Far from Stability. 9th Int. Conf. on Atomic Masses and Fundamental Constants. July, 1992, p.PH18.

78. Stoica A.D., Strelkov A.V., Shvetsov V.N. Dynamic Convertors of the Ultracold Neutrons. JINR Comm., É3-92-116, Dubna, 1992 (In Russian).

79. Sukhovoj A.M. The Main Peculiarities of Complex Nuclei Compound States γ-Decay. In: Nuclear Structure and Nuclear Reactions at Low and Intermediate Energies. Dubna, 1992, Contributions, p.71.

80. Sukhovoj A.M. Determination of the Radiative Strength Function. In: Int. Nuclear Physics Conference. Wiesbaden, Germany, 1992. Book of Abstracts. Ed. by U.Grundinger, p.26.

81. Sukhovoj A.M. Radiative Strength Function Determination in the $(n, 2\gamma)$ Reaction for Soft Primary Transition in Heavy Nuclei. In: Proc. of the X Int. Physics School on Neutron Phys. and Nucl. Energy. Ed. by W.Andrejtscheff, O.Elenkov. Inst. for Nucl. Res. and Nucl. Energy, Sofia, 1993, 200-212.

82. Vasilieva E.V., Kulik V.D., Kulikov E.V., Lebedev N.A., Le Khong Khiem, Novgorodov A.F., Popov Yu.P., Sukhovoj A.M., Pham Dinh Khang, Khitrov V.A., Kholnov Yu.V. Using the $\gamma\gamma$ Coincidences Method with Summing the Amplitudes of the Coinciding Pulses in the Investigation of the Decay Schemes of the Radioactive Nuclei. The γ-Transition Scheme of the $^{170}Lu \rightarrow ^{170} Yb$ Decay. Izv. RAN, ser. fiz., 1992, v.56, No.5, c.2-17 (in Russian).

83. Vasilieva E.V., Vojnov A.V., Kulik V.D., Popov Yu.P., Sukhovoj A.M., Khitrov V.A., Kholnov Yu.V., Shilin V.N. A New Way of Subtracting the Compton Background in Studying the $\gamma\gamma$-Coincidences by the Method of Summing the Amplitudes of the Coinciding Pulses. JINR P6-92-148, Dubna, 1992 (in Russian).

84. Vasilieva E.V., Vojnov A.V., Kulik V.D., Popov Yu.P., Sukhovoj A.M., Khitrov V.A., Kholnov Yu.V., Shilin V.N. The Techniques of Analyzing the Non-Statistical Behavior of the Radiative Strength Function at the Thermal and Resonance Neutron Capture. JINR É3-92-245, Dubna, 1992 (in Russian).

85. Vasilieva E.V., Vojnov A.V., Kulik V.D., Popov Yu.P., Sukhovoj A.M., Khitrov V.A., Kholnov Yu.V., Shilin V.N. The Analysis of the Non-Statistical Behavior of the Radiative Strength Function at the Thermal and Resonance Neutron Capture. Yad. Fiz., 56 (1993) 13-22 (in Russian).

86. Vasilieva E.V., Vojnov A.V., Kestarova O.D., Kulik V.D., Sukhovoj A.M., Khitrov V.A., Kholnov Yu.V., Shilin V.N. The Two-Quantum Cascades of the Thermal Neutron Capture in Sm-149. Izv. RAN, ser. fiz., v.57, 9, 1993, p.128 (in Russian).

87. Vasilieva E.V., Vojnov A.V., Kestarova O.D., Kulik V.D., Sukhovoj A.M., Khitrov V.A., Kholnov Yu.V., Shilin V.N. The Cascade Gamma-Decay of the Gd-156 Compound State. Izv. RAN, ser. fiz., v.57, 10, 1993, p.98 (in Russian).

88. Vasilieva E.V., Vojnov A.V., Kestarova O.D., Kulik V.D., Sukhovoj A.M., Khitrov V.A., Kholnov Yu.V., Shilin V.N. The Intense Two-Quantum Cascades and the Decay Scheme of the Dy-164 Compound State. Izv. RAN, ser.fiz., v.57, 10, 1993, p.109 (in Russian).

89. Vasilieva E.V., Vojnov A.V., Kestarova O.D., Kulik V.D., Popov Yu.P., Sukhovoj A.M., Khitrov V.A., Kholnov Yu.V., Shilin V.N. On the Possibility of the Excitation Energies of the Intense Gamma-Cascades Transition Levels Being Equidistant. Izv. RAN, ser. fiz., v.57, 9, 1993, p. 118 (in Russian).

90. Vesna V.A., Gledenov Yu.M., Okunev I.S., Parzhitskii S.S., Popov Yu.P., Shulgina E.V. P-Odd Correlations in the Reactions $^6Li(n,\alpha)^3H$ and $^{10}B(n,\alpha)^7Li$ with Polarized Neutrons. In: Book of Abstracts. Int. Nucl. Phys. Conf., Wiesbaden, Germany, July 26 - August 1, 1992. Ed. by U.Grundinger. GSI, p.1.4.10.

91. Vesna V.A., Okunev I.S., Gledenov Yu.M., Parzhitskii S.S., Popov Yu.P. A Search for p-Odd Effects in Reactions $^{10}B(n,\alpha)^7Li$ and $^6Li(n,\alpha)T$. In: Int. Symp. on Weak and Electromagnetic Interactions in Nuclei. JINR E1,3,6,15-92-241, Dubna, 1992, p.22.

92. Vesna V.A., Gledenov Yu.M., Okunev I.S., Parzhitskii, Popov Yu.P., Shulgina E.V. Search for P-Odd Effects in the Reactions $^6Li(n,\alpha)^3H$ and $^{10}B(n,\alpha)^7Li$ with Polarized Neutrons. In: Int. Seminar on the Interactions of Neutrons with Nuclei. Dubna, 14-17 April, 1992. JINR, E3-92-128, Dubna, 1992, p.19.

Theory

1. Belyaev V.B., Fiedeldey H., Rakityansky S.A., Sofianos S.A. Nuclear Transitions in Muonic Molecules. In: Proc. of 14th European Conf. on Few-Body Problems in Physics. Amsterdam, 1993, p.76.

2. Bunatian G.G. Nucleon Polarizability in Free Space and in the Nuclear Medium. Yad. Fiz., 1992, v.55, issue 12, p.3196-3228 (in Russian).

3. Bunatian G.G. Description of a Nucleon in Nuclear Matter. In: Contribution Papers of the International Conference of the Structure of Baryons and Related Mesons - "Baryons'92". New Haven, USA, June 1-4, 1992. In: Book of Abstracts of the Int. Nucl. Phys. Conf. Wiesbaden, Germany, July 26 - August 1, 1992.

4. Bunatian G.G. Nucleon Polarizability in Free Space and in Nuclear Matter. ibid.

5. Bunatyan G.G., Kämpfer B. Properties of ρ- and ω-Mesons in Dense and Hot Nuclear Matter near the Critical Pion Mode Scattering. FZR Preprint 92-08, Dresden, 1992.

6. Bunatian G.G., Kämpfer B. Quasiparticle Description of a Strongly Interacting Pion Gas. FZR Preprint 93-28, 1993; Submitted to Phys. Lett.

7. Furman W.I., Kadmensky S.G., Tchivilsky Yu.M. Shell Model Approach to the Description of Cluster Radioactivity of Heavy Nuclei. In: Clustering Phenomena in Atoms and Nuclei. Springer Verlag, Berlin, 1992, p.295.

8. Furman W., Kadmensky S., Tchuvilsky Yu. Some Predictions of New Spontaneous Cluster Emitters. In: Proc. 2nd Int. Conf. on Atomic and Nucl. Clusters'93. Santorini, Greece, June 29 - July 2, 1993, p.44.

9. Furman W.I., Kadmensky S.G., Tchuvilsky Yu.M. Results of Shell-Model Theory of Cluster Radioactivity. Ibid., p.45.

10. Furman W.I. Nuclear Physics with Neutron at Dubna. Present Status and Trends. In: Collection of Abstracts of Workshop on Scientific Cooperation Between FRG Research Centers and JINR. JINR, 92-510, Dubna, 1992, p.24-27.

11. Ignatovich V.K. The Ultracold Neutron Dispersion Law in the Medium. JINR Preprint, P3-92-130, Dubna, 1992 (in Russian).

12. Ignatovich V.K. Propagation of the Acoustic Waves in the Elastic Layered Media. Akust. zhurn., 1992, Ô.38, 1, pp.70-78 (in Russian).

13. Ignatovich V.K. Electromagnetic Model of the Ball Lightning. JINR Preprint, P3-92-209, Dubna, 1992 (in Russian).

14. Ignatovich V.K. Classical Interpretation of the Quantum Mechanics. JINR, P4-92-389, Dubna, 1992 (in Russian).

15. Ignatovich V.K. Joint Bragg-Laue Diffraction. Report at the Fourteen European Crystallography Meeting. ECM-14, 2-7.08, 1992, Enschede.

16. Ignatovich V.K. Quantum Mechanics of Ultracold Neutrons. Report on the Conference Wave-Particle Duality, Trani, Italy, 24.09-30.09.1992.

17. Ignatovich V.K. Time-of-Flight Fourier-Spectroscopy with Polarized Beams. Proc. of the ISSI, 1-4 September, Dubna, 1992. JINR, E3-93-65, Dubna, 1993, p.69.

18. Kadmensky S.G., Furman W.I., Tchuvilsky Yu.N. Spectroscopic Factors and Classification of the Even-Even Nucleus Cluster Decays. Nuclear Spectroscopy and the Atomic Nucleus Structure. Moscow, Nauka, 1992, p.174 (in Russian).

19. Kadmensky S.G., Kurgalin S.D., Mikheev V.L., Furman V.I., Tchuvilsky Yu.M. Cluster Radioactivity of the Nuclei with $A < 208$. Izv. RAN, 1993, v.57, No.1, p.12-16 (in Russian).

20. Kadmensky S.G., Kurgalin S.D., Furman W.I., Tchuvilsky Yu.M. Semi-Empirical Method of the Analysis of the Relative Probabilities of the Heavy Cluster Spontaneous Emission. Yad. Fiz., 1993, v.56, 8, p.80-89 (in Russian).

21. Pupyshev V.V., Rakityansky S.A. Semianalytical Method for Treatment of the N-Body Problem with Complex Total Energy within the Hyperspherical Approach. JINR preprint, E4-93-27, Dubna, 1993; Yad. Fiz., 1993, v.56, p.46 (in Russian).

Applied Studies

1. Burkovskaya T.E., Frontasyeva M.V., Gundorina. Elemental Bone Composition of Rats Flown in Biosatellite "Cosmos-2044". Int. Conf. Nuclear Analytical Methods in the Zife Sciences, 13-17 September 1993, Prague, Czech Republic, p.40.

2. Burkovskaya T.E., Frontasyeva M.V., Gundorina S.F. Kinetics of Elemental Content Changes of Bone Tissue of Mice During Evolution under Hypokinetic Stress. Int. Conf. Nuclear Analytical Methods in the Zife Sciences, 13-17 September 1993, Prague, Czech Republic, p.60.

3. Dermendjiev E. et al. An Experimental Facility for Studying Delayed Neutron Emission. Comm. JINR, E13-93-6, Dubna, 1993.

4. Diyachenko V.M. et al. Absolute Calibration of the KNT-8 Fission Chambers. JINR Rapid Comm., No. 2(53)-92, Dubna, 1992, p.45-50.

5. Frontasyeva M.V., Gundorina S.F., Gorbunov A.V., Onischenko T.L. Effect of the Production of Phosphorous Fertilizers on Environment. Recent Developments of Radioanalytical Methods at the IBR-2 Pulsed Fast Reactor. Proc. of MTAA-8, 16-20 Sept., 1991, Vienna, Austria; Journal of Radioanalytical and Nuclear Chemistry, 1992, v.167, No.1.

6. Frontasyeva M.V. et al. Activation Studies of Concrete Binding Agent Ingredients Used for Nuclear Radiation Shielding. Kernenergie, 1992, 34, p.7-8.

7. Frontasyeva M.V., Nazarov V.M., Steinnes E. Mosses as Monitors of Heavy Metal Deposition: Comparison of Different Multi-Element Analytical Techniques. Int. Conf. Heavy Metals in the Environment. Sept. 1993, Toronto, Canada, vol. 2, p.17 (submitted to the Journal of Radioanalytical and Nuclear Chemistry).

8. Gorbunov A.V., Frontasyeva M.V. et al. Effect of Agricultural Use of Phosphogypsum on Trace Elements in Soils and Vegetation. The Science of the Total Environment, 1992, 122, p.337-346.

9. Gorbunov A.V., Gundorina S.F., Frontasyeva M.V. The Effect of Sample Size on the Representativity of Ecological Sample Studied by NAA. In: II Int. Workshop on Neutron Activation Analysis in Environment. Dubna, 15-28 Sept., 1992. JINR, E14-92-364, Dubna, 1992.

10. Nazarov V.M., Frontasyeva M.V., Pavlov S.S., Sysoev V.P. Recent Developments of Radioanalytical Methods at the IBR-2 Pulsed Fast Reactor. Proc. of MTAA-8, 16-20 Sept., 1991, Vienna, Austria; Journal of Radioanalytical and Nuclear Chemistry, Articles, 1992, v.167, No.1.

11. Nazarov V.M., Borzakov S.B., Herrera E., Diaz O., Montero M.E. Investigation of REE and other Trace Elements Distribution along Oil Wells by Means of NAA. Proc. of the Second Int. Symp. on Nuclear Analytical Chemistry (NACII). Toronto, Canada, 3-5 June, 1992.

12. Nazarov V.M., Frontasyeva M.V., Lavdanskij P.A., Stephanov N.I. NAA for Optimization of Radiation Shielding of Nuclear Power Plants. Proc. of the Second Int. Symp. on Nuclear Analytical Chemistry (NACII). Toronto, Canada, 3-5 June, 1992.

13. Nazarov V.M. Use of Pulsed Neutron Sources in Analytical Applications. Proc. of the Second Int. Symp. on Nuclear Analytical Chemistry (NACII). Toronto, Canada, 3-5 June, 1992.

14. Nazarov V.M. Radioanalytical Methods at the IBR-2 Pulsed Fast Reactor. Proc. of the Annual Meeting of the Americal Nuclear Society. Boston, Massachusetts, June 7-12, 1992.

15. Nazarov V.M., Serebryanny L.R., Kuznetsov M.P., Vostokova T.A., Koryakin V.S. Snow Cover as a Witness of Environmental Pollution from Norilsk Copper-Nuckel Plant in the Maimyr Peninsula, Northern Siberia. II Int. Workshop on Neutron Activation Analysis in Environment. Dubna, 15-18 Sept., 1992. JINR, E14-92-364, Dubna, 1992.

16. Nazarov V.M. Use of IBR-2 Pulsed Fast Reactor in Analytical Applications. II Int. Workshop on Neutron Activation Analysis in Environment. Dubna, 15-18 Sept., 1992. JINR, E14-92-364, Dubna, 1992.

17. Nazarov V.M. Radioanalytical Methods at the IBR-2 Pulsed Reactor. 1992 Annual Meeting Boston, Massach., June 7-12, 1992. Transaction of the American Nuclear Society, vol.65, Tansao 65, 1-580 (1992) p.173.

18. Nazarov V.M. et al. An Analyzer for the Determination of Protein Concentration in Corn. Conference on Industrial Radiation and Radioisotope Measurement Applications. September 8-11, 1992. Supplement number 1 to vol. 65, Tansao 65, 1-80 (1992).

19. Nazarov V.M. et al. Regent Developments of Radioanalytical Methods at the IBR-2 Pulsed Fast Reactor. Journal of Radioanal. and Nuclear Chem., vol.167, No.1 (1993).

20. Nazarov V.M. et al. Fine-Powder Al_2O_3 and SiO_2 for Preparation of Multielement Standards for Rare-Earth Element Analysis. Journ. of Radioanal. and Nuclear Chem., vol. 168, No.1 (1993) 163-168.

21. Nazarov V.M., Frontasyeva M.V., Chinaeva V.P., Borzakov S.B. NAA Biomonitoring of the Environment with Mosses and Pine Tree Needles. Int. Conf. Nuclear Analytical Methods in the Zife Sciences, 13-17 September 1993, Prague, Czech Republic, p.18.

22. Oganessyan Ju.Ts., Karamyan S.A., Nazarov V.M., Sheglovski Z. Observation Neutron Radioactive Capture Reaction on Exotic Isomer $^{178m2}Hf$. JINR Rapid Comm., No. 3(54)-92, Dubna, 1992.

23. Ostrovnaya T.M. et al. Software for INAA on the basis of Relative and Absolute Methods Using Nuclear Data Base. II International Workshop on Neutron Activation Analysis in Environment. Dubna, 15-18 Sept., 1992. Collected reports, Dubna, 1993.

24. Polushkin V.N., Buev A.R. Investigation of the high temperature superconducting screen with the help of the magnitometer based on the radiofrequency high-temperature squid. JINR Preprint, P13-92-42, Dubna, 1992 (in Russian).

25. Vostokova T.A., Ilina Y.A., Nazarov V.M. NAA as Applied to Trace Elements Distribution Determination in Environmental Samples from Frans Iosifa Land. 2 International Workshop on Neutron Activation Analysis in Environment. Dubna, 15-18 Sept., 1992. Collected reports, Dubna, 1993.

Neutron Sources

1. Aksenov V.L., Dikansky N.A., Lomidze V.L., Novokhatsky A.V., Popov Yu.P., Rudenko V.T., Skrinsky A.N., Furman W.I. Proposal for the Construction of the New Intense Resonance Neutron Source (IREN). JINR, E3-92-110, Dubna, 1992.

2. Krasnykh A., Popov Yu., Rudenko V., Somov L., Men'shikov L., Prusakov V., Subbotin. SCANUR: Subcritical Reactor with Electron Linac for Transmutation of Nuclear Wastes. In: Proc. of IEEE Particle Accelerator Conf., Washingron, D.C., May 17-29, 1993, v.1, p.552.

3. Lomidze V.L., Rogov A.D. Using of the Interactive Version GEANTS3 Code for Analysis of Neutron Source. Presented to the Int. Conf.: Mathematical Methods and Supercomouting in Nuclear Application. 19-23 Apr., 1993, Karlsruhe, FRG.

4. Lomidze V.L., Rogov A.D. The Reflection of the 40 MeV Electrons by the Sharp-Angle Tungsten Target and the Fuel Pin Meltdown Accident Analysis of the IBR-30 Booster. Report during the Int. Seminar on Neutron Interactions with Nuclei. Dubna, April 14-17, 1992.

5. Novokhatsky A.V., Aleksandrov A.V., Avilov M.S. et al. Linear Accelerator for Intense Resonance Neutron Source (IREN). In: Proc. of the Int. Workshop on C-tau Factory. Dubna, 1993.

6. Pepyolyshev Yu.N., Malyshev E.K., Chuklyaev S.V. Secondary Emission Detectors to Measure Dose Rate of γ-radiation of Nuclear Reactors and Accelerators. The IXth Conference on Radiation Control of Intensive Fluzes of Ionizing Radiation. Abstracts of Reports. Obninsk, March 24-26, 1992 (in Russian).

7. Pepyolyshev Yu.N., Dzwinel W. The Possibility of Efficient Control of Product Quality with an Aid of Methods Classifying Data with Many Parameters. JINR Comm., H10-92-143, Dubna, 1992 (in Russian).

8. Pepyolyshev Yu.N., Chuklyaev S.V., Odintsov Yu.N., Koshelev A.S. Secondary Emission Detectors (SED-2) to Measure Dose Rate of γ-Radiation. Atomnaya Energiya., 1993, v.75, issue 4 (in Russian).

9. Rogov A.D., Shabalin E.P. Comparative Potentialities of Different Variatns to Up-Date the IBR-2 Pulsed Neutron Source. In: Int. Workshop "Pulsed Nuclear Reactors: New Possibilities for Scientific Research". Dubna, 1992 (in Russian).

Measurement and Computation Complex

Arkhipov V.A., Ishmukhametov M.Z., Solodilov A.V. Automation of the radiation monitoring at the JINR reactors. In: XV Int. Symp. on Nuclear Electronics. D13-92-581, Dubna, 1993.

2. Barabash I.P. et al. The Measurement Module for the Ultracold Neutron Experiments. JINR Comm., 13-92-274, Dubna, 1992 (in Russian).

3. Bogdzel A.A., Vagov V.A., Lyapin D.I., Salamatin I.M., Sirotin A.P., Tishin V.G. Digital Information Filtering in the UKOR Multidimensional Spectrometer. JINR Comm., 13-92-121, Dubna, 1992 (in Russian).

4. Bogdzel A.A. et al. Prompt Gamma-Rays Yields at Individual Fission Resonances of ^{239}Pu by Resonance Neutrons. JINR E7-92-95, Dubna, 1992, p.305-311.

5. Bogdzel A.A. et al. ibid., p.312-313.

6. Bogdzel A.A. et al. A PC/AT-Based Multiparameter Nuclear Data Acquisition System. In: Proc. of Seventh Symp. on Microcomputer and Microprocessor., vol.1. April, 1992. House of Technics, Budapest, Hungary.

7. Bogdzel A.A., Nguyen Chung Tuan. The PC/AT Based Multidimensional Spectrometrical Information Acquisition System. In: XV Int. Symp. on Nuclear Electronics. JINR, D13-92-581, Dubna, 1993 (in Russian).

8. Brankowski E. et al. The Multidetector System of Registering and Storing the Spectrometrical Information Based on the 64K x 24bit Memorizing Device. JINR Comm., 13-92-120, Dubna, 1992 (in Russian).

9. Brankowski E. et al. The Bit Registering and Storing Multidetector System. In: XV Int. Symp. on Nuclear Electronics. JINR, D13-92-581, Dubna, 1993 (in Russian).

10. Cheremukhina G.A. et al. A Two-Dimensional Detector with Delay Line Readout for Slow Neutron Fields Measurements. JINR, E13-92-52, Dubna, 1992.

11. Ermakov V.A., Kim Khen Do. The Digital Filtering Unit. JINR Comm., P13-92-112, Dubna, 1992 (in Russian).

12. Ermakov V.A., Zen En Ken, Khim Khen Do. The POISK Multiparameter Measurement System Based on the CAMAC Units and the Pravets-16 Personal Computer. JINR Comm P13-92-210, Dubna, 1992 (in Russian).

13. Janeva N., Toshkov S., Georgiev G., Sirakov I., Tishin V.G., Zamyatnin Yu.M. A Setup for Precise Measurement of Resonance Neutron Capture by Self/Indication. Nucl. Instr. Meth. Phys. Res. A, 1992, v.313, No. 1,2, p.266-272.

14. Korneev D.A. et al. The Structure of the Spectrometrical Experiment Automation System Software Founded on Databases. In: XV Int. Symp. on Nuclear Electronics. JINR, D13-92-581, Dubna, 1993 (in Russian).

15. Natkaniec A., Ostrovnoi A.I., Sukhomlinov G.A., Tishin V.G. Computer-Aided Systems for the IBR-2 Spectrometers (CAS . IBR-2 Project). JINR-FRG Cooperation in Neutron Physics. Results of 1992 and Plans for 1993. JINR 92-563, Dubna, 1992, p.17-19.

16. Vagov V.A., Walther K., Sirotin A.P., Tishin V.G., Voitus K. The Readout, Handling, and Control System of the NSHR High-Resolution Spectrometer at the IBR-2 Reactor. JINR Comm., 13-92-122, Dubna, 1992 (in Russian).

17. Vladimirov V.A. et al. Operating Some Final-Control Devices of the TEKST and DVR Facilities at the IBR-2 and IBR-30 Reactors. JINR Comm., 13-92-123, Dubna, 1992 (in Russian).

18. Vladimirov V.A. et al. Operating Some Final-Control Devices of the TEKST and DVR Facilities at the IBR-2 and IBR-30 Reactors. In: XV Int. Symp. on Nuclear Electronics. JINR, D13-92-581, Dubna, 1993 (in Russian).

19. Zanevsky Yu.V. et al. Two-Dimensional High-Resolution Multiwire Detector for an X-Ray Diffractometer. JINR Preprint, 18-92-180, Dubna, 1992(in Russian).

20. Zanevsky Yu.V. et al. Two-Dimensonal High-Resolution Multiwire Detector for an X-Ray Diffractometer. Crystallography, v.38, issue 2, 1993, p.252-260 (in Russian).

6.1. CONDENSED MATTER PHYSICS

CONTENTS

The Phase Diagram of Hematite in an External Magnetic Field
V.V.Nietz

Diffraction Investigation of the Dynamic Hysteresis Following Spin-Flop Transition in Uniaxial Antiferromagnetics in a Pulsed Magnetic Field
D.Georgiev, V.V.Nietz, A.P.Sirotin

Texture Investigations of Geological Samples at the NSHR Diffractometer
K.Walther, N.N.Isakov, A.N.Nikitin, D.I.Nikolayev, K.Ullemeyer, J.Heinitz

Neutron Diffraction at High Pressure with Diamond and Sapphire Anvils at the IBR-2 Reactor
A.M.Balagurov, B.N.Savenko, V.P.Glazkov, V.A.Somenkov

Small-angle scattering

SANS Studies on Hydrating Cement Paste and SSNTD
F.Haussler, M.Hempel, F.Eichhorn, A.Hempel, H.Baumbach

SANS-Investigation of the Micelle System C_{14}DMAO in D_2O at High Hydrostatic Pressure
N.Gorski, J.Kalus, A.I.Kuklin, L.S.Smirnov

The Study of Micellar Solutions of Ethoxylated Diisononylphenol by Small-Angle Neutron Scattering
L.A.Bulavin, V.M.Garamus, Yu.M.Ostanevich

Inelastic scattering

Structure of Liquid Helium-4 Excitation Spectrum
N.M.Blagoveshchenskii, I.V.Bogoyavlenskii, L.V.Karnatsevich, Zh.A.Kozlov, V.G.Kolobrodov, V.B.Priezzhev, A.V.Puchkov, A.N.Skomorokhov, B.S.Yarunin

Inelastic Neutron Scattering in PbF_2
Zh.A.Kozlov, I.Padureanu, S.N.Rapeanu, Gh.Rotarescu, V.A.Semenov

Localized Vibrations of Nitrogen in Interstitial Phases of Ta-N
S.I.Morozov, V.V.Kazarnikov

Localized Vibrations of Host Atoms in Zr-O Interstitial Solid Solutions
S.I.Morozov

Oxygen Atom Vibrational Excitations in Y-O-H Solid Solutions
S.I.Morozov, V.V.Sumin

Effect of Nitrogen on Lattice Dynamics of the Austenitic Fe-Cr-Mn-Ni Alloys
S.A.Danilkin, V.P.Minaev, V.V.Sumin

The Analysis of Incoherent Neutron Scattering on Liquid Pottassium at 340-550 K
M.V.Zaezjev, M.N.Ivanovski, A.G.Novikov, V.V.Savostin, O.V.Sobolev, A.L.Shimkevich

Neutron Scattering Studies of Phase Transitions in Protonated and Deuterated Triammonium Hydrogen Disulphate
L.Bobrowicz, I.Natkaniec, M.Mroz, W.Nawrocik, W.Wojtowicz

Neutron Scattering Studies of Ammonium Dynamics and Phase Transition in $K_{1-x}(NH_4)_xSCN$ at 10 K
I.Natkaniec, L.S.Smirnov, A.I.Soloviev, S.I.Bragin

Vibration Spectrum of the Ice III
I.Natkaniec, L.S.Smirnov, A.N.Ivanov

Investigation of the Temperature Dependence of Static and Dynamic Disorder in the $K_{1-x}(NH_4)_xSCN$ System
I.Natkaniec, L.S.Smirnov, S.I.Bragin, A.I.Soloviev

The Search for the Crystal Electric Field in the Compounds of the ReNiSn (Re-Ce, La, Nd) Type
P.A.Alekseev, E.S.Clementyev, V.N.Lazukov, I.P.Sadikov, A.Yu.Muzychka, I.L.Sashin

Crystal Field in the Set of $RECu_2Si_2$ Compounds (RE - Pr, Nd, Tb, Ho, Er, Yb)
E.A.Goremychkin, A.Yu.Muzychka

Density of Vibrational States of Silicon Nitride
I.Markichev, E.Sheka, N.Goncharova, I.Natkaniec, A.Muzychka, V.Chukalin, V.Khavryutchenko, E.Nikitina

Density of States of Bulk and Surface Vibrations of Highly Disperse Al
I.Markichev, E.Sheka, I.Natkaniec, A.Muzychka, V.Khavryutchenko

Density of Vibrational States in Thiol Capped CdS Particles Using Inelastic Neutron Scattering
I.Markichev, E.Sheka, I.Natkaniec, A.Muzychka, V.Khavryutchenko, Y.Wang, N.Herron

Inelastic Neutron Scattering (INS) Investigation of Hydrogen Capture by Crystal Lattice Defects
V.V.Sumin, C.Gantulga

Polarized Neutron

Polarized Neutron Reflectivity of Epitaxial Thin Magnetic Films
O.McGrath, V.V.Pasyuk, H.J.Lauter, A.V.Petrenko, D.Givord

Interface Magnetization in a Pd/Co/Pd Ultra-Thin Film Studied by PNR
V.V.Pasyuk, H.J.Lauter, M.T.Johnson, F.J.A. den Broeder, E.Janssen, J.A.C.Bland, A.V.Petrenko, J.M.Gay

Polarized Neutron Reflectrometry Study on Magnetic Multilayers for Nuclear Resonant Scattering Experiments
V.V.Pasyuk, D.L.Nagy, H.Lauter, A.V.Petrenko

New Aspects in Employing Magnetic Anisotropic FeCo Thin Films as Neutron Polarizes
D.A.Korneev

A possible observation of the Depinning Line in $YBa_2Cu_3O_{7-}$ Ceramics from Neutron Polarization Studies
V.L.Aksenov, Yu.V.Bugoslavsky, E.B.Dokukin, V.K.Ignatovich, A.A.Minakov, Yu.V.Nikitenko, A.V.Petrenko, S.A.Sergeenkov

Neutron Depolarization Studies of Magnetization Process on Superparamagnetic Cluster Structures
S.Ligenza, E.B.Dokukin, Yu.V.Nikitenko

THE NEW FOURIER DIFFRACTOMETER AT THE IBR-2 REACTOR: DESIGN AND FIRST RESULTS

V.L.Aksenov, A.M.Balagurov, V.G.Simkin and Yu.V.Taran
Frank Laboratory of Neutron Physics, JINR, Dubna, Russia
V.A.Trounov, V.A.Kudrjashev, A.P.Bulkin and V.G.Muratov
S-Petersburg Nuclear Physics Institute, Gatchina, Russia

A high-resolution neutron powder Fourier diffractometer (HRFD) has been constructed at the pulsed reactor IBR-2 in Dubna[1] and the very first high-resolution spectra measured (Fig.1). The diffractometer uses the Reverse Time-Of-Flight (RTOF) method[2] in the data acquisition system. The design avails of both the high luminosity of the IBR-2 reactor and the high resolution of a Fourier chopper and reveals good prospects for structural and residual stress studies. The high resolution of the HRFD is provided by high frequency of neutron beam modulation (~150 kHz). High intensity level is ensured by high transmision of Fourier chopper (~0.25) and a large solid angle (0.1 sr) of the time focused detector system. Additional modulation of the beam by neutron source pulses makes possible a considerable (by 10 or more times) decrease in correlation background level as compared with that of a Fourier diffractometer at a steady state reactor.

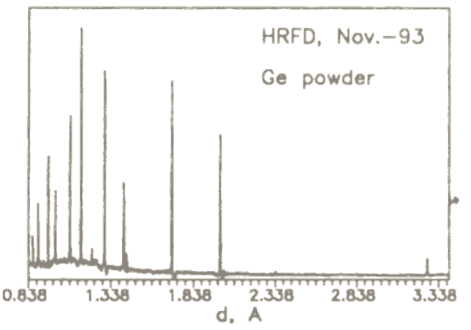

Fig.1. Diffraction pattern of Ge powder, measured on HRFD.

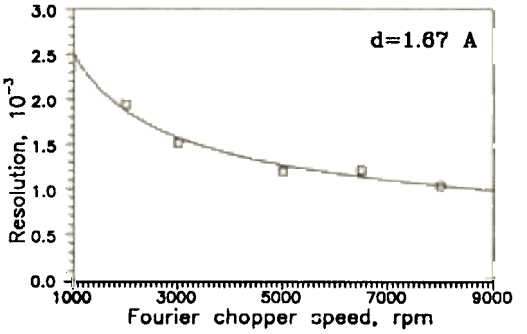

Fig.2. The dependence of the resolution on the maximum chopper speed.

The results of preliminary measurements have confirmed that the Fourier technique in combination with the IBR-2 pulse reactor gives diffraction patterns of good quality both with respect to resolution and intensity. The resolution very close to 0.001 was achieved (Fig.2) and the expected value of $\Delta d/d$ equal to 0.0005 can be reached after the diffractometer units are aligned. The structural study oppotunities with the new Fourier diffractometer are expected to be just the same as HRPD (RAL) offers.

1. V.L.Aksenov, A.M.Balagurov, V.A.Trounov, P.Hiismaki et al, Communication of JINR, E13-92-456, Dubna, 1992
2. P.Hiismaki, H.Poyry, A.Tiitta, J Appl.Cryst. 1988, 21, p.349

ESTIMATION OF RESIDUAL STRESS IN ROLLED IRON-DISKS BY STRAIN MEASUREMENTS USING THE HIGH RESOLUTION FOURIER DIFFRACTOMETER OF REACTOR IBR-2

V.L. Aksenov, A.M. Balagurov, G.D. Bokuchava, J. Schreiber*, Yu.V. Taran

Frank Laboratory of Neutron Physics, JINR, Dubna, Russia
*Fraunhofer-Institute for Nondestructive Testing, Department of Acoustic Methods for Nondestructive Evaluation and Quality Assurance, Dresden, Germany

Variation of internal stress states in cold rolled sheet metal can essentially influence the result of forming processes. Therefore it is important to controll the forming process by a practicable in line testing method. For this purpose magnetic [1] and ultrasonic [2] nondestructive methods are available. However, it is necessary to calibrate these techniques [3] to get results, which can be used for a reliable assessment of rolled plates for the further forming process.

This paper describes a calibration procedure making use of the neutron diffraction method. With the help of the high resolution Fourier diffractometer at the pulsed reactor IBR-2 in Dubna [4] the strain tensor was measured at selected points of cold rolled iron-disks (2.5 mm thickness). As the fluctuations of residual stress in the disk are of interests at a lateral scale of about 10x10 mm^2 the gauge volume of the neutron diffraction was chosen in correspondence with that.

The complete strain tensor ε_{ij} is determined from the measured reverse time of flight (RTOF) diffraction spectra for different orientations of the scattering vector. The size of stress states are averaged inside the scattering volume. This averaging makes the components of the internal stress states belonging to the normal direction of the disk plane to be vanished. Therefore the determination of the main components of the local strain and stress is reduced to a quasi-two-dimensional problem.

Analysing the positions of the available eight Bragg reflexes the corresponding crystallite lattice plane spacing d^{hkl} is obtained. The lattice spacing of the unstrained state d_0^{hkl} was known from RTOF spectrum for the annealed powder sample of the disk material. Thus taking the quantities $\Delta^{hkl}=(d^{hkl}-d_0^{hkl})/d_0^{hkl}$ and the direction cosines of the scattering vector the strain components ε_{ij}^{hkl} is calculated applying the least squares method. Additionally to that information Rietveld Refinement is carried out to get ε_{ij} averaged with respect to the different diffraction planes (hkl). Now the quantity Δ is calculated by the fitted lattice constant a, i.e. $\Delta=(a-a_0)/a_0$. Furthermore, the systematic deviations of the measured intensities of the Bragg peaks from the Rietveld fit for ideal

isotropic powder samples provided information on the change in the texture at different inspection points of the disk.

On the basis of the diffraction results an assessment of the magnetic and ultrasonic methods for the estimation of residual stress in the cold rolled iron-disks was made. The characteristic parameters of the Barkhausen noise, i.e. noise amplitude, coercitive field strength at different measuring frequencies, and others [1], as well as of the ultrasonic technique (sound velocity for different wave modes and measuring frequencies [2]) are determined for the considered disks. The comparison of these results with the neutron data are used to propose a reasonable measuring concept for practical applications to forming processes with cold rolled sheet metal.

References

[1] Dobmann G., Höller P., Non-Destructive Determination of Material Properties and Stresses, in Proc. of the 10th Intern. Conf. (Glasgow) on NDE in the Nuclear and Pressure Vessel Industries, (Ohio: ASM International 1990), p. 641

[2] Spies M., Schneider E., Nondestructive analysis of the deep-drawing behaviour of rolled sheets by ultrasonic techniques; in Proceedings of the 3rd International Symposium on Nondestructive Characterization of Materials, Eds. P. Huller, V. Hauk, G. Dobmann, C. Ruud, R. Green (Berlin: Springer-Verlag 1989), p. 296-302

[3] Allen A.J., Calibration of portable NDE techniques for residual stress measurements, in Hutchings M.T. and Krawitz A.D., Measurement of Residual and Applied Stress Using Neutron Diffraction (Dordrecht: Kluwer Academic Publishers and NATO Scientific Affairs Dvision 1992), p. 559

[4] Balagurov A.M., Simkin V.G., and Taran Yu. V., Possible utilization of high resolution Fourier diffractometer at the IBR-2 for strain measurements, EPDIC-III (Wien, 1993)

Atomic and Magnetic Structure of $YBa_2(Cu_{1-x}{}^{57}Fe_x)_3O_{6+y}$ Studied by Neutron Diffraction on Isotope Enriched Samples

A.M.Balagurov[1], F.Bouree[2], I.S.Lyubutin[3], I.Mirebeau[2]

1 – Frank Laboratory of Neutron Physics, JINR, Dubna, Russia
2 – Laboratoire Leon Brillouin, Saclay, France
3 – Institute of Crystallography, Moscow, Russia

Copper atoms in the superconductor $YBa_2Cu_3O_7$ can be easily substituted by two and three valent metals. This fact is widely used to study the role of some Y123 structural elements in the formation of superconducting properties and to study the problem of the coexistence of superconductivity and magnetism in this compound.

Copper substitution in Y123 for iron or other 3d-metals destroys the superconducting properties of this compound. The mechanism of this phenomenon is still not very clear. On the whole, it is attributed to a modification of the charge transfer from chains to planes. For example, for the $YBa_2(Cu_{1-x}Co_x)_3O_{6+y}$ (Y123-Cu/Co) system, it was suggested/1/ that removal of O^{2-} from pure Y123 is equivalent an increase of Co^{3+} content at the Cu1 site because the Cu2-O1 distances are changed by the same means in both cases. But for the Y123-Cu/Fe system, in our study/2/, it was found that the Cu2-O1 distance does not depend on iron concentration. Moreover, as follows from data published in/3/ for the Y123-Cu/Ni system the Cu2-O1 distance decreases if Ni concentration in a sample increases.

Modification of the magnetic structure by substituting copper for iron is another interesting question of the Y123 compound. In addition to the structural data, of special interest is a comparison of the Y123-Cu/Fe and Y123-Cu/Co systems, i.e., the magnetic moment of Co-atoms is also very high. On the whole, these systems reveal many common features, but at the same time, no long range magnetic order was found in the oxygen saturated Y123-Cu/Fe system, though it was well established in the Y123-Cu/Co system.

In paper/4/ a new analysis of the neutron structural data for the Y123 system is made and new data about the magnetic order in this compound are analyzed.

Neutron diffraction experiments were performed with the DN-2 diffractometer at the IBR-2 pulsed reactor in Dubna and with the constant wavelength diffractometers G6-1 and 3T2 at the Orphee reactor in Saclay.

The structure of $YBa_2(Cu_{1-x}{}^{57}Fe_x)_3O_{6+y}$ both oxygen saturated and oxygen deficient samples was refined by the Rietveld method. The atomic coordinates do not change

very much with x, remaining at y≈1, practically the same as in pure Y123 despite the tetragonal symmetry of the structure. At y≤0.5 the coordinates are also typical for pure Y123 with oxygen partially removed (Fig.1).

In spectra obtained with the G6-1 spectrometer we observed three magnetic reflections at *1/2,1/2,l*, with half integer *l* values (*l=1/2, 3/2 and 5/2*). The intensity of those peaks is comparable to that of the impurity peaks but they can be clearly distinguished through their temperature dependence.

Nuclear and magnetic Rietveld refinement have been performed on some spectra obtained with the G6-1 spectrometer using the program FULLPROF. The magnetic moments μ_{Cu1} and μ_{Cu2} were refined assuming a collinear structure with alternating antiferromagnetic planes along the *c* axis, and spin components in the *a–b* plane.

The magnetic moments are plotted as a function of temperature in Fig.2. We note that the moment on the Cu1 sites is antiparallel to the neighboring moment on the Cu2 sites, so that the sequence + - + - + - of AF planes is observed along the *c* axis. The Neel temperature increases with iron concentration, together with the amplitudes of the mean moment.

Our study confirmed in general and extended the magnetic phase diagram of this compound in the deoxygenated state, published earlier in[5] from Mossbauer measurements and in[6] from neutron scattering data. The question for next experiments would be the intermediate (x≈0.02 – 0.07) region between the state with moments ordered on Cu1 sites only and the state with long-range order on both Cu1 and Cu2 sites, where the data are not fully agree each other.

References

1. Sonntag R., Hohlwein D., Hoser A., Prandl W., Schafer W., Kiemel R., Kemmler-Sack S., Losch S., Schlichenmaier M., Hewat A.W.
Physica C, 1989, v.159, p.141

2. Balagurov A.M., Lyubutin I.S.
Communication of JINR, P14-92-579, Dubna, 1992

3. Balagurov A.M., Piechota J., Pajaczkowska A.
Solid St. Comm., 1991, v.78, p.407

4. Balagurov A.M., Bouree F., Lyubutin I.S., Mirebeau I.
Physica C, to be published

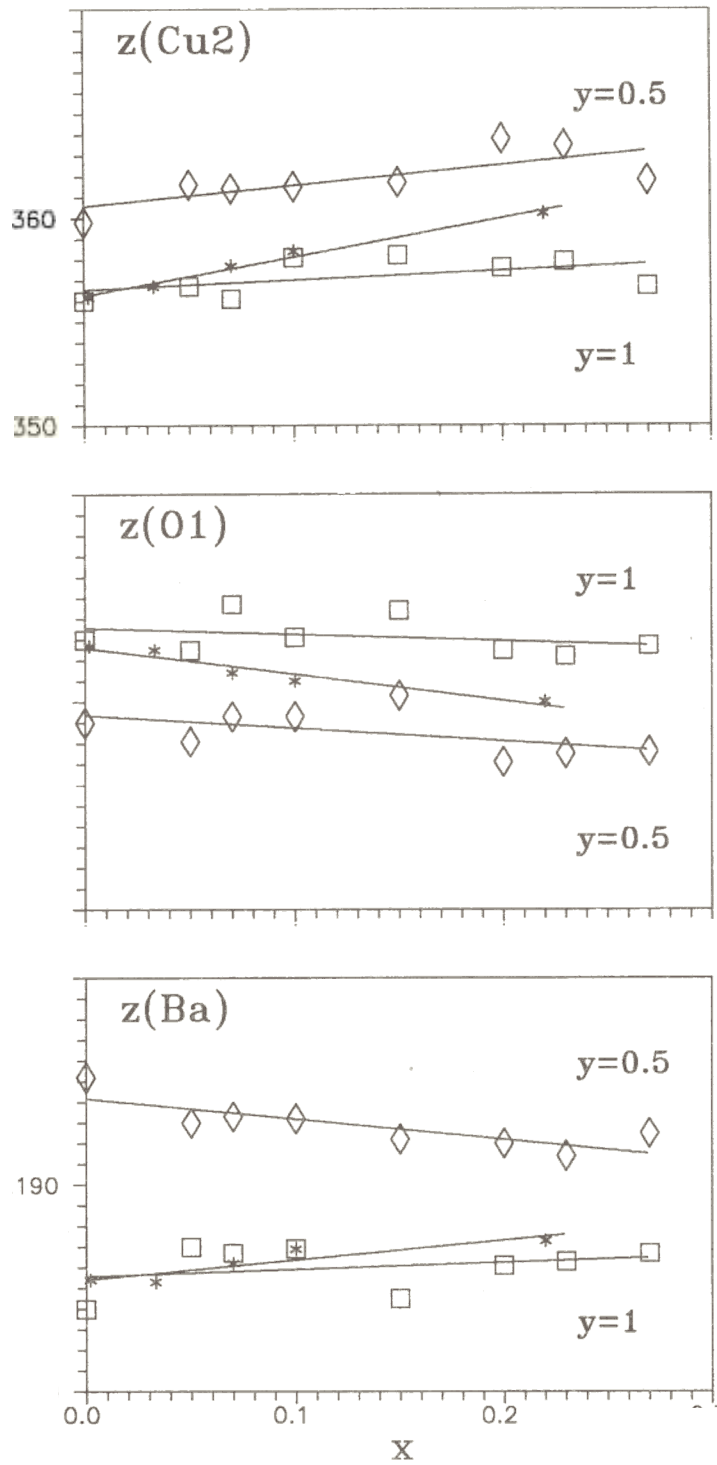

Fig.

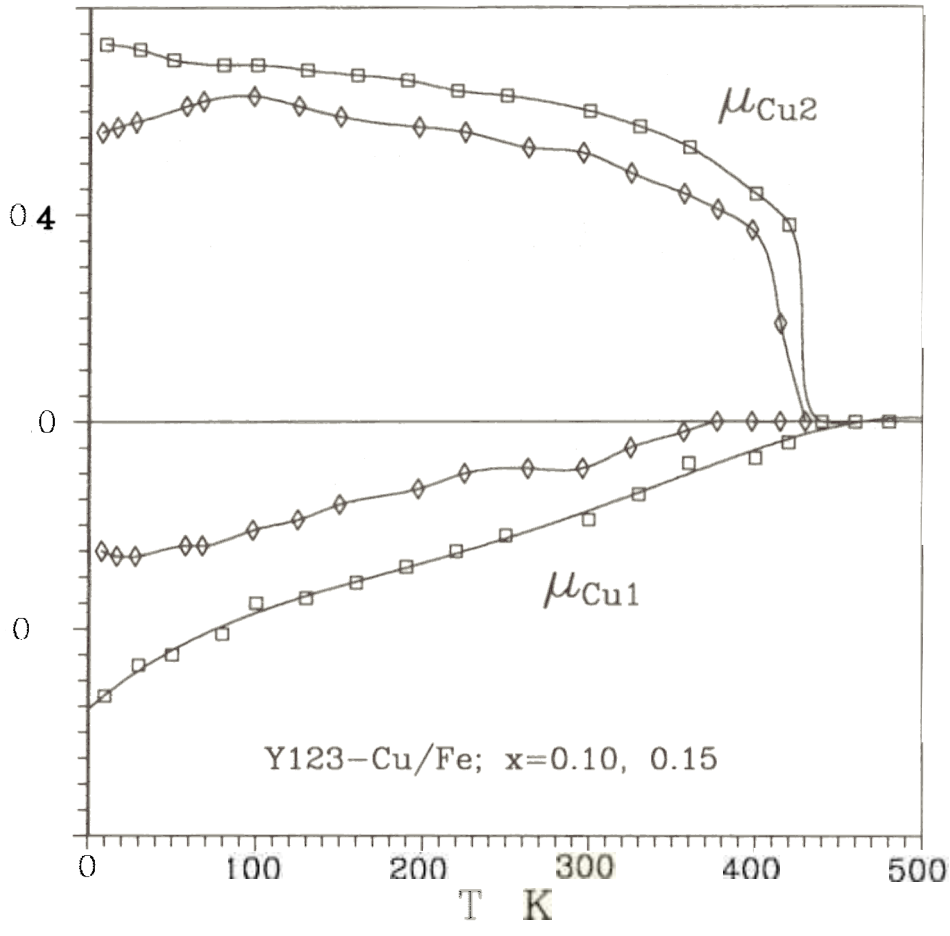

Fig.

NEUTRON INVESTIGATION OF La_2CuO_4 AND $(Nd_1Ce)_2CuO_4$ SINGLE CRYSTALS.

By A.M.Balagurov, S.N.Barilo, A.I.Beskrovnyi, N.N.Bydanov, K.V.Gamayunov, E.E.Rider, V.A.Sarin, Laboratory of Neutron Physics, Joint Institute for Nuclear Research, Dubna, Obninsk Branch of Karpov Physical Chemistry Institute, Obninsk, Russia.*

The purpose of this work was to study regularities of the structure defects caused by nonstoichiometry, to determine fine cationic and anionic distributions. The investigations of regularities of the reciprocal lattice, the definitions of twinning law, check of crystal quality were fulfilled on the time-of-flight diffractometer DN-2 with the help of position sensitive detector at the pulsed reactor IBR-2 in Dubna. The neutron diffraction measurements for precise structure calculation were done on the 4-circle diffractometer Syntex PIN at the reactor VVR in Obninsk (λ=1,167Å, sin θ/λ=0,81).

There were two samples of La_2CuO_4. The sample S1 was annealed and quenched at 1150°C, the sample S2 - at 400°C. Neutron experiments for these samples were done at 18°C and 300°C. The parameters of elementary cell are

		SP.GR.	a, A	b	c	V, A^3
18°C	S1	C mca	5,369(3)	13,144(9)	5,389(3)	380,3(5)
	S2	C mca	5,363(2)	13,147(13)	5,389(2)	380,6(5)
300°C	S1	14/mmm	3,811(2)		13,208(8)	191,8(3)
	S2	14/mmm	3,810(2)		13,214(8)	191,8(3)

L.S. refinement of structure parameters at 300°C gave R-factors 0,025 for 141 independent reflections for S1 and 0,028 for 143 independent reflections for S2 and next results. In position (e,4mm) parameters z/c are La 0,36119(6) and for O1 0,1833(1) as for S1 and S2. Site occupations for all atoms in S1 and S2 are exactly 1. But the parameters of thermal vibrations are systematically higher for all atoms in S1

		B eq., A^2	B11	B22	B33
La	S1	1,10(1)	1,22(2)	B11	0,87(3)
	S2	0,92(2)	1,04(3)	B11	0,68(4)
Cu	S1	0,98(2)	0,66(3)	B11	1,62(4)
	S2	0,79(2)	0,48(3)	B11	1,43(4)
O1	S1	2,56(3)	3,24(5)	B11	1,20(5)
	S2	2,33(3)	3,01(6)	B11	0,97(6)
O2	S1	1,52(3)	0,69(4)	1,37(4)	2,52(5)
	S2	1,32(3)	0,47(5)	1,22(5)	2,28(6)

Two samples with the composition $Nd_{2.05}Cu_{0.95}O_x$(N1)and $Nd_{1.90}Ce_{0.18}Cu_{0.92}O_x$(N2) were investigated at 18°C. The parameters of elementary cell are

	SP.GR.	a, A	c	V, A^3
N1	14/mmm	3,9450(8)	12,170(3)	189,4(1)
N2	14/mmm	3,8480(1)	12,093(4)	188,5(2)

L.S. refinement of structure parameters gave R-factor 0,027 for 139 independent reflections for N1 and 0,028 for 139 independent reflections for N2. The main results are

		x/a	y/b	z/c	B eq., A^2	cite occupation
Nd	N1	0,0	0	0,35098(8)	0,63(1)	1,002(5)
	N2	0	0	0,3515(2)	0,47(5)	0,965(5)
Cu	N1	0	0	0	0,68(2)	1,00
	N2	0	0	0	0,57(7)	1,00(3)
O1	N1	0	0,5	0	0,94(2)	0,993(7)
	N2	0	0,5	0	0,96(9)	1,00(3)
O2	N1	0	0,5	0,25	0,85(2)	0,995(7)
	N2	0	0,5	0,25	0,74(3)	0,985(6)

Because the lengths of neutron scattering for Nd and Ce are different but for Nd and Cu are approximately equal we can propose from our experimental results and compositions the next crystal chemistry formula for N1: $Nd_2(Cu_{0.95}Nd_{0.05})O_{3.98}$ and for N2: $(Nd_{0.91}Ce_{0.09})_2(Cu_{0.92}Nd_{0.08})O_{3.94}$.

NEUTRON DIFFRACTION STUDY OF THE MODULATED STRUCTURE OF $Bi_2Sr_{2,43}Y_{0.6}Cu_2O_{8+\gamma}$

A.I.Beskrovnyi[a], *Z.Jirak*[b], *M.Nevrila*[b] *and I.G.Shelkova*[a]

[a] *Frank Laboratory of Neutron Physics, JINR, 141980 Dubna, Moscow Region, Russia*

[b] *Institute of Physics, 16200 Prague 6, Cukrovarnicka, Czech Republic*

The $Bi_2(Sr,Ca)_{n+1}Cu_nO_{2n+4}$ cuprate based crystals (n=1,2,3) show structural modulation, depending on the content and amount of oxygen present. The modulation can be commensurate or incommensurate. The reason for appearance of modulation lies in existence of an additional oxygen atom inserted in a Bi-O-Bi ribbon after each modulation period in the direction of the modulation vector with the period 4-5 times the period of the basic cell.

The investigations were performed on the time-of-flight neutron diffractometer DN-2 at JINR, Dubna. The sample measuring $2 \times 2 \times 0.3mm^3$ was scanned in the reciprocal space of the *hol*, *okl*, *hko*, *hhl*-planes. The refined structural parameters are : A_{maa}, $a = 5.461\mathring{A}$, $b = 5.456\mathring{A}$, $c = 30.48\mathring{A}$. The superstructure reflections of the first and second order were observed. The positions of the satellites show that the structural modulation is defined by the wave vector $\tau = [0.233(2), 0, 1]$. The period of modulation $p = a/\tau^*$ is close to 4.25 a, what means, that it can be considered approximately commensurate with a 17 times enlarged cell in the a-direction, space group P_{naa}. The observed structural modulation has a peculiarity consisting in the following. Besides the first additional oxygen atom, existing in the Bi-plane with a period 4.25 a, there is inserted with the same period one more additional oxygen atom between the neighbouring ribbons in the Bi-planes. The increased oxygen content given by $\gamma = 0.5(1)$ compensates the effect of trivalent yttrium. The positions of atoms and the amplitudes of modulation have been determined.

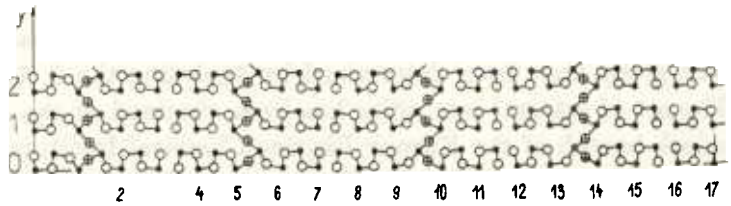

The $BiO_{1+\gamma/2}$ arrangement in $Bi_2Sr_{3-x}Y_xCu_2O_{8+\gamma}(x \sim 0.6)$. Oxygen atoms $O(4)$ are shown by open circles, the extra atoms $O(5)$ (within the chains along the x-axis) and $O(5')$ (between the chains) are marked by crosses.

NEUTRON STRUCTURE INVESTIGATION OF SINGLE CRYSTALS OF THE $BaBiO_3$ – $KBiO_3$ SYSTEM

V.A. Sarin, A.M. Balagurov, A.I. Beskrovnyi, S.S. Negovelov
Laboratory of Neutron Physics, Joint Institute for Nuclear Research

Ye.E. Rider, L.Ye. Fykin
Obninsk branch of the Karpov Physico-Chemical Institute

D. Hohlwein
Hahn–Meitner Institut, Berlin

Among the non-copper superconductors, $Ba_{1-x}K_xBiO_3$ single crystals have been known to have the highest T_c. A number of purely structure problems was supposed to have been solved by means of the neutron investigation of the single crystals of this system with x=0, 0.11, 0.16, 0.22, 0.43, 1.0. The first problem was to ascertain with the help of the coordinate detector whether there is the incommensurate phase in this system. The second problem was to solve the structure of $KBiO_3$ single crystal about which there has been no single crystal data. The third problem was to evaluate precisely the cation and anion distribution, anisotropic parameters of the thermal oscillations of atoms, and possible nonstoichiometry.

By now, the stage of studying the high-symmetry (cubic) phases with x=0.22 (T_{exp}=300°C), x=0.43, and x=1.0 ($KBiO_3$) has been completed.

1. In the number of experiments on the single crystals with x=0.43 and 1.0 performed at the DN-2 diffractometer (Laboratory of Neutron Physics, JINR) and at the Weissenberg neutron goniometer (HMI, Berlin), no satellites as an indication of noncommensurate or modulated phase have been detected. Thus, even if the incommensurate or modulated structure does exist, its crystallites are too small and their coherency region is insufficient for the neutron diffraction.

2. The first stage of the neutron structure analysis of $KBiO_3$ single crystals has been caried out at the neutron Weissenberg goniometer (HMI). The unit cell parameter a=10Å and the I3m space group have been determined by analysing the 0, 1, and 2 developed layer lines. The set of integral intensities has been obtained at the 4-circle goniometer Syntex (Obninsk branch of the Karpov Physico-Chemical Institute). The structure has been solved automatically by the PATS program and then with the help of the nuclear density differencial syntheses. The least squares refinement has been performed by use of the CSD programs complex. The structure data is presented in the Table 2. In the structure of $KBiO_3$, large K cations are statistically disordered along the body diagonal in the cavities between the Bi–O octahedra. In this compound, Bi has the valency of 5^+.

3. In the structures with x=0.22, 0.43, and 1.0, no oxygen nonstoichiometry has been detected to an accuracy of 0.01 formula units. In structures with xleq0.5, Ba is replaced by K in its position (which is logical in view of the closeness of their ion radii). However, the primitive cubic cell (x=0.43) does not remain as the K content increases, and $KBiO_3$ has a complicated body-centered cell with disordered K positions. Strong anisotropy of thermal oscillations of oxygen atoms has been detected in the studied compounds.

Table 1. The compounds studied

Compound	T_{exp}	Space group	a, Å	Molecules per cell	Number of reflections for LS refinement	Crystal volume, mm^3
$KBiO_3$	room	Im3	10.006(7)	12	129	~0.9
$Ba_{0.78}K_{0.22}BiO_3$	~300°	Pm3m	4.333(3)	1	74	30
$Ba_{0.57}K_{0.43}BiO_3$	room	Pm3m	4.281(2)	1	52	1.9

Table 2. Refinement results

Atom	x/a	y/b	z/c	Thermal factor B, Å^2	Position multiplicity	Population
			$KBiO_3$, R=0.04			
Bi	0.5	0	0.3393(4)	0.48(8)	12	1
O1	0	0	0.3619(6)	0.8(2)	12	1
O2	0.2885(5)	0	0.3382(5)	1.05(12)	24	1
K1	0	0	0	1.4(6)	2	0.70(9)
K2	0.159(2)	x	x	3.2(6)	16	0.61(3)
K3	1/4	1/4	1/4	1.9(6)	8	0.125(4)
			$Ba_{0.78}K_{0.22}BiO_3$, R=0.01			
Bi	1/2	1/2	1/2	0.720(6)	1	1
Ba	0	0	0	1.69(1)	1	0.77
K	0	0	0	1.69(1)	1	0.23
O	1/2	1/2	0	2.93	3	1
			$Ba_{0.57}K_{0.43}BiO_3$, R=0.28			
Bi	1/2	1/2	1/2	0.42(3)	1	1
Ba	0	0	0	0.91(6)	1	0.56(3)
K	0	0	0	0.91(6)	1	0.44(3)
O	1/2	1/2	0	1.41	3	1

PHASE TRANSFORMATIONS IN MATERIALS STUDIED BY TOF NEUTRON THERMO-DIFFRACTOMETRY.

A.M.Balagurov and G.M.Mironova
Laboratory of Neutron Physics, JINR, 141980 Dubna, Moscow Reg., Russia

ABSTRACT

On the TOF neutron diffractometer DN-2 at the IBR-2 pulsed reactor in Dubna it is possible to measure the complete powder diffraction pattern in several minutes or sometimes seconds. The wide range of d-spacing is available for diffraction studies together with small angle scattering measurements. In this report the recent results of the real time studies of phase transformation in powders are presented.

INTRODUCTION

It is well known that the powder diffractometer can be optimized in two alternative modes: either high resolution or high intensity. The first kind of instruments is destined mainly for the precision structural studies, whereas the second one is developed for studies of samples that are either very small or are in extreme environments, but mainly for transition phenomena studies by the real-time technique.

At present there are several neutron powder diffractometers which have high $\Delta d/d$ resolution (about 0.001). The best of them such as D2B in ILL and HRPD at ISIS with resolution better than 0.001 became famous owing to very high quality of structural data obtained.

Another kind of instruments - high intensity diffractometers - are not widespread nowadays, there exist two or three instruments which offer the possibility to measure the whole diffraction pattern in several minutes. At the most known of them - D1B in ILL - a lot of the real-time neutron diffraction experiments were performed during the last decade [1].

Since 1985, the real-time diffractometry has been developing on the time-of-flight instrument - the DN-2 neutron diffractometer at the IBR-2 pulsed neutron reactor in Dubna [2]. In a short time a number of experiments were performed and it was shown [3,4] that the TOF-diffractometer is very suitable not only for the reversible phase transition studies, as it was known long ago, but also for the irreversible processes studies. It should be mentioned that there are several plans to build high intensity diffractometers which would offer the possibility to measure neutron powder diffraction spectra within a minute even in seconds time intervals [5], but at present, on our knowledge, the acquisition of the whole neutron diffraction pattern in such a short time is possible at the DN-2 diffractometer only.

DN-2 - TIME-OF-FLIGHT HIGH INTENSITY DIFFRACTOMETER

The design and performance of the DN-2 TOF-diffractometer were described several times elsewhere (see, for example, [6]). The main features of DN-2 are as follows: high total neutron flux (10^7 n/cm^2/s), medium TOF resolution ($\Delta d/d$=0.025/d, where d is in Å), very high signal-to-noise ratio, the possibility to use neutrons with a very long wavelength without overlapping (in real experiments up to 20 Å) due to the low source repetition frequency (5 s^{-1}). The detector system consists of one linear PSD and several ^{3}He counters enclosed in individual shielding and placed at various scattering angles very close to the sample position: the sample-detector distance can be varied from 30 to 130 cm. The high count rate is provided by large beam cross section, S=15·180 mm^2, and large solid angle of the detectors. For example, the count rate of the 90-degree detector is as high as 10^5 n/s for 10 cm^2 cross section sample with 0.2 probability of scattering. The software of RT-experiments includes the special graphics program and the package for the analysis of the diffraction pattern evolution. At the final stage the spectra are analyzed by the Rietveld method. Figure 1 shows an example of the evolution of the neutron diffraction pattern during the thermal treatment of powder $TiD_{0.74}$ and in figure 2 the results of multiphase Rietveld refinement at several temperatures are illustrated.

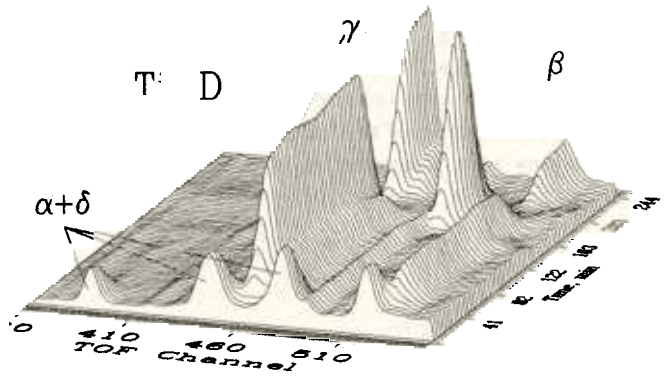

Figure 1. The evolution of the neutron diffraction pattern during the thermal treatment of $TiD_{0.74}$ as measured for d-spacing range 1.7 - 2.7 Å. The sample was heated up from 293 K to 873 K (β -phase) and then cooled down.

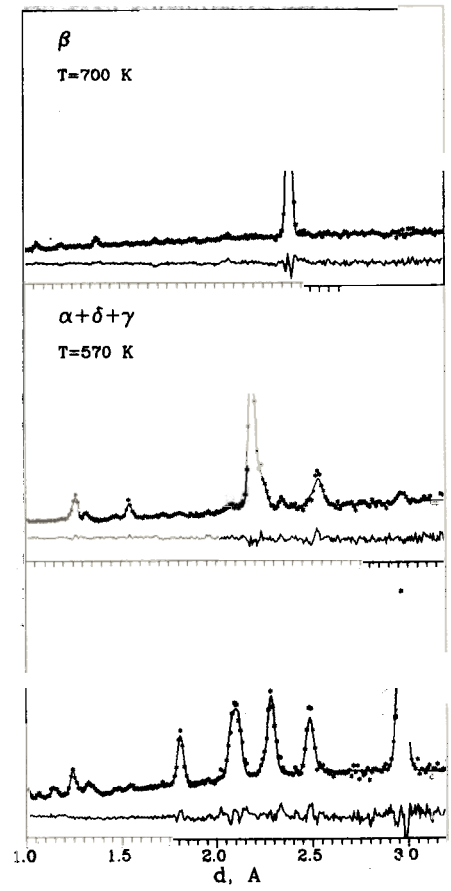

Figure 2. Multi-phase Rietveld analysis of Ti-D diffraction patterns measured at several temperatures. Crystal data of phases are:
α - Ti, $P6_3/mmc$, a=2.965 Å, c=4.634 Å; β - $TiD_{0.74}$, Im3m, a=3.383 Å; γ - $TiD_{1.56}$, Fm3m, a=4.386 Å; δ - $TiD_{0.96}$, Cccm, a=4.164 Å, b=4.232 Å, c=4.573 Å.

EXAMPLES OF APPLICATION

Though the RT neutron diffraction is a relatively new technique, the list of possible applications of the method is already quite long [1,3]. Our practice of DN-2 operation includes: isothermal kinetic study of the reaction between water and calcium aluminate [2], isotope H-D exchange in the lipid multilayer [7], polymorphic transformation in the Ti-D system [8], solid state chemical reaction - formation process of high-T_c Y123 ceramics [9] and some others.
Many of these experiments have been performed in a thermo-diffractometry mode, i.e. when the diffraction pattern was measured at constant time intervals, t_s, the temperature of the sample was continuously varied in a predetermined range along the time scale. The rate of temperature variation was determined by several factors: neutrons count rate, the temperature gradient in the sample, and sometimes by the beam-time available. Typically, in our experiments t_s was between 20 s and 5 min.

Phase transitions of high pressure metastable ice VIII [10]

In ice, as it was shown recently [11], in addition to some crystal phases, two amorphous phases of different density: low (*lda*) and high (*hda*) density, do also occur. These amorphous phases can be extracted from hexagonal ice of high pressure. Another possibility to obtain *lda* and *hda* from the quenched high pressure phase VIII was reported in [12], where a series of transitions were observed: VIII→*lda*→Ic→Ih, here Ic is the cubic phase, Ih is the hexagonal phase. It was suggested that the low density phase, *lda*, was formed from a high density phase, *hda*, but attempts to observe this process had failed.
We studied [10] phase transitions of heavy ice from the quenched phase VIII when heated from 94 to 240 K by the real time neutron diffraction method with the temporal resolution of 5 min to find the transition VIII→*hda*. The sample (99% D_2O, weight 0.3 g), was compressed at room temperature to the pressure of ~ 2.6 GPa, held under those conditions for 1 h to establish equilibrium, cooled down to 100 K and then the pressure was lowered to the atmospheric pressure. Figure 3 shows the sequence of diffraction patterns measured during the heating of this quenched phase. Experimental data show that the initial phase, ice VIII, remains to a temperature of 130 K. At temperatures 130-135 K the diffraction pattern changes dramatically in 5 min.

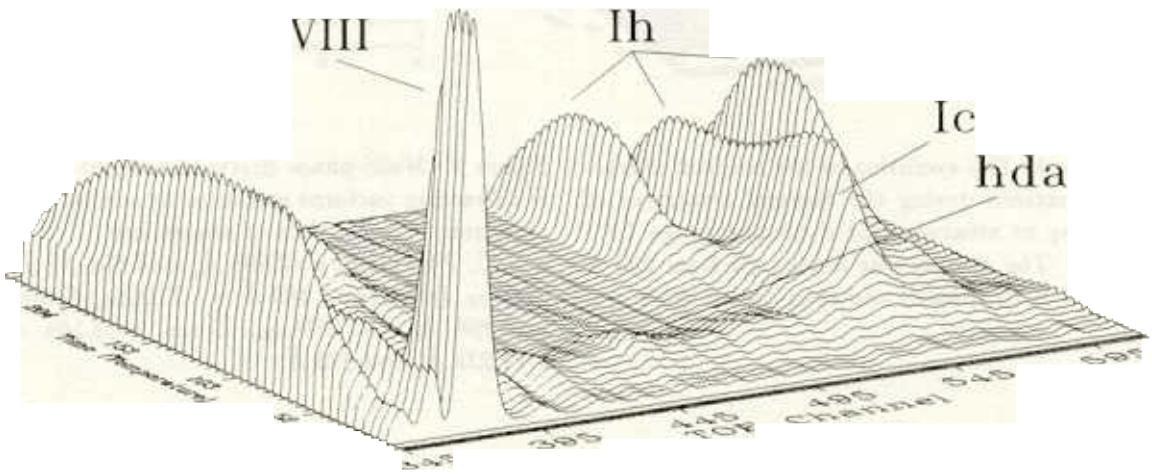

Figure 3. Neutron diffraction patterns of heavy ice in the temperature interval 94 - 290 K The heating was carried out at $\Delta T/\Delta t$=1 deg/min. T=94 K corresponds to zero time.

The narrow peaks corresponding to a crystalline phase of ice vanished and two broad peaks at d_1=3.65 Å and d_2=3.01 Å appeared. The peak with a larger d had a structural feature near 3.85 Å. The values given above are in virtually complete agreement with the values d=3.85 Å and 2.99 Å which were measured earlier for amorphous phases of high- and low-density ice, while d=3.65 Å corresponds to a (111) reflexion for a cubic phase of Ic. The mixture of phases remained to 150-160 K, and at T=160 K a transition to a cubic Ic phase occurred, and later, to the hexagonal one, Ih. The transition Ic→Ih had the complex nature: in the beginning the ordering of D_2O in the basic plane of Ih occurred, then these planes were ordered with respect to each other. Thus, in this experiment the transition of ice VIII to an amorphous ice, *hda*, was observed for the first time. It was also found that amorphous phases of two densities, *hda* and *lda*, can coexist and that the Ic→Ih transition was of a complex nature.

The study of the phase transition in $CuLi_{0.1}V_{0.1}Fe_{1.8}O_4$

The copper ferrite $Fe_{1-\delta}Cu_\delta[Fe_{1+\delta}Cu_{1-\delta}]O_4$ has the inverse spinel structure and appears in two crystal forms: cubic Fd3m at high temperature and tetragonally deformed $I4_1/adm$ with a distortion parameter $\gamma=c/a\sim1.06$ when slowly cooled down to room temperature. The phase transition occurs due to the cooperative Jahn-Teller effect. In the existing theory of this phenomenon parameters δ and γ are related with each other and this relation can be tested in diffraction experiment. A real time neutron diffraction study with temporal resolution of 80 s was performed to examine the tetragonal-cubic phase transition in $CuLi_{0.1}V_{0.1}Fe_{1.8}O_4$ [13]. The sample temperature was varied as shown in figure 4. Figure 5 shows the characteristics of the crystal that were determined by the Rietveld analysis.

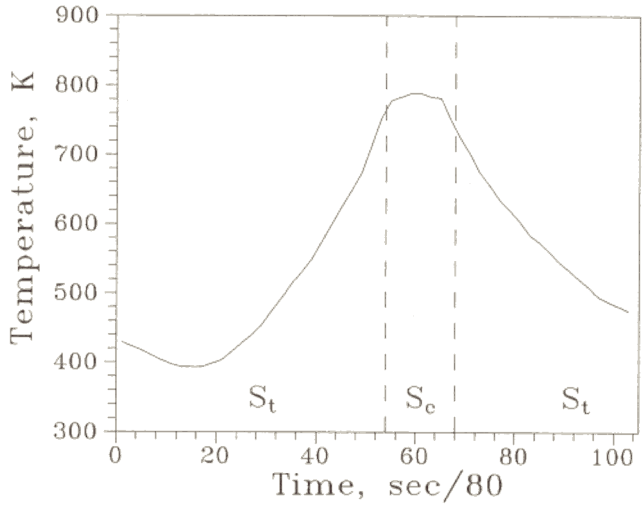

Figure 4. The variation of the temperature during the experiment with the $CuLi_{0.1}V_{0.1}Fe_{1.8}O_4$. The regions are marked where tetragonal (S_t) and cubic (S_c) phases occurred.

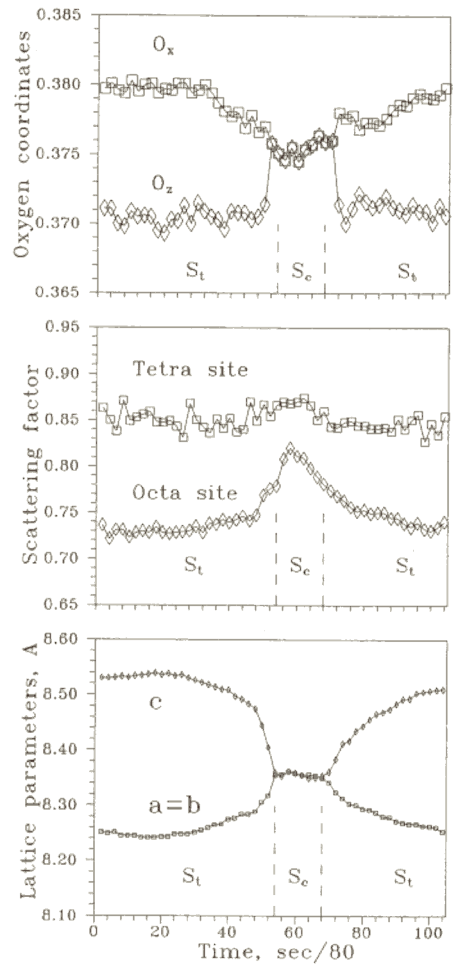

Figure 5. Time (temperature) dependence of: lattice parameters, scattering factors of A- and B-sites and oxygen coordinates of $CuLi_{0.1}V_{0.1}Fe_{1.8}O_4$.

The variation of scattering factors, $g_I = b_I \exp(-B_I \kappa)$, where b is coherent scattering length, B is the temperature parameter, κ is momentum transferred, I indicates octa- (A) or tetrahedrall (B) sites in the unit cell, can be referred to the effect of cation diffusion between A and B sites. This effect is more distinct in figure 6, where the difference of g_A and g_B is shown.

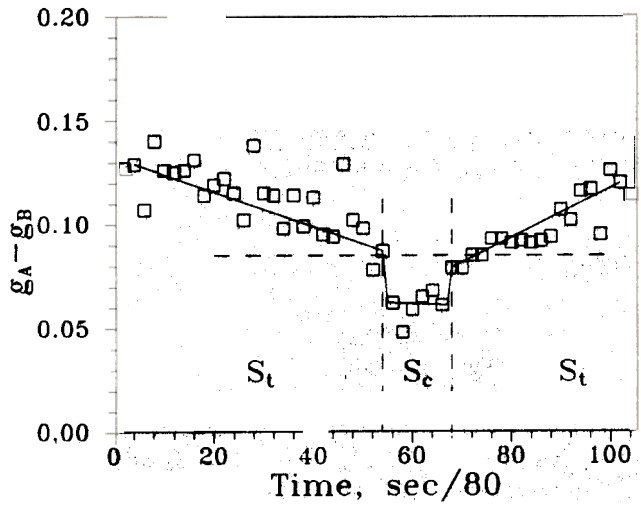

Figure 6. Time (temperature) dependence of the difference between scattering factors of A- and B-sites. The solid lines are guides to the eyes.

The annealing of the melt-quenched $BiSrCaCu_2O_x$ material

One of the most attractive features of TOF diffractometer is its possibility to measure the diffraction pattern and small-angle neutron scattering (SANS) together. An example of the results which can be obtained in a such experiment is shown in figures 7 and 8.

Figure 7. The evolution of the diffraction pattern of the melt-quenched $BiSrCaCu_2O_x$ during heating from 290 K to 1340 K and then cooling down to room temperature. The (002) 12 Å and 15 Å diffraction peaks from (2201) and (2212) phases are clearly seen.

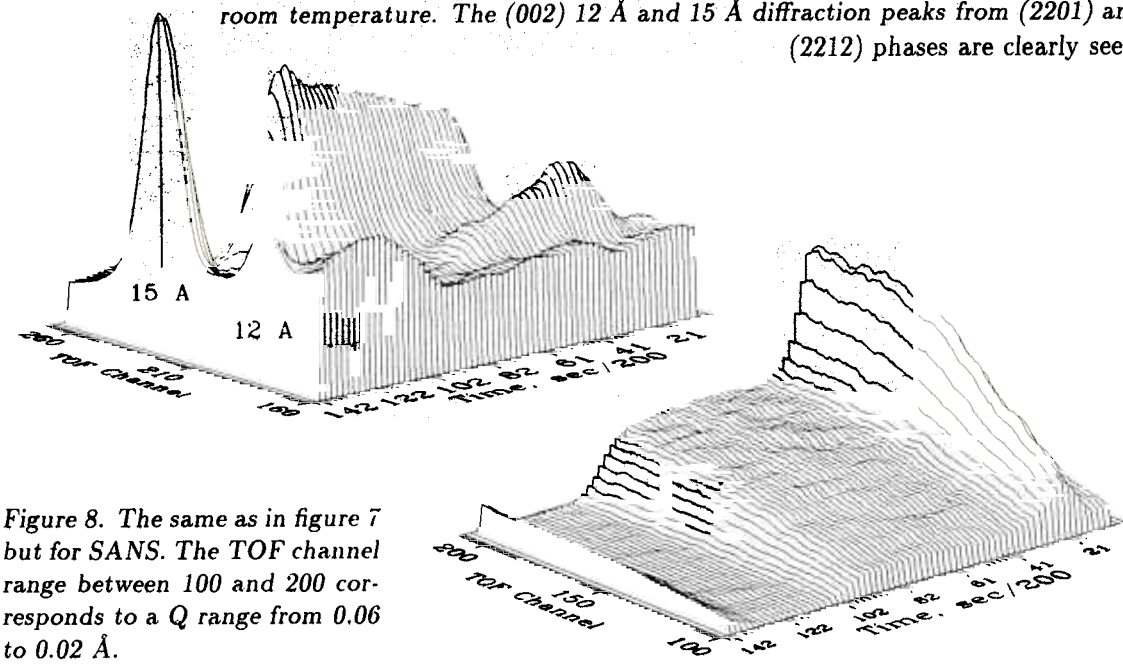

Figure 8. The same as in figure 7 but for SANS. The TOF channel range between 100 and 200 corresponds to a Q range from 0.06 to 0.02 Å.

The sample was the $BiSrCaCu_2O_x$ material melt-quenched from the temperature of 1340 K, heated up to 973 K for 5 h, then melted at 1150 K and cooled down. During the first stage of the annealing for 2 h two well known crystal phases of the Bi-Sr-Ca-Cu-O system were formed sequentially: (2201) and (2212). The (002) diffraction peaks with d=12 Å and 15 Å from the basis plane of that structures are clearly seen in figure 7. Just before the beginning of the (2201) phase formation, significant small-angle scattering arose at the nucleation of this phase (figure 8). During the (2212) phase formation there was no evidence of any nucleation. Only this long-period phase, (2212), was retained after the additional annealing for 3 h. The diffraction pattern and small-angle scattering disappeared after the material was melted. During the cooling down both of crystal phases appeared almost simultaneously, at first (2212), not long after (2201), but SANS intensity remained very low.

CONCLUSION

The real-time studies have good perspectives at the IBR-2 reactor. In principle, it is possible to increase the count rate by several times and thus to obtain the opportunity of studying the transition phenomena in crystals with a time of spectrum acquisition less than one minute. Moreover, in appropriate cases it would be possible to obtain useful information in one pulse (1 ms temporal resolution) of IBR-2 operation [4].

These investigations are supported financially by the Russia Acad. Sci. under the projects 90287 and 91069

REFERENCES

1) Pannetier, J.: in: Chemical crystallography with pulsed neutrons and synchrotron X-rays, edited by M.A.Carrondo and G.A.Geffrey, Dordrecht: Reidel, 1988, 313.
2) Balagurov, A.M., Mironova, G.M.: JINR Rapid Communication, 1986, 19-86, 50, Dubna, Russia (In Russian)
3) Balagurov, A.M., Mironova, G.M., Novozchilov, V.E., Ostrovnoy, A.I., Simkin, V.G., Zlokazov, V.B.: J.Appl.Cryst., 1991, 24, 1009
4) Mironova, G.M.: Proceedings of the EPDIC 1, Material Sc.Forum, 1991, 79-82, 487
5) Jorgensen, J.D., Cox, D.E., Hewat, A.W., Yelon, W.B.: in: Scientific opportunities with advanced facilities for neutron scattering, Shelter Island Workshop, 1984, 45
6) Balagurov, A.M.: Physica B, 1991, 174, 542
7) Balagurov, A.M., Mironova, G.M.: Krystallografia, 1991, 36, 314 (In Russian)
8) Balagurov, A.M., Bashkin, I.O., Kolesnikov, A.I., Malijshev, V.Ju., Mironova, G.M., Ponjatovskij, E.G., Fedotov, V.K.: Fiz.Tverd.Tela, 1991, 33, 1256 (In Russian)
9) Balagurov, A.M., Mironova,G.M.: Sverhprovodimost, 1990, 3, 545 (In Russian)
10) Balagurov, A.M., Barkalov, O.I., Kolesnikov, A.I., Mironova, G.M., Ponjatovskij, E.G., Sinicijn, V.V., Fedotov, V.K.: Pis'ma Zh. Eksp. Teor. Fiz., 1990, 53, 30 (In Russian)
11) Mishima, O., Calvert, L.D., Whalley, E.: Nature, 1985, 76, 314
12) Klug, D.D., Handa, Y.P., Tse, J.S., Whalley, E.J.: J.Chem.Phys., 1989, 90, 2390
13) Balagurov, A.M., Kozlova, E.P., Mironova, G.M., Onyszkiewicz, I.: phys.st.solidi, to be published

TIME-RESOLVED DIFFRACTION AND SMALL ANGLE NEUTRON SCATTERING STUDY OF THERMAL BEHAVIOR OF $YBa_2Cu_3O_{7-x}$ COMPOUND OVER A TEMPERATURE RANGE 900-1470 K.

G. M. Mironova

The use of high-T_c ceramic superconductors for practical applications is limited by their low current densities. It is believed that the low current densities result from the presence of grain boundaries [1], porosity, crystallographic anisotropy of individual grains [2], and cracks resulting from the thermal expansion anisotropy [3]. In order to obtain high critical current densities in bulk forms of YBCO it will be necessary to produce a textured microstructure such that the high j_c directions in the basal plane are aligned in the direction of current travel. Of different methods, directional solidification has been found to produce the highest transport and magnetization j_c values [4]. To develop this technique the knowledge of processes taking place at melting-solidification of YBCO is necessary. It is clear that the knowing of how the second phase material exists in the system is of great importance in order to control the microstructure of YBCO superconductor prepared by melt processing. It is very important also to know if the cracks originate during the solidification process or the subsequent oxygen anneal.

Although there are a lot of investigations on the equilibrium phase diagrams of the ternary Y_2O_3-BaO-CuO system, very little is known about phase transformations of the Y-Ba-Cu-O system near the 1:2:3 stoichiometric composition below and above the melting point.

The objective of our paper [5] was to elucidate the kinetic behavior of $YBa_2Cu_3O_{7-x}$ compound in the course of melting-solidification cycle using direct information about atomic structure and large-scale inhomogeneities in the sample from diffraction spectra and SANS.

The experiment was carried out in real-time mode on the TOF diffractometer DN-2 at the reactor IBR-2 [6]. Two ^3He detectors placed at angles of scattering (2θ) of 170° and 0.8° were available providing diffraction and SANS spectra from the sample every 100 sec. The ceramic sample of $YBa_2Cu_3O_{7-x}$ (T_c ~ 90 K) was placed into the tube furnace and annealed as is shown in Fig. 1(a).

In Fig. 2 (a, b) the time (temperature) evolution of diffraction and SANS spectra in the course of the first melting-solidification cycle is presented. As to diffraction spectra, one can see the sharp transition, resulting in disappearance of the $YBa_2Cu_3O_{7-x}$ compound and appearance of a new crystal phase with very low scattering capacity due to its high dispersity. This phase was identified as "green" phase Y_2BaCuO_5. There are no evidence of another crystal compounds just above the temperature of melting (~1070 °C). Increased incoherent background under diffraction lines indicates the existence of a liquid phase. From earlier studies [7] it may have approximate composition $Y_{0.01}Ba_{0.25}Cu_{0.74}O$. In this part our findings are consistent with the previous data [7,8]. Under subsequent cooling a hysteresis takes place: the solidification occurs at ~970 °C in the same abrupt manner. The quantity of "green" phase diminished but the third crystal phase appeared identified as Y_2O_3. The phase ratio depends on the highest temperature reached in the experiment, the

rate of heating and cooling, the dispersity of initial sample. A number of additional phases were encountered in other our experiments. For the reaction under discussion, the following sequence of phase transformations in the course of melting-solidification is suggested:

$$YBa_2Cu_3O_{7-x} \rightarrow Y_2BaCuO_5 + \textit{liquid} \rightarrow YBa_2Cu_3O_{7-x} + Y_2BaCuO_5 + Y_2O_3$$

Fig. 3 shows the diffraction spectra from the sample before melting (a, b), in the molten state (c) and after solidification (d). The second cycle of melting (T_{max}= 1470 K) - solidification resulted in increase of "green" and Y_2O_3 phases and in decrease of $YBa_2Cu_3O_{7-x}$ phase.

The information about large-scale inhomogeneities provided by SANS is unique and very interesting. In Fig.1(e) one can see abrupt decreasing of SANS at temperatures of ~970 and ~1070 °C. The last effect must be ascribed to melting transition. The first one we attribute to unknown phenomena connected with a small increase of density of the sample and disappearance of a large amount of planar defects (accompanied by oxygen release) which play a crucial role in oxygen transport through the bulk.

There exist numerous data on two thermal effects detectable above 900 °C [9]. Some authors left it unexplained, while others attribute this effect (970 °C in air) to the melting of $BaCuO_2$. We hope that our interpretation is reasonable and correlates with many experimental studies on the J_c dependence versus sintering temperatures. It is well established that the J_c drastically drops in the samples processed at temperatures near 970 °C. Our finding shows that at this temperature on heating a drastic change in a microstructure takes place. After this temperature structural parameters behavior changes as well (Fig.1(b,c)). The lattice parameter *a* becames constant (or even has negative thermal expansion coefficient). The effect at 970 °C is irreversible. A long time is needed for soaking a sample at several temperatures to form the appropriate microstructure again.

References:

1) Ekin J.W.: Adv. Ceram. Mater., 1987, 2, 586
2) Ekin J.W. et al.: J. Appl. Phys., 1987, 62, 4821
3) Keester K.L. et al.: J. Cryst. Growth, 1988, 91, 295
4) Jin S. et al.: Appl. Phys. Lett., 1988, 52, 2074
5) Mironova G.M.: Materials Science Forum, 1993, v. 133-136, pp. 847-852
6) Balagurov A.M., Mironova G.M., ibid, pp. 397-402
7) Clarke D.R. et al.: J. Am. Ceram. Soc., 1989, 72(7), 1103
8) Takada J. et al.: Jap. J. Appl. Phys., 1987, 26, L1707
9) Costa G.A. and Ferretti M.: J. of Less-Comm. Metals, 1990, 157, 77

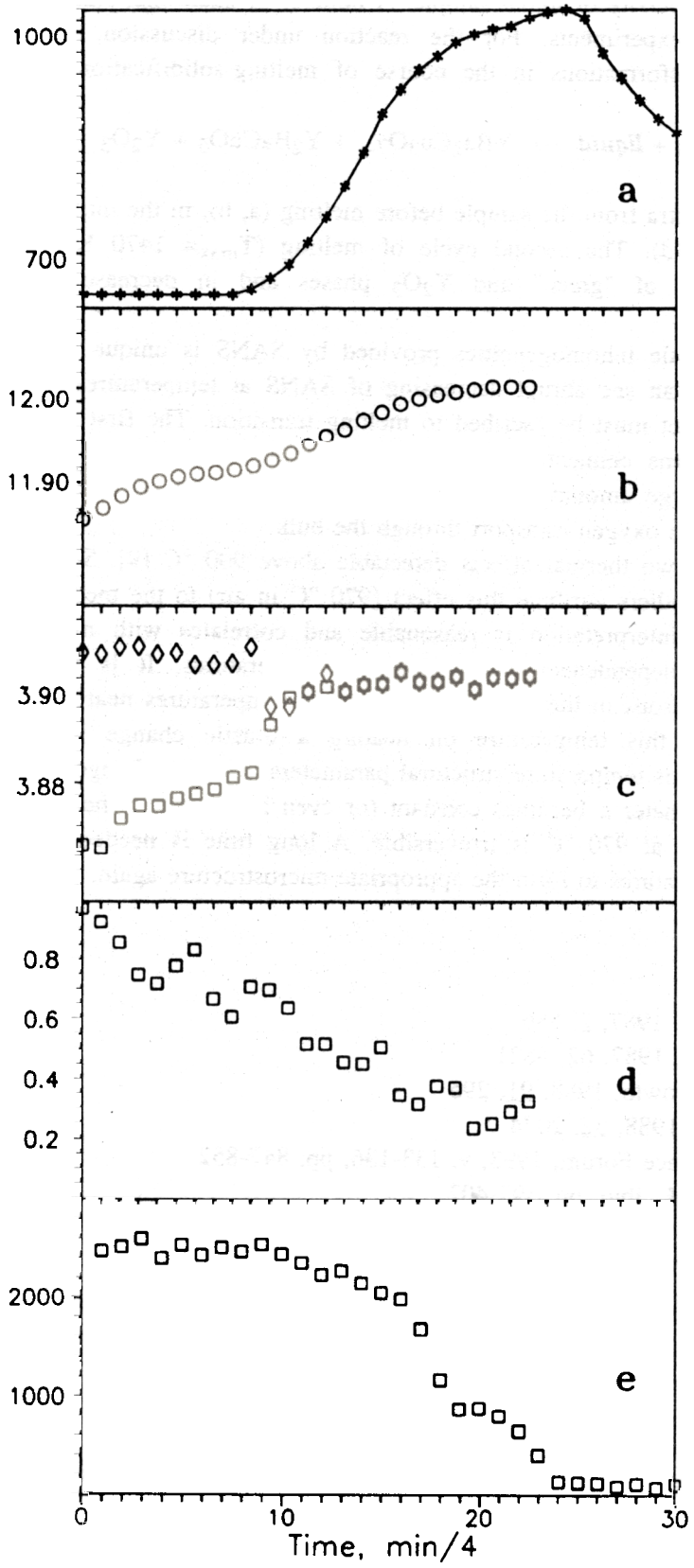

Fig.1(a). Temperature versus time in the course of heating-cooling

Fig.1(b-d). Time-temperature evolution of lattice parameters derived by profile refinement of diffraction spectra

Fig.1(e). Time-temperature evolution of SANS intensity in the vicinity of $Q=0.018$ Å^{-1}

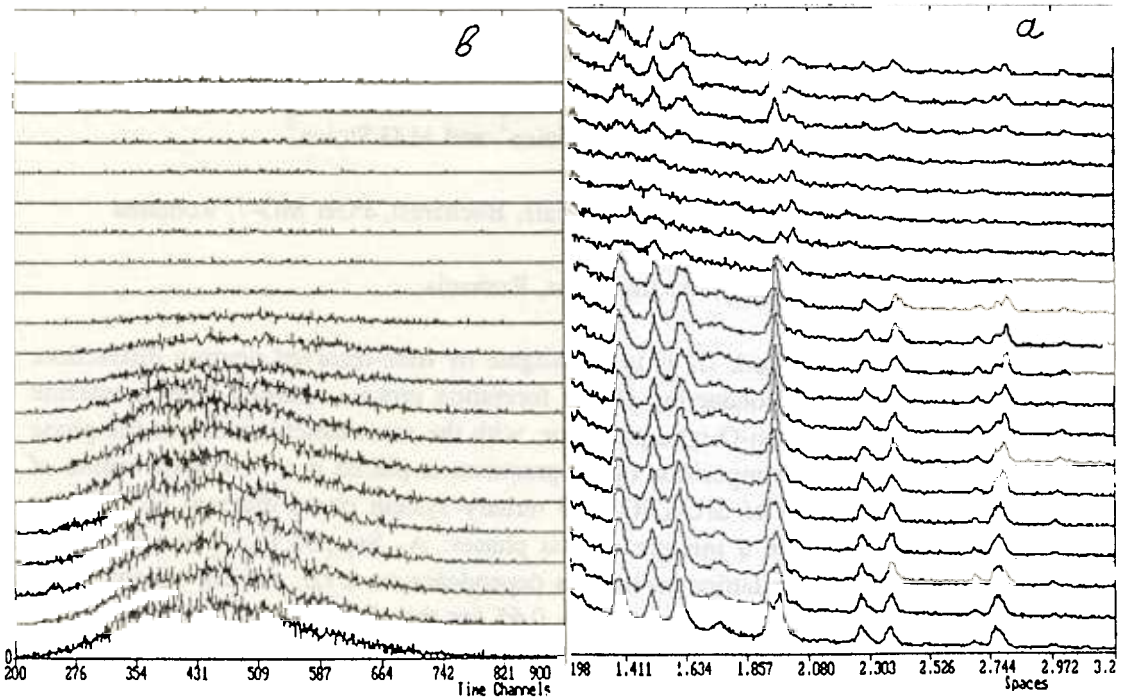

Fig.2. Time-temperature evolution of diffraction and SANS spectra during melting-solidification process.

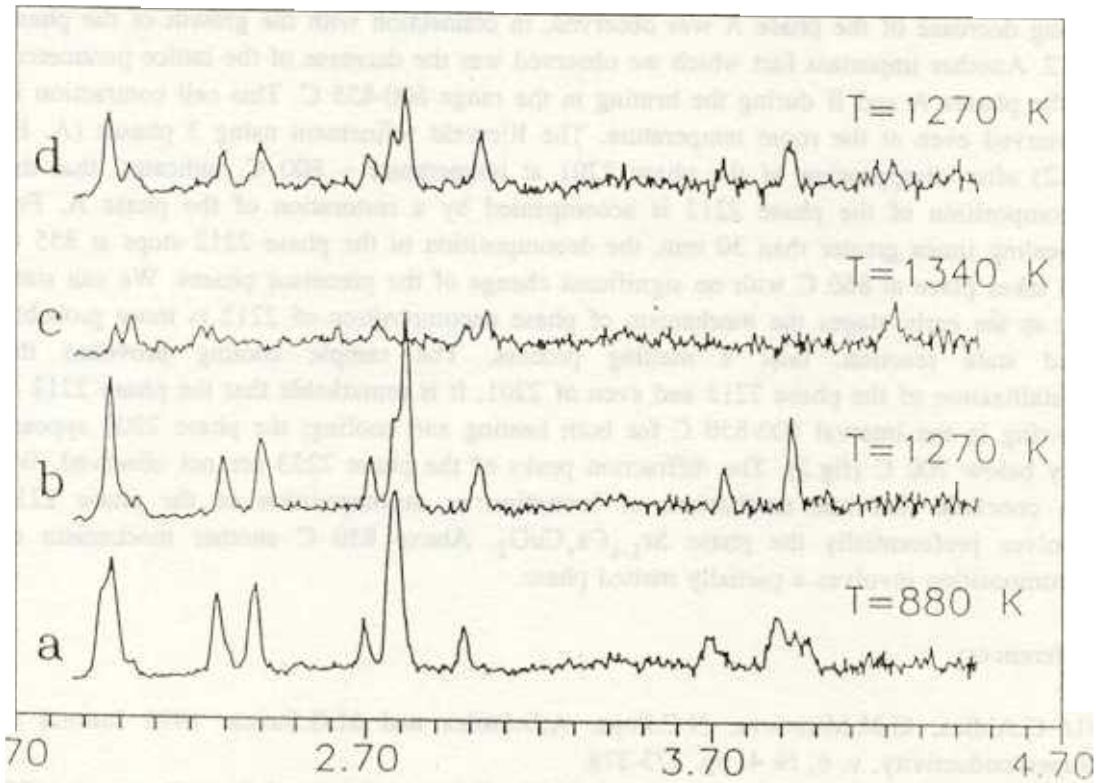

Fig.3. The diffraction spectra of sample before melting (a, b), in the molten phase (c) and after solidification (d)

TIME-RESOLVED NEUTRON DIFFRACTION STUDY OF THE SUPERCONDUCTING PHASE FORMATION PROCESS IN THE Bi(Pb)-Sr-Ca-Cu-O SYSTEM

G.Aldica G.M.Mironova[2], N.C.Popa A.D.Stoica[1] and M.G.Stoica[3]

[1] Institute of Physics and Technology of Materials, Bucharest, POB MG-7, Romania
[2] Laboratory of Neutron Physics, JINR, Dubna
[3] Institute for Electronic Components, Bucharest, Romania

The purpose of the present work /1/ is to investigate by time-resolved neutron diffraction, the early stages of the superconducting phases formation process, starting from a mixture of Bi_2O_3(PbO) and a Sr-Ca-Cu-O type precursor, with the same stoichiometry as the phase 2223. The starting nominal composition of the precursor is placed in a two-phase region of the room temperature action of SrO-CaO-CuO ternary system phase diagram /2/. By this reason the precursor must be a mixture of two phases: A- $Sr_{1-x}Ca_xCuO_2$ and B- $Sr_{2(1-x)}Ca_{2x}CuO_3$. Considering the lattice parameters dependence on x /2/, we can conclude that the value of x is ~ 0.35 for the phase A and ~ 0.65 for the phase B. The resulting Sr-Ca-Cu-O compound was mixed with Bi_2O_3 and PbO powder. The nominal cation ratio was Bi:Pb:Sr:Ca:Cu=1.7:0.3:2:2:3. This material was examined by neutron diffraction in the course of heating to observe the phases evolution. After appearance of the phases 2201 and 2212 (fig.1), the Rietveld refinement with four phases (A, B, 2201, 2212) was used. A strong decrease of the phase A was observed, in connection with the growth of the phase 2212. Another important fact which we observed was the decrease of the lattice parameters of the phases A and B during the heating in the range 800-855 C. This cell contraction is conserved even at the room temperature. The Rietveld refinement using 3 phases (A, B, 2212) after disappearing of the phase 2201 at temperature ~ 800 C, indicates, that the decomposition of the phase 2212 is accompanied by a restoration of the phase A. For annealing times greater than 30 min, the decomposition of the phase 2212 stops at 855 C and takes place at 860 C with no significant change of the precursor phases. We can state that in the early stages the mechanism of phase decomposition of 2212 is more probable solid state reaction, later a melting process. The sample cooling provokes the crystallization of the phase 2212 and even of 2201. It is remarkable that the phase 2212 is growing in the interval 800-850 C for both heating and cooling; the phase 2201 appears only below 700 C (fig.2). The diffraction peaks of the phase 2223 are not observed. We can conclude that one mechanism of formation or decomposition of the phase 2212 involves preferentially the phase $Sr_{1-x}Ca_xCuO_2$. Above 850 C another mechanism of decomposition involves a partially melted phase.

References:

/1/ G.Aldica, G.M.Mironova, N.C.Popa, A.D.Stoica and M.G.Stoica. 1993 Journal of Superconductivity, v. 6, № 4, pp. 273-278.
/2/ Liang Jingkui, Chen Zhan, Wu Fei and Xie Sishen. 1990 Solid State Commun. v.75, p. 247.

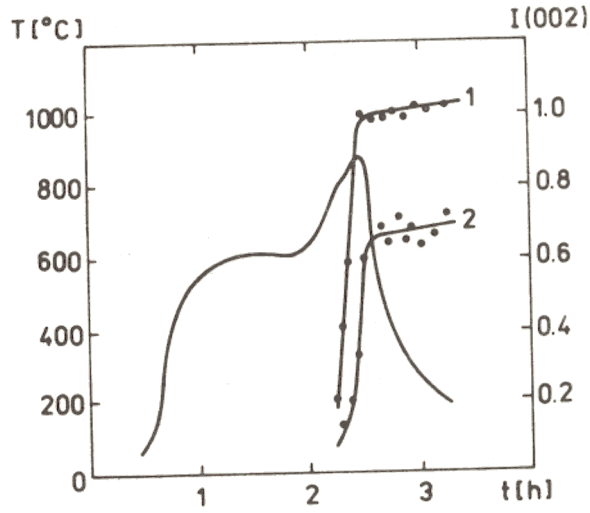

Figure 1. Time dependence of the sample temperature (left scale) and the integral intensity of the (002) peak (right scale) for the first series of measurements.
(1) 2201 phase; (2) 2212 phase.

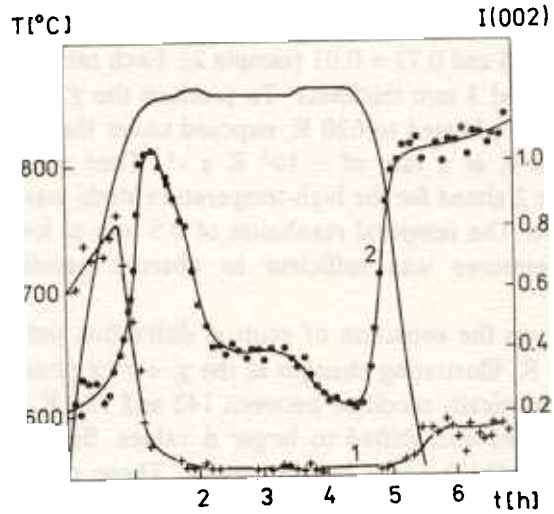

Figure 2. Time dependence of the sample temperature (left scale) and the integral intensity of the (002) peak (right scale) for the second series of measurements.
(1) 2201 phase; (2) 2212 phase.

A Real - Time Neutron Diffraction Study of Phase Transitions in the Ti-D System After High- Pressure Treatment

A.I.Kolesnikov[1], A.M.Balagurov[2], I.O.Bashkin[1], V.K.Fedotov[1], V.Yu.Malyshev[1], G.M.Mironova[2], and E.G.Ponyatovsky[1]

1 Institute of Solid state Physics, Russian Academy of Science, Russia
2 Frank Laboratory of Neutron Physics, JINR, Russia

The present real-time study of phase transitions in pressure-treated Ti-D 0.75 was carried out by simultaneous measurement of neutron diffraction and SANS. The total sequence of structural transformations

$$\chi \rightarrow \kappa + (\tilde{\alpha}) \rightarrow \gamma + \tilde{\alpha} \rightarrow \alpha + \delta = \beta \qquad (1)$$

was investigated (only last one is reversible), and most structures were further detailed. We parenthesize the $\tilde{\alpha}$ phase after the first transition to indicate that this phase was not a product of the transition, but arose during further evolution.

Two samples were prepared by reaction of high-purity titanium with gaseous deuterium from thermally decomposed TiD 2. To obtain fine-grained polycrystalline deuterides and to reduce their texture, the titanium rod was cold rolled by ~70% before hydrogenation. Deuterium content was determined from weight gain, and it was x=0.74±0.01 (sample 1) and 0.73 ± 0.01 (sample 2). Each sample consisted of 10 discs of 6.7 mm diameter and 3 mm thickness. To produce the χ phase, the samples were compressed to 60 kbar , heated to 620 K, exposed under these conditions for 10 min and quenched to 80 K at a rate of ~ 10^3 K s -1. Then pressure was lowered to atmospheric. Sample 2 aimed for the high-temperature study was air-heated from 77 K to room temperature. The temporal resolution of 0.5 min at low temperatures and 1 min at high temperatures was sufficient to observe peculiarities of the phase transformations.

Figure 1 shows the evolution of neutron diffraction patterns and SANS over interval 137 to 240 K, illustrating changes at the $\chi \rightarrow \tilde{\alpha} + \gamma$ phase transformation. The diffraction pattern drastically modified between 142 and 151 K. Peak (111) decreased in intensity by ~5 times and shifted to larger d values. Simultaneously, superlattice reflections (110) and (112) arose in the pattern. These changes in the diffraction pattern can be explained by displacement of deuterium from octahedral to tetrahedral sites concomitant with ordering on alternate {110} planes and increase in volume of the unit cell. Further modifications of the diffraction spectrum displayed structural and chemical changes within the κ phase and its discontinuous transformation to the γ phase. Drastic changes in microstructure occurred at 215 K, as is seen from evolution of SANS spectra. It is possible to connect this effect with better resolved (002), (200) and (020) peaks. The anomalous temperature behavior of lattice parameters seems to indicate strong D-D interaction in κ and γ phases.

Evolution of the neutron diffraction pattern from TiD 0.73 measured on heating from 480 to 760 K followed by cooling to 515 K is shown in Figure 2. It is

seen that the crystal structure of $\tilde{\alpha}$ Ti in ($\tilde{\alpha}$+γ)-TiD 0.73 prepared by rapid heating of the χ phase to room temperature differed from that of α-Ti, but gradually approached the latter eutectoid transformation in the single-phase state, the β phase, where deuterium occupied only tetrahedral interstitial positions in the BCC metal sublattice. The reverse transformation to the α+δ state took place on cooling. As is seen from SANS measurements, precipitated α-Ti had much larger grain size compared to $\tilde{\alpha}$-Ti and α-Ti precipitated on heating the high- pressure χ phase. For more details see /1/.

References

[1] A.I.Kolesnikov, A.M.Balagurov, I.O.Bashkin, V.K.Fedotov, V.Yu.Malyshev, G.M.Mironova, and E.G.Ponyatovsky. J.Phys.: Condens. Matter 5 (1993) 5045-5058

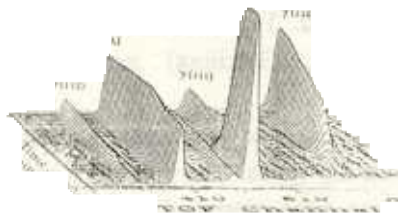

Fig.1. Evolution of the neutron diffraction pattern from $TiD_{0.74}$ (sample 1) measured at the angle $2\vartheta = 152^o$ during the χ to $\alpha + \gamma$ transformation on heating (time interval t_1 to t_2 in figure 2a, i.e. $T = 130$ to $300K$). Numbers of the time-of-flight (TOF) channels are proportional to neutron wavelengths and interspace distances.

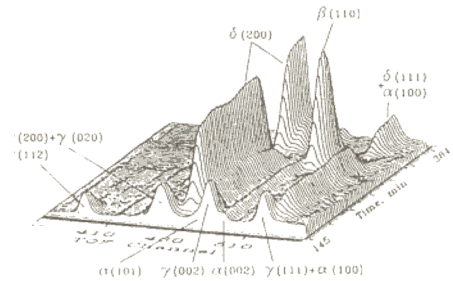

Fig.2. Evolution of the neutron diffraction pattern from $TiD_{0.73}$ measured at angle $2\vartheta = 160.8^o$ on heating from 480 to 760 K followed by cooling to 515 K (time interval t_1' to t_2 in figure 2b). Representative peaks only are indicated.

PECULIARITIES OF LOW TEMPERATURE PHASE IN $PbMg_{1/3}Nb_{2/3}O_3$

A.M.Balagurov S.B.Vakhrushev[2], A.A.Naberezhnov[2], B.N.Savenko[1]

- JINR, Dubna; 2- FTI, St.-Petersburg

ABSTRACT

In recent years the phase transitions and structure of low temperature phases in the disordered perovskitelike compounds have been the subject of intensive experimental investigations, but their macroscopic nature and the role of structural disorder are not understood yet. A crystal $PbMg_{1/3}Nb_{2/3}O_3$ (PMN) belongs to this class of disordered system. In PMN nonisovalent ions (Mg^{2+} and Nb^{5+}) are randomly distributed in crystallographically equivalent positions. This random charge distribution generates local electric fields randomly distributed in strength and direction as well as random interaction between dipole moments. This paper presents the results of neutron scattering measurements on PMN in temperature range from 300K to 90K and in applied along [110] direction electric field. The measurement have been performed on triple axis spectrometer "Neutron-3" (PNFI, Gatchina) and on neutron diffractometer DN-2 (JINR, Dubna).

It was confirmed the existence of two types of quasielastic scattering (QES) in the vicinity of Bragg's reflections of (2h+1 2k+1 2l) and (2h 2k 2l) types. The intensity of the first increased strongly with a fall of the temperature and two-dimensional distribution of QES intensity revealed a transversal character of scattering relatively the reciprocal lattice vector. On the contrary in the second case the QES intensity was temperature independent and longitudinal. Under applied electric field it was found that the Bragg' s intensity increased with an increase of field. On other hand the first part of QES (in particular in vicinity of (110) and (330) reflections) decreased with the increase of electric field. For the temperature below the FC and ZFC splitting points [1,2] we observed a threshold value of applied electric field for the (330) Bragg's peak intensity and QES in vicinity of this reflection. For example at 180K and electric field $\approx 6.5 \cdot 10^3$ V/m Bragg's peak intensity achieved practically a saturation and the first part of QES was completely suppressed. It is necessary also to point out that the (600) Bragg's peak intensity increases faster than the intensities of (200) and (400) reflections when the temperature decreases. This fact enables us to confirm that the growth of Bragg's peak intensities is not concerned with the extinction effects. So the obtained data allow to do the following conclusion:

- the observed transversal QES is the critical scattering is concerned with the ferrofluctuations in PMN crystal;
- the dependencies of Bragg's peak intensity and intensity of critical scattering have a thresholdlike character;
- the second part of observed QES is a Huang's scattering;
- an absence of critical scattering in vicinity of (2h 2k 2l) reflection only, a suppression of this scattering (and a growth the Bragg's peaks intensities) in applied external electric field allow us to confirm that as into in PMN there are random shifts of ions from their symmetrical positions.

References:

1. Vakhrushev S.B. et al. 1989 Phisica B 156 & 157 90
2. Vakhrushev S.B. et al. 1990 Ferrelectrics 90 173

MELTING - FREEZING OF THE METALLIC MERCURY IN THE POROUS GLASS

S.B.Vakhrushev[1], Yu.A.Kunzerov[1], A.A.Nabereznov[1], B.N.Savenko[2]

1 - A.F.Ioffe Phys.-Tech. Institute, St.-Petersburg, Russia
2 - FLNP JINR, Dubna, Russia

In a recent time a considerable interest has appeared for the investigation of the physical properties of ultradispersive materials. One of most peculiar parts is related to studies of the phase transformations in micropaticles. It is clear that phase transition should be destroyed in the limit of extremely small size. In present paper we are discribing the results of the investigation of the liquid-solid phase transition in the ultradispersive mercury obtained by filling of the porous glass with metallic mercury. The distribution function of the porus size was measured by mercury porosimetry. It was shown that in our samples distribution was quite narrow with average porus size of about 70Å. The glass was filled with Hg at high pressure and after pressure removal nearly 95% of mercury remained inside glass. Sample size was ~0.5x0.5x2 cm^3. It was placed in the close cycle refrigerator. Temperature was controlled with the precision of about 0.5K and temperature gradient along the sample was of the same order of magnitude. Neutron diffraction measurements were performed on the DN-2 TOF difractometer with point detector, placed at angle $2\theta=150$.

At room temperature no diffraction peaks were observed. In cooling solidification started at 205K resulting in the appearance of Bragg peak. The intensity of the peaks I(T) was increasing with temperature decrease indicating probably the increasing of the concentration of solid phase - Fig.1. At T<100K the saturation of I(T) dependency was observed. The low temperature diffraction pattern exactly coincided with the diffractogramm of the bulk mercury, but all peaks were broadened. One should mention that the widening should exists both for the independent Hg clusters with 70Å diameter and for fractal cluster consisting of the connected microregions, but the exact lineshape should be different. In the present work the lineshapes were not studied because of relatively poor instrumental resolution. The measurements in the heating regime have revealed extremely large hysteresis of the I(T) dependency. At the moment the physical nature of the hysteresis is under discussion as well as "diffuseness" of the I(T) in the cooling branch and "sharpness" at the heating branch. These phenomena would be discussed in more detailed in the foregoing paper. At present time we would like to mention that results of neutron experiments exactly correspond to the results of the specific heat measurements on the same samples as it be easily seen from Fig.2.

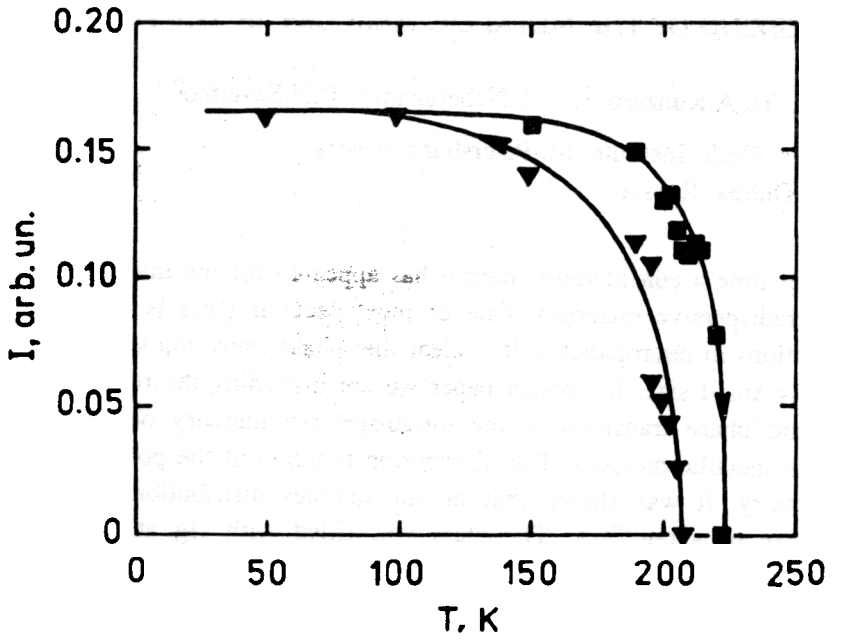

Fig. Temperature dependency of (110) diffraction peak intensity during cooling and heating.

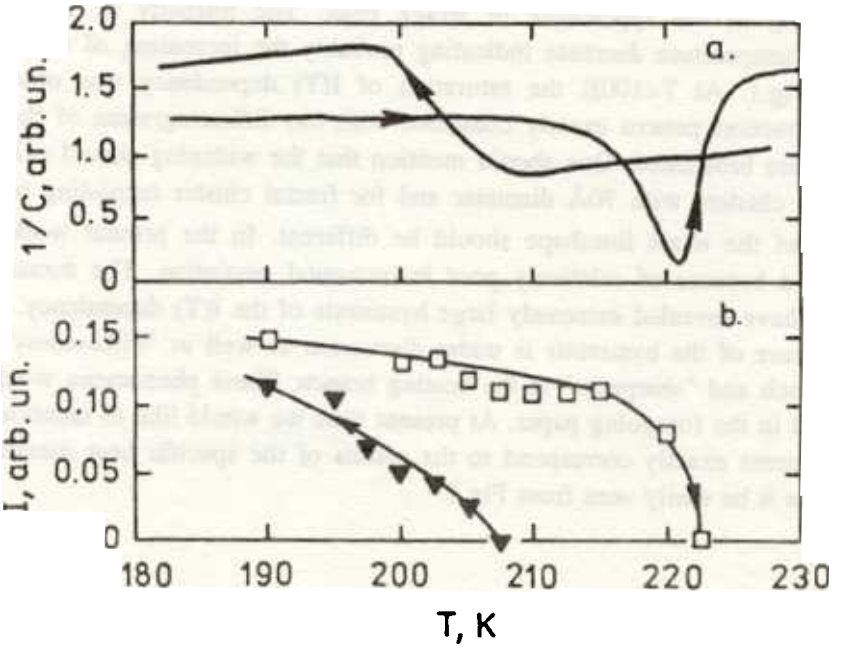

Fig.2 a) Temperature dependence of the inverse specific heat.

b) Temperature dependence of the (110)peak intensity in the transition region.

THERMAL DIFFUSE SCATTERING IN $Sr_xBa_{1-x}Nb_2O_6$.

F.Prokert[a], B.N.Savenko[b], A.M.Balagurov[b]

a) - Research Center Rossendorf, IIM, Germany
b) - FLNP JINR, Dubna, Russia

At the time-of-flight spectrometer DN-2, installed at the pulsed reactor IBR-2 in Dubna $Sr_xBa_{1-x}Nb_2O_6$ mixed single crystals (SBN-x) of different compositions ($0.50 \leq x \leq 0.75$) were investigated between 15 K and 773 K. The diffraction pattern along [001] at the scattering plane (110) and (100), respectively, were found to be strongly influenced by the thermal diffuse scattering (TDS). The appearance of the TDS from the long-wavelength acoustic modes of vibration in single crystals is characterized by the ratio of the velocity of sound c_s to the velocity of neutron v_n [1]. Due to the nature of the TOF Laue diffraction technique used on DN-2, the TDS around a Bragg peak has a rather complex profile. An understanding of the TDS close to Bragg peaks is essential in allowing the extraction of the diffuse scattering occuring at the diffuse ferroelectric phase transition in SBN crystals.

There are three regions of v_n to be considered in calculating the nature of this scattering. If $c_s < v_n$, the TDS rises to a maximum at the Bragg peak and scattering is allowed at all points in the reciprocal space. If $c_s > v_n > c_s \cos\theta$, where θ is half the scattering angle, the TDS rises to a steep maximum on either side of the Bragg peak at θ_B and scattering between these maxima is forbidden [2]. Finally, if $c_s \cos\theta > vn$, there is *one maximum* only, and this is associated with *phonon annigilation* for $\theta > \theta_B$ and *phonon creation* for $\theta < \theta_B$.

The third region, already studied in barium fluoride [3] on SXD at ISIS, has been examined now using SBN crystals and the results agree with the theoretical predictions.

Fig.1 is a contour plot near $2\theta = 90$, showing scattering close to the reciprocal lattice point (002). The TDS occurs only on one side of the Bragg peak, which is characterized by the TOF and the Bragg angle θ_B. TDS appears at shorter TOF than t_B if $\theta < \theta_B$ and longer TOF if $\theta > \theta_B$. From the curve calculated for the central position of the TDS [3] we get $c_s = 2.90\ kms^{-1}$. This value is not far from $3.16\ kms^{-1}$ determined from the elastic constant $c_{44} = (5.2+0.5)\ 10^{10}\ Nm^{-2}$ (and the density $\rho = 5.2\ gsm^{-3}$) for the elastically isotropic case which is approximately given here.

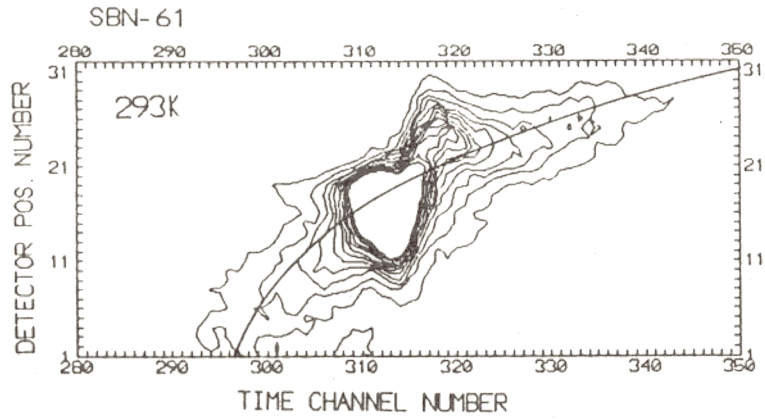

Fig.1 Contour plot of (002) reflection of SBN-61 around $2\theta = 90°$ on DN-2. The detector positions 1 - 32 cover the 2θ - range 83.9° - 96.1°. Time channal width 64 μs.

References

[1] P.Schofield and B.T.M.Willis, *Acta Cryst.* A43, 803-809 (1987)

[2] C.J.Carlile and B.T.M.Willis, *Acta Cryst.* A45, 708-715 (1989)

[3] C.J.Carlile, D.A.Keen, C.C.Wilson, and B.T.M.Willis, *Acta Cryst.* A48 826-829 (1992)

STUDY OF ANTIFERROMAGNETIC ORDERING IN $HoFeO_3$ INDUCED BY AN EXTERNAL MAGNETIC FIELD.

S.A.Buiko, K.Krezhov, V.V.Nietz, G.Pasazhov, A.P.Sirotin

Frank Laboratory of Neutron Physics

Diffraction measurements using a single-crystal sample placed in a pulsed magnetic field to study the earlier observed effect of antiferromagnetism induced in rare-earth sublattices have been continued.

In $HoFeO_3$ four sublattices of iron ions experience antiferromagnetic ordering along the c-axis (a, b, c – are three orthogonal axes of the orthorhombic cell) and holmium ions are in paramagnetic state. Under the action of magnetic field (along the b-axis) the antiferromagnetic ordering of four Holmium sublattices along the a-axis, perpendicular to the applied field, is induced. Besides that the antiferromagnetic ordering in iron sublattices occurs also along the a-axis, however with the alternation of the signs of magnetic moments, different from that of the main antiferromagnetism.

Though the appearence of additional components of antiferromagnetic ordering in the applied magnetic field is necessarily determined by crystal symmetry, their quantitative values, which are first of all dependent on antisymmetric exchange interactions Fe-Fe and Fe-Ho, have not been calculated yet.

The diffraction reflections (102), (104), (201), (302), which are not present in the initial state have been measured. As an example a series of neutron-diffraction patterns for (102) is given in Fig.1 for the magnetic field pulse amplitude of 77 Oe and the indicated temperatures. The time dependence on magnetic field (in relative units) is shown here too.

The results of processing neutron-diffraction patterns for (102) and (201) measured at the temperature of 93 K is given in Fig.2. The (201) peak is determined by the antiferromagnetic ordering of only holmium ions, and the (102) peak — by the insertion of iron and holmium ions. Comparison of these data shows that the antiferromagnetism is induced in both subsystems along the a-axis. The temperature dependence on holmium "antiferromagnetic susceptibility" is represented in Fig.3.

The theoretical analysis of the obtained data will allow to determine a number of essential constants for antisymmetric Fe-Fe and Fe-Ho exchange interactions.

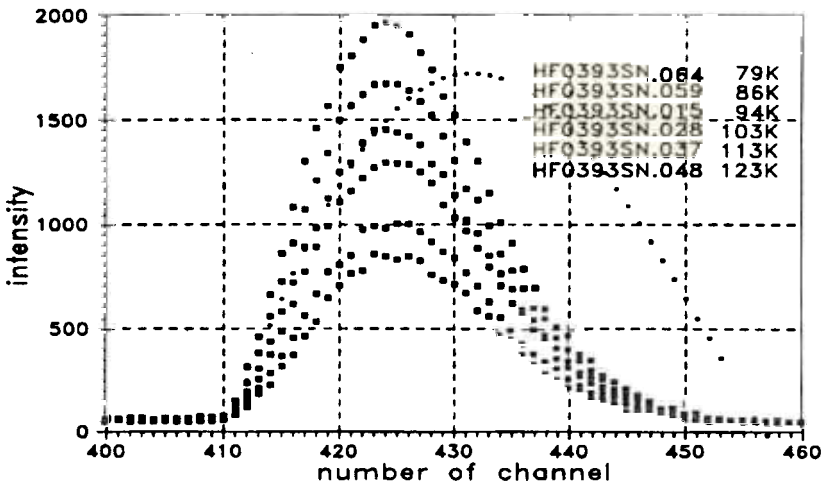
2000
1500
1000
500
0
intensity
400
410
420
430
440
450
460
number of channel
HF0393SN.064 79K
HF0393SN.059 86K
HF0393SN.015 94K
HF0393SN.028 103K
HF0393SN.037 113K
HF0393SN.048 123K

Fig.1.

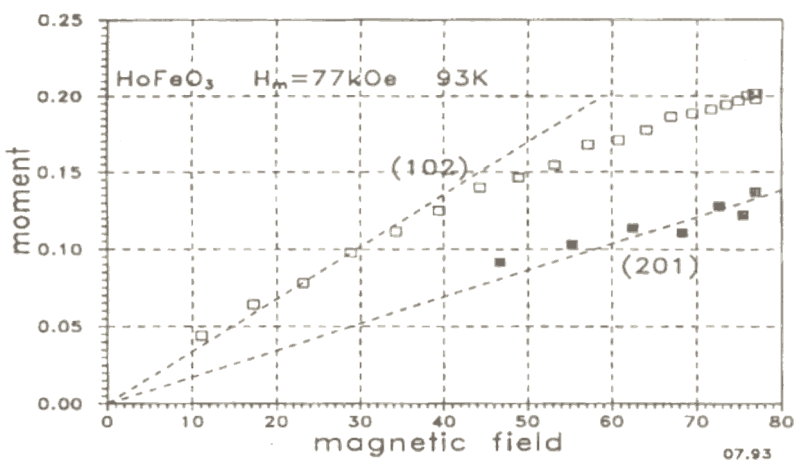
0.25
0.20
0.15
0.10
0.05
0.00
moment
HoFeO3 Hm=77kOe 93K
(102)
(201)
0
10
20
30
40
50
60
70
80
magnetic field
07.93

Fig.2.

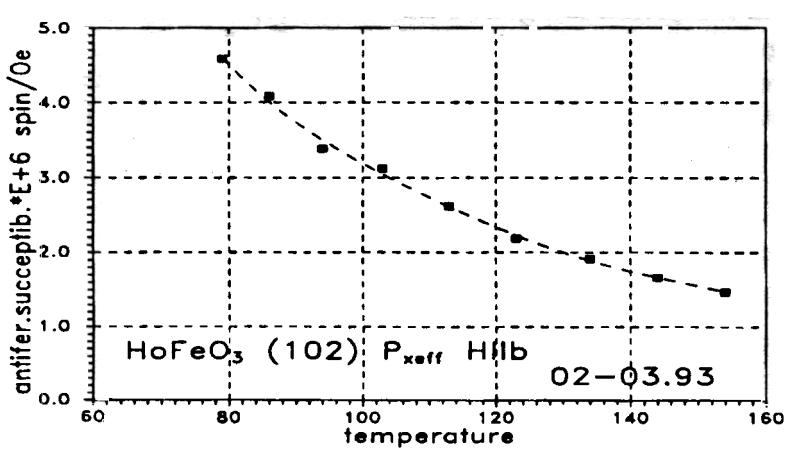
5.0
4.0
3.0
2.0
1.0
0.0
antifer.succeptib.*E+6 spin/Oe
HoFeO3 (102) Pxeff Hllb
02-03.93
60
80
100
120
140
160
temperature

THE PHASE DIAGRAM OF HEMATITE IN AN EXTERNAL MAGNETIC FIELD

V.V.Nietz

Frank Laboratory of Neutron Physics

In connection with measuring hysteresis phenomena following spin-flop transition in antiferromagnetics with uniaxial anysotropy with the SNIM-2 spectrometer, the phase diagram of hematite (α-Fe_2O_3) in an external magnetic field has been calculated. We could assume that the maximum width of the experimental hysteresis loop is directly connected with the magnetic field range within the limits of metastability for two possible phase states in the spin-flop transition. This range, in its turn, is determined by the ratio of the 1st and 2nd constants of anisotropy. The phase diagram calculation with the known values of these constants shows that the experimental hysteresis loop width is at least twice less than the calculated one.

In addition, on the phase diagram some peculiarities have been found which are not encountered in other cases of phase transitions. The section of this diagram for certain values of anisotropic constants is shown in Figure 1. The complication of the phase diagram is caused by the emergence of one more phase state (III) besides two basic ones (I and II). In the figure: C is a critical point of the first-order phase transition between the states I and III, $TC2$ is a tricritical point which unlike typical cases is not connected with the first-order transition line. In the $(TC2-C)$ interval the minimum of the state III originates. In the $(a-C)$ interval the minimum of the state I dissapears (when H_z increases). Over the $(b-c)$ line the minimum of the state II originates so that beginning from the point $TC2$ it also becomes the line of the second-order phase transition between the states II and III. In the interval $(d-F)$ the states I and II and in the interval $(F-C)$ the states III and II satisfy the equilibrium condition. While the anisotropic constant K_1 is decreasing which corresponds to a temperature rise, the points F and C become closer and finally for $K_1 = 156\ Oe$ (at the temperature of 160 K) these points converge into one supercritical point. This anomalous point on the phase diagram unites properties of both critical and tricritical points. The exhibition of specific peculiarities in the behaviour of the system in its vicinity should be expected.

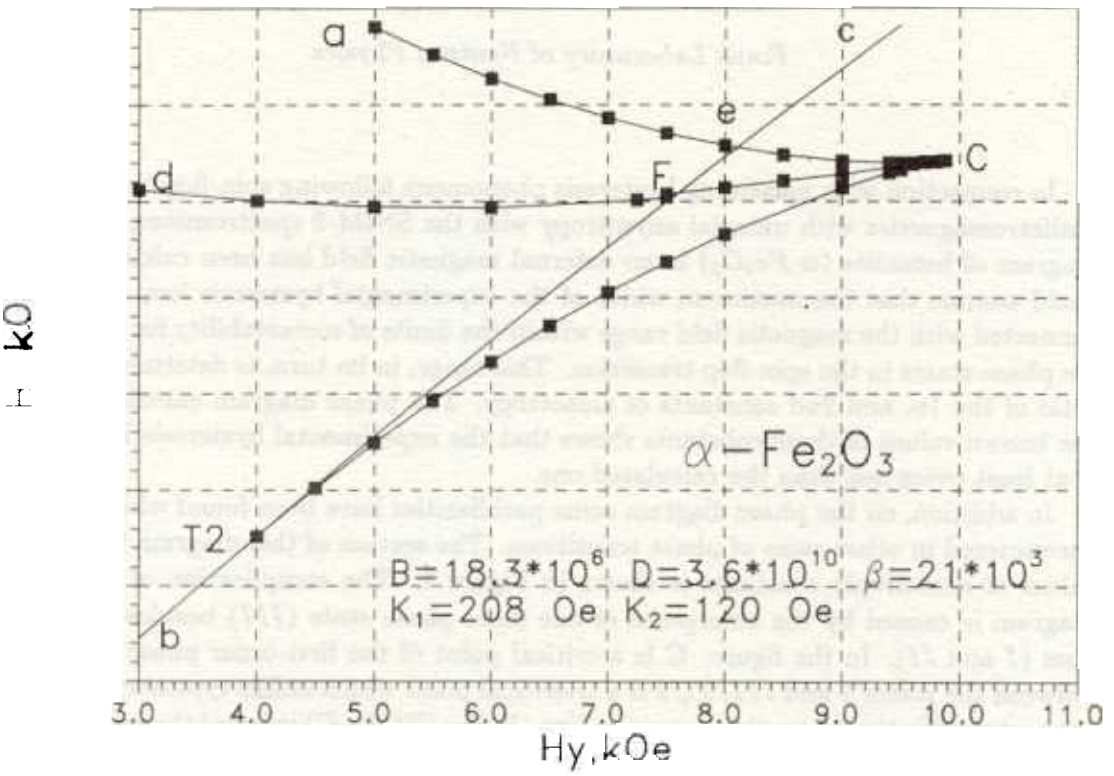
a
c
e
C
d
F
T2
b
$\alpha-Fe_2O_3$
B=18.3*10^6 D=3.6*10^10 β=21*10^3
K1=208 Oe K2=120 Oe
3.0
4.0
5.0
6.0
7.0
8.0
9.0
10.0
11.0
Hy,kOe

Fig.

DIFFRACTION INVESTIGATION OF THE DYNAMIC HYSTERESIS FOLLOWING SPIN-FLOP TRANSITION IN UNIAXIAL ANTIFERROMAGNETICS IN A PULSED MAGNETIC FIELD

D.Georgiev, V.V.Nietz, A.P.Sirotin

Frank Laboratory of Neutron Physics

Investigations of the kinetics of re-orientation spin-flop phase transition in antiferromagnetics with a rhombohedric structure have been continued with the SNIM-2 spectrometer.

The dimensions of Cr_2O_3 and α-Fe_2O_3 single-crystal samples are $5 \times 6 \times 8mm$. Magnetic field pulses have the shape of a half-period sinusoid and the duration of 735 μs on the bottom. The time resolution for transition processes is approximately 4 μs. The crystal basis plane (111) is vertical. The magnetic field is perpendicular to the (111) plane, i. e. it is parallel to the initial direction of antiferromagnetic vector.

Since the observed hysteresis exhibits itself only at a rather fast field change, it is of a dynamic character. The hysteresis can be naturally considered to be the consequence of the coexistence of two states in some definite field range, with one of them being metastable. According to the theory this range is determined by the ratio of the 1st and 2nd anisotropic constants. In the case of Cr_2O_3 it is impossible to compare the experimental data with the theory since it cannot be said with any certainty whether the obtained hysteresis loops are utmost and the 2nd anisotropic constant is unknown either. The phase diagram calculation for α-Fe_2O_3 in a magnetic field has shown that the experimental hysteresis loop width is at least twice less than the calculated range of metastability.

References

[1] D.Georgiev, V.V.Nietz, A.P.Sirotin, A.A.Yakovlev
Temperature and field dependences of neutron scattering intensity at coherent spin-flop transition in Cr_2O_3,
JINR, P14-92-400, Dubna, 1992 (in Russian)

[2] D.Georgiev, V.V.Nitz, A.P.Sirotin
Hysteresis phenomena at spin-flop transition induced by the pulsed magnetic field
JINR, P14-92-401, Dubna, 1992 (in Russian)

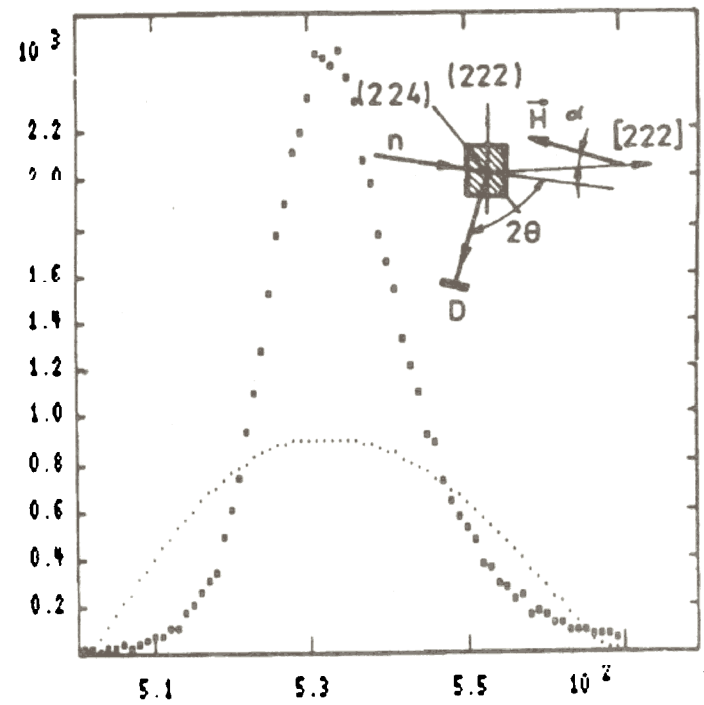

Fig.1 The neutron-diffraction pattern of reflection (224) for Cr_2O_3 at $H = 0$, together with the field pulse. The time channel number is shown on the horisontal axis (the channel width $\tau = 16\mu s$) The geometry of the experiment is also given.

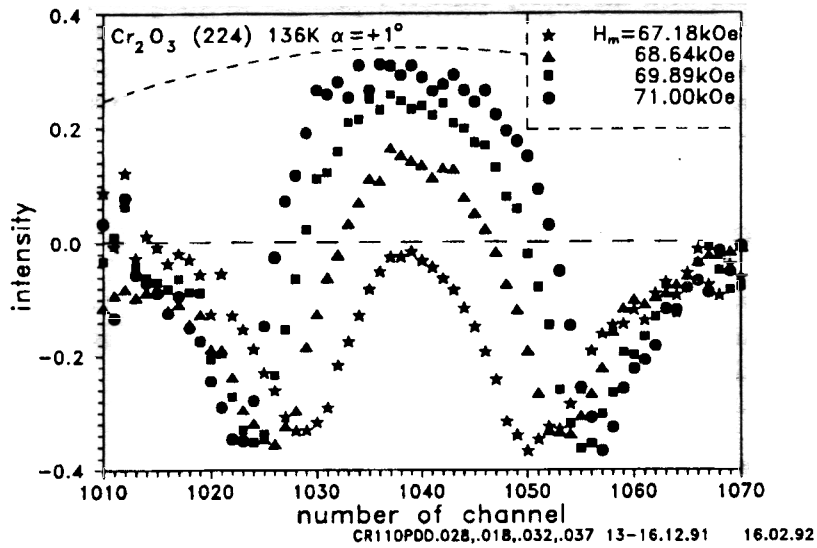

Fig.2 The normalized difference neutron-diffraction patterns $(I_H - I_O)/I_O$ (I_H, I_O – the patterns with and without a magnetic field respectively) for Cr_2O_3 , obtained at $2\Theta = 90°$, the channel width $\tau = 8\mu s$ and the indicated in the insert magnetic pulse amplitudes. The dashed line shows the magnetic field variation in relative units. α – is the angle between the field direction and the anisotropic axis on the horizontal plane, which determines the direction of magnetization rotation at an increase of the field.

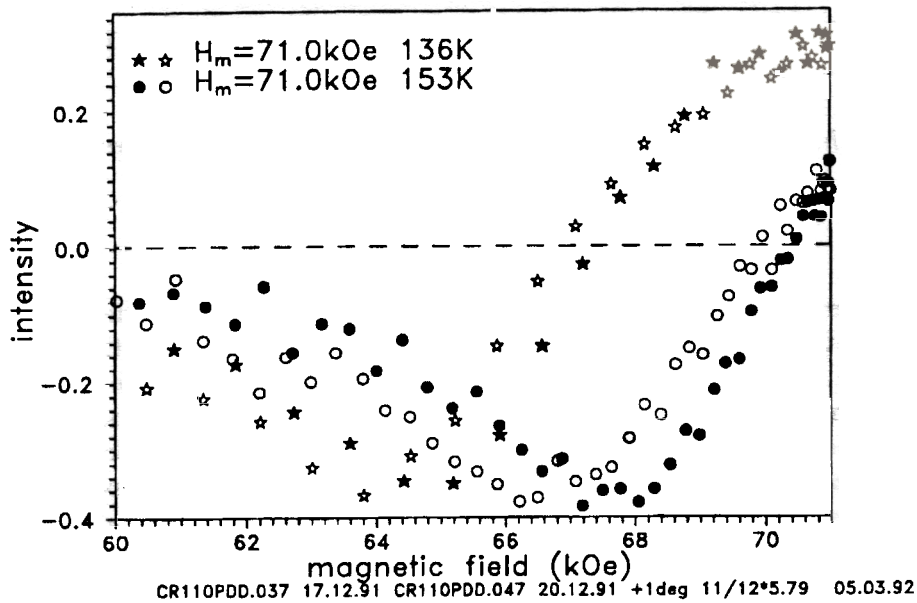

Fig.3 The scattering intensities in dependence on magnetic field value for Cr_2O_3 at two indicated temperatures. Full stars and circles correspond to the field growth and blank – to the field decrease.

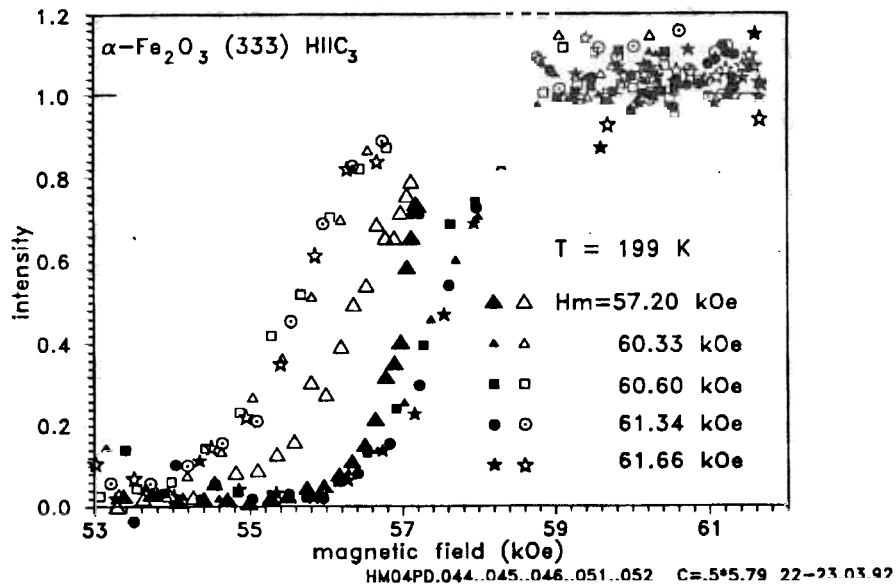

Fig.4 The scattering intensities in dependence on magnetic field value for the (333) diffraction peak of α-Fe_2O_3 for the indicated pulse amplitudes. At a sufficiently high value of the pulsed magnetic field amplitude the hysteresis loop achieves an utmost shape and maximum width.

TEXTURE INVESTIGATIONS OF GEOLOGICAL SAMPLES AT THE NSHR DIFFRACTOMETER

K. Walther, N.N. Isakov, A.N. Nikitin, D.I. Nikolayev, K. Ullemeyer, J. Heinitz
Joint Institute for Nuclear Research, Dubna, Russia

The preferred orientation of crystallites deviating from isotropic orientation distribution is called texture. For geological materials deformation processes active in the Earth's crust are the main mechanism influencing texture development. These processes acting under extreme physical conditions are very slow and therefore cannot be investigated by direct methods. Texture analysis would provide interesting information about the deformation history of rocks. For a better understanding of the processes acting in the crust it is also important to simulate the texture forming mechanisms and investigate experimentally the deformation of geological samples and composites. Ref. [1] reports on the results of simulating the texture development in high temperature quartz applying a thermoactive model of dislocation slip. Ref. [2] proposes a model for a texture rise in an initially isotropic polycrystalline quartz aggregate under non-uniform strain directed parallel to the crystallographic axes. The model bases on the notion of the behaviour and the properties of quartz near the $\alpha - \beta$ transition point. In cooperation with the Institute of High Pressure in Troitsk, Russia, and the Research Center Rossendorf, Germany, much effort has been made to develop high pressure facilities to investigate texture modification processes in geological materials directly in a neutron beam. Two high-pressure cells are in construction: one for a working temperature up to 1100 K and single-axis compression up to 1.5×10^5 H for samples with a volume up to 20 cm^3. The second, for a temperature up to 600 K under a hydrostatic pressure of 1.5 GPa and single-axis compression up to 5×10^4 for samples of 4 cm^3. Ref. [3] reports details of that complex.

Time-of-flight neutron diffraction is the most perspective method to investigate the texture of geological samples. It allows high resolution and large sample volumes and simultaneous measurement of a large number of pole figures. The work on the determination of textures of geological materials [4,5] with the NSHR diffractometer was continued . New data were obtained about the texture of polyphase samples containing quartz, plagioclase, and biotite [6].

Figure 1 shows a time-of-flight spectrum of a three-phase granulite measured at the NSHR diffractometer. Although the resolution is high, $\Delta d/d = 0.5\%$, the spectrum has a complicated character with many overlapping peaks because of the polyphase composition of the sample and the low symmetry of its constituents.

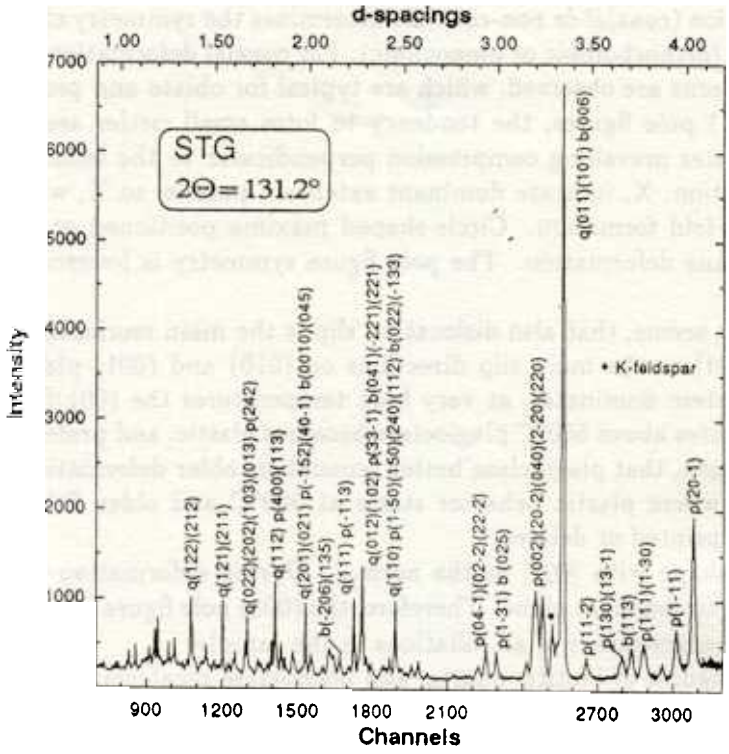

Fig. 1. Time-of-flight spectrum of sample STG containing quartz, biotite and plagioclase.

Quartz is common in many rocks, if present, its ductile properties mainly determine the rheological behavior of the rock. On the other hand, a broad spectrum of quartz textures is observed. It was found, that the normal to (110) is the dominant slip direction. The main slip planes are the basic, rhombohedral and prismatic planes. Under deformation the slip plane becomes parallel to the shear plane, and the slip direction parallel to the direction of shear. Moreover, the strain path and the magnitude and symmetry of strain also influence the resulting texture.

Figure 2 illustrates the reference system commonly used in geology. The XY plane is the foliation plane, the X direction is the lineation direction. Pole figures are generally given in the XZ section. The X,Y,Z axes are interpreted to represent the main axes of the strain tensor.

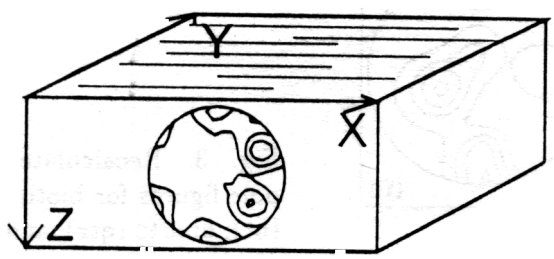

Fig. 2. The geological reference system.

The symmetry of deformation (coaxial or non-coaxial) determines the symmetry of the observed preferred orientation (orthorhombic or monoclinic). For coaxial deformation two main types of orientation patterns are observed, which are typical for oblate and prolate strain. In the (110) and (001) pole figures, the tendency to form small circles around the foliation normal, Z, indicates prevailing compression perpendicular to the foliation. Small circles around the lineation, X, indicate dominant extension parallel to X, which is commonly observed during fold formation. Circle-shaped maxima positioned on the XZ-circle give evidence for plane deformation. The pole figure symmetry is lowered by non-coaxial strain.

In the case of plagioclase it seems, that also dislocation slip is the main reorientation mechanism with [100] and [001] as the main slip directions on (010) and (001) planes. Usually the (010)[001] slip system dominates, at very high temperatures the (001)[100] system activates. At temperatures above 500°C plagioclase becomes plastic, and preferred orientation develops. That means, that plagioclase better remembers older deformational events in contrast to quartz, where plastic behavior starts at 300°C and older Fabrics textures are more or less over printed or deleted.

Biotite has a platy grain shape with [001] as the normal. During deformation that normal becomes perpendicular to the shear plane. Therefore, the (001) pole figure contains general information about the orientations of all foliations in the sample.

Figure 3 shows some pole figures of biotite, quartz, and plagioclase recalculated from the orientation distribution function. The (001) pole figure of biotite has a sharp, almost axial-symmetric maximum in the Z direction. That points to a dominant XY-foliation which developed under coaxial compression. The (110) pole figure of quartz has circle-shaped main maxima near the X direction. No tendency to form small circles can be observed. In contrast to biotite, that indicates plane deformation with extension parallel X. Furthermore, the quartz (110) pole figure is characterized by the fact, that the circle connecting the three maxima departs from the XZ section. Correspondingly, the maximum in the (001) pole figure is shifted from the center.

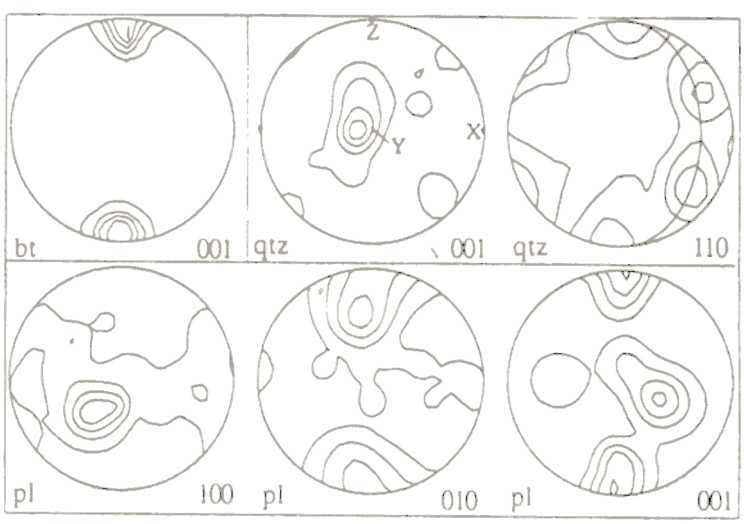

Fig. 3. Recalculated pole figures for biotite (bt), quartz (qtz), and plagioclase (pl).

The observed textures of quartz and biotite might be interpreted as follows: the (001) pole figure of biotite reflects the bulk final strain characterized by a tensor with the axes, X, Y, and Z (Fig.2). The quartz texture gives information about the last stage of deformation and evidences for an oblique deformation regime. The interpretation of the plagioclase texture is at the state of beginning, because of the absence of sufficient information on the reorientation mechanisms acting during texture formation. The characteristic maximum of the (010) poles in the Z direction might be evident for the dominance of (010) as slip plane.

References.

/1/ K. Walther et al.: Simulation of deformation textures of high-temperature quartz. (in Russian), Fiz. Zemli, 1993, No. 6, p. 45-48.

/2/ A.N. Nikitin, I.K. Arhipov & K. Walther: A Model of Induced Anisotropy in crystalline Rocks. XXIII General Assembly of the European Seismological Commission, Activity Report 1990-1992 and Proceedings, vol. 2, pp. 359-362, Prague, 1992.

/3/ J. Heinitz et al.: A High-Pressure Device for In-Situ Measurements in a Neutron Beam. Textures and Microstructures, 1994 (in press).

/4/ K. Helming, W. Voitus & K. Walther: Progress in Texture Investigation at the Pulsed Reactor IBR-2. Physika B, 1992, 180 & 181, pp. 1025-1028.

/5/ K. Walther et al.: Diffraction studies of the texture of geomaterials at the high resolution neutron diffractometer NSHR at FLNP JINR. (in Russian), Fiz. Zemli, 1993, No. 6, pp. 37-44.

/6/ S. Siegesmund, K. Helming & R. Kruse: Complete Texture Analysis of a Deformed Amphibolite: Comparison betrween Neutron Diffraction and U-Stage Data. J. Struct. Geol., vol. 16 (1994), pp. 131-142.

NEUTRON DIFFRACTION AT HIGH PRESSURE WITH DIAMOND AND SAPPHIRE ANVILS AT THE IBR-2 REACTOR

A.M.Balagurov, B.N.Savenko
Joint Institute for Nuclear Research, Dubna, Russia
V.P.Glazkov, V.A.Somenkov
RSC "Kurchatov Institute", Moscow, Russia

The new high-luminosity neutron diffractometer, MAN, for investigating microsamples at ambient and high pressures is now operating on channel 12 at the IBR-2 reactor (see Fig.1). A ring of 16 detectors is positioned on the vertical plane perpendicular to the incident beam. By moving the ring along the beam, the scattering angle is varied from 45° up to 135°. First test experiments have demonstrated the possibility of measuring samples with a volume of $0.05 to 1.5\ mm^3$ with this diffractometer. The crystal structure of DyD_3 was investigated with diamond anvils at pressures of up to 120 *kbar* to search for the phase transition predicted on the basis of the resistivity data in [1,2] to occur at about 100 *kbar*. The initial hexagonal structure was found to be stable over the entire pressure range (Fig.2). Magnetic ordering in ($\alpha - Fe_2O_3$ hematite was investigaed at 45 *kbar*. Transition to a new state with intermediate moment directions [3] has been confirmed. Additional data about intensities of reflections with larger Q have been collected.

1. I.O.Bashkin, E.G.Ponyatovskii, M.E.Kost. Phys.Stat.Sol.(b), 83 (1977), 517-520.
2. A. Sawaoka, K. Wakamori, S.M.Filipek. Proc.JIMS-2, Hydrogen in Metals. 1980, 141-147.
3. I.N.Goncharenko, O.A.Lavrova, V.A.Somenkov, G.Andre, J-M.Mignot, I.Mirebeau, J.Rossat-Mignot. Abstr. of Russian-French Seminar, Gatchina, 1993

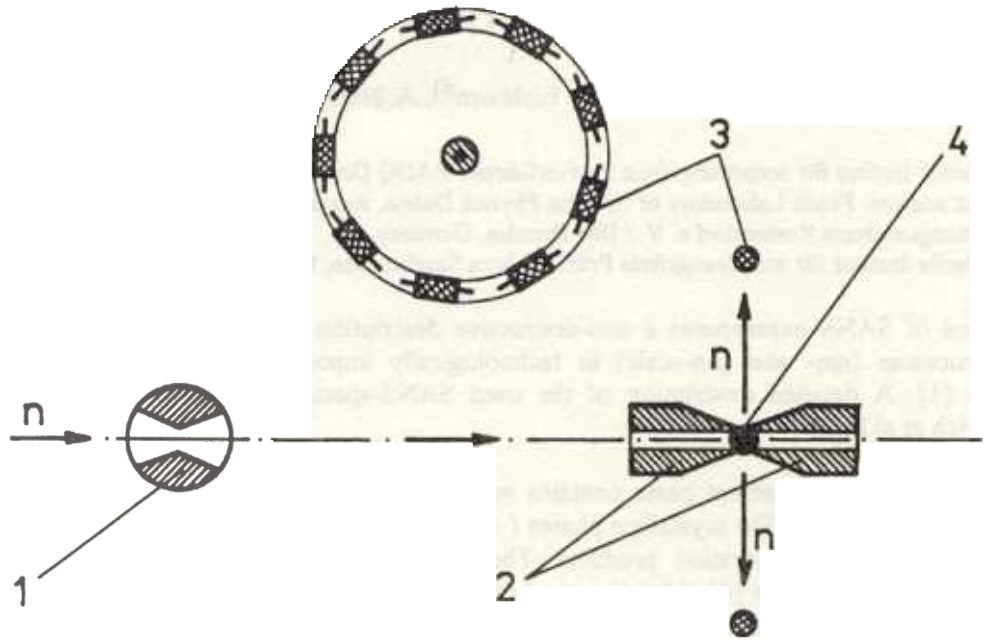

Fig.1. The diffractometer layout: 1 - mechanical chopper, 2 - anvils, 3 - detector ring, 4 - sample.

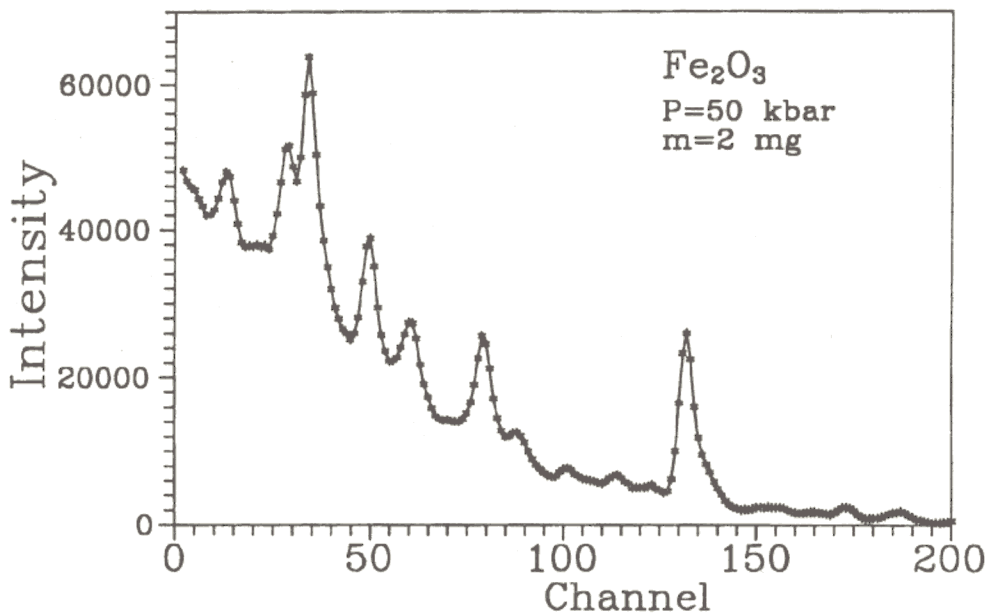

Fig.2. The diffraction pattern from hematite measured at P=50 kbar.

SANS Studies on Hydrating Cement Paste and SSNTD

F. Häußler*), M. Hempel*), F. Eichhorn#), A. Hempel#),H. Baumbach+)

*)Fraunhofer-Institut für zerstörungsfreie Prüfverfahren / EADQ Dresden, Germany
present address: Frank Laboratory of Neutron Physics Dubna, Russia
#) Forschungszentrum Rossendorf e. V. / IIM Dresden, Germany
+)Fraunhofer-Institut für zerstörungsfreie Prüfverfahren Saarbrücken, Germany

By means of SANS experiments a non-destructive description of statistically representative microstructures (nm- and µm-scale) in technologically important disordered materials is possible [1]. A detailed description of the used SANS-spectrometer MURN is given by Ostanevich et al.[2,3].

A hardening Portland cement paste contains many crystalline and non-crystalline phases in various ranges of sizes. The crystalline phases (e.g. Portlandite, Calcite) are embedded in the amorphous phases of hydration products. The kernel of the hydrating grain consists of unreacted Portland cement [4]. After the onset of hydration the evolution of the inner structure is observable by the evolution of typical parameters of the SANS curve.

The influence of the dry Portland cement (particle size: (1 ...150) µm, specific surface area (BLAINE): 0.25 m^2 /g [5]) and silica fume (sphere-like particles (diam.50% smaller than 0.25 µm) specific surface area (BLAINE): 20 m^2 /g [6]) on the scattering signal is investigated by special SANS measurements. A dry powder of silica fume (SF), of ordinary Portland cement (PZ), and a mixture of them (with a SF-PZ-mass ratio of 0.109) were put in a sandwich-like container formed of a plastic hollow ring and two circular plates of quartz glass on the faces of this ring. The obtained SANS-data for all the samples studied have been plotted as [$Q^4 \cdot d\Sigma/d\Omega$ (Q)] versus Q. Figure 1 shows different scattering patterns of the behaviour of dry powder samples. The Porod's potential law holds for the samples of the mixture of SF and PZ. Based on the smaller size range of the SF-particles a steeper increase of the macroscopic cross-section by decreasing of Q is expected. The exponents A(2) of the scattering curves of dry Portland cement and dry silica fume, calculated by the fit procedure FUMILI, deviate from 4.0 by about 4%. Accordingly, the calculated surface area of these samples have to be considered as an estimate [7]. The surface area per unit volume of PZ and SF is estimated. The results are summarized in table 1.

Table 1: Surface measurements of dry powder samples of anhydrous ordinary Portland cement, silica fume and their mixture

Sample	Exp./ ΔExp.	Porod constant Kp/ΔKp/ $10^{36} m^{-5} sterad^{-1}$	Surface area per unit vol. S/Vg/ΔS/Vg/ $10^6 m^{-1}$	Specific surface area S/mg/ΔS/mg/ $m^2 g^{-1}$
anhydrous Portland cement (PZ)	-3.84/ 0.01	3.23 / 0.14	3.43 / 0.11	1.94 / 0.10
anhydrous Silica fume (SF)	-4.17/ 0.01	3.10 / 0.11	2.81 / 0.09	4.77 / 0.25
mixture of anhydrous SF & PZ	-4.00/ 0.01	3.33 / 0.13	-	-

The samples of a hardened cement paste are prepared from ordinary Portland cement and water (D_2O) with a given water to cement ratio of 0.38. In order to observe the hydration progress after the onset of hydration (at the last measurements the sample were 620 days old) the cement paste was put in a sandwich-like container formed of a plastic hollow ring and two thin 30 μm thickness plastic foils on the faces of this ring to reduce the vapour (water) exchange. Changes in the mass of a sample due to evaporation of water were registered. The thicknesses of these plastic rings were 0.50 mm, 1.05 mm, and 1.70 mm.

Both the potential law of the scattering curve and the macroscopic cross section $d\Sigma/d\Omega$ vary. In the measured Q-region the hardening cement paste do not exhibit a Porod-like behaviour. The power law of $\propto Q^{-A(2)}$ is observed for $Q < 1$ nm [7]. Figure 2 gives a survey of the evolution of the exponents A(2) of the SANS curves. The exponents A(2) of the FUMILI calculations are varying in dependence on the hydration time and lie in an interval from about 2 to 4. This is believed to be associated with fractal behaviour. This might arise from the deposition of a C-S-H gel on the cement clinker grain/pore boundary and the roughening of water intrudes to form the inner product [1]. The area of the rough surface depends on the scale of observation [8]. In the case of self-similar surface structures (surface fractals) the exponent of Q is between -3 and -4. In addition the thickness of the hydrating cement paste samples proves to be a significant parameter for studying the cement hydration in real-time experiments. Comparing the evolution of the exponent A(2), after the hydration time of 92 days the exponents describing the potential behaviour decreased. Bevore reaching a nearly common value of A(2) the minima of all these evolution curves at the hydration time of about 400 days are visible in figure 2. Hence these experimental results might be caused by changes of the microstructure during the hydration process.

Assuming a logarithmic normal distribution for the size (geometric radius R) of spherical particles (pores or grains of different phases) the most probable radius R_0 (centre of distribution) and the dispersion of that distribution ($p \propto$ FWHM) for hydrating samples within the first 92 days after the onset of hydration is given in table 2. The results using a calculation procedure discussed in G. Walther et al. [9] show that the mean particle size reaches its final value already in the early stage of hydration whereas the dispersion of the particle size increases during a longer period [10].

Table 2: Parameters (the most probable radius R_0 and the full width at half maximum [FWHM]) of a logarithmic normal distribution for spherical particles in dependence on the time after the onset of hydration of Portland cement paste

Hydration time / d	R_0 / nm	FWHM / nm
1	3.3 ± 0.1	3.1 ± 0.1
60	2.8 ± 0.5	4.3 ± 0.2
92	3.1 ± 0.4	4.5 ± 0.1

All these experimental results give rise to the conclusion that further investigations, especially theoretical ones, are necessary for the correct interpretation of the experimental curves and the evaluation of structural data (nm-level) on the cement paste.

Furthermore, latent ion tracks in solid state nuclear track detectors (SSNTD) before and after etching are studied by SANS [11]. Passing the SSNTD charged particles (protons and havier particles) form latent tracks. The parameters of these tracks vary with the atomic number and

the energy of the incident particles. Therefore SSNTD represent passive detectors for ionizing radiation and can be used for the registration and identification of charged particles. On the other hand with the help of special etching procedures the design and the production of nuclear filters with defined porous radii in the µm-level is achievable. First experiments by SANS on the MURN facility are realized [12]. Essentially the study of the influence of partial annealing and of other environmental conditions on the storage of irradiated detectors over a long period requires the analysis of the latent tracks. Semenyuk, Svergun et al.[13] have investigated different types of nuclear filters by small angle X-ray scattering. Both latent and etched tracks in PETP are studied. Irradiated and etched ion tracks are shown in Fig. 3. The slope of the scattering curve using the Guinier plot indicates the size range of the radial extension of the etched track. Without any assumptions about the form of the scattering objects the radii of gyration R_g calculated from the slope of the scattering curve correlate with the radii r measured by a gas penetration method. For the further interpretation of the scattering data via modelling additional data about the latent tracks are necessary. This modelling is a useful help for the quantitative analysis of SANS data. For this analysis, the form of the latent tracks, i.e. the matter density distribution (profile) parallel and perpendicular to the track axis, the exact track density of the irradiated region, i.e. homogeniety of the track distribution, and other parameters are needed.

The authors wish to gratefully acknowledge late Prof. Yu. M. Ostanevich of FLNP JINR for his permanent interest, fruitful discussions and the support for the work until his sudden death in 1992. We thank our colleagues from the SANS group, especially A. I. Kuklin, for their helpful discussions and help in the SANS experiments. The experiments in the field of SSNTD are supported by Dr. W. Birkholz. These experiments were done by cooperation with the colleagues of the JINR Dubna / Laboratory for Nuclear Research Dr. V. P. Perelygin, Dr. M. Danziger, Dr. P. Yu. Apel, Dr. S. G. Stetsenko and Mr. A. Schulz.
The work reported has been performed with partial support of the Bundesminister fuer Forschung und Technologie through grant no. 03-DU3FHG and 03-EI3ROS. The authors are fully responsible for the contents of this publication.

(1) A. J. Allen, J. Appl. Cryst. 24 (1991) p. 624
(2) User Guide, Neutron Experimental Facilities at JINR, Dubna, USSR 1991
(3) Yu. M. Ostanevich, Time-of-flight small-angle scattering spectrometers on pulsed neutron sources, Makromol. Chem., Macromol. Symp. 15 (1988) p. 91
(4) S. Röhling, M. Nietner, Betontechnik 9 (1988) p. 52
(5) Analytic protocol of the Chemiewerk Coswig/Germany, 1985
(6) W. Altner et al. , Betontechnik 4 (1989) p.117
(7) F. Häußler, F. Eichhorn, H. Baumbach, Description of the Structural Evolution of a Hydrating Portland Cement Paste by Small-Angle Neutron Scattering (SANS), accepted for publication in *Physica Scripta* (proceedings of the Euroconference 1993, Studsvik (Sweden))
(8) L. Auvray and P. Auroy, Scattering by interfaces:variation on Porod's law. I: Neutron, X-Ray and Light Scattering, ed. by P. Lindner and Th. Zemb, Elsevier Science Publishers B.V., 1991, p. 199
(9) G. Walther et al., J. Appl. Cryst 18 (1985) p. 205
(10) F. Eichhorn, F. Häußler, and H. Baumbach, Structural Studies on Hydrating Cement Pastes, *Journal de Physique IV* (proceedings of the IX. International Conference on Small Angle Scattering) 3 (1993) p. 369

W. Birkholz, F. Häußler, S. G. Stetsenko, Investigation of Latent Ion Tracks in SSNTD with Small Angle Neutron Scattering, Proceedings *II International Workshop "Solid State Nuclear Track Detectors and their Applications"*, Dubna 1993, E7-93-61, p. 29

(12) W. Birkholz, F. Häußler, V. P. Perelygin, S.G. Stetsenko, P. Vater, Study of latent heavy ion tracks in SSNTD by small-angle neutron scattering, *16th International Conference on Nuclear Tracks in Solids*, Beijing (China),7. - 11. September 1992

A.V. Semenyuk et al., Small-angle x-ray scattering investigation of the pore structure of nuclear filters, *J. Appl. Cryst.*424 (1991) p. 809

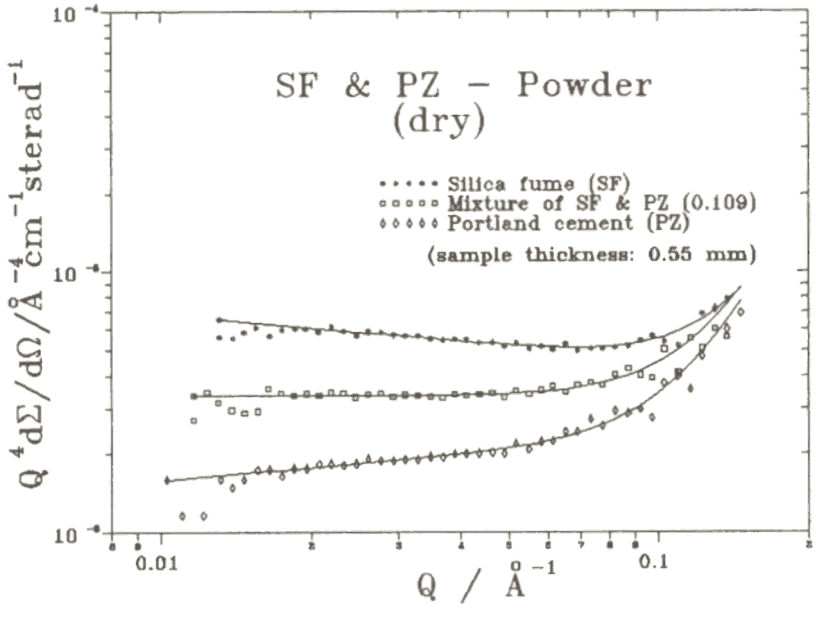

FIGURE 1: The Porod-plot for dry powder samples of ordinary Portland cement (PZ), silica fume (SF) and a mixture of PZ and SF

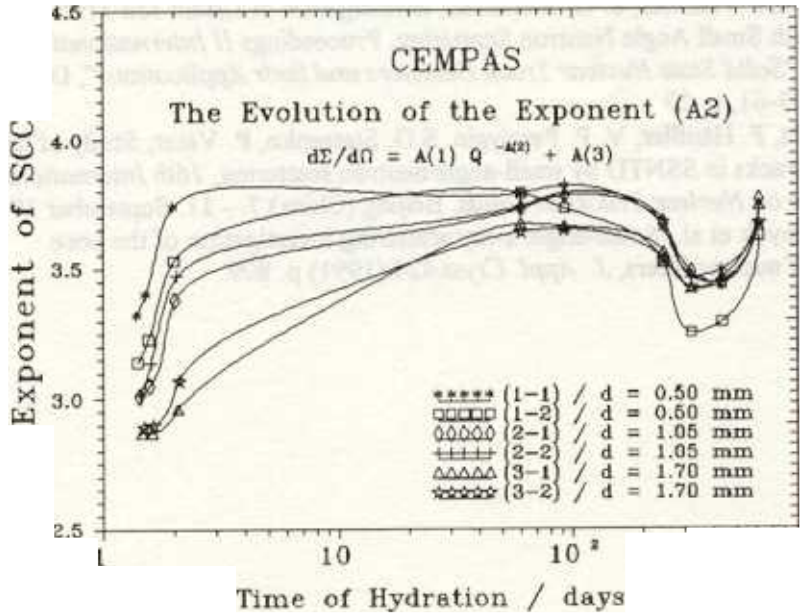

FIGURE 2: The evolution of hardening cement paste in dependence on the hydration time and the sample thickness

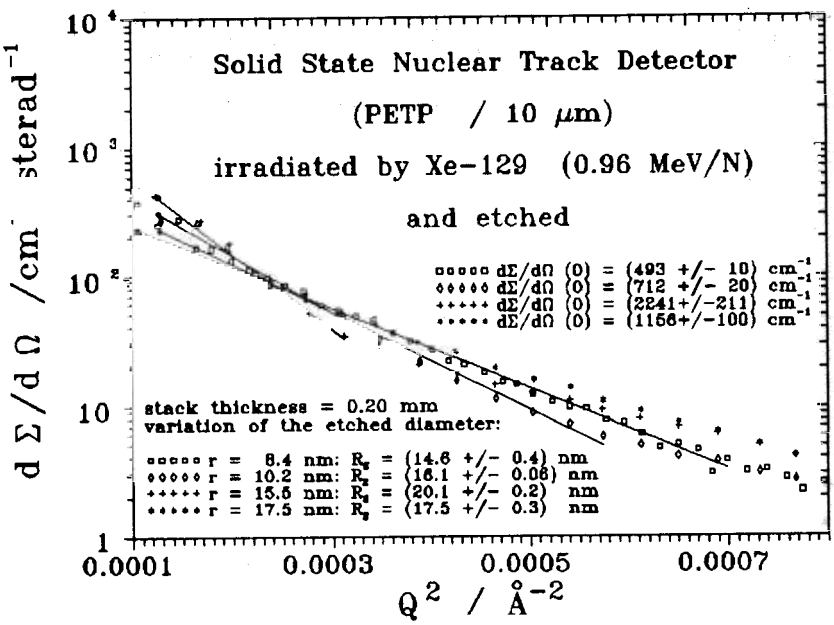

FIGURE 3: Ion tracks in SSNTD after the first step of etching. A correlation between the radii measured by SANS and gas penetration (r) is shown.

SANS-investigation of the micelle system C_{14} DMAO in D_2O at high hydrostatic pressure

N .Gorski,* J.Kalus,** A.I.Kuklin,*** L.S.Smirnov***

* FZ-Rossendorf, Germany; JINR,Dubna,Russia
** University Bayreuth, Germany
*** JINR, Dubna, Russia

Introduction

Pressure (along with temperature) is one of the important characteristics, which determines the properties of matter. Neverthless, pressure is not widely used in small angle neutron scattering investigations of micelle systems because of technical complications.
The main aim of our experiments is to obtain information about the behaviour of surfactant solutions under pressure. It is necessary to note, that under the influence of pressure phase transitions within the mezophase range.

SANS Experiments

Were done with MURN the time-of-flight spectrometer at the pulsed reactor IBR-2, JINR, FLNP. We used a wavelength range from 0.7 to 10 Å and a time-averaged flux of thermal neutrons on the sample of about 10^7 neutrons $cm^{-2}s^{-1}$. The length of the scattering vector Q was varied from 0.01 to 0.2 $Å^{-1}$. The important feature of the "MURN" spectrometer is the use of an internal standard scatterer (metallic vanadium) which guarantees absolute calibration of the measured cross section with an overall systematic error less than 10%.

The high pressure chamber (HPC)

HPC is made from the Ti/Zr alloy with a "0"cohernt scattering length. This chamber is a 130 mm high cylinder with the 33 mm external diameter and the 11 mm internal diameter. The working range is from 0 up to 1000 MPa. The pressure was created by a press.

The Micelle system

The concentration of the micelle system C_{14}DMAO (tetradecyldimethylaminoxide) in D_2O was C=55 mM. The shape of micelle with this concentration is a cylinder with the radius R= 20.6Å and the mean length L=150Å. The experimental background was formed by heavy water. The samples were exposed to radiation for 1 to 4 hours.The temperature was 24° C, the pressure - 0.1; 210; 421; 632; 842 MPa. For estimating the possibility of using this chamber for conducting experiments we compared the data measured with the cell of the 1 mm useful thickness with the data measured for the reported chamber under the pressure P=0.1 MPa. Comparison of the scattering curves (Fig.1) indicates good agreement within the range Q ≥0.03$Å^{-1}$.

Results and Discussion

As is seen from Fig.2, an increase of pressure to 210 MPa leads to a great change in the scattering curves . A further increase of pressure (up to 842 MPa) does not affect the curves so much: the shape of the curve does not vary appreciably with increasing pressure, and only intensity increases. The reason for this change is the increasing micelle concentration due to heavy water compressibility. For comprison with the experimental data the fit-curves for the cylinder (Fig.3), for the disk (Fig.4) and the ellipsoid (Fig.5) are presented. The calculated values are listed in Tab. 1. As is seen from figures 2-5 the scattering curves have the maximum at $Q \approx 0.18$ Å^{-1}. But this maximum does not exist at the pressure $P = 0.1$ MPa. If assumed, that with increasing pressure a layered structure appears, then from equation $d = 2\pi/Q_{max}$ we obtain the interlayer repeat distance d of about 34 Å. We plan to conduct additional experiments for further detalization of micelle structure at high pressure.

Finaly, many thanks are due to Mrs Drozdova for numerous corrections of our English.
N.Gorski gratefully acknowledges the support of **BMFT** (contract 03-DU3 ROS /A.8-K16).

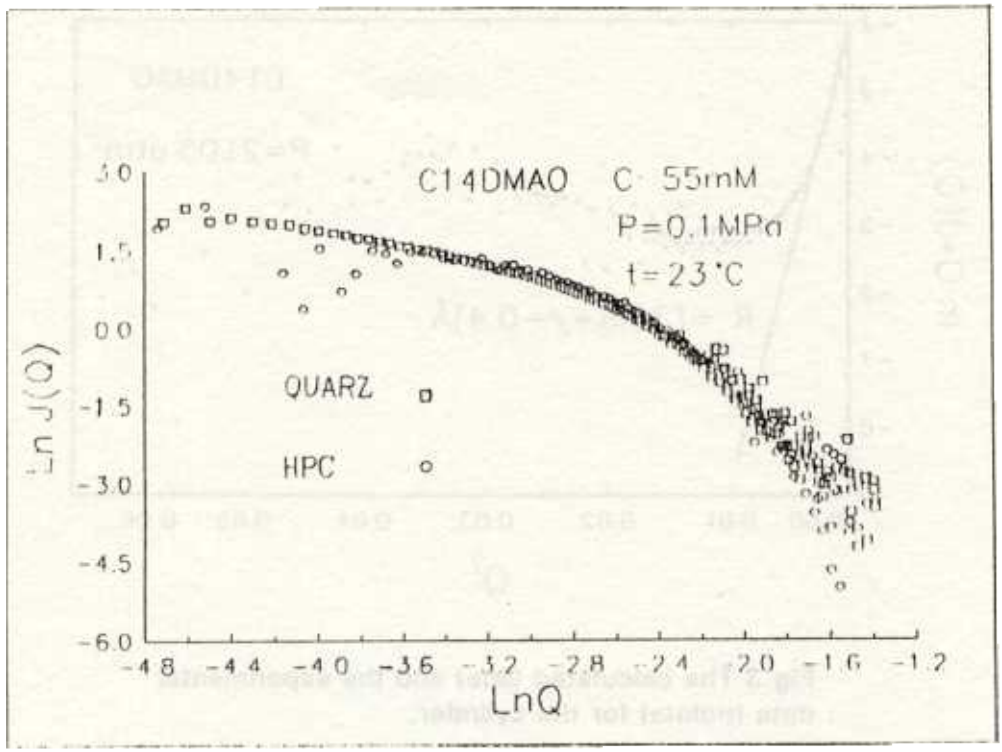

Fig.1 The scattering dependence for the C_{14} DMAO-solution in D_2O in the cell and in the high pressure chamber.

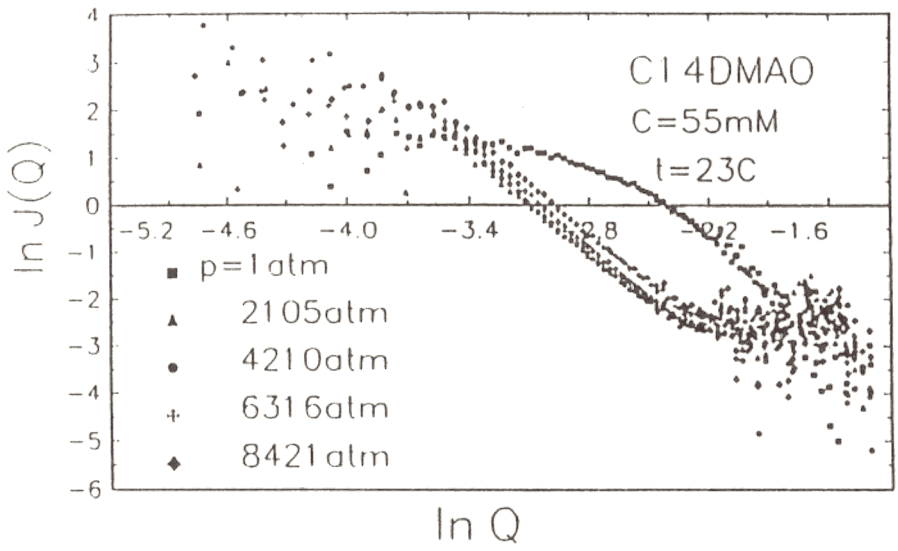

Fig.2 The small-angle scattering patterns of C_{14}DMAO as a function of pressure at T = 24° C.

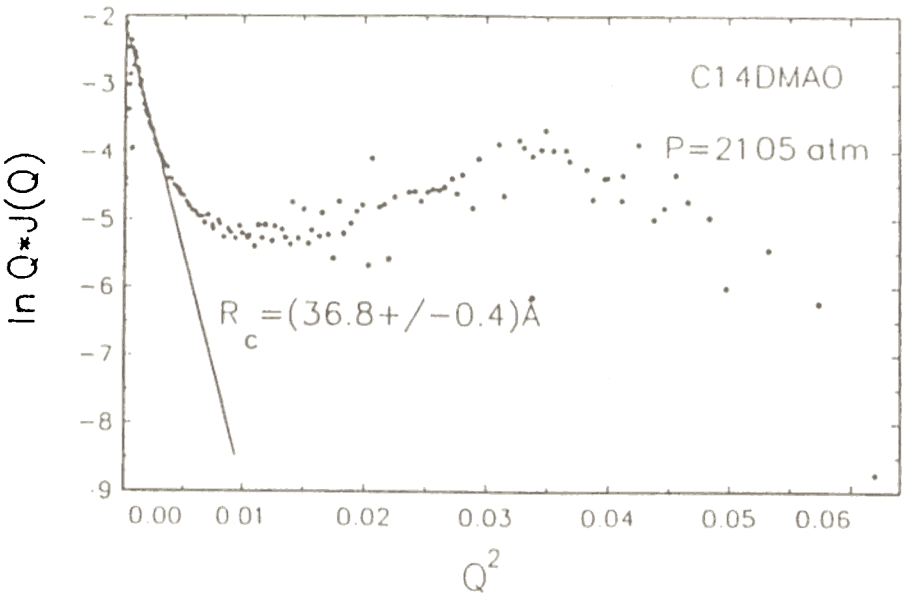

Fig.3 The calculated (line) and the experimental data (points) for the cylinder.

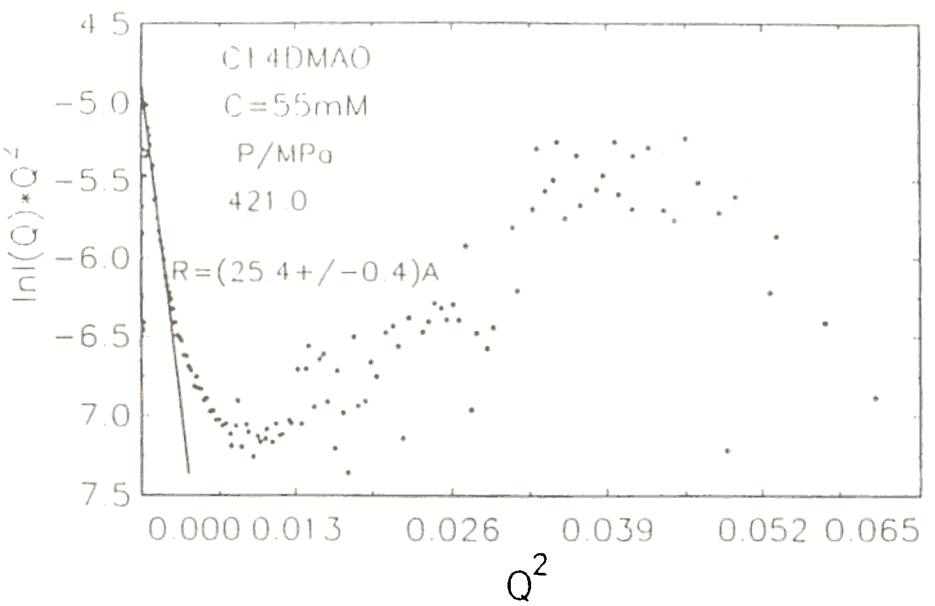

Fig.4 The calculated (line) and the experimental data (points) for the disk.

P (MPa)	R_c (Å)	R (Å)	R_t (Å)	(Å)	R (Å)	HL (Å)	Porod n
0.	14.5±0.	20.6±0.2					
210	36.8±0.4	52.0±0.6	19.6±0.4	68.1±1.4	91.7	37.0	
421	40.5±0.2	57.3±0.3	25.4±0.4	88.1±1.3	97.6	40.4	
632	38.0±0.4	53.8±0.5	19.6±0.2	67.8±0.7	87.5	37.0	3.74
842	37.4±0.4	52.8±0.5	19.5±0.2	67.6±0.9	84.7	33.8	

Tab.1 : The values calculated in the frame of different models

Rc,Rt - the radius of gyration of the cylinder and the thickness of the disk respectively.
$R=\sqrt{2}\,R_c$ - the radius of the cylinder, $t=\sqrt{12}\,R_t$ - the thickness of the disk.
Hl,R - the half radius of the ellipsoid.

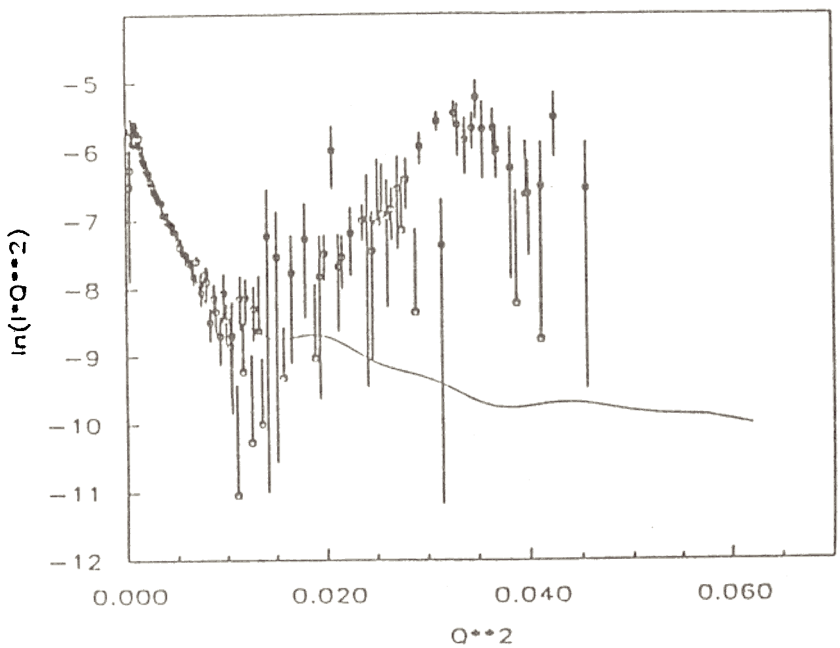

Fig.5 The calculated (curve) and the experimental data (empty squares) for the ellipsoid.

The Study of Micellar Solutions of Ethoxylated Diisononylphenol by Small-Angle Neutron Scattering

Bulavin[1] L.A., Garamus V.M., Ostanevich Yu.M.

1 - Physical Faculty, Kiev University, Kiev, Ukraine

The application of non-ionic surfactants in enhanced oil recovery has recently attracted considerable interest owing to their favourable characteristics under reservoir conditions. Because the structure of micellar solutions of surfactants, i.e., the size, shape and concentration of micellar associates (micelles), may play a fundamental role in the shaping of interface phenomena in oil/water systems it is been investigated on many occasions [1].

The structure of micellar associates is intimately connected with surfactant molecular formula. The one of parameters is number of alkyl chains. The surfactants with different number of alkyl chains are a objects of study [2]. The chosen surfactant has two alkyl chains and is close to industrial ones. Both factors make it very interesting object of studying.

Small angle neutron scattering is a powerful technique that is able to investigate, not only the above mentioned parameters but also the intermicellar interactions.

Oxyethylated diisononylphenol $(C_9H_{19})_2C_6H_4(OC_2H_4)_nOH$ (ODNP), where n=20 is the main component, was received from the Institute of Bioorganic Chemistry and Petroleum Chemistry, Kiev, Ukraine [3]. The ODNP is mixture of equal part of 2,4 and 3,4 diisononylphenol . The critical micelle concentration (CMC) in aqueous solution was measured by the surface tension method [4]. The CMC was $5.06 \cdot 10^{-5}$ mol/l at 20 °C. The cloud point is 70.8 °C. Existing of second chain may play the important role in systems where one of components is ODNP and the surface tension (oil/surfactant/water) is 10^{-2} - 10^{-5} mN/m.

Experiments with increasing surfactant concentration, from $3.83 \cdot 10^{-4}$ to $5.7 \cdot 10^{-2}$ mol/l, were performed at 18-20 °C. In data analysis we used Guinier's approximation $(d\Sigma(q)/d\Omega = d\Sigma(0)/d\Omega \exp(-q^2 R_g^2/3))$. We concluded that micelles do not growth. Because Guinier's radius is practically equal to 40.0 ± 1.5 Å and radius of equivalent homogeneous sphere is equal to 51.5 ± 2 Å for concentrations to $1.22 \cdot 10^{-2}$ mol/l . Another argument, that micelles do not increase size, is the measurement of Porod's field of q range. For $8.1 \cdot 10^{-3}$ and $5.7 \cdot 10^{-2}$ mol/l were performed experiments under large q. The scattering curve were modelled by Porod's approximation A/q^4 and incoherent background. We obtained that the ratio between A parameters of total micelle surface is equal to 7.5 ± 0.5 that is equal to ratio between

concentrations. That is why, we can conclude that micelles do not growth in concentration range to $5.7 \cdot 10^{-2}$ mol/l . Micellar surface is equal to $2.4 \cdot 10^4 \text{Å}^2$.

The difference cross section in zero angle per one ODNP molecule $d\Sigma(0)/d\Omega/N$ vs. surfactant concentration is showed in fig.1. The like maxima were obtained in [5]. From decreasing part of curve (fig.1) we obtained B = - (38 ± 2). The second virial coefficient of the system of monodisperse hard spheres is equal to -8. Such increasing of B may be connected with two factors: polydispersity and hyd-ration forces between micelles [6]. The appear of maximum may be connected with changed of micellar interaction. The repulsion between micelle become more than the attraction under increasing surfactant concentration.

We performed cycle experiments on contrast variation. The average scattering length density of the surfactant micelles ρ was obtained after the building linear dependence $(d\Sigma(0)/d\Omega)^{1/2}$ vs. ρ_s. The obtained ρ is $(9.4 \pm 0.4) \cdot 10^9$ cm^{-2} . The calculated (table data) scattering lengths density is equal to $5.0 \cdot 10^9 cm^{-2}$. This difference may indicate on hydration of C_2H_4O [7]. In the case of hyd-ration of oxyethylene groups the part of micelle becomes smaller and it's scattering length density increases. We obtained one hydrated water molecule per one oxyethylene group. This value is less than maxima possible one [8].

The aggregation number of the micelles was obtained by the free article of $(d\Sigma(0)/d\Omega)^{1/2}$ vs. ρ_s and was equal to 430 ± 30.

The scattering data were analyzed by reverse Fourier transformation [9]. The contrast profile is showed in fig.2. For test of results the convolution and direct Fourier transformation of data (fig.2) were performed. Obtained curve consistented with original one.

We can conclude that the scattering length density of micelles is slowly de-creased from centre to boundary of micelle. This result may be connected with hydration.

References:

1. Lindman B., Wennerstrom H. in: Topics in Currrent Chemistry / v.87, p.1 (1980).
2. Aveyard R., Binks B.P., Clark S. et al. / Coll. & Surf. v.59 p.97-111 (1991).
3. Pop G.S., Glavati O.L., Geresh P.A., et al. / Author Receipt of USSR 1629308 " The Composition for Oil Recovery ".
4. Pop G.S., Kurilo S.M., Mischenko N.I. / Reports of Ukraine AS v.8 p.32-36 (1992)
5. Plestil J., Ostanevich Yu.M. et al. / J. Appl. Cryst. v. 24, p.659-664 (1991).
6. Monohar C., Kelkar V.K. et al. / Chem. Phys. Lett. v. 171, p.451-456 (1990).
7. Berr S.S., Marriott Jones R.R. et al. / J.Phys.Chem. v.90, p. 6492 (1986).
8. N. Schonfeldt "Grenzflachenaktive Athylenoxid-Addukte" / Wissenschaftliche Verlagesellschaft MBH Stuttgart 1976
9. Glatter O. / Acta Phys. Austriaca v.1-2, p.83-102 (1977).

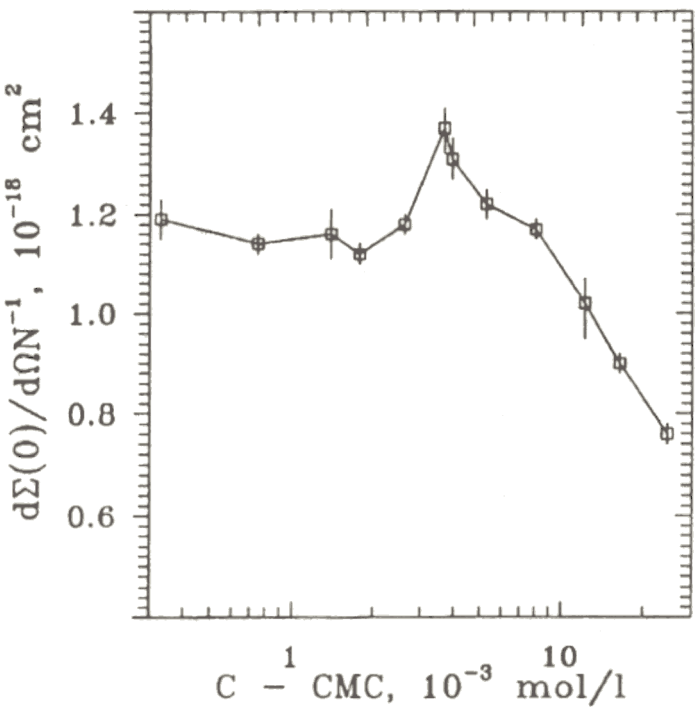

Fig.1. Normalized difference cross section of scattering $d\Sigma(0)/d\Omega/N$ vs. surfactant concentrations.

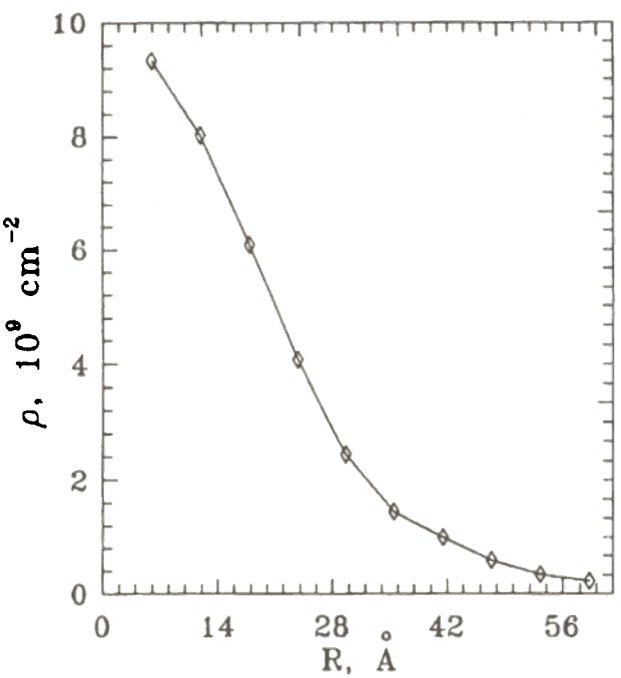

Fig.2. The profile of micelle density of scattering lengths.

STRUCTURE OF LIQUID HELIUM-4 EXCITATION SPECTRUM

N.M. Blagoveshchenskii , I.V. Bogoyavlenskii , L.V. Karnatsevich , Zh.A. Kozlov ,V.G. Kolobrodov , V.B.Priezzhev , A.V.Puchkov , A.N. Skomorokhov , B.S.Yarunin

Inst.of Physics and Power Engineering, Obninsk, 249020, Russia
Inst.of Physics and Technology, Kharkov, 310108, Ukraine
Joint Inst.for Nuclear Research, Dubna, 141980, Russia

Held in 1993 the high-precision investigation of liquid helium-4 excitation spectrum with the wave vectors (q) less than one of roton by means of the cold neutron inelastic scattering has shown that the experimental spectrum of one-particle excitations has complex structure, both in normal and superfluid phases [1].

One can observe two branches of the excitations in normal phase, $T>T_\lambda$: narrow one (os) is detected only in the phonon region, at $q<0.65$ $\mathring{A}^{-1}$, and wide branch survives at all q. An additive branch (n) at $q> 0.48$ $\mathring{A}^{-1}$appears in the superfluid phase, $T<T_\lambda$. Thus, main transformation of the helium excitation spectrum structure takes place in two ways. Firstly, when helium transforms from He II to He I, secondly in the tight wavevector's region, namely, 0.48 $\mathring{A}^{-1}$ $<q<0.65$ $\mathring{A}^{-1}$ both in normal and superfluid phases (Fig.1).

The experimental data obtained commonly agrees with the liquid helium conception developed in last few years by Griffin, Glyde etc. [2] based on the fundamental studies of Pines, Nozieres, Belyaev and others. In the frame of these theories each component of the spectrum structure observed get the definite physical sense. Such way the narrow component (n) intrinsic for superfluid phase only, is to be interpreted as an elementary excitations-quasiparticle spectrum (Landau's dispersion law). The narrow component of phonon region in normal phase (os) one can identify like a collective zero-sound mode; in superfluid phase one being regarded as the superposition of this mode with the phonon part of the quasiparticle spectrum. The nature of the (w)-component, detected in both phases, is less understandable. One can link it with the scattering on the thermally excited quasiparticles or with the quasicrystal structure of liquid or with other mechanisms.

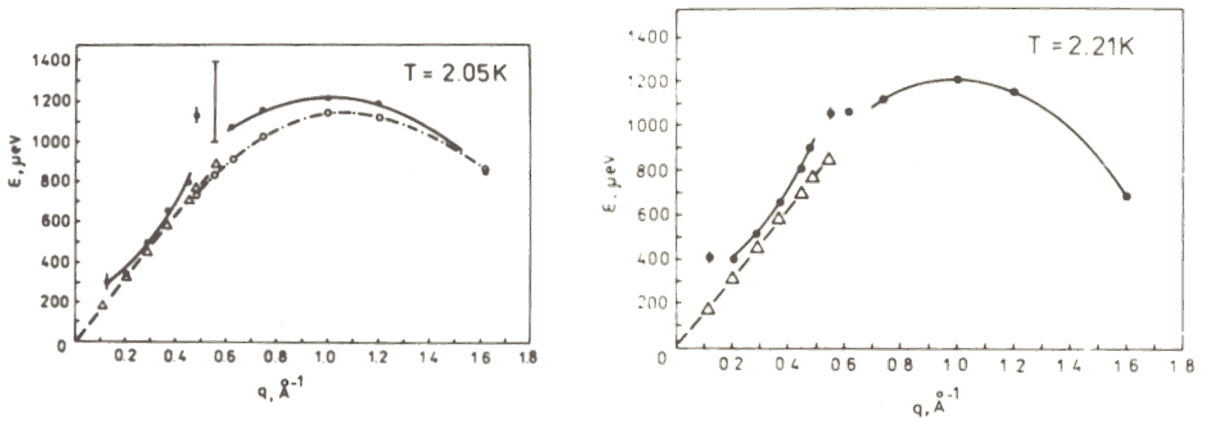

Fig. 1. Liquid helium-4 dispersion curves at the temperatures 2.05 and 2.21 K for the next components: (n) - empty circles; (w) - solid circles; (os) - triangles.

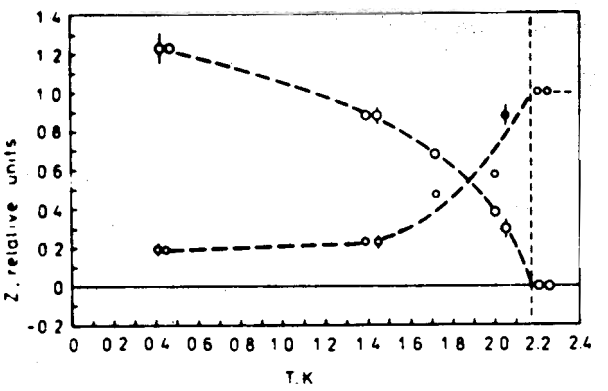

Fig. 2. Temperature dependencies of intensities for the next components: (n) -empty circles; (w) - solid circles. Curves are normalized by 1 for the (w) at $T > T_{\lambda}$.

According to Griffin and Glyde conception, the temperature dependence of the narrow (n) component strength reflects the T-dependence of the bose-condensate in liquid helium. This leads to the principal new opportunity to investigate the bose-condensate phenomenon (Fig.2).

The direct experimental decomposition of the scattering spectra into several branches is the important result which allows, in principle, to study the character and peculiarities of each type of inelastic neutron scattering separately. Theoretically this decomposition is just not properly developed.

1. N.M.Blagoveshchenskii, I.V.Bogoyavlenskii, L.V.Karnatsevich, Zh.A.Kozlov, V.G.Kolobrodov, A.V.Puchkov, A.N.Skomorokhov, JETP Lett.,v.57,No.7,(1993),428; and Proc.of XX Inter.conf.on Low Temp.Phys., #PD-38, Eugene,USA,1993.
2. H.R.Glyde and A.Griffin, Phys.Rev.Lett.,65(1990)1454. H.R.Glyde, Phys.Rev., 45(1992)7321.

INELASTIC NEUTRON SCATTERING IN PbF_2

Zh. A. Kozlov
LNP, JINR, Dubna
I. Padureanu, S. N. Rapeanu, Gh. Rotarescu
Central Institute of Physics, Bucharest, Romania
V. A. Semenov
Institute of Physics and Power Engineering, Obninsk, Russia

Many materials with fluorite structure exhibit a specific heat anomaly at a temperature T_c well bellow their melting temperature T_m ($T_c \sim 0.8\ T_m$). This anomaly is accompanied with the onset of dynamical disorder in the anion sublattice /1/. A series of data suggest this disorder. However the extent of this disorder is inclear in fully. A study of the lattice dynamics of fast ion conductors is of current interest. Neutron beam techniques /diffraction, quasielastic and inelastic scattering of neutrons/ are ideally suited to study the behavior of the ions in these systems /2,3/.

The aim of the present work is to provide the information on the nature of the dynamical anion disorder lead fluorine, PbF_2, from inelastic neutron scattering. PbF_2 has a simple cubic array of anions with cations at every other body center. This compound possesses the highest ionic conductivity and lowest transition temperature /T_c =710 K/ of the fluorites.

On the spectrometer DIN-2PI we have measured the neutron inelastic scattering in PbF_2 at the temperatures 293 K and 823 K. Two incident energy, E_0 =2.84 and 10.4 meV, were used. The scattered spectra were observed via neutron energy gain. A simple measurement were made on the spectrometer IN4 in Grenoble by a neutron energy loss method /4/. Fig. 1 and fig. 2 shows the time-of-flight spectra of neutrons scattered from PbF_2 at 293 K and 823 K. The ordinate is the sum over scattering angles of 71° to 134°. The data were corrected for background. The energy resolution was less than 4-5% in all the region of energy transfers. The spectra were normalized to a constant value.

The phonon density of state PbF_2 calculated in /5/ shows the peak at 6.5 meV derives from the transverse acoustic modes and the peaks of 13,27 and ~40 meV derive from optic modes /in fig. 1-2 the short lines show the calculated position of the peaks/. There is

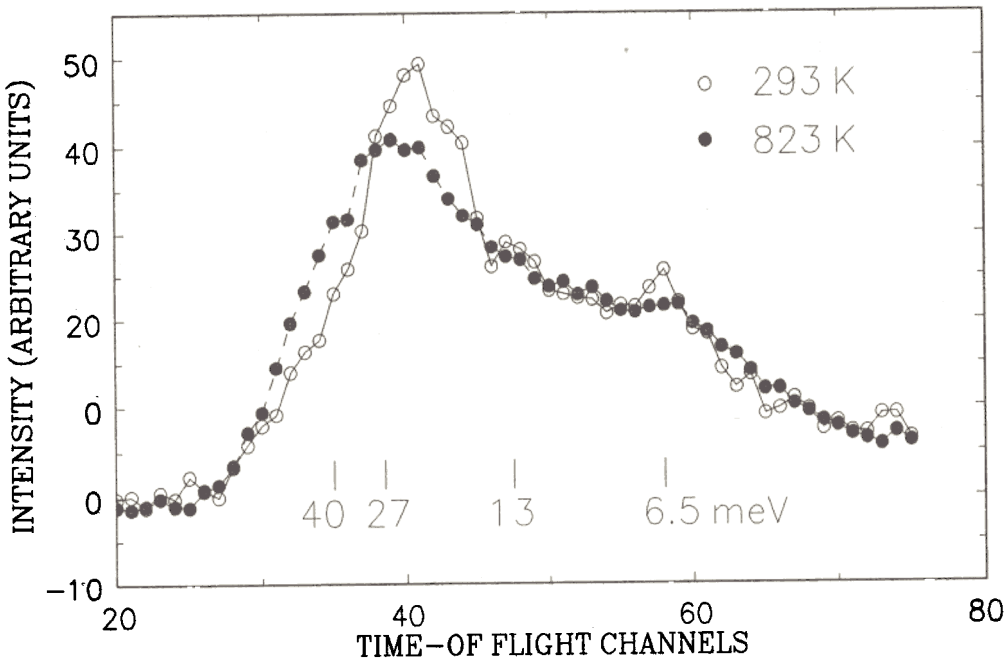

Fig.1. The time-of-flight spectrum of neutrons scattering from PbF_2 for E =2.84 meV.

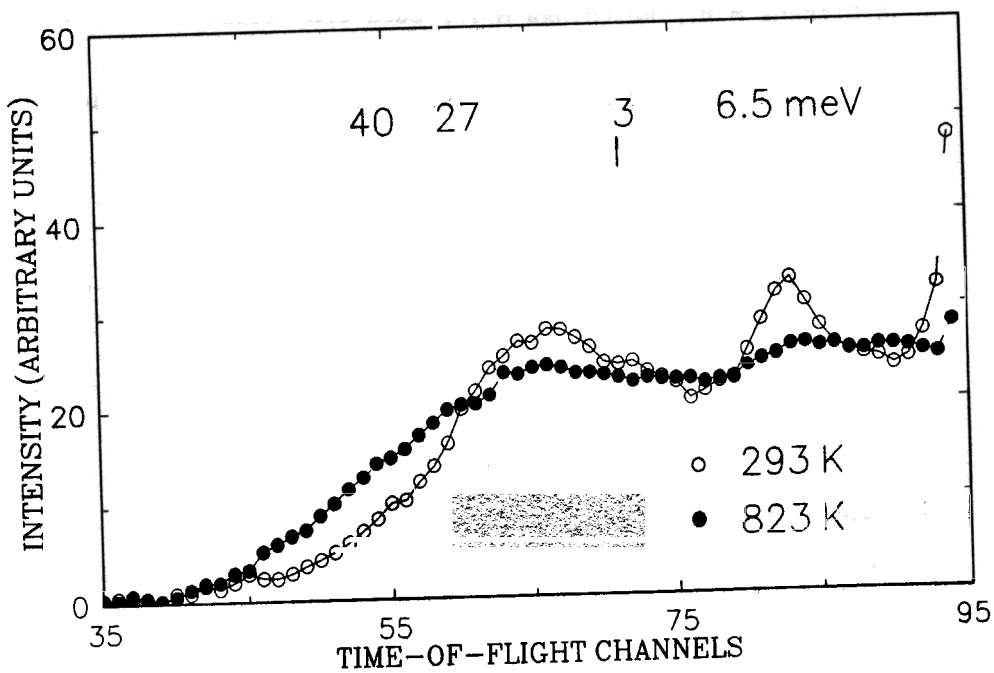

Fig.2. The time-of-flight spectrum of neutrons scattering from PbF_2 for E =10.4 meV.

a gap at ~33 meV. The calculated density-of-states agrees well with the experimental distribution function for phonons in PbF_2 measured at 10 K /5/. As the temperature is raised the peaks become broadened and smoothed. This effect exhibits already at the room temperature. At 823 K the left slope of the spectrum is been extend to the high energies. The elastic peak decreases visibly /no shows/. As the temperature increases the multiphonon processes increase in importance. In order to determine the frequency distribution the contribution of these processes must be extracted from the measured intensity. At the same time it is seen that both acoustic and optic spectra take place at 823 K. It means no complete disorder of the anion sublattice occurs.

1. Catlow C.R.A., Comins J.D., Germano F.A., Harley R.T. and Hayes W. J. Phys. C: Solid State Phys. 11 /1978/ 3197-3211.
2. Salamon M.B. /ed./ Physics of Superionic Conductors, 1979, Topics in Current Physics N15 /Berllin: Springer/.
3. Hutchings M.T., Clausen K., Dickens M.H., Hayes W., Kjems J.K., Schnabel P.G. and Smith C. J. Phys. C: Solid State Phys. 17 /1984/ 3903-3940.
4. Dickens M.H., Hutchings M.T., Suck J.B. Solid State Commun. 34 /1980/ 559-565.
5. Dickens M.H. and Hutchings M.T. J. Phys. C: Solid State Phys. 11 /1978/ 461-468.

LOCALIZED VIBRATIONS OF NITROGEN IN INTERSTITIAL PHASES OF Ta-N

S.I.Morozov, V.V.Kazarnikov
Institute of Physics and Power Engineering, Obninsk, Russia

The results of inelastic neutron scattering (INS) measurements of $TaN_{0.45}$ spectra are presented. Localized vibration spectra of nitrogen in the α and β phases were investigated and interatomic force constants of N and Ta coupling were obtained.

The INS-experiment was performed on the DIN-2PI spectrometer at room temperature. The initial energy of neutrons was 10 meV and the gain-energy processes were registered.

Fig. 1 shows the vibration spectra of nitrogen in $TaN_{0.45}$. Strong peak at ε=74 meV is a threefold degenerated excitation of N in β-phase Ta_2N. This kind of structure corresponds to the cubic symmetry of octahedral site (O-site) nitrogen occupies.

Two small peaks can be seen at ε=52 and ε=89 meV (fig.1) along with the ε=74 meV main peak. They correspond to the vibrational spectra of nitrogen in α-Ta-N-phase which coexists with the β-phase in our sample. These data are close to the data [1] for α-phase Ta-N.

The experimental data of interstitial atoms vibrational energies in α Ta-N and metal-impurity (Me-X) coupling constants are given in Table. The relation between Me-X central force constants γ and experimental vibrational frequency of an atom in an O-site can be presented as [2]:

$$\gamma = \frac{m\omega_1^2}{2}\left[\frac{m}{\quad}\left(\frac{\langle\omega^2\rangle}{\omega_1^2}\right)\right]^{-1} \qquad (1),$$

where ω_1 is the interstitial atoms local mode frequency, and $\langle\omega^2\rangle$ is the mean square frequency of host atom vibrations.

The correlation between nitrogen atom vibrational frequency and Me-X distance R_{om} (without accounting of host atom static displacement) is seen in Table. The dependence of $\hbar\omega$ on R_{om} for Ta-N phases is described by a linear function in a first approximation. Furthermore all data available on optical mode excitations energies $\hbar\omega$ of nitrogen in interstitial phases (Ti,Zr,V,Ta) -N can be well represented by the same relationship (see fig.2).

Along with the nitrogen local excitations earlier described we also see peaks at ε=36±2.4 and ε=45±3.2 meV the nature of which is not clear. In our opinion it is a result of interstitial atom vibrations or their complexes.

Table

Metal-Impurity coupling force-constants and nitrogen excitation energy in MeN_x interstitial phases.

Phase	Struct. of met. latt.	Excitat. energy, meV	Excitat. Width, meV	Coupling const, γ $*10^4 \frac{dyn}{sm}$	O-site radii Å	Lattice paramet. Å
α-$TaN_{0.03}$	BCC	59±2.2 89±4.5	7±2 13±5	9.0±0.6 20.4±2.1	2.345 1.658	a=3.317
β-$TaN_{0.45}$	HCP	74±0.9	8±1	14.1±0.3	2.147	a=3.048 c=4.918

LOCALIZED VIBRATIONS OF HOST ATOMS IN Zr-O INTERSTITIAL SOLID SOLUTIONS

S.I.Morozov, Institute of Physics and Power Engineering, Obninsk, Russia

Investigation of the detailed structure of Zr-O and Ti-O alloys vibration spectra has been performed. The localized states (LS) of the host atoms which are the nearest neighbors to the interstitials have been observed in the gap between continuous metal atoms spectra and localized impurity vibration excitations (see fig.1).

It is necessary to note that the intensity of these metal atom LS in inelastic neutron scattering spectra are much less than the split-mode intensities of the V-group transition metals with oxygen we observed earlier [1]. Nevertheless the energies of the split-modes both in hexagonal structures and in V-O BCC and BCT-structures may be described as a mean-field approximation by an equation which connects the quasi-molecular vibrational frequency ω_{qm} with the continuous spectra bound frequency ω_b and interstitial local vibrational frequency ω_l [2]:

$$\omega_{qm}^2 = 0.9\omega_b^2 + \frac{m}{2M + m}\cdot\omega_l^2$$

where m and M are the mass of interstitial and host atoms, respectively.

In spite of a good agreement between estimated values and experimental data [2] there is no answer why we can observe split-modes very well in BCC-structures, worse in BCT, and poorly in HCP-structures.

It is not clear whether it is a result of different nuclear cross section of the concrete alloy or impurity concentration effects or defect point symmetry effects. To answer this question it is necessary to perform calculations of the solid solution vibrational spectra with the Me-X (X=O,N,C) interaction potential model.

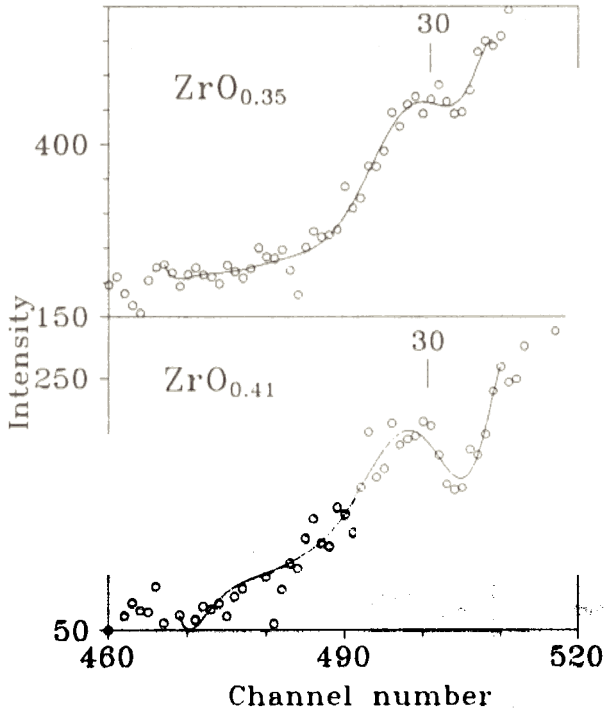

Fig.1. Localized vibrations of host atoms in ZrO_x interstitial solid solutions. Energies $\varepsilon=\hbar\omega=E-E_0$ of rows - marked peaks are indicated in meV. Here E_0 and E are initial and final energies of neutrons.

1. S.A.Danilkin et al. Fiz. Tverd. Tela, 1980, v.22, p.3327.
2. S.I.Morozov. Preprint IPPE-2190. Obninsk. 1991 (in Russian).

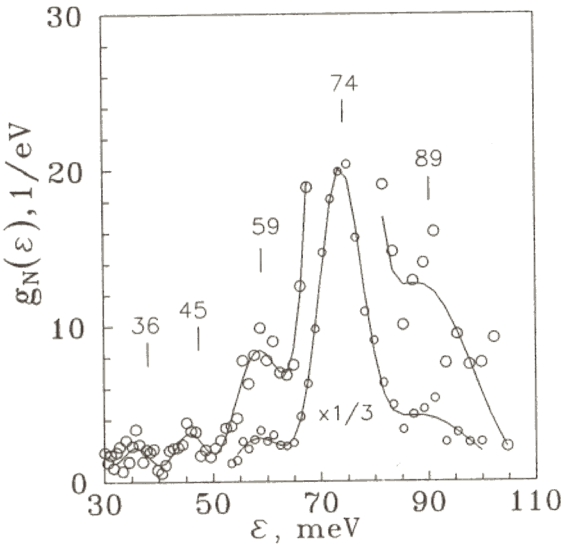

Fig.1. Nitrogen vibration spectra (α+β phases) in $TaN_{0.45}$. Energy of vibrations $\varepsilon=\hbar\omega$ is indicated in meV.

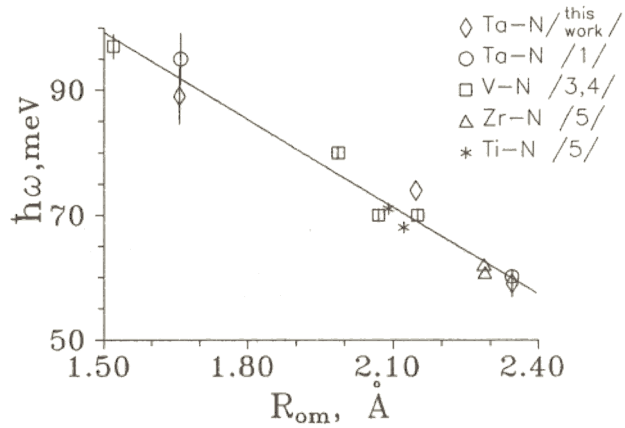

Fig.2. Nitrogen atoms excitation energies versus octahedral site radii of host-atom lattice in Me-N interstitial phases. Experimental data have been taken from [1-5] and this work.

REFERENCES:

1. S.A.Danilkin et al. Fiz. Tverd. Tela, 1989, v.31, p.8 (in Russian).
2. S.I.Morozov. Preprint IPPE-2190, Obninsk, 1991 (in Russian).
3. S.I.Morozov et al. Preprint IPPE-1931. Obninsk, 1988 (in Russian).
4. S.A Danilkin et al. Physica B, 1991, v.174, p.241.
5. S.I.Morozov et al. Fiz. Tverd. Tela, 1987, v.29, p.1653 (in Russian).

OXYGEN ATOM VIBRATIONAL EXCITATIONS IN Y-O-H SOLID SOLUTIONS

S.I.Morozov*, V.V.Sumin**

* Institute of Physics and Power Engineering, Obninsk, Russia
** Frank Laboratory of Neutron Physics, JINR, Dubna

Investigations of yttrium-hydrogen solid solution by the inelastic neutron scattering (INS) method have shown for the first time that the shape of hydrogen vibrational spectra do not correspond to interstitial site symmetry [1]. The existence of two peaks in the INS-spectra of hydrogen atoms in the $YH_{0.1}$ alloy occur to be connected with different vibration frequencies polarized parallel to the c axis and perpendicular to the c axis. There is a question if this kind of effect can appear in yttrium alloys with interstitial atom more heavier and greater than hydrogen. The alloy $YO_{0.03}H_{0.03}$ has been investigated by INS-method in this connection.

The measurements were performed on the DIN-2PI spectrometer at an initial neutron energy of E_0=10 meV. INS-spectrum of localized vibrations (LV) of oxygen and hydrogen is shown on fig.1.

The hydrogen LV-spectrum (ε'_H=100 meV, ε''_H=134 meV) is similar to that which has been observed for $YH_{0.1}$ [1]. The oxygen vibration spectrum in $YO_{0.03}H_{0.03}$ includes two peaks (ε'_O=40 meV and ε''_O=50 meV) and consequently do not correspond to the symmetry of cubic octahedral sites which oxygen atoms occupied in the Y-lattice.

In all INS-spectrum of interstitial solid solutions with an HCP-structure of the host lattice, the p-element's LV have been observed as an isolated threefold degenerated peak [2]. The splitting of local mode peaks as in case of Y-H interactions so Y-O once is able to explain by the displacement of impurity atoms from the center of interstitial site.

Interstitial atoms dynamics may be described by the Me-X model of effective pair potential. The minimum of this potential is at $R_0=R_M+R_X$, where R_M, the host atoms metallic radii, and R_X, the interstitial atoms' Pauling radii. For Y-O this value R_0=2.46 Å is markedly less than the distance from lattice point to octahedral site center of R_O=2.55 Å. At this conditions the potential profile of force-field in which the interstitial is found probably has two minima. We can expect a clearly seen splitting of the local mode under such form of the Me-X potential.

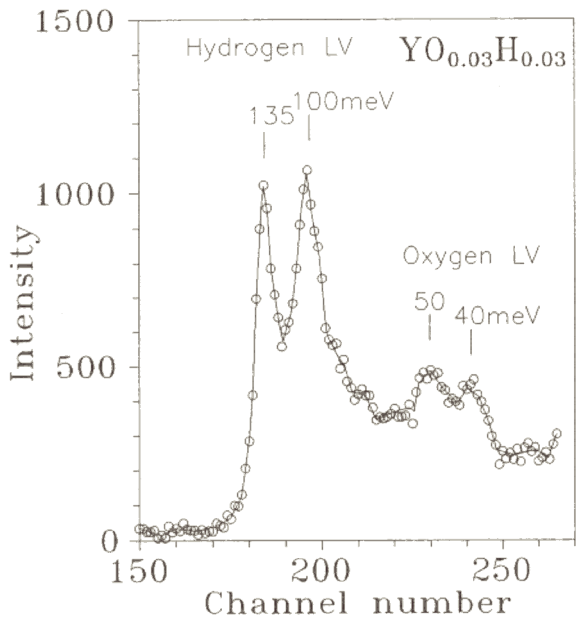

Fig.1. $YO_{0.03}H_{0.03}$ **INS-spectrum of oxygen and hydrogen localized vibrations. Energies** $\varepsilon=\hbar\omega=E-E_0$ **of row-marked peaks are indicated in meV. Here** E_0 **and E are initial and final energies of neutrons. Pure Y INS-spectrum is subtracted.**

REFERENCES:

1. I.S.Anderson et al. Phys. Rev. Lett., 1986, v.57, p.2822.
2. S.I.Morozov et al. Fiz. Tverd. Tela, 1987, v.29, p.1653 (in Russian).

EFFECT OF NITROGEN ON LATTICE DYNAMICS OF THE AUSTENITIC Fe-Cr-Mn-Ni ALLOYS

S.A.Danilkin*, V.P.Minaev*, V.V.Sumin**

* Institute of Physics and Power Engineering, Obninsk, Russia.
** Joint Institute for Nuclear Research, Dubna, Russia

1. Nitrogen alloying additions increase the strength of the austenitic steels. The INS study provides important information for interatomic force constants determination and the changes that may occur during alloying. In recent papers /1,2/ austenitic Fe-Cr-Mn and Fe-Cr-Ni alloys with nitrogen content in the range of 0.05-1.0 wt.% have been studied. In this work the INS measurements of the austenitic Fe-Cr-Mn-Ni f.c.c. alloys (C-0.07 wt.% ,Mn-9.64% ,Si-0.45% ,S-0.004%,P-0.008%, Cr-18.48% ,Ni-16.13%) with a nitrogen content of 0.06-0.50 wt.% are presented /3/.

The frequency spectra were measured with the DIN-2PI direct geometry spectrometer.

The frequency spectrum of Fe-18Cr-10Mn-16Ni alloy consists of two parts (Fig.1):

1) ε=0-40 meV - metal atom vibrations. Two peaks in the spectra correspond to transversal vibrations (ε_t) at 23.8 meV and longitudinal vibrations (ε_l) at 32.0 meV.

2) nitrogen atom vibrations peak at 79 meV (Table).

Metal atom spectrum.

As seen in Fig.1 and from the $\langle\varepsilon^2\rangle$ values given in the Table, the metal atom spectrum of alloys studied does not depend on nitrogen content. This contrasts with earlier results for Fe-Cr-Mn steels when the decrease in the frequency spectrum parameters (2-3% per wt. for $\sqrt{\langle\varepsilon^2\rangle}$, ε_t and ε_m) was observed /1,2/. According to the Gruneisen equation with γ=1.98 and $\Delta a/ca$=0.034 a reduction of metal atom frequencies ($\Delta\varepsilon/c\varepsilon$=-0.05) was expected for Fe-18Cr-10Mn-16Ni steels. But additional Me-N bonds increase the $\langle\varepsilon^2\rangle$ and, also, nitrogen produces perturbation of the electron screening. Therefore, probably, for the Fe-18Cr-10Mn-16Ni alloys studied a compensation of this effects takes place and no concentration dependence is observed. A similar compensation of the lattice dilation and even an increase in the metal atom frequencies caused by nitrogen and oxygen interstitials were observed earlier for V, Nb and Ta /4/.

Nitrogen atom vibrations.

The energy (ε_N), width ($\Delta\varepsilon_N$) and intensity (I_N) of the nitrogen vibration peak are given in Table. The tendency to reduce the ε_N with nitrogen content is observed ($\Delta\varepsilon_N/c\varepsilon_N$=-0.043±0.042). This value is in agreement with Gruneisen equation estimations (-5%).

The nitrogen vibration peak width and intensity increase with nitrogen content approximately in a linear fashion (Table). This shows that nitrogen atoms are mainly in a solid solution and precipitation of nitrides does not occur. This contrasts with results we obtained for carbon steels with appropriate metal element content- Fe-21Cr-3Mn-21Ni. For carbon steel the linear dependence of the lattice parameter vs. carbon content was observed only up to 0.2%. At higher carbon content the slope of the a(c) dependence decreases and additional peaks corresponding to the carbide phases appear in frequency distribution. Therefore the solid solution hardening does not take place in carbon austenitic steels studied with high interstitial content.

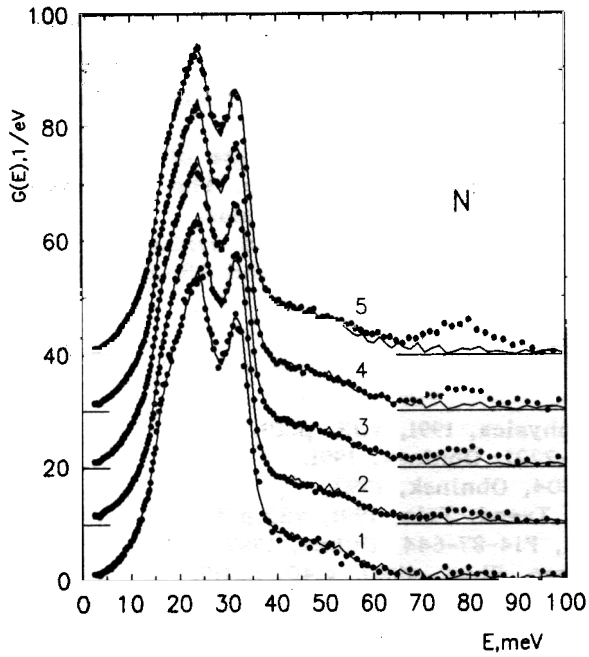

Fig.1 Frequency spectra of nitrogen austenitic steel Fe-18Cr-10Mn-16Ni with nitrogen content:
1 - 0.13%
2 - 0.17%
3 - 0.30%
4 - 0.34%
5 - 0.50%
Solid line shows the frequency spectrum of steel containing 0.06% N.

TABLE

Nitrogen atom content, lattice parameter and frequency spectrum parameters in the Fe-18Cr-10Mn-16Ni steel.

No.	%wt.N	o a.A	Frequency spectra parameters $\langle\varepsilon^2\rangle$ [1]	ε_N [2]	$\Delta\varepsilon_N$ [2]	I_N [3]
1.	0.06	3.588	538±15			
		(3.588)	(534±15)	-	-	-
2.	0.14	3.592	536±15	80.5±1.3	7.4±1.6	9.3±2.0
3.	0.17	3.596	538±15	79.7±0.9	8.0±1.3	13.8±3.0
4.	0.30	3.600	537±15	80.1±0.9	11.2±1.0	28.5±5.0
5.	0.35	3.600	539±15	79.4±1.2	10.8±1.1	31.8±6.0
		(3.600)	(525±15)	(75.7±2.1)	(13.5±2.2)	(27±8)
6.	0.50	3.604	538±15	78.7±0.9	13.9±1.3	65.0±9.0
		(3.604)	(522±15)	(76.5±1.3)	(17.1±1.7)	(65±10)

1) $\langle\varepsilon^2\rangle$ - moment of the metal atoms frequency spectrum, meV^2.
2) ε_N, $\Delta\varepsilon_N$ - energy and width of the nitrogen peak, meV.
3) I_N - nitrogen peak area
Values in parenthesis are given for alloys after deformation.

2. The same Fe-18Cr-10Mn-16Ni alloys with nitrogen content 0.06, 0.35 and 0.50 % were studied after cold deformation (ε_d=90%). The lattice parameter and nitrogen peak intensity remains practically unchanged after deformation (Table) and ,obviously, nitride precipitation does not take place.

The smoothing of the peaks in metal atom spectrum and increase of the density of states at ε=5÷15 meV was observed in deformed specimens. The deformation decrease the $\langle\varepsilon^2\rangle$ values and frequencies of the nitrogen atoms.

Effects of enhancement of low-frequency modes were observed earlier in the frequency spectra of deformed Re and Re-Mo alloys /5/, Nb and Nb-Zr alloys /6/, in deformed Cu /7/.

REFERENCES:

1. V.G.Gavriluk, S.A.Danilkin et al Metallophysica, 1991, v.13, p.29.
2. S.A.Danilkin,V.P.Minaev, V.V.Sumin PhEI-2221, Obninsk, 1991.
3. V.G.Gavriluk, S.A.Danilkin et al PhEI-2304, Obninsk, 1993.
4. S.A.Danilkin, V.P.Minaev, V.V.Sumin Fiz. Tverd. Tela, 1991, v33,p.3.
5. A.V.Belushkin, M.G.Zemlianov et al JINR, P14-87-644, Dubna, 1987.
6. E.L.Wolf,R.J.Noer, G.B.Arnold J. Low Temp. Phys., 1980, v.40, p.419.
7. J.Bevk, Phil. Mag.,1973, v.28, p.1379.

THE ANALYSIS OF INCOHERENT NEUTRON SCATTERING ON LIQUID POTASSIUM AT 340K - 550K

M.V.Zaezjev, M.N.Ivanovski, A.G.Novikov,
V.V.Savostin, O.V.Sobolev, A.L.Shimkevich

Institute of Physics and Power Engineering, Obninsk, Russia

We present here the data for atomic dynamics of liquid potassium obtained from inelastic neutron scattering experiments on DIN-2PI spectrometer. The details about the spectrometer and experiment itself can be find elsewhere [1, 2]. In this report the results of incoherent neutron scattering analysis are given including two parts concerned with the inelastic and quasi-elastic components of double-differential scattering cross section (DDS).

A) The analysis of inelastic component was aimed to get the frequency spectra (FS) of the velocity autocorrelation function (the FS of atomic vibrations) in liquid potassium for three temperatures: 340K, 440K and 550K. For data processing the program code SLOWN [3] was used. To take into account the remarkable coherent part of potassium scattering cross section the program code based on the incoherent approximation was supplemented by the subroutine for coherent effects calculation using the viscoelastic model of Lovesey [4]. The FSs of liquid potassium obtained for three temperatures mentioned above are shown on Fig. 1. The comparison of 340K experimental spectrum with the corresponding curve for the solid potassium (300K, [5]) reveals the disappearance in liquid the structure features of FS existing in solid. At the same time the good agreement between our experimental FS and the results of molecular dynamics simulation for 340K [6] can be underlined. From Fig. 1 d, where experimental curves for three temperatures are plotted together, it follows that the temperature dependence of the FS in the temperature interval under our measurements should be estimated as a weak one.

A possible way for physical interpretation of the experimental FSs consists in the assumption they are the sums of two partial distributions corresponding to longitudinal and transversal modes. Using for partial curves the form proposed in [7] we can write:

$$g(\varepsilon) = g_L(\varepsilon) + g_T(\varepsilon) = \frac{4\varepsilon^2}{\sqrt{\pi}}\left[\frac{A_L}{\varepsilon_L^3}\exp(-\varepsilon^2/\varepsilon_L^2) + \frac{A_T}{\varepsilon_T^3}\exp(-\varepsilon^2/\varepsilon_T^2)\right], \qquad (1)$$

where ε_L and ε_T - are excitation energy maxima of partial curves (1); A_L and A_T - are their relative weights ($A_L + A_T = 1$). Describing the experimental curves at each temperature by the expression (1) and assuming temperature independence of these weights we find out ε_L and ε_T in the temperature range 340K - 550K demonstrated the approximately linear temperature dependence:

$$\varepsilon_{L,T} = \varepsilon^0_{L,T} - a_{L,T}T \, . \qquad (2)$$

The descriptions of the experimental FSs by expression (1) are plotted on Fig. 1 as a solid lines.

Given the atomic vibration FS of the substance, it is possible by using well-known expressions to get a number of microdynamic characteristics of this substance. So, in particular for three temperatures mentioned we calculate: the velocity autocorrelation function; the mean-square displacement of an atom as a function of time; the mean-square amplitude of atomic vibrations; the force constant for interatomic force field, averaged over directions (for details see [1]).

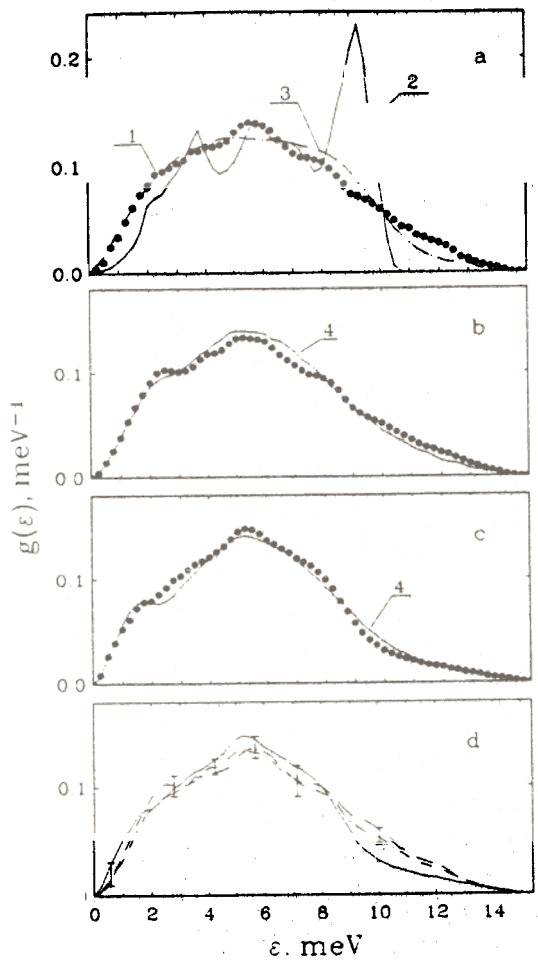

Fig. 1. The frequency spectrum of atomic vibrations in liquid potassium.
a - 340K; b - 440K; c - 550K;
1 - experiment;
2 - solid potassium (300K) calculation [5];
3 - molecular dynamics simulation (340K) [6];
4 - calculation by exp. (1);
- - - 340K;
- · - 440K;
——— 550K.

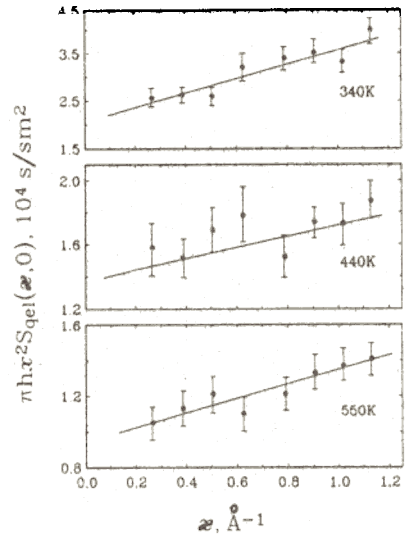

Fig. 2. The dependence of $\pi\hbar\text{æ}^2 S_{q.el.}(\text{æ},\varepsilon=0)$ vs. æ in the framework of the mode-coupling theory [11]; points -experiment; solid lines -calculation by the exp.(4).

Along with microdynamic characteristics the knowledge of FS allows for the estimation some of thermodynamic properties of the substance. For example, the isochoric specific heat of liquid potassium was calculated by taking into account for anharmonic effects arisen from the temperature deformations of FS. Within the experimental accuracy our results are in accordance with the reference data [8]. Gruneisen parameter was also derived from the expression

$$\gamma_G = - \frac{\partial \bar{\varepsilon}}{\bar{\varepsilon}\ \alpha_p\ \partial T} \qquad (3)$$

where $\bar{\varepsilon} = \int \varepsilon\ g(\varepsilon)\ d\varepsilon$

the excitation energy, averaged over FS, and α_p - the temperature coefficient of thermal expansion at a constant pressure. Within the accuracy of experimental data γ_G does not depend of temperature and its value is not far from that, obtained for solid potassium near the melting temperature [9].

B) Using the data obtained in preceding section the quasi-elastic component of DDSs was separated and transformed in the scattering low $S(æ,\varepsilon)$ at æ = const. It was concluded that under our experimental conditions there is no any remarkable presence of the coherent effects in the quasi-elastic scattering. The natural line of the quasi-elastic scattering low was approximated by lorenzian and its half-width $\Delta E(æ^2)$ for three temperatures can be satisfactory described on the basis of the mixture diffusion model [10] supposing the existence in the melt of the jump and continuous diffusive motions. But the values of some parameters get in the framework of this model cast doubt upon the activation mechanism of the diffusion. That is why we made an effort to apply the mode-coupling theory, which gives for $S_{q.el.}(æ,\varepsilon=0)$ in reduced units the expression [11]:

$$\pi\hbar æ^2 S_{q.el.}(æ,\varepsilon=0) = \frac{1}{D}[1 + \alpha æ + O(æ^{3/2})]\ , \qquad (4)$$

where $\alpha = \left(\frac{2D}{\omega_0}\right)^{1/2}$, $\omega_0 = 72\left(\frac{\pi\rho D}{kT}\right)^2 (D + \nu)^3$,

D - diffusion coefficient, ρ - density, ν - kinematic viscosity. It was found that at 550K and 440K the expression (4) describes the experimental results of $S_{q.el.}(æ,\varepsilon=0)$ rather satisfactory (Fig. 2) and gives for D and ν the estimations not far from tabulated ones. And vice versa near the melting point (at 340K) there is no agreement between the coefficient of self-diffusion and viscosity get from (4) and their known values.

REFERENCES

1. Abramov A.V. et al. Soviet Atomic Energy,1989, v.66,№3,p.345 (in Russian).
2. Zaezjev M.V. et al. Russian J. Phys. Chem., 1994, v. 68, № 2, p. 240.
3. V.I.Ionkin et al. Jadernye Konstanty, 1989, № 1, p. 19 (in Russian).
4. Lovesey S. J. Phys. C, 1971, v. 4, № 18, p. 3057.
5. Gurskii Z.A., Chushak Ya.G. Phys. Stat. Sol. (b), 1990,v. 157, № 2,p. 557.
6. Gonzales Miranda J.M. J. Phys. F, 1986, v. 16, № 1, p. 1.
7. Hubbard J., Beeby. J.L. J. Phys. C, 1969, v. 2, p. 556.
8. Handbook of Thermodynamic and Transport Properties of Alkali Metals. Ed. R.Ohse. Blackwell Sci. Publ., London, 1985, ch.6.
9. Shouten D., Swenson C. Phys. Rev., 1974, v. 10B, № 6, p. 2175.
10. Oscotskii V.S. Phisica Tverd. Tela, 1963, v.5, № 4, p. 1082 (in Russian).
11. Verkerk P. Nuovo Cimento, 1990, v. 12D, № 4-5, p. 441.

Neutron Scattering Studies of Phase Transitions in Protonated and Deuterated Triammonium Hydrogen Disulphate

L. Bobrowicz[1] I. Natkaniec* , M. Mroz** , W. Nawrocik** and W. Wojtowicz***

* Joint Institute for Nuclear Research , Dubna , Russia
** A. Mickiewicz University , Poznan , Poland
*** Pedagogical University , Zielona Gora , Poland

Triammonium hydrogen disulphate , $(NH_4)_3H(SO_4)_2$, undergoes four phase transitions at atmospheric pressure above the liquid nitrogen temperature [1] and one phase transition below it [2] :

Phase I is the trigonal R3m , the room temperature phase I is monoclinic with the space group A2/a , phase III is also monoclinic [3].

In the deuterated triammonium hydrogen disulphate , $(ND_4)_3D(SO_4)_2$, phase V does not exist and the crystal shows four phase transitions below room temperature [4] :

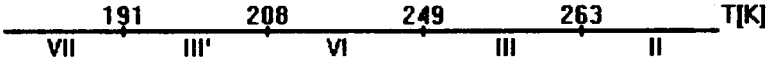

We report results of neutron diffraction (ND) and inelastic incoherent neutron scattering (IINS) of normal and deuterated crystals. Experiments were conducted on the multipurpose neutron spectrometer NERA - PR at the IBR - 2 pulsed reactor.

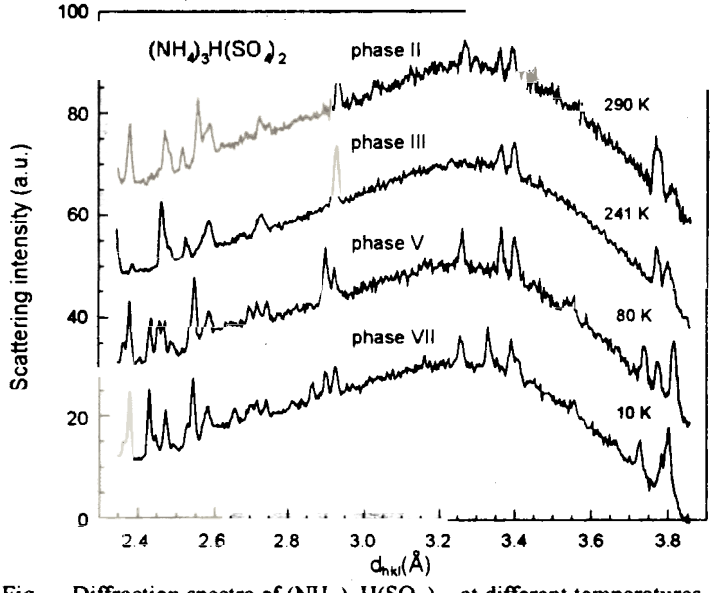

Fig. Diffraction spectra of $(NH_4)_3H(SO_4)_2$ at different temperatures.

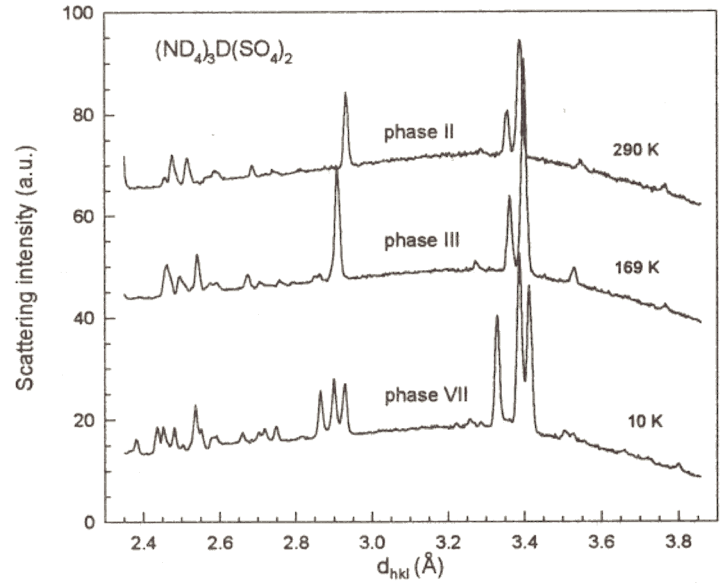

Fig.2. Diffraction spectra of $(ND_4)_3D(SO_4)_2$ at different temperatures.

Figures 1 and 2 show the diffraction spectra for normal and deuterated crystals at different temperatures. For the $(NH_4)_3H(SO_4)_2$ crystal considerable differences in the structure of phases II , III , V and VII have been observed. For the deuterated crystal we have observed phases II , III and VII only. The temperatures of the phase transitions indicate that deuterium exchange in the crystal is of about 85%.

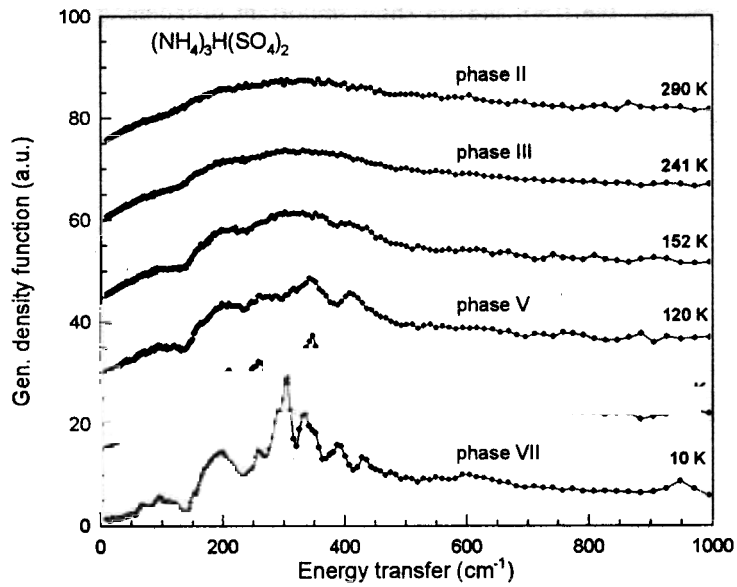

Fig.3. Temperature dependence of IINS spectra of $(NH_4)_3H(SO_4)_2$ crystal.

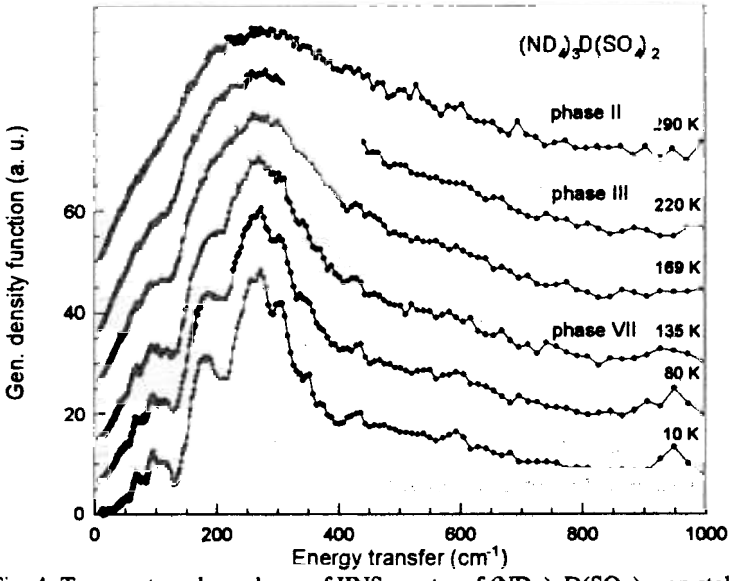

Fig. 4. Temperature dependence of IINS spectra of $(ND_4)_3D(SO_4)_2$ crystal

Examination of the IINS spectra of $(NH_4)_3H(SO_4)_2$ and $(ND_4)_3D(SO_4)_2$ (fig. 3 and 4) shows that they vary considerably with temperature , especially in the 150 - 450 cm^{-1} range. For both compounds , the frequency shift versus temperature are generally small; the significant change has only been observed at the V - VII phase transition in $(NH_4)_3H(SO_4)_2$. The IINS spectra of phases V and VII triammonium hydrogen disulphate consist of numerous bands chracteristic of an ordered crystal. When the temperature increases , the IINS spectra show important broadening due to orientational disorder of ammonium ions.

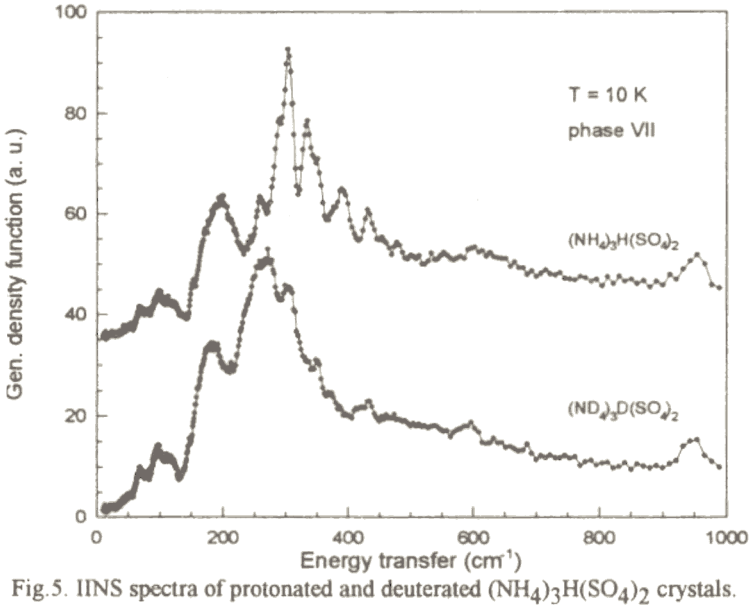

Fig.5. IINS spectra of protonated and deuterated $(NH_4)_3H(SO_4)_2$ crystals.

Fig. 5 shows IINS spectra of protonated and deuterated crystals at 10 K (phase VII). A comparison of the Raman , infrared [5] and IINS spectra in this phase shows that they are similar exept for isotope effect for the ammonium bands.

Acknowledgments

The authors express their sincere thanks to T. Sarga and S. I. Bragin for their valuable help with the neutron scattering measurements.

References:

1. K.Gesi , Phys. Status Solidi (a) , 33 , 479 (1976).
2. K. Gesi , Jap. J. of Appl. Phys. , 19 (6) , 1051 (1980).
3. S. Suzuki and Y. Makita , Acta Cryst. , B34 , 732 (1978).
4. T.Osaka , Y. Makita and K. Gesi , J. Phys. Soc. Jpn. , 49 , 593 (1980).
5. M.Kamoun , A. Lautie , F. Romain and A. Novak , J. Raman Spectrosc. , 19 , 329 (1988).

Neutron scattering studies of ammonium dynamics and phase transition in $K_{1-x}(NH_4)_xSCN$ at 10K.

I. Natkaniec, L.S.Smirnov, A.I.Solov'ev, S.I.Bragin
Frank Laboratory of Neutron Physics, JINR, Dubna

KSCN and NH_4SCN crystals have layered structures of SCN and K or NH_4 ions. These crystals undergo a phase transition from the high temperature tetragonal phase I at T_c=413 and 391K, respectively, to the the orthorhombic phase II, which is associated with the ordering of linear SCN ions and with two NH_4 ions. At about 360K, orthorhombic NH_4SCN transforms in to the monoclinic phase III with ordered orientation of other two-tetrahedral NH_4 ions. We investigated the elastic and inelastic incoherent neutron scattering from the mixed $K_{1-x}(NH_4)_xSCN$ system on the NERA-PR time-of-flight inverted geometry spectrometer to study the influence of composition and symmetry of the dynamics of ammonium ions.

Powder samples of $K_{1-x}(NH_4)_xSCN$ with x=0, 0.005, 0.05, 0.15, 0.34, 0.50, 0.60, 0.68, 0.75, 0.85, 0.95 and 1 were prepared by evaporation of appropriate aqueous solutions at 350K. The structural parameters obtained by neutron powder diffraction are presented in Fig.1. One can see, that the transformation from the phase II to the phase III has its origin at x=0.75. The determined concentration dependence of the generalized phonon density of states G(E) in the one-phonon incoherent scattering approximation for $K_{1-x}(NH_4)_xSCN$ is presented in Fig.2.

For diluted ammonium solutions (x=0.15) the unit cell parameters are close the those of pure KSCN. The G(E) functions exhibit rotational tunneling transitions at about 30 cm^{-1}, as well as localized translational (195 and 228 cm^{-1}) and torsional (295 and 327 cm^{-1})vibrations of NH_4 ions. With increasing ammonium concentration the unit cell volume and orthorhombic distortion increase, showing some saturation effect for 0.50<x<0.75. Localized vibrations for these concentrations of ammonium form broad bands, with maxima corresponding to the following frequencies: 180, 220, 292 and 327 cm^{-1}. The linear behavior of the G(E) functions below 30 cm^{-1} speaks of the static disorder of NH_4 ions (orientational glass) at 10K in the above indicated concentration range of the ammonium in the orthorhombic phase. Phase transition to the ordered monoclinic phase III occurs at about 75% ammonium concentration. A significant increase of the unit cell volume is observed at this transition. In the ordered phase of ammonium thiocyanate the torsional band shifts to higher frequencies and splits into four sub-bands, corresponding to 318, 352, 380 and 409 cm^{-1}. The translational band of NH_4 vibrations becomes narrower and shows maxima at 179 and 193 cm^{-1} which values are close to the corresponding frequencies in the orthorhombic phase.

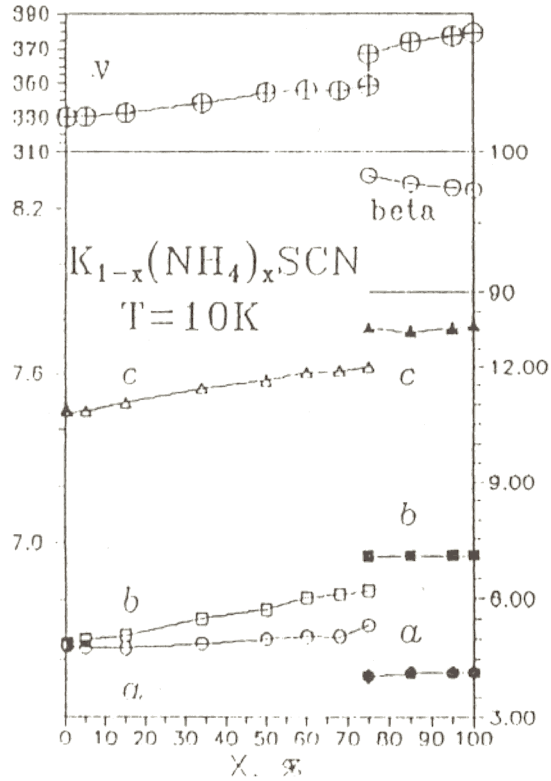

Fig.1. Unit cell parameters and the volume of potassium—ammonium thiocyanate solid solutions at 10 K.

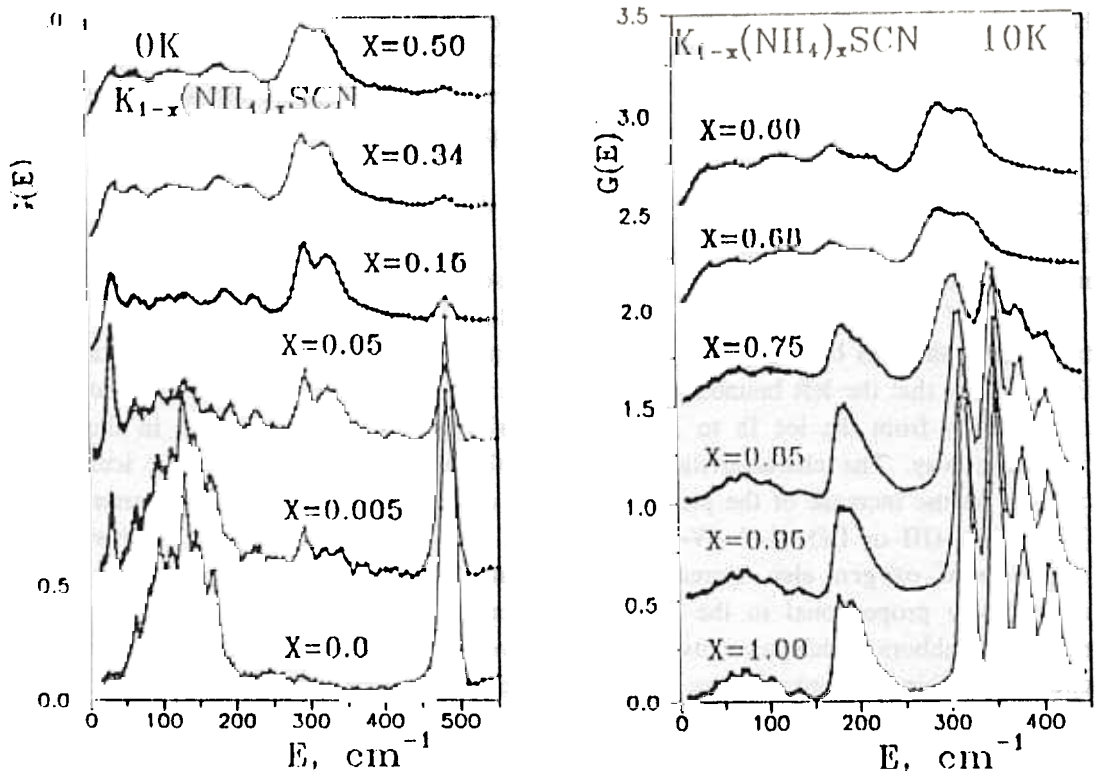

Fig.2. Generalized phonon density of states $G(E)$ of potassium—ammonium thiocyanate solid solutions normalized to the same area in the frequency range $(0-500)cm^{-1}$.

VIBRATION SPECTRUM OF THE ICE III

I. Natkaniec, L.S. Smirnov
Frank Laboratory of Neutron Physics
Joint Institute for Nuclear Research, Dubna, Russia
A.N. Ivanov
The Institute for Physics of High Pressures, RASc, Troitsk

The ice is unique object for studying the effect of the orientational disorder upon the vibration spectrum. To investigate the ices Ih, Ic, II, III, IX, V, and VI is possible only under the pressure of up to 20 kbar and at the temperature below 270K. Some of these phases of ice are fixed by means of the quenching method [1].

The vibration spectrum of the quenched ices Ih, II, IX, V, and VI have been studied by means of the inelastic incoherent neutron scattering (IINS) at different pulsed sources [2,3]. The crystal structure of ice in these phases varies from totally disordered with respect to the hydrogen position to partly or totally ordered. The structure of the ice III is similar to that of the ice IX and differs from the latter in the ordering degree [4]. It is tetragonal, the space group is $P4_12_12$, Z=12, the unit cell parameters are a=6.6662 A and c=6.9358 A. The unit cell parameters are close tothose of the ice IX. However, some researchers [5] insist that the ice III cannot be produced by the use of quenching.

The IINS measurement of the ice III has been carried out *in situ* with the help of the clamped high pressure cell [3] at the NERA-PR neutron spectrometer with the use of the pyrolytic graphite analyzer crystal. The ice III has been produced by the isobaric cooling of the high pressure cell with the sample in the flow cryostat down to T=250K with the initial pressure at the room temperature P=3 kbar. The further cooling down to 200K has allowed comparing spectra of the ices III and II. The obtained generalized phonon densities of states G(E) of the ice III (250K), the ice II (200K) as well as G(E) of the ices Ih and II at 80 K measured earlier are shown in Fig. 1 for comparison.

G(E) of ice consists of the libration zone, which is isolated from the region of translation phonons by a gap. The G(E) dependences for the ices Ih, III, and II in Fig. 1 show that the left boundary of the libration zone shifts to lower energies at thetransition from the ice Ih to II. This regularity may be accounted for in the following way. The characteristic property of the crystal structures of the ices consists in the increase of the phases density in moving along the p--T diagram ((Ih or Ic)--(III or IX)--II-V--IV--VI--VIII), but the distance between the nearest neighbors of oxygen also increases. The orientational intermolecular interaction is inversely proportional to the power dependence of the distance between the nearest neighbors which accounts for the observed behavior of the libration zone energy. Within one phase, the distance between the nearest neighbors of oxygen decreases with the increaseof pressure, and the libration energy increases. Earlier we observed this in the ice II [3].

References:
1. P.V. Hobbs. Ice Physics, 1974.
2. J.C. Li et al. J. Chem. Phys., v.94, N10, 1991
3. O.I. Barkalov et al. Annual Report, FLNP JINR, 1991, Dubna, pp. 219-221
4. J.D. Londono et al. J. Chem. Phys., v.98, N6, pp. 4878-4888, 1993.
5. B. Minceva-Sukarova et al. J. Phys. C: Solid State Phys., v.17, pp. 5833, 1984.

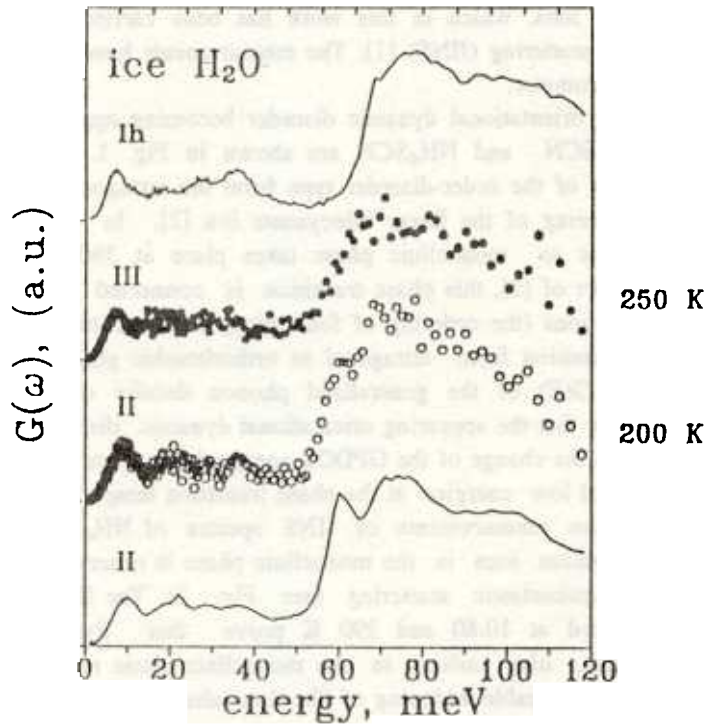

Fig. 1. Weighted phonon densities of states G(E) of the different phases of ice measured in situ in the high pressure cell with the initial pressure (from above down) P_{in} and following temperatures:

P_{in}=0.01kbar at 80K - ice Ih
P_{in}=3kbar at 250K -ice III .
P_{in}=3kbar at 200 -the ice II
P_{in}=3kbar at 80K - the ice II.

INVESTIGATION OF THE TEMPERATURE DEPENDENCE OF STATIC AND DYNAMIC DISORDER IN THE $K_{1-x}(NH_4)_xSCN$ SYSTEM

I. Natkaniec, L.S. Smirnov, S.I. Bragin, A.I. Solov'ev
Frank Laboratory of Neutron Physics
Joint Institute for Nuclear Research, Dubna, Russia

The x-T phase diagram of $K_{1-x}(NH_4)_xSCN$ shows that this compound is an interesting object for investigation into the temperature dependence of static and dynamic disorder of ammonium and thiocyanate ions, which in this work has been carried out by means of inelastic incoherent neutron scattering (IINS) [1]. The measurements have been performed at the NERA-PR neutron spectrometer.

The results of studying orientational dynamic disorder becoming apparent in the region of phase transitions in KSCN and NH_4SCN are shown in Fig. 1. At 413 K KSCN undergoes a phase transition of the order-disorder type from the tetragonal to orthorhombic phase related with the ordering of the linear thiocyanate ion [2]. In NH_4SCN, a phase transition from orthorhombic to monoclinic phase takes place at 360 K. According to interpretation by the authors of [3], this phase transition is connected with orientational ordering of two ammonium ions (the ordering of four thiocyanate and two ammonium ions takes place at the phase transition from tetragonal to orthorhombic phase at 390 K). The temperature dependences G(E) of the generalized phonon density of states (GPDOS) presented in this work prove that the appearing orientational dynamic disorder of SCN and NH_4 ions manifests itself in the change of the GPDOS energy dependence from the Debye to the linear one in the region of low energies at the phase transition temperature.

However, our temperature measurements of IINS spectra of NH_4SCN show that the dynamic disorder of ammonium ions in the monoclinic phase is observed right up to 200 K which is manifested by quasielastic scattering (see Fig. 2). The IINS spectra of $K_{0.15}(NH_4)_{0.85}SCN$ measured at 10.80 and 290 K prove that dynamic disorder of ammonium ions is present, like earlier, in the monoclinic phase manifesting itself by quasielastic scattering and considerable widening of libration subzones (Fig. 3, T=290K) as well as by overlapping with translation optical phonons.

In NH_4SCN, orthorhombic phase exists in a very narrow temperature interval of 360 to 390K. Due to dynamic disorder, this makes impossible to investigate the libration zone. At the concentration of $x<0.75$, a possibility of measuring the libration zone energy of ammonium ion in the orthorhombic lattice of $K_{1-x}(NH_4)_xSCN$ appears. In the concentration interval from, say, x=0.30 to x=0.75, an orientational glass state caused by frozen static orientational disorder of ammonium ions arises in this compound at 10K. The static disorder causes widening of the libration zone, and for x=0.60 (see Fig. 4) the dynamic disorder is observed already at T=80K with the considerable presence of quasielastic scattering.

In the diluted solution region of a mixed crystal at the concentration of $x<0.15$ the low energy excitation of ammonium ions is observed at 10K. As the temperature increases, the dynamic disorder intensifies and transforms into jump diffusion (see Fig. 5).

1. I. Natkaniec, L.S.Smirnov, A.I.Solov'ev, S.I.Bragin, Proceedings of LT-20, Aug. 4-11, 1993, Eugene. OREGON, USA.
2. O. Blaschko, W. Schwarz, W. Schranz, A. Fuith. Ferroelectrics, 1991, v.124, N1-4, pp. 139-144.
3. W. Schranz, A. Fuith, H. Warkanek, R. Blinc, et al. Ferroelectrics, 1992, v.125, N1-2, pp. 257-262.

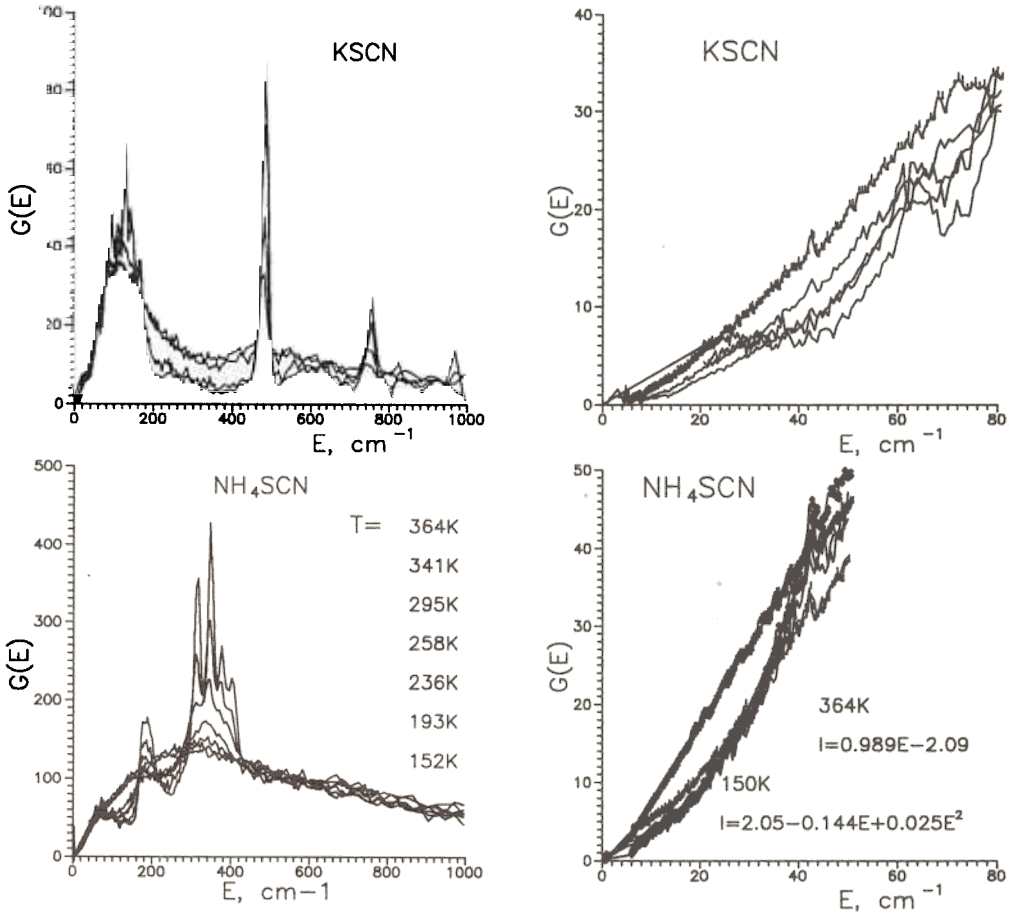

Fig 1. G(E) in the region of the order-disorder phase transition from tetragonal to orthorhombic phase for KSCN and in the region of transition from orthorhombic to monoclinic phase for NH_4SCN.

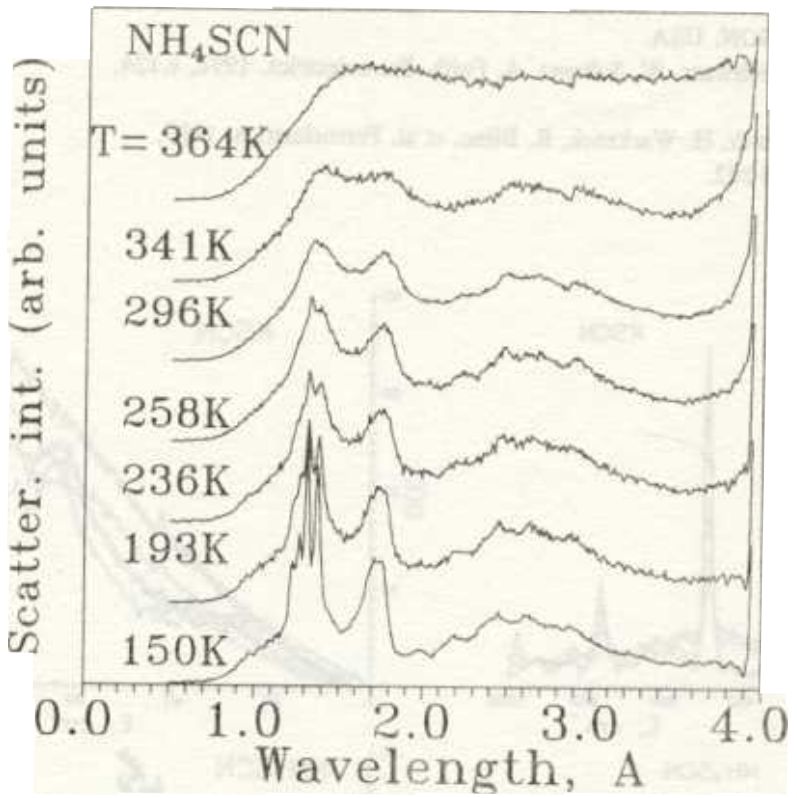

Fig 2. Temperature dependence of IINS spectra intensity for NH_4SCN.

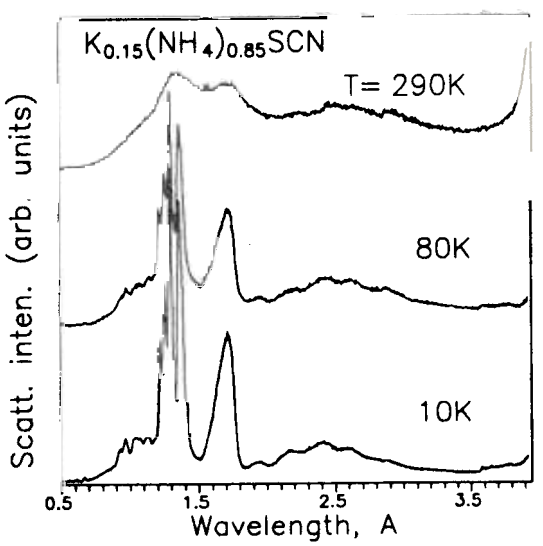

Fig 3. Temperature dependence of IINS spectra intensity for $K_{0.15}(NH_4)_{0.85}SCN$.

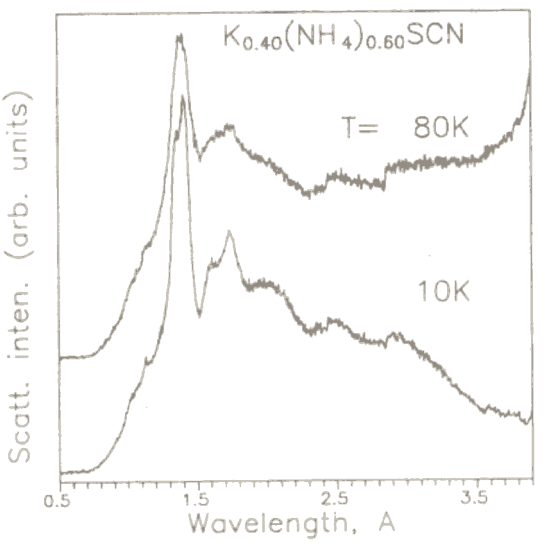

Fig 4. Temperature dependence of IINS spectra intensity for$K_{0.4}(NH_4)_{0.6}SCN$.

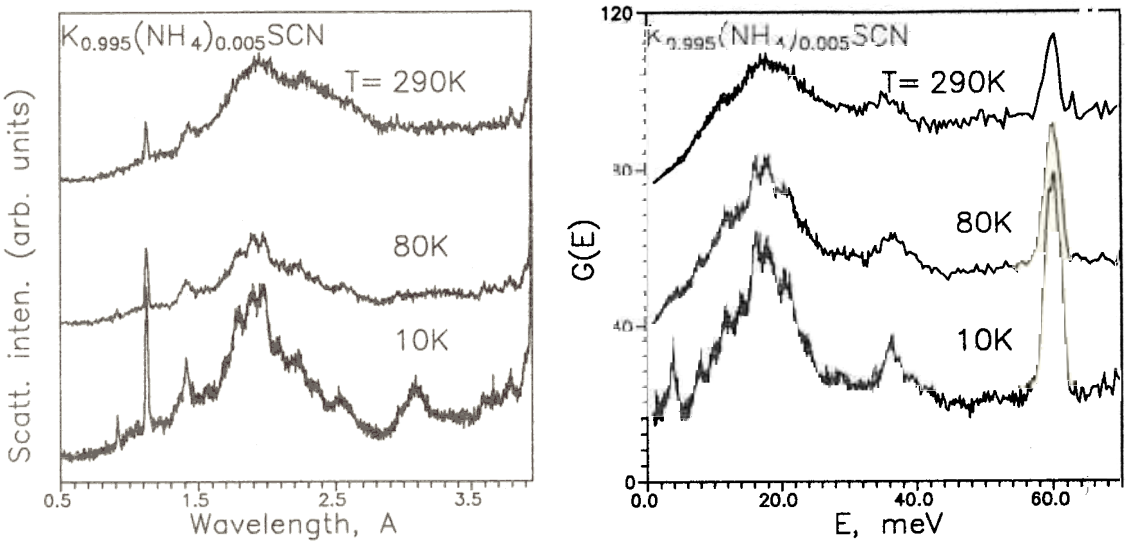

Fig 5. Temperature dependence of IINS spectra intensity and G(E) for $K_{0.995}(NH_4)_{0.005}SCN$.

THE SEARCH FOR THE CRYSTAL ELECTRIC FIELD IN THE COMPOUNDS OF THE ReNiSn (Re – Ce, La, Nd) TYPE

P.A. Alekseev, E.S. Clementyev, V.N. Lazukov, I.P. Sadikov
Russian Research Center "Kurchatov Institute", Moscow

A.Yu. Muzychka, I.L. Sashin
Frank Laboratory of Neutron Physics
Joint Institute for Nuclear Research, Dubna

In the recent time, the intensive investigations of the valency-instable CeNiSn system which has a gap in the electron states spectrum at the Fermi level are carried out [1,2]. In ascertaining the gap forming mechanism, the issue of characteristic energy of interaction between 4f electrons of Ce and crystal electric field (CEF) is vital. Namely, the ratio of the ground level splitting energy of Ce and the temperature at which violation of the coherency regime in the spin subsystem takes place (T=40°K) [3] is important. The magnetic excitations spectrum of the CeNiSn system is described by the quasi-elastic Lorentz peak with the half-width $\Gamma/2\approx3.5$ meV [2], i. e. no CEF effects are observed in it. One of the possible ways of assessing the magnitude of the 4f multiplet splitting in the CEF of the CeNiSn system is measuring the magnetic scattering spectrum of the $Ce_{1-x}La_xNiSn$ sample in which replacing Ce by La ion that has greater ion radius may lead to decreasing Ce valency down to transition into the Ce^{3+} state. Thus, measurements of the L_{III} of the ions absorption verge in the $Ce_{0.3}La_{0.7}NiSn$ sample at T=300K have proved abscence of the Ce^{4+} state within the limits of experimental accuracy. To assess splitting in the CEF for CeNiSn is also possible by using CEF Hamiltonian parameters which have been determined in an isostructure compound based on an ion with the integer-valued valency, for example, $Nd_xLa_{1-x}NiSn$. In this work, the inelastic neutron scattering from the $Ce_{0.3}La_{0.7}NiSn$ and $Nd_{0.3}La_{0.7}NiSn$ samples has been studied. The unit cell parameters of the latter sample are close to those of CeNiSn. The measurements have been performed at the KDSOG time-of-flight spectrometer at 10, 80, and 300K at the scattering angles 2θ=30 to 90° and fixed final energy of neutrons E_f=4.9 meV. The mass of polycrystal samples was about 150 grams.

Fig. 1 shows the magnetic component of the neutrons scattering function S_{mag}(E) of $Ce_{0.3}La_{0.7}NiSn$ at T=10K. The spectrum is well fitted by the quasi-elastic spectral function with half-width $\Gamma/2\sim4.6\mp2$ meV. The increase of the temperature up to 80K leads only to slight widening of the Lorentz function width ($\Gamma/2\approx5$ meV). At T=300K, no magnetic component of the scattering has been discerned. The observed spectral response, like in the case of CeNiSn, manifests instability of the 4f shell of $Ce_{0.3}La_{0.7}NiSn$ at low temperatures. Thus, for assessing the splittinng of the 4f Ce multiplet in the CeNiSn CEF only the second possible method that consists in measuring the magnetic neutrons scattering from Nd_{3+} ions in CeNiSn lattice may be applied. Fig. 2 shows the spectral functions S(E) of neutron scattering for the $Nd_{0.3}La_{0.7}NiSn$ and LaNiSn samples at T=80K. The diference between S(E) measured for these samples is the magnetic component of the inelastic neutrons scattering from the neodymium ions caused by CEF effects. The peaks in the magnetic scattering spectrum corespond to transitions between the 4f levels of the $Nd3+$ ion multiplet splitted in the CEF. 10-fold degenerate

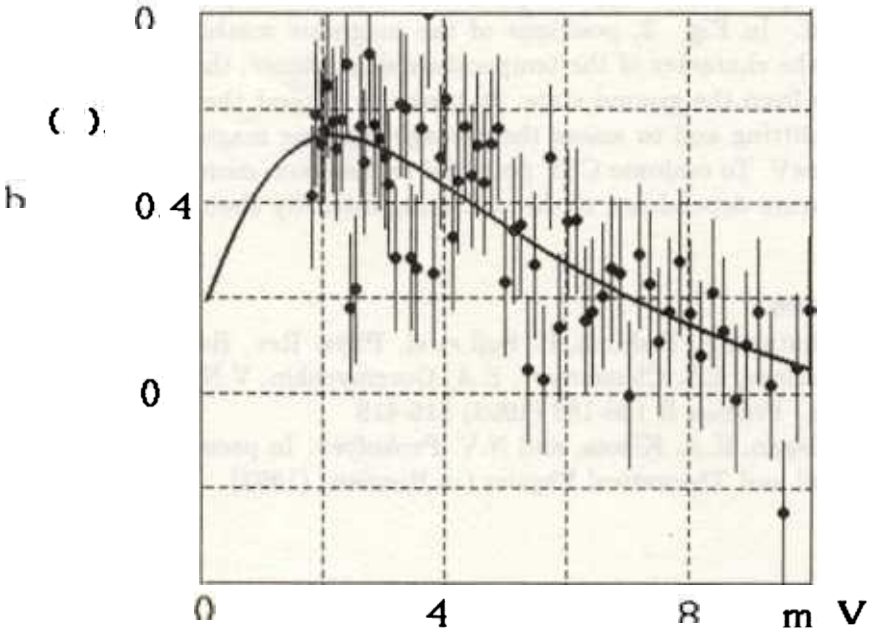

Magnetic component of neutrons scattering function S(Q) for $Ce_{0.}$ $La_{0.}$ $Ni_{0.}$ $Si_{0.}$

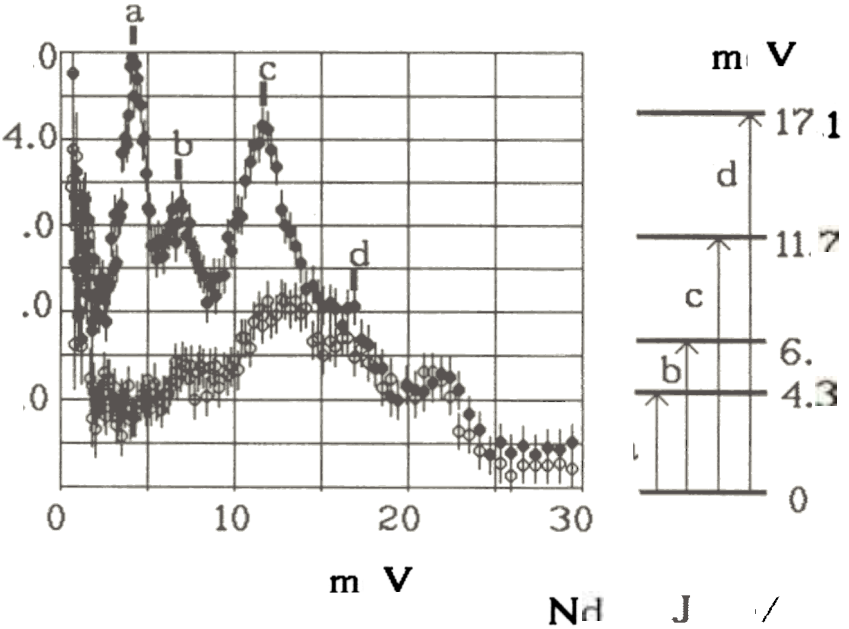

Nd J /

Fig. pectral neutrons scattering function he $Nd_{0.}$ $La_{0.}$ $Ni_{0.}$ and LaNi samples T 80K

ground multiplet of the Nd_{3+} ion splits into 5 Kramers doublets in the low-symmetric CEF of RNiSn. In Fig. 2, positions of the magnetic scattering peaks are marked. Judging from the character of the temperature dependence, they may be attributed to the transitions from the ground state. It allows to suggest the probable scheme of the Nd_{3+} levels splitting and to assess the average splitting magnitude for Ce in CeNiSn which is $\approx$20 meV. To evaluate CEF potential parameters, more detailed measurements of the temperature dependence of the scattering intensity should be carried out.

References

1. T. Takabatake, F. Teshima, H. Fuji et al. Phys. Rev. B41 (1990), 9607

2. P.A. Alekseev, E.S. Clementyev, E.A. Goremychkin, V.N. Lazukov, I.P. Sadikov, and I.L. Sashin. Physica B 186-188 (1993) 416-418

3. Yu.M. Kagan, K.A. Kikoin, and N.V. Prokofyev. In press, Letters to the Journal of Experimental and Theoretical Physics (in Russian) (1993)

CRYSTAL FIELD IN THE SET OF $RECu_2Si_2$ COMPOUNDS (RE -- Pr, Nd, Tb, Ho, Er, Yb)

E.A. Goremychkin, A.Yu. Muzychka
Frank Laboratory of Neutron Physics,
Joint Institute for Nuclear Research, Dubna, Russia

The isostructure compounds $RECu_2Si_2RE$ (RE is a rare earth element, Tr is a transition metal) demonstrate different physical properties. Depending on the kind of RE and Tr, they may exist as normal antiferromagnetics (AF), medium valence compounds (MVC), or as a systems with heavy fermions (SHF).

Determining the crystal field (CF) parameters in the Ce compound [1] has been chosen as an initial point of studying CF in the $RECu_2Si_2$ series. The purpose of this work is studying of the CF regularities in normal representatives of the series as well as comparing them with the anomalous compounds (SHF and MVC)

The results of the $NdCu_2Si_2$ investigations have already been published [2]. Besides, by the present time the CF parameters in the Pr, Ho, and Er compounds have been determined reliably enough (Fig. 1 a, b for Er).

The analysis has been based on the superposition model (SM) in which CF is represented as a superposition of the contributions of the coordination spheres containing different ions. The magnitude of each sphere contribution is determined by the factor called internal parameter of the sphere.

The main conclusions are:

1. The CF parameters of the 4th and 6th order are determined by the two nearest coordination spheres: Cu and Si. Thus, for each compound of the series we have four characteristic internal parameters: $A_4(Si)$, $A_6(Si)$, $A_4(Cu)$, $A_6(Cu)$.

2. In normal AF, $A_4(Si)$ is much lower than $A_4(Cu)$ while in the $CeCu_2Si_2$ SHF the contribution of Si prevails. This indicates that it is Si ligands that are responsible for the anomalous properties of $CeCu_2Si_2$ [3].

3. In Nd, Ho, Er compounds, monotonous growth of the internal parameters is observed as the RE ordinal number increases. Simultaneously, the spheres radii monotonously decrease. Each of these regularities may be the cause of the CP monotonous change. We hope that it will be after processing the Tb compound results that the issue of the main cause clears up because its ordinal number lies between those of Nd and Ho while the Si coordination sphere radius is smaller than that in $ErCu_2Si_2$.

4. It seems that the monotonous CF change along the set of RE is the property of the normal representatives of these series. $CeCu_2Si_2$ has anomalously large $A_4(Si)$ while its ordinal number is the lowest and the sphere radius is the largest. Similar CF behavior in $PrCu_2Si_2$, though it is less distinct, is a surprise. It calls the "normality" of this compound under question. The final CF picture in this series should be evaluated on the grounds of the $YbCu_2Si_2$ MVC results which currently are under procession.

RE	Radius Si	$A_4(Si)$	$A_6(Si$	Radius Cu	$A_4(Cu)$	$A_6(Cu)$
Ce	3.136	-8.3		3.218	3.1	
Pr	3.130	-3.2	3.9	3.216	4.4	2.6
Nd	3.115	0.6	9.1	3.208	6.6	6.6
Tb	3.021	?	?	3.186	?	?
Ho	3.040	1.0	24.9	3.181	12.0	18.6
Er	3.024	1.2	29.18	3.178	12.6	21.6

References:

1. E.A.Goremychkin and R.Osborn Phys.Rev. B 47, 14280 (1993)

2. E.A.Goremychkin, A.Yu.Muzychka and R.Osborn Physica B 179, 184 (1992)

3. P.M.Levy and S.Zhang Phys.Rev.Lett., 62 (1989)

Fig.1 Time-of-flight spectra of magnetic responce of $ErCu_2Si_2$ a)T=10K b)T=80K

a)

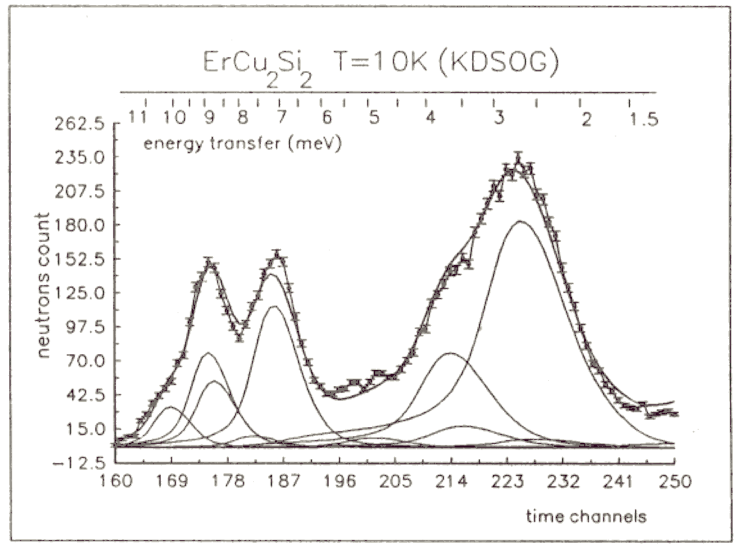

b)

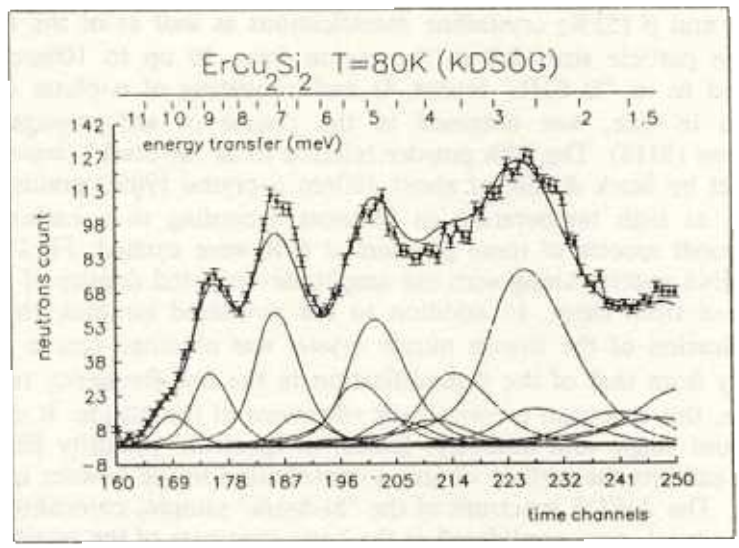

DENSITY OF VIBRATIONAL STATES OF SILICON NITRIDE

I.Markichev, E.Nikitina, E.Sheka
Patrice Lumumba Peoples' Friendship University, Moscow, Russia

V.Khavryutchenko
Institute of Surface Chemistry, Ac.Sci.Ukraine, Kiev, Ukraine

I.Natkaniec, A.Muzychka
Frank Laboratory of Neutron Physics,
Joint Institute of Nuclear Research, Dubna, Russia

During two past decades, powdered Si_3N_4 has received considerable attention due to its broad application to a structural ceramics fabrication. In practice, the above chemical formula represents a family of materials in which the species constitutes the major phase only. The properties of each family member depends, in part, on the microstructure developed during manufacturing. An INS study of the vibrational spectyra of five members of the family has been performed. The results are presented in Fig.1.

The first powder was obtained in the course of $SiCl_4$ decomposition by a plasma induced gaseous reaction in a nitrogen-ammonia flow.The product was treated by heating at 450°C for 100 hours in a nitrogen atmosphere to remove the NH_4Cl by-product. The final powder was amorphous with a specific area of $50 m^2 / g$ and consisted of practically ideal spherical particles of 17nm average diameter. The powder is denoted below as "Cl-plasma" (see curve 1). A part of this sample was exposed to the ambient atmosphere for a week. This sample is referred to as "Cl-plasma/air" (curve 2). The third powder, referred to as "Si-plasma" (curve 3), was also produced by a plasma induced but direct silicon nitridation reaction. The powder is a mixture of α (45%) and β (55%) crystalline modifications as well as of the amorphous phase. The average particle sizes fall in the region from 30 up to 100nm. The fourth powder, referred to as "Si-SHS" (curve 4) and consisting of α-phase (80%) grains of about 100nm in size, was obtained in the course of self-propagating high-temperature synthesis (SHS). The fifth powder referred to as "Si-Stark" (curve 5) was a commercial product by Stark & Co. of about 100nm α-crystal (90%) grains produced by nitriding silicon at high temperature in furnaces according to a carbothermal reaction. The vibrational spectra of these powders at 80K were studied. Fig.1 shows the normalized TOF INS spectra along with the amplitude-weighted density of states (AWDS) spectra obtained from them. In addition to the powdered samples, the spectrum for the α-modification of the silicon nitride crystal was obtained (curve 6 in Fig.1b). It differs slightly from that of the β-modification in the low-frequency region $\leq 400 cm^{-1}$ only. Hence, this spectrum presents bulk vibrations of the nitride. It serves as a reference for spectrum shape and intensity. Excess in spectrum intensity followed by a change in shape exhibits the surface vibration contribution to the powder spectrum.

The AWDS spectrum of the "Si-Stark" sample, coinciding with the spectrum of the α-crystal, was considered as the basic spectrum of the powder core. Extracting this spectrum from the others gave the spectra of the surface zones shown in Fig.2. The presented spectra exhibit the differences in the composition of the surface zones. A spectrum of a NH_4Cl crystal is given in Fig.2 (curve 7) for comparison.

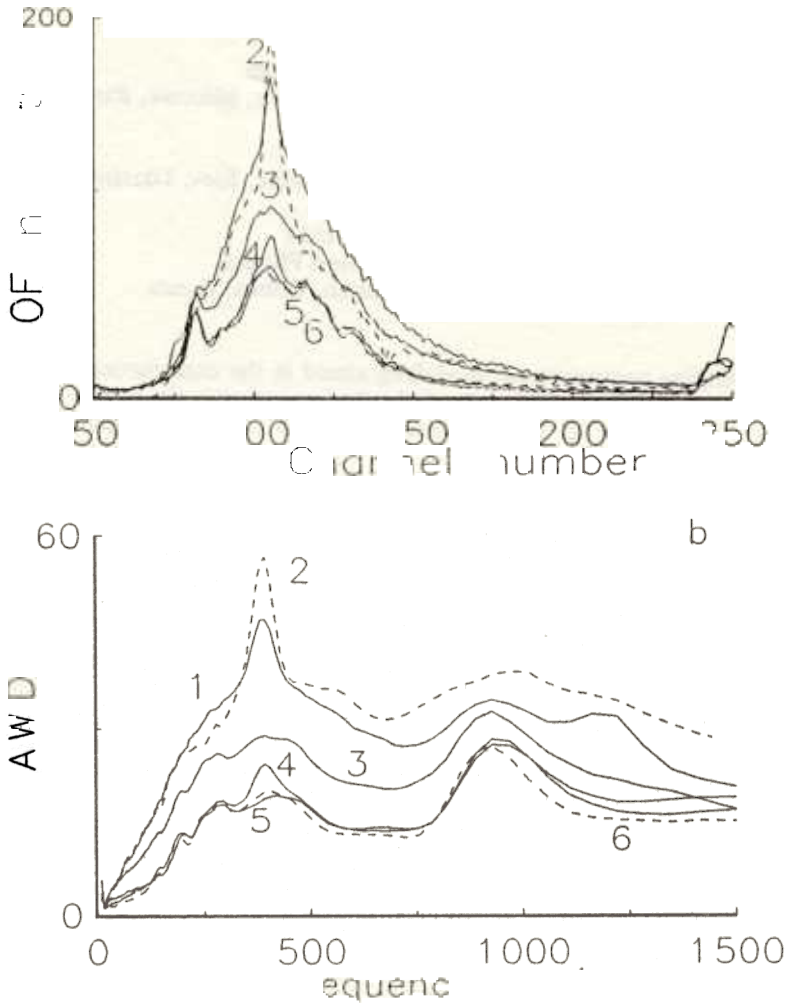
200
OF
0
50
00
50
200
250
C ıar ıel ıumber
b
60
AWD
0
500
1000
1500
equenc

Fig.

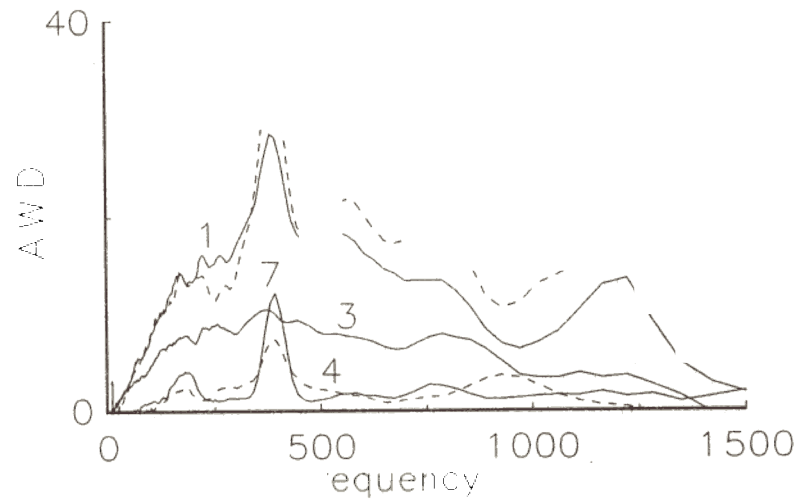
40
AWD
0
500
1000
1500
equency

Fig

DENSITY OF STATES OF BULK AND SURFACE VIBRATIONS OF HIGHLY DISPERSE Al

I.Markichev, E.Nikitina, E.Sheka
Patrice Lumumba Peoples' Friendship University, Moscow, Russia

V.Khavryutchenko
Institute of Surface Chemistry, Ac.Sci.Ukraine, Kiev, Ukraine

I.Natkaniec, A.Muzychka
Frank Laboratory of Neutron Physics,
Joint Institute of Nuclear Research, Dubna, Russia.

We are performing computational modelling aimed at the construction of a microscopic picture of the surface of aluminum. The surface vibration spectrum is the basis for the modeling proof. To get such a spectrum an experimental INS study has been undertaken. Thedouble amplitude-weighted spectra of a and highly disperse Al particles (the average size is 600 Å) were obtained at 80K. The first (curve 1 in Fig.1) represents the spectrum of the bulk vibrations of aluminum. In the second case the AWDS spectra have been recorded for two samples, namely, for an *as prepared* Al powder in an argonatmosphere (see curve 2 in Fig.1) and the powder after water adsorption on it at 290K (Fig.2). A comparative study of the spectra presented in Fig.1 shows a quite pronounced excess in the scattering intensity, in the case of the particles, caused by the surface vibration contribution.

As seen from Fig.2, water adsorption produces a significant increase in the particle spectrum intensity as well as a change in its shape. These phenomena might be connected with two effects, namely, the sensitivization of surface vibrations by the adsorbed molecules through a "rider effect" as well as the water vibrations themselves. However, make a more precise analysis of the data more accurate measurments of the AWDS particle spectrum is necessary.

Fig.1

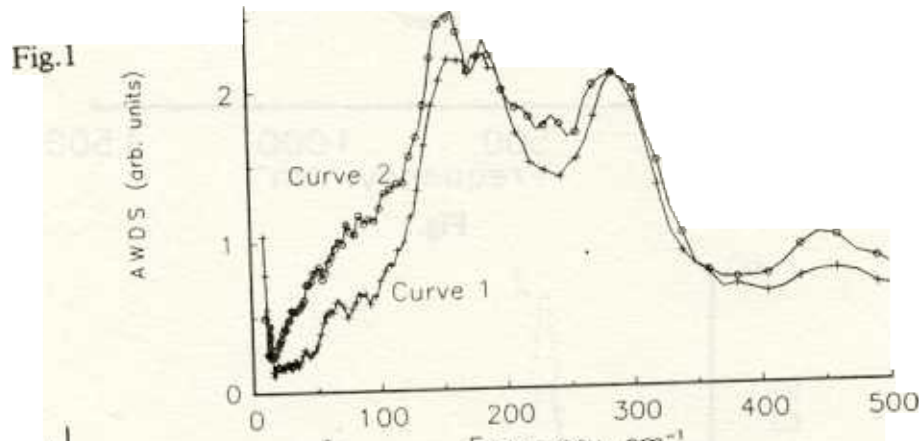

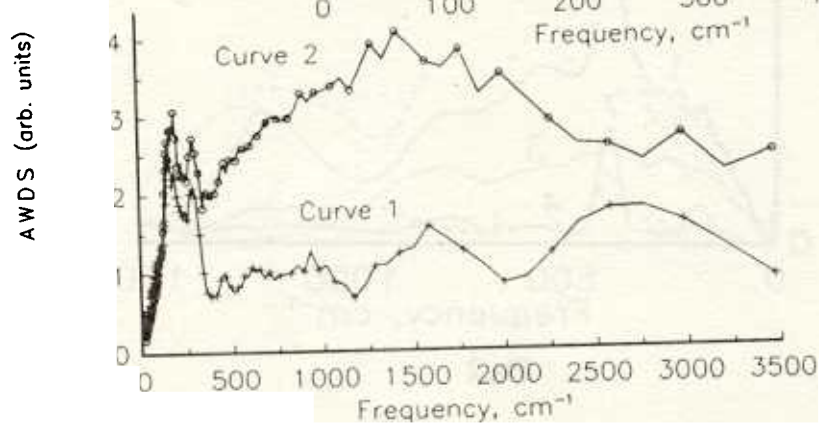

Fig.2

DENSITY OF VIBRATIONAL STATES IN THIOL CAPPED CdS PARTICLES USING INELASTIC NEUTRON SCATTERING

I.Markichev, E.Sheka
Patrice Lumumba Peoples' Friendship University, Moscow, Russia

V.Khavryutchenko
Institute of Surface Chemistry, Ac.Sci.Ukraine, Kiev, Ukraine

I.Natkaniec, A.Muzychka
Frank Laboratory of Neutron Physics,
Joint Institute of Nuclear Research, Dubna, Russia.

Colloidal semiconductor compounds are currently under intense investigation as examples of nonmolecular materials which demonstrate the quantum confinement effect (1).The particle size is a few nanometers so surface atoms constitute a significant part of the material. The interface between the particle core and surrounding atoms greatly affects the properties of these surface atoms.

We have studied vibrational spectra of capped clusters of CdS where the capping groups are thiophenolate ions (SPh^-) The formula of the clusters is $N(CH_3)_4]_8*(Cd_{20}S_{13}SPh_{22})$.Here tetramethylammonia cations compensate the negative charge of the thiophenolate groups. The CdS core size is of 1nm.

Fig.1 shows the spectrum of the double amplitude-weighted density of vibrational states (AWDS) of the cluster obtained by inelastic neutron scattering at 10K. Naturally cadmium is a good thermal neutron absorber so the presented spectrum exhibits the vibrations of the hydrogenically enriched capping surface zone only. A well defined structure corresponds to molecular group vibrations. It is obvious that the thiophenolate ions are the main contributers to the spectrum. To trace the difference in ion vibrations with respect to the thiophenol molecules, the solid thiophenol AWDS spectrum was obtained as well (see Fig.2).

To assign the vibrational modes and to model cluster structure we have performed a quantum chemical calculation of athiophenol molecule and a model thiol capped cluster. Curve 2 in Fig.2 presents the calculated AWDS spectrum of the thiophenol molecule obtained without any adjusting parameters. The pure AWDS function being a set of 33 δ-functions has been convoluted with a resolution function simulating that of the KDSOG-M spectrometer at the IBR-2 reactor in Dubna. As seenfrom the figure, the calculated spectrum fits the experimental one quite well if one takes into account the spectrum alterations caused by solidification.

The capped cluster has been modelled by a cluster having the formula SCd_4SPh_8, consisting of 101 atoms. Its fully optimized structure is shown in Fig.3. Curve 2 in Fig.1 presents the calculated AWDS spectrum of the cluster genrated as in the case of the thiophenol molecule spectrum above without any adjusting parameters and with the same convolution function. As seen, the calculated spectrum fits the experimental one well. This supports the validity of the cluster structure shown in Fig.3 and the quantum chemically calculated force field. The spectra calculation has been performed for internal coordinates to assign the vibrational modes and to reveal the difference in the thiophenol spectrum after capping.

Wang Y., Herron N. J.Phys.Chem., v95 (1991) 525

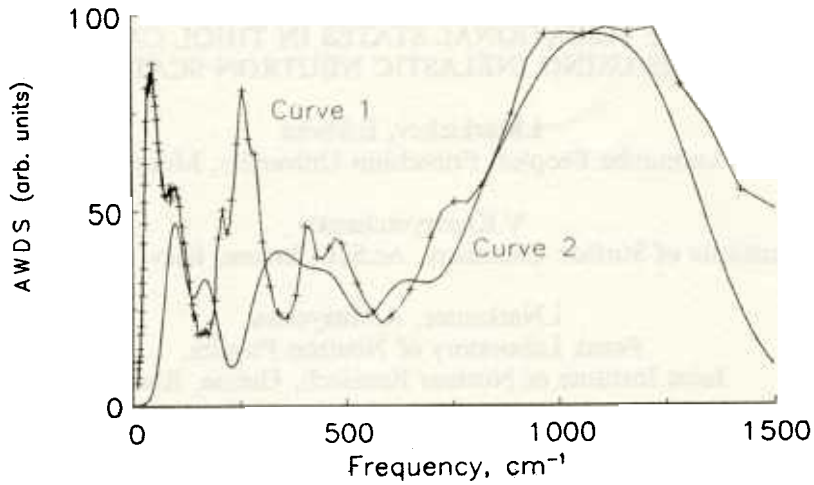
100
50
0
AWDS (arb. units)
Curve 1
Curve 2
0
500
1000
1500
Frequency, cm⁻¹

Fig.1

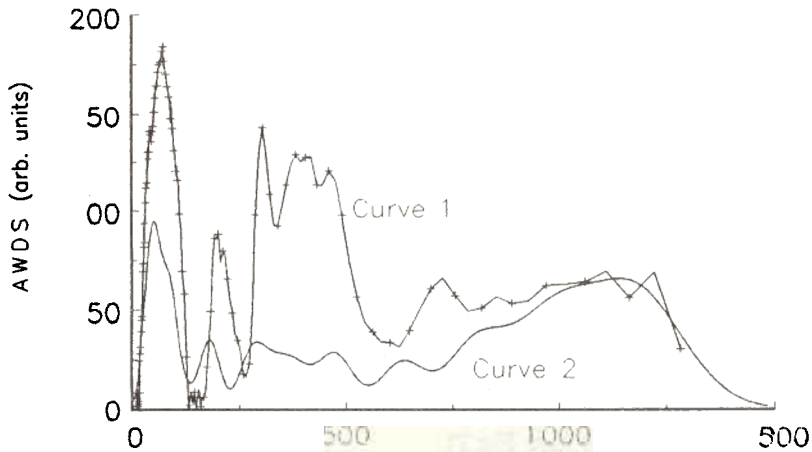
200
50
00
50
0
AWDS (arb. units)
Curve 1
Curve 2
0
500
1000
500
Frequency, cm⁻¹

Fig.2

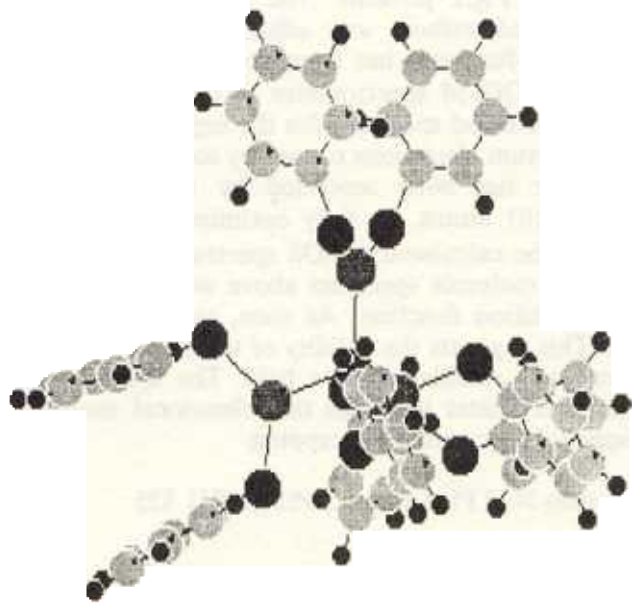

INELASTIC NEUTRON SCATTERING (INS) INVESTIGATION OF HYDROGEN CAPTURE BY CRYSTAL LATTICE DEFECTS

V.V. Sumin, C. Gantulga
Frank Laboratory of Neutron Physics
Joint Institute for Nuclear Research, Dubna, Russia

The effect of hydrogen capture by crystal lattice defects consists of suppressing hydride formation with a temperature decrease, at the expense of high enthalpy of the hydrogen complex formation, with some crystal lattice defects.

This phenomenon has been well studied in niobium, where interstitial atoms of dissolved nitrogen or oxygen or dissolved interstitial atoms of titanium form traps.

In tantalum, hydrogen capture has not been studied yet. However, investigations of fast ion channeling show this metal to be interesting for the following fact: deuterium, when captured by nitrogen atoms, is not only kept by the latter in a solid solution, but also changes the number of its neighboring atoms from tetrahedron to octahedron.

The INS method is an effective means of studying hydrogen capture by defects. In this work, nitrogen atoms and the more complicated vanadium plus nitrogen complex have been used as hydrogen traps in tantalum.

Highly purified tantalum, as well as $TaN_{0.02}$ and $TaV_{0.03}N_{0.02}$ alloys, which are solid solutions, have been used in this work. Pure tantalum and these alloys were saturated by hydrogen up to 1 atomic % from the gas phase.

The INS spectra of alloys, with and without hydrogen, were measured with the KDSOG-M spectrometer at three temperatures: room, 90K, 22K. The hydrogen contribution to the INS spectra was obtained by subtraction. Following that, then the spectra were processed to obtain the partial hydrogen density of states.

The hydrogen local modes in pure tantalum are 118 and 168 meV (see Fig. 1), which are close to the literature data. At 22K, where all hydrogen precipitates into the hydride phase, the hydrogen vibration energies shift into the high-frequency region, up to 127 and 182 meV, with widths of these vibrations considerably narrowing (see Fig. 1).

In tantalum with nitrogen or nitrogen and vanadium additions, the hydrogen peak positions do not change at the measured temperatures, which confirms hydrogen capture by these defects. The local mode widths decrease from 28 to 10 meV for the 118 meV low-frequency peak as the temperature decreases from room to 22K. These widths remain about twice as wide as those for pure tantalum at all temperatures.

In the $TaN_{0.02}$ alloy at 20K and in the $TaV_{0.03}N_{0.02}$ alloy at 90K, an additional peak with an energy of about 80 meV appears. Meanwhile, the wide high-frequency peak apparently splits into two peaks with energies of 170 and 210 meV (see Fig. 2).

The appearance of the additional peak at 80 meV and the splitting of the twice degenerated high-frequency peak shows a more complicated character of the defect complexes with hydrogen in tantalum than in niobium. Probably, hydrogen partially moves over into the octahedron position with vibration energies of 80 and 210 meV, which follows from the data on channeling. It is also possible that in this complex hydrogen occupies a less symmetrical position in the tantalum lattice than the tetrahedra position in niobium.

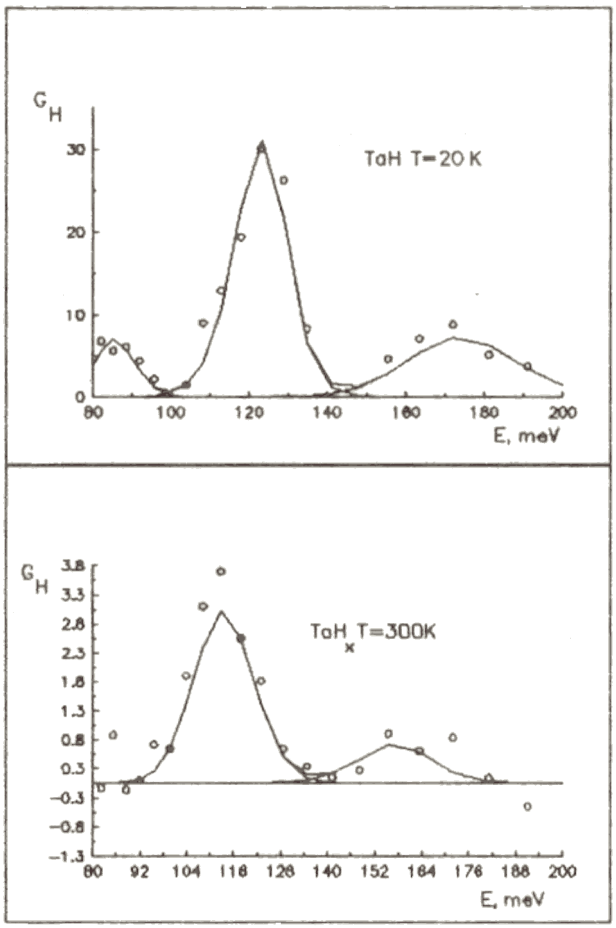

Fig.1 Hydrogen local modes in pure tantalum

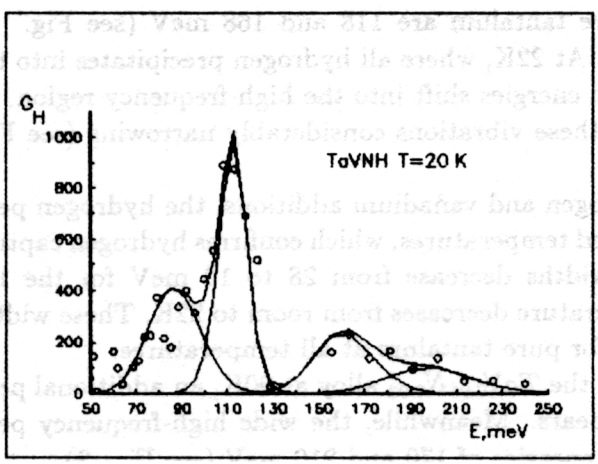

Fig.2 Hydrogen local modes in Ta-V-N solid solution

Polarized Neutron Reflectivity of Epitaxial Thin Magnetic Films

O.McGrath[1], V.V.Pasyuk[2], H.J.Lauter[3], A.V.Petrenko[2] and D.Givord[1]

[1] Laboratoire Louis Neel, CNRS, BP 166, F-38042 Grenoble, France
[2] FLNP, JINR, 141980 Dubna, Moscow Region, Russia
[3] ILL, BP 156, F-38042 Grenoble Cedex, France

The symmetry breaking at an interface gives rise to large surface magnetic anisotropies. Much scientific work has been devoted recently to studying surface anisotropies, but the exact origins still remain unclear.
In order to study this phenomen we realized three films of:
W(110)(50Å)/Fe(110)d/W(110)(500Å)/$Al_2O_3(11\bar{2}0)$ where d= 90 Å, 20 Å, and 4 Å. A detailed study of the magnetic and structural properties of the 90 Å and 20 Å films has been conducted. Analysis of the 4 Å film is in the process of being completed.

One of the most stringent means of analyzing the quality of the films is by polarized neutron reflectivity (PNR). The experimentally obtained reflectivities for the 90Å film and for the 20Å film were fitted. This enabled the exact determination of the film thicknesses. In addition the fits were obtained without introducing any noticable roughness parameters ($<z^2><$ 3Å), thus indicating clean interfaces. Finally bulk magnetisation per atom (2.2 μ_B) were used in the fit throughout the film thickness (the measurement was performed in saturating external magnetic field). This indicates no enhancement/reduction of magnetic moment at the interfaces, to within experimental accuracy, as one would expect for the (110) face of a bcc structure.

The investigation of Tb/Fe films deserved to the basic understanding of ferromagnetism. Ferromagnetism occurs due to exchange interactions. Three types of exchange interactions are known. They are:
-3d-3d exchange ie transition metal exchange
-4f-4f exchange ie rare-earth exchange, commonly called RKKY exchange and finally
-3d-4f exchange.
Due to the complexity of the magnetic systems in which 3d-4f exchange interactions occure ie mainly intermetallic alloys, this exchange mechanismn is poorly understood.

Thus recently we discovered that it was possible to epitaxially deposit Tb(4f) on Fe(3d) in the following configuration: W/Tb(0001)/Fe(110)/W(110)/Al_2O_3. This system is a model system for studying the above mentioned interactions. In particular it is predicted that a Tb film couples antiferromagnetically to the Fe at low temperatures. A variant is that only about two layers of Tb adjacent to the Fe are antiferromagnetic with respect to the Fe but in further layers the direction of magnetisation turns again by 180 deg.

PNR experiments were performed at room temperature on SPN at the IBR-2. The reflectivity data for the Tb(53Å)/Fe(100Å) composition are shown in the figure. The data could be fitted with the bulk magnetisation value of Fe and no magnetisation of the Tb. However the average density of the Fe layer is reduced by about 8% with respect to the bulk density. Increasing the Fe layer from 100Å to 165Å the density decrease is even about 16%. This indicates that beyond a certain thickness island growth may appear.

The low temperature data (T = 80 K) show differences with respect to the room temperature one and are in progress of being analysed to determine the interaction between Fe and Tb (3d-4f coupling).

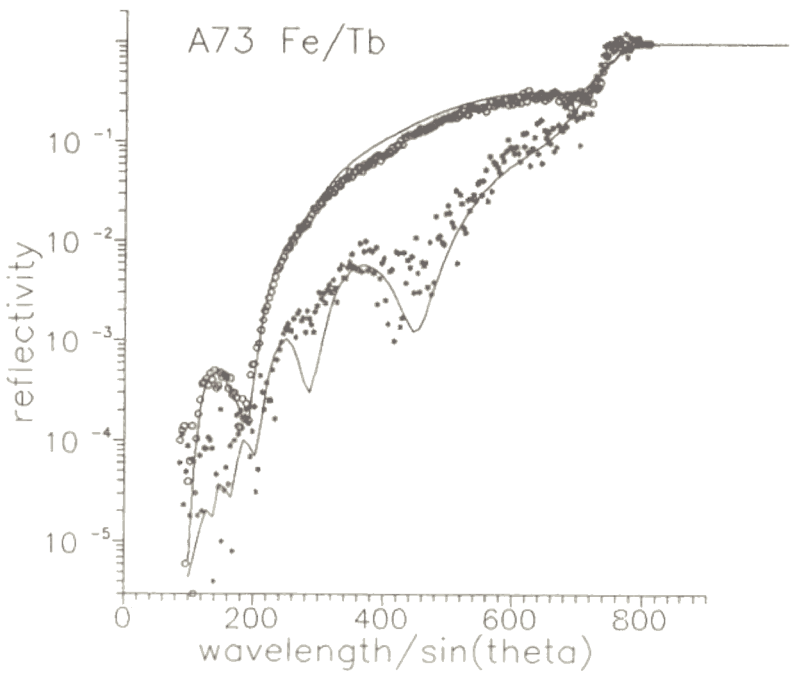

Figure: PNR data as a function of $4\pi/Q$ (Q = momentum transfer) for the Tb/Fe sample. R^+ (o) and R^- (*) are the reflectivities for the neutron spin parallel or antiparallel, respectively, with respect to the external saturating magnetic field.

Interface Magnetisation in a Pd/Co/Pd Ultra-thin Film Studied by PNR

V.V.Pasyuk[1], H.J.Lauter[2], M.T.Johnson[3], F.J.A. den Broeder[3], E.Janssen[3], J.A.C.Bland[4], A.V.Petrenko[1] and J.M.Gay[5]

[1] FLNP, JINR, 141980 Dubna, Moscow Region, Russia
[2] ILL, BP 156, F-38042 Grenoble Cedex 9, France
[3] Philips Research Laboratories, PB 80.000, 5600 JA Eindhoven, The Netherlands
[4] Cavendish Laboratory, Cambridge CB3 OHE, UK
[5] CRMC2, Luminy, Case 913, F-13288 Marseille, France

A Polarized Neutron Reflectivity (PNR) study was performed on SPN at the IBR-2 reactor for the investigation of the magnetisation profile of the sandwich Pd/Co(21Å)/Pd (in a saturating magnetic field) prepared by high vacuum vapor deposition on a Au film deposited on a Si-substrate.

Surface and interface magnetism and magnetic properties of ultra-thin films are extensively studied due to the fact that new magnetic features are expected to arise from the breakdown of three dimensional crystal symmetry. The enhancement of the Co magnetic moment was theoretically predicted in Co/Pd [1] thin films. In Pd the d band is not completely filled, therefore for 3d monolayers on Pd a strongly increased 3d-4d hybridization arises. Due to the large spin-susceptibility of Pd one expects also that the magnetic 3d overlayers induce sizable moments in the Pd substrate. The effect of an interface and of film thickness upon the magnetic properties can be studied due to recent progress in techniques used to synthesize high quality ultra-thin films. A PNR study was carried out to measure the absolute value of the magnetic moment per atom in an ultra-thin Co(21 Å) single film sandwiched by Pd and to determine also the magnitude of a possible induced magnetic moment in the Pd at the Co/Pd interface.

Prior to the neutron study the samples were characterized by Surface Magneto Optic Kerr Effect (SMOKE) and Vibrating Sample Magnetometer (VSM) measurements. The structural composition was determined by chemical analysis, X-ray and neutron reflectivity measurements. In the neutron study a saturating external magnetic field was turned perpendicular to the surface of the film, thus the neutron reflectivity becomes spin-independent and the nuclear profile is measured [2,3]. For some parameters the different measurements were complementary, but in general an excellent agreement of all parameters was obtained [3,4]. The composition of the film was determined to be: Si(111)/Au(220Å)/Pd(272Å)/Co(20.9Å)/Pd(70Å).

The VSM measurement indicated already an about 10% enhanced magnetisation then expected from the Co thickness of 21 Å. The neutron-spin depended reflectivities with

a saturating magnetic field of 3.5 kOe parallel to the film surface are shown in figure 1. The amplitude of the first oscillation between R^+ and R^- reflects the average magnetisation of the Co-layer. The fits to the experimental data were made by using the thicknesses and neutron-optical potentials which were obtained by the previously mentioned characterization studies. Only the magnetic contribution from the Co layer was a free parameter. The solid lines represents a fit to the data with 1.84 μ_B per Co atom throughout the Co layer (1.73 μ_B for bulk Co).

The spin-asymmetry S, shown in figure 2, can be expressed as:
$S=S_m/P=(1/P)*(R^+ - R^-)/R^- + R^+)$
S_m is the measured spin-asymmetry and P is the wavelength dependent polarization of the neutron beam. The solid line shows the best fit to the data and corresponds, as the fit in figure 1, to the enhanced magnetic moment of 1.84 μ_B per Co atom. The region in Q, where the enhancement of the magnetic moment is the most obvious, is enlarged in the insert. The dashed line is calculated with the bulk moment of Co. The difference to the fitted curve is evident, however a determination of a profile, e.g. higher magnetisation at the two interfaces, is within the statistical error.
A very similar curve with respect to the fitted curve (full line) is obtained using the bulk magnetic moment of Co and an average induced moment of 0.4 μ_B in a 5 Å thick layer of Pd adjacent to the Co. In order to distinguish between the two possibilities: an enhanced Co magnetic moment or an induced Pd magnetic moment (or a mixture between both) [3,4], one neds to measure reflectivities for higher Q values.
Recent measurements extending to higher momentum transfers which are in the process of being analyzed will allow to distinguish between the two solutions found in the presented experiment.

[1] R.Wu, C.Li and A.J.Freeman, J Magn.Magn.Mat. 99 (1991) 71
[2] S.S.Parkin, V.R.Deline, R.O.Hilleke and G.P.Felcher, Phys.Rev.B42 (1990) 10583
[3] V.V.Pasyuk, H.J.Lauter, M.T.Johnson, F.J.A.den Broeder, E.Janssen, J.A.Bland and A.V.Petrenko, Appl.Surf.Science 65/66 (1993) 118
[4] V.V.Pasyuk, H.J.Lauter, M.T.Johnson, F.J.A.den Broeder, E.Janssen, J.A.Bland, A.V.Petrenko and J.M.Gay, J.Mag.Mag.Mat., 121 (1993) 180

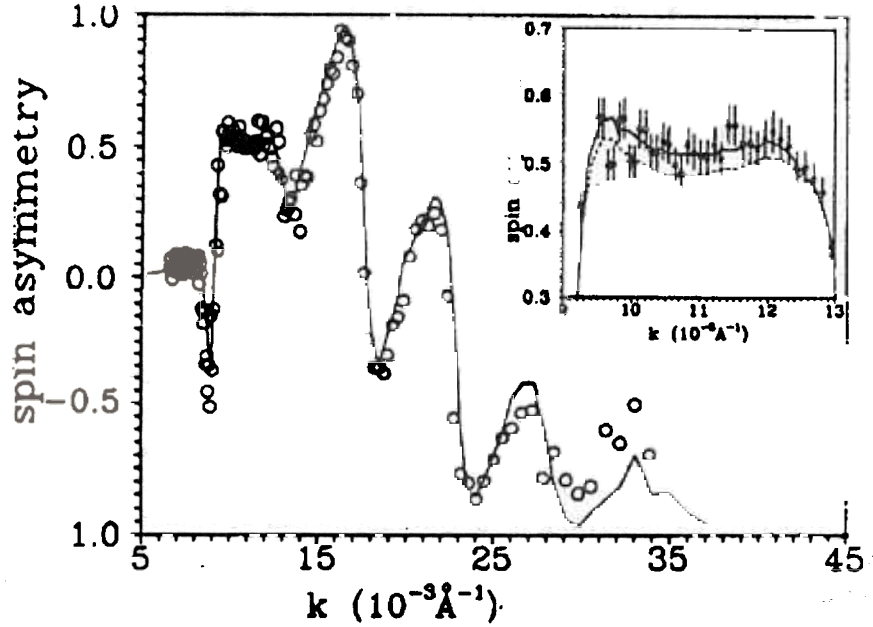

Figure 1: Neutron spin-dependent reflectivity curves R^+ (o) and R^- (+) for the Pd/Co/Pd sample measured in a magnetic field of 3.5 kOe parallel to the surface of the sample. The solid line shows the best fit to the data.

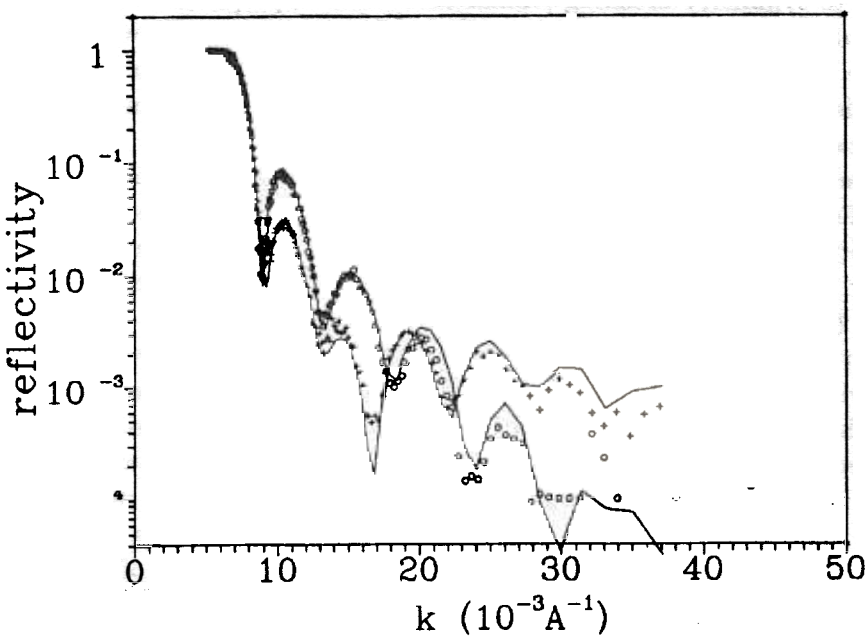

Figure 2: Measured and calculated spin-asymmetries for the Pd/Co/Pd sample. The dashed line in the insert corresponds to the bulk magnetisation per Co atom, the solid line is calculated for the enhanced moment of 1.84 μ_B per Co atom. A very similar curve is obtained with the parameters of the bulk Co magnetisation and 0.4 μ_B induced magnetic moment in a 5 Å thick layer of Pd at each Co/Pd interface.

Polarized Neutron Reflectometry Study on Magnetic Multilayers for Nuclear Resonant Scattering Experiments

V.V. Pasyuk[1], D.L. Nagy[2], H. Lauter[3] and A.V. Petrenko[1]

[1] Frank Laboratory of Neutron Physics, JINR, 141980 Dubna, Russia
[2] KFKI Research Institute for Particles and Nuclear Physics,
H-1525 Budapest, P.O.B. 49, Hungary
[3] ILL, B.P. 156, F-38042 Grenoble, France

Magnetic multilayers composed of alternating ^{56}Fe and ^{57}Fe layers are good candidates of monochromators for neutron scattering as well as for Mössbauer spectroscopy. In the case of neutron scattering the magnetic scattering length is the same for the two isotopes but the nuclear scattering length is different. By varying the composition in each bilayer properties for polarising monochromators can be explored. The film of an alternating Fe-isotope structure is in addition a nuclear resonant periodic structure and can be used as monochromators with μeV bandwidth for temporal Mössbauer spectroscopy at synchrotrons. In particular multilayers prepared from epitaxial layers will have appropriate bandwidth, high acceptance, high nuclear and low electronic reflectivity.

An advantage of these Fe-multilayers is that there is no structural interface leading to effects due to symmetry breaking (enhanced moments, perpendicular anisotropy, etc.) and to structural roughness (mechanical strain at interfaces). However, if such multilayers are grown by conventional sputtering techniques, they can be still influenced by amorphisation and interdiffusion both resulting in a roughness and a degradation of coherent scattering and magnetic properties.

In the presented study we investigated the isotope distribution and magnetisation of an ^{56}Fe/^{57}Fe multilayer containing 15 bilayers prepared by J.Korecki (AGH, Cracow, Poland) with molecular beam epitaxy (MBE). The sample is grown on float glass and covered by a 90 Å thick Al layer. The study was performed with polarized neutron reflectivity (PNR) on SPN at the IBR-2.

In the figure the measured reflectivity curves are shown for the two spin states of the neutrons with respect to the external magnetic field of 1 kOe applied along the sample surface. The small oscillations at low Q represent the total thickness of the film. The peak at about 0.12 Å^{-1} is the Bragg-peak arising from the multilayer structure with its bilayer thickness of 52 Å. The limited number of bilayers gives rise to a broadened peak. The slight shift of the peak position given by the two neutron spin states reflects the fact that the multilayer does not consist of an integer number of bilayers, but that a layer of ^{57}Fe is added on top.

Thus it has been shown that multilayers of different isotopes of Fe can be grown by MBE such that a Bragg-peak can be measured with PNR. The quality of the interfaces will be deduced from the on-going data analysis. It seems that after this first successfull step a way was found for the preparation of efficient μeV monochromators for nuclear resonant scattering experiments at synchrotrons.

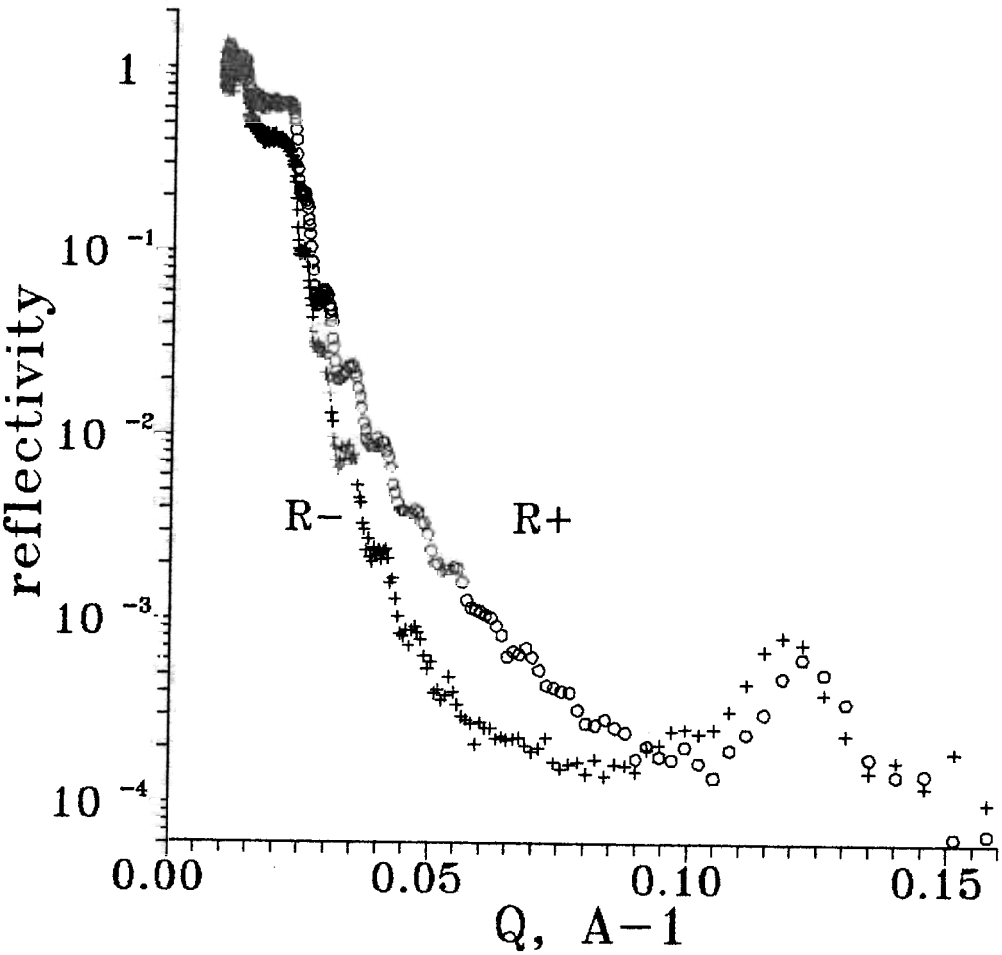

Figure: Measured reflectivities of a Fe-isotope multilayer structure for the neutron spins parallel (R^+) (o) and antiparallel (R^-) (+) with respect to the saturating external magnetic field of 1 kOe (oriented parallel to the sample surface) as a function of the momentum transfer Q. The composition of the multilayer is Al/^{57}Fe/15(^{56}Fe/^{57}Fe)/floatglass.

New aspect in employing magnetic anisotropic FeCo thin films as neutron polarizers

D.A.Korneev

Laboratory of Neutron Physics, Joint Institute for Nuclear Research
141980 Dubna, Moscow region, Russia

ABSTRACT

Reversal of the beam polarization vector is a necessary procedure in carrying out experiments with polarized neutrons. At present a number of methods and set-ups (spin-flippers) are widely used in experiments utilizing thermal polarized neutrons. A new way to achieve neutron beam polarization of a necessary sign during the process of neutron specular reflection from ferromagnetic anisotropic mirrors is proposed. The results of its check-up testing with a polarized neutron beam are given. The measured spin reversal probability by this method is near to unity, and, practically, it does not depend on the neutron wavelength. The application of the given way lets one exclude the spin-flipper as an element of polarized neutrons set-ups.

INTRODUCTION

Neutron reflection from the surface of ferromagnetic films is a widespread method of getting thermal polarized neutron beams. D.Hughes and M.Burgy were the first to use a ferromagnetic mirror as a neutron polarizer[1]. Hereafter this technique was being extensively developed (see[2], for instance). Polarizing mirrors on the base of the FeCo alloy sputtered on the absorbing sublayer TiGd, multilayer thin film structures with alternate layers of ferromagnetic and non-ferromagnetic materials are much used nowadays. Mirror polarizers make it possible to choose the right ferromagnetic alloy reflecting only the neutrons which spins are parallel to a magnetic induction vector of a mirror. As a result the spins of the reflected neutrons are directed towards an external magnetic field. A high value of polarizability ($95 - 97\%$), weak spectral dependence of polarization and ease of operation make wide use of neutron mirror polarizers at stationary as well as at pulsed neutron sources.

A change of sign of a polarization beam, i.e. mutual reverse of a polarization vector and an external magnetic field is very important during polarized neutron experiments. To realize this one needs spin-flippers - the devices for mutual reverse of the external magnetic field and beam polarization. Spin-flippers impair polarization spectral characteristics and limit the luminosity of set-ups. For example, a well-known Drabkin spin-flipper has a bounded region of neutron spin reverse.

A new way of obtaining beams of different polarization signs with the help of thin magnetic anisotropic films is discussed in this paper. The experimental results of the check-up are presented.

THE GROUND OF THE NEW METHOD OF POLARIZATION

As it is known, the ferromagnetic with a flat boundary can be described by the following jump of the neutron optical potential

$$U\pm = U_n \pm \mu(4\pi M_p), \tag{1}$$

where $U_n = 4\pi\frac{\hbar^2}{2m} \cdot N \cdot b$ is a neutron nuclear optical potential, N is a number of nuclei per unit volume, b is an average neutron scattering length, M_p is the projection of a magnetic moment on a reflecting surface. The fact that a neutron spin is equal to one half results in the existence of two potentials. Thus, if one chooses the right ferromagnetic alloy, then

$$U_- = U_n - 4\pi\mu M_p \quad 0.$$

As a result only the neutrons with a magnetic moment facing away from the vector $\vec{M}_p$ will be reflected from the matter boundary, because $U_+ = U_n + 4\pi\mu M_p > 0$. A very important fact should be noted here: during the neutron magnetic moment interaction with the boundary of ferromagnetic matter, the derection of polarization in the reflected beam is determined only by the direction of the vector $\vec{M}_p$. The magnetic field vector does not enter into the equation (1). Thus, it is easy to show that in the system of coordinates connected with the external magnetic field $\vec{H}$ polarization in the reflected beam will depend on the angle θ between the vectors $\vec{M}_p$ and $\vec{H}$, i.e.

$$P(\theta) = P_o(\lambda) \cdot Cos(\theta), \tag{2}$$

where $P_o(\lambda)$ is mirror polarizability along the $\vec{M}_p$ direction.

From (2) it follows that

$$P(\theta = 0) = -P(\theta = \pi) \tag{3}$$

Therefore, for a polarizer where M_p does not depend on H, the change of mutual orientations of vectors $\vec{P}$ and $\vec{H}$ in a reflected beam can be achieved by the magnetic field reverse.

Single-axis anizotropic magnetic films with a rectangular hysteresis loop, see Fig.1, are the ones which are practically free from the dependence of M_p on H in the interval of $|H| < H_c$. From this it follows that for the films with such a hysteresis loop the change of the field sign at $|H| < H_c$ will result in the change of sign of the reflected beam polarization.

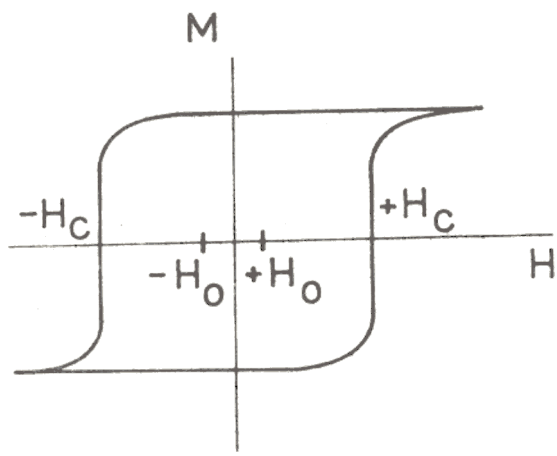

Fig.1. The typical magnetization reversal curve of a single-axis anisotropic film, when the magnetic field is directed to the "easy axis" of anisotropy of a film. In the region $-H_o < H < H_o$ the dependence of the magnetic moment $\vec{M}_p$ of a film on the volume and direction of an external magnetic field H is absent.

EXPERIMENTAL CHECK-UP OF THE METHOD

To examine the suggested technique we have used a polarizing mirror with the $Fe(40)Co(60)$ film (1500$\AA$ thick) with the $Ti(85)Gd(15)$ sublayer sputtered on a float glass plate. The film was being sputtered in the magnetic field of 250 Oe at the temperature of a glass plate equal to 150 ^oC. Single-axis anisotropy of the film occurred due to the magnetic field. The value of the film coercive force was $H_c = 95$ Oe. The mirror was placed into a polarized beam behind a polarizing neutron guide. A change of polarization of an incident beam was performed by a spin-flipper. The mirror was put into a gap of the electromagnet allowing one to change both the value and sign of a magnetic field. The $\vec{H}$ vector coincided with the anizotropy axis of the film. Magnetic field behaviour at the electromagnet inlet provided the adiabatic guide of the spin at any field direction in the gap. Reflected intensities N_+ (spin-flipper "off") and N_- (spin-flipper "on") for different values of fields in the electromagnet were measured with the ^3He detector. A combination of the measured intensities was analysed:

$$\frac{N_+ - N_-}{N_+ + N_-} = P_o \cdot P_m(H), \qquad 4)$$

where P_o is incident beam polarization, P_m is mirror polarizability. Equation (4) is true for the case that spin reverse probability by a spin-flipper is $f = 1$. In our case the latter condition was realized with an accuracy of $5 \cdot 10^{-3}$ in the region of a neutron wave length $\lambda < 6\AA$.

THE MEASUREMENT OF FIELD DEPENDENCE OF P_m

At first the mirror was magnetized by a negative magnetic field of 500 Oe. After that the field decreased to zero and then increased in a positive direction. Fig.2 shows the experimental dependence of $P_o \cdot P_m(H)$ on the magnetic field. Here P_o and $P_m(H)$ are an average over the spectrum beam polarization and mirror polarizability, respectively. It is seen from the shape of a curve that in $H < 80$ Oe $P_o \cdot P_m(H)$ does not depend on the value of an applied field; in this case it is negative. It means that the magnetization vector $\vec{M}_p$ is opposite to the external field. In the fields $H > 80$ Oe the reversal of magnetization begins; the process ends in the fields of ≥ 200 Oe. Then at a decrease of the field $P_m(H)$ does not depend on the field and it is positive. It means that the magnetization vector $\vec{M}_p$ is parallel to $\vec{H}$. Therefore the bottom and top parts of the experimental curve correspond to opposite and unidirectional orientations of the vectors $\vec{M}_p$ and $\vec{H}$, respectively.

The measurements have shown that $P_m = -P_m'$ with a high degree of accuracy (about $5 \cdot 10^{-3}$) in the region $H \leq 70$ Oe, where P_m and P_m' mirror polarizabilities correspond to the bottom and top parts of a hysteresis loop.

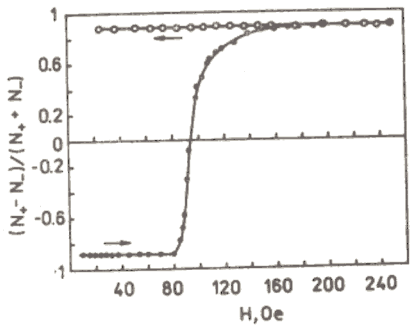

Fig.2. The experimental dependence of $P_o \cdot P_m(H) = \frac{N_+ - N_-}{N_+ + N_-}$ on the external magnetic field parallel to the "easy axis" of the anisotropic $FeCo$ film. At first the film was magnetized in the opposite direction to the external magnetic field. The reversal of magnetization of the film leads to the changing of sign of film polarizability.

THE MEASUREMENT OF WAVELENGTH DEPENDENCE OF P_m

For spectral properties check-up of mirror polarizability we have measured $P_o \cdot P_m$ according to a neutron wave length in the fields $H_1 = -8$ Oe and $H_2 = +8$ Oe.

Fig.3 shows experimental functions $P_o \cdot P_m$ for these values of the fields. The ratio $\frac{P_m(\lambda,H_1)}{P_m(\lambda,H_2)}$ got from the experimental curves 1 and 2 differs from -1 no more than $5 \cdot 10^{-3}$ in the measured interval of neutron wave lengths $\lambda = 1.5 \div 6\mathring{A}$.

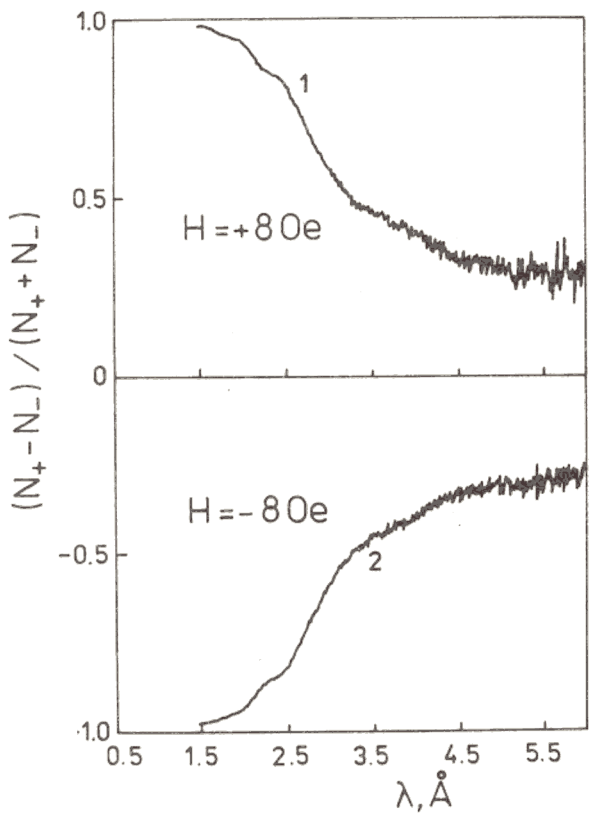

Fig.3. The experimental wavelength dependence of $P_o \cdot P_m(H) = \frac{N_+ - N_-}{N_+ + N_-}$ for the $FeCo$ single-axis anisotropic film: curves 1,2 correspond to the magnetic field equal to +8 Oe and −8 Oe, respectively. The changing of sign of the external magnetic field leads to the changing of sign polarizability of the film in a wide range of the wavelengths.

CONCLUSION

A new method of getting polarized neutrons with a necessary sign of polarization by specular reflection from a magnetic anisotropic film is suggested. Its checkup on the single-axis anisotropic $FeCo$ film have shown that the reflected beam polarization and the external magnetic field change their sign simultaneously. The efficiency of the change of sign of neutron beam polarization due to the change of sign of an external magnetic field is near to unity and is independent of a neutron wave length.

The application of the given method allows one to perform the mutual reverse of a neutron spin and external magnetic field not using a spin-flipper.

ACKNOWLEDGMENTS

The author is indebted to Drs. A.V.Petrenko, E.B.Dokukin, V.V.Pasyuk for the help in carrying out the measurements and to Dr. A.F.Schebetov for the FeCo films preparation.

Thanks are due to Mrs. T.A.Filimonycheva who made a translation of the paper into English.

REFERENCES

1. D.J.Hughes, M.T.Burgy, "Reflection of Neutron from Magnetized Mirrors *Phys.Rev.*, 81, 498, (1951)
2. W.G.Williams, *"Polarized Neutrons"*, Oxford, Clarendon Press, (1988)

V.L.Aksenov, Yu.V.Bugoslavsky [1], E.B.Dokukin, V.K.Ignatovich,
A.A.Minakov[1], Yu.V.Nikitenko, A.V.Petrenko, S.A.Sergeenkov

Frank Laboratory of Neutron Physics,
Joint Institute for Nuclear Research,
Dubna 141980, Moscow region, Russia

A POSSIBLE OBSERVATION OF THE DEPINNING LINE IN $YBa_2Cu_3O_{7-\delta}$ CERAMICS FROM NEUTRON POLARIZATION STUDIES

Abstract

Using the experimental data on neutron depolarization in superconducting $YBa_2Cu_3O_{7-\delta}$ ceramics obtained by means of the high flux pulsed reactor IBR-2 in Dubna, we discuss a possible manifestation of the so-called depinning line, $H^*(T)$, which separates pinned vortices from the freely moving ones.

Our previous measurements [1] conducted in applied magnetic fields up to 0.5 T, confirmed in general the well-known behaviour of the neutron depolarization $P(H)$ in type-II superconductors. Yet, near T_c we observed the appearence of an extra anomaly in $P(H)$ dependence. It was interesting to get more information about the nature and evolution of this anomaly at higher magnetic fields. This is the main goal of the present paper.

The investigations of the superconducting $YBa_2Cu_3O_{7-\delta}$ ceramics (T_c = 90.4 K) were carried out on the polarized neutron spectrometer SPN-1 on the high flux pulsed reactor IBR-2 of the Frank Laboratory of Neutron Physics, JINR, Dubna. The detailes of the experimental method and the sample's parameters are given in [1]. In the depolarization experiments, the temperature and magnetic field dependence of depolarization of the neutron beam $P(H,T)$ is measured. The neutron wavelength used in our experiments had varied from 0.5 to 15Å. The measurements have been taken at temperatures from 77 to 250 K. To illustrate the obtained results, Fig.1 shows the field dependence of the polarization of the sample taken at $T = 86$ K for increasing field mode. It is seen that in addition to the polarization minima at $H = H_1$ and $H = H_2$ (which have been discussed in [1]), there is a region (starting at $H = H_d$) of quasiperiodic (oscillating) behaviour of $P(H)$. In the backward regime (with decreasing the field), the minima become even deeper (as compared to the forward mode). Fig.2 depicts the temperature dependence of the threshold field $H_d(T)$ (curve 2). For comparison, the same figure shows the corresponding behaviour of the upper critical field $H_{c2}(T)$ (curve 1) for the same sample deduced from the resistivity measurements in applied magnetic field. Clearly, both curves exhibit a linear temperature dependence (near T_c), i.e. $H_d(T) = H_d(0)(1 - T/T_c)$, where $H_d(0) \simeq 84$ kOe. Since for $YBa_2Cu_3O_{7-\delta}$

[1]General Physics Institute,Russian Academy of Sciences,Moscow

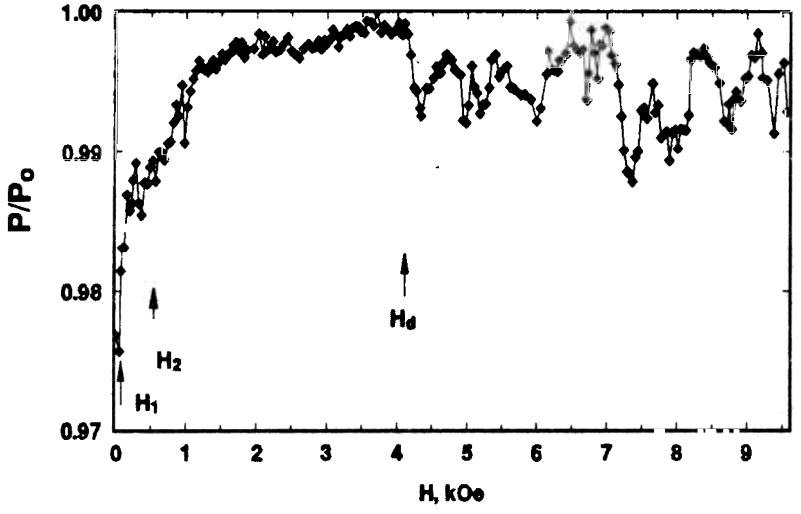

Figure 1: Field dependence of normalized polarization $P(H)$ at $T = 86\ K$ for increasing field mode.

ceramics [2] $H_{c1}(0) \simeq 0.5\ kOe$ and $H_{c2}(0) \simeq 200\ T$, we conclude that our sample is in the mixed state and, thus, the above-mentioned quasiperiodic behavior of $P(H)$ can be attributed to the neutron scattering by Abrikosov vortices.

Let us discuss briefly a possible origin of the observed anomaly of $P(H)$. Taking into account the field dependence of the critical current density $j_c(H)$ (e.g., in the critical state model $j_c(H) \propto (H + H_0(T))^{-1}$), one can approximate the volume pinning force density $F_p(H) = H \cdot j_c(H)$ as [3]: $F_p(H) = b(1-b)$, where $b \equiv H/H^*(T)$ and $H^*(T)$ is the so-called "depinning" field. It is important to stress that in contrast to the conventional (low-T_c) superconductors where pinning reaches its maximum value at $H \simeq \frac{1}{2} \cdot H_{c2}(T)$, in high-$T_c$ materials the magnitude of the depinning field lies essentially below H_{c2} [4]. Assuming that $H_d(T)$ corresponds to the onset of the depinning line $H^*(T)$, we can propose the following interpretation of the anomalous behaviour of $P(H)$ above $H_d(T)$. Namely, the higher the applied magnetic field, the more rigid becomes the vortex lattice. Correspondingly, polarization $P(H)$ increases (see Fig.1), tending to reach its maximum value. At $H = H_d(T)$, vortices start to depin from their pinning sites (which in turn depend on the applied field via $F_p(H)$). This results in a "softening" (melting) of the vortex lattice. According to this picture, it seems quite plausible to assume that neutron scattering by vortices which are still pinned will be highly depressed (this gives rise to the appearence of the maxima above $H_d(T)$) in comparison with the freely moving (unpinned) vortices which will dominate the neutron scattering data (resulting in the appearence of the minima of $P(H)$, see Fig.1). It is worthwhile to mention

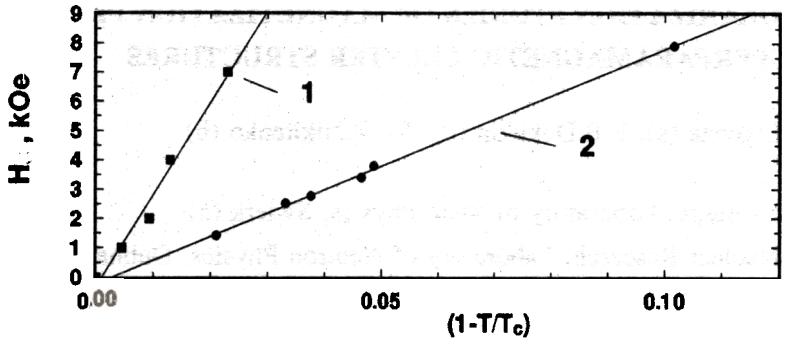

Figure 2: Temperature dependence of the upper critical fied H_{c2} (curve 1) and the threshold field H_d (curve 2) for given $YBa_2Cu_3O_{6.9}$ sample.

that the absolute value of our threshold field $H_d(0) \simeq 84\ kOe$ is in a rather good agreement with the estimates of the depinning field $H^*(0)$ known for $YBa_2Cu_3O_{7-\delta}$ compound [4].

In summary, we presented our recent experimental data on the polarized neutron scattering by superconducting $YBa_2Cu_3O_{7-\delta}$ ceramics and discussed the possibility of a direct observation of the depinning line $H^*(T)$ separating freely moving (above $H^*(T)$) Abrikosov vortices from the pinned ones (below $H^*(T)$).

The authors would like to acknowledge the colleagues with whom we have had the collaboration in the work. Particular thanks go to Dr. V.K.Fedotov, S.V.Kozhevnikov and Ch.Surkovski.

Part of this work has been supported by Russian Foundation for Fundamental Research (Grant 93-02-2535).

References

[1] Aksenov V.L, Dokukin E.B., Nikitenko Yu.V., Petrenko A.V. and Sergeenkov S.A., Physica Scripta **T48** (in press).

[2] Harshman D.R. and Mills A.P., Phys.Rev.B **45**, 10684 (1992).

[3] Fietz W.A. and Webb W.W., Phys.Rev. **178**, 657 (1969).

[4] Civale L., McElfresh M.W., Marwick A.D., Holtzberg F., Feild C., Thompson J.R. and Christen D.K., Phys.Rev.B **43**, 13732 (1991).

NEUTRON DEPOLARIZATION STUDIES OF MAGNETIZATION PROCESS ON SUPERPARAMAGNETIC CLUSTER STRUCTURES

S.Ligenza (a), E.B.Dokukin (b), Yu.V.Nikitenko (b).

Institute of Atomic Energy, Laboratory of State Physics, Swierk (a)
Joint Institute for Nuclear Research, Laboratory of Neutron Physics, Dubna (b)

Neutron depolarization studies are made on polycrystalline Li-Ti-Zn ferrite system exhibiting the superparamagnetic behaviour due to the magneto-crystalline cluster structure [1]. The magnetization processes investigated by neutron depolarization measurements on magneto-crystalline cluster structure have been performed for the first time. The magnetization is measured by using neutron spin precession time-of-flight method on polarized neutron beam [2] at pulsed reactor IBR-2 in Dubna. The analyses of neutron depolarization with respect to the wavelength dependence are performed for different values of external magnetic field $\mathbf{H}_{ex}$. The oscillations of polarization are observed versus the neutron wavelength. Basing on the wavelength dependence of the neutron polarization, the mean magnetic induction is estimated as a function of external magnetic field using a least square fit procedure and the classical model assumption of neutron depolarization given by Halpern and Holstein [3]. The magnetic induction $\langle \mathbf{B} \rangle$ inside sample, versus $\mathbf{H}_{ex}$ is interpreted using the Langevin function. The running of estimated magnetization curve is explained assuming an existence of the "cluster field" connected with a dipole interclusters interaction. The value of this "cluster field" is taken as proportional to the magnetic moment of clusters and depends on the value of external applied field $\mathbf{H}_{ex}$.

It is established that this cluster interaction depends on the $\mathbf{H}_{ex}$ in a power equal $(4/3)^2$. During the analysis of the depolarization measurements the perpendicular magnetization induction $\langle \mathbf{B} \rangle_{\perp}$ is determined as a function of $\mathbf{H}_{ex}$. For the $\langle \mathbf{B} \rangle_{\perp}(\mathbf{H}_{ex})$ relation the unexpected maximum of perpendicular magnetic induction appeared at external field $\mathbf{H}_{ex}$=44*Oe*. The existence of perpendicular$\langle \mathbf{B} \rangle_{\perp}$ with distinct maximum is interpreted as due to the superparamagnetic cluster structure and is connected with appearing of intercluster interactions.

REFERENCES

[1] S.Ligenza and M.Konwicki, Phys. stat. solidi(a) **109**, 319(1988).

[2] Dokukin,E.B., Korneev,D.A., Loebner,W., Pasjuk,V.V., Petrenko,A.V. and Rzany,H., J.de Physique **49**, C8-2073 (1988).

[3] Halpern O. and Holstein T., Phys.Rev. **59**, 960(1941)

6.2. NEUTRON NUCLEAR PHYSICS

CONTENTS

Measurement of P-odd Asymmetry in the $^{10}B(n,\alpha)^{7}Li$ reaction
V.A.Vesna, Yu.M.Gledenov, I.S.Okunev, S.S.Parzhitskii, Yu.P.Popov, E.V.Shulgina

Investigation of Charged Particles Emission Reaction Induced by Fast Neutrons
Yu.M.Gledenov, G.Khuukhenkhuu, Yu.P.Popov, Bao Shanglian, Tang Guoyou, Cao Wentian, Qu Decheng, Chen Zemin, Chen Yingtang, Qi Huiquan

Interaction of Polarized Neutrons with a Polarized Lanthanum Target and Structure of the Neutron Cross Section up to 20 eV
V.P.Alfimenkov, Yu.D.Mareev, V.V.Novitsky, L.B.Pikelner, V.R.Skoy

Study of the Depolarization of Resonance Neutrons in an Experiment to Search for the T-Noninvariance
V.P.Alfimenkov, Yu.D.Mareev, V.V.Novitsky, L.B.Pikelner, V.R.Skoy, C.R.Gould, D.G.Haase, N.R.Roberson

Multiplicity of Gamma-Rays in Neutron Resonances of ^{176}Hf and ^{179}Hf
G.P.Georgiev, Yu.V.Grigoryev, G.V.Muradyan, N.B.Yaneva

Situation in Study of Electric Polarizability and Mean Square Charge Radius of the Neutron
Yu.A.Alexandrov

On the Electric Polarizability of the Neutron
Yu.A.Alexandrov, L.Koester, L.V.Mitsyna, P.Prokofiev, G.S.Samosvat, J.Tambergs, W.Waschkowski

UCN High Density Pulse Source at the BIGR Reactor (Arzamas-16) and Neutron Lifetime Experiment
A.V.Strelkov, V.N.Shvetsov, A.D.Stoica

A Moving Converter as a Possible Tool for Producing Ultracold Neutron at Pulsed Neutron Sources
Yu.Pokotilovski

On Experiment Verification of the Skobeltsin-Baldin Hypothesis of Emission of a Nonstable Particle Following the Decay of ^{214}Bi
Yu.N.Pokotilovski, G.G.Takhtamyshev

Mossbauer Effect Based Experiments to Search for New Light Bosons
Yu.Pokotilovski

Some Aspects of Estimation of n,e-amplitude and Neutron Polarizability
V.G.Nikolenko, A.B.Popov

Properties of ρ - and ω -mesons in Dense and Hot Nuclear Matter Near the Critical Pion Mode Softening
G.G.Bunatian, B.Kampfer

Quasi-Particle Description of a Strongly Interacting Pion Gas
G.G.Bunatian, B.Kampfer

Quantum Phenomena at Fast Modulation of a Neutron Wave
D.V.Amandzolova, A.I.Frank, V.G.Nosov

Interaction of Waves and Particles with Layered Media (all media can be considered to be layered)
V.K.Ignatovich

Promising and Crucial Examples of Cluster Radioactivity Processes
S.G.Kadmensky, V.I.Furman, Yu.M.Tchuvil'sky

Possible equidistance of the excitation energies of the intermediate levels of intense γ-cascades

V.A.Khitrov, Yu.V.Kholnov, Yu.P.Popov, A.M.Sukhovoj, E.V.Vasilieva, A.V.Vojnov

Frank Laboratory of Neutron Physics, Joint Institute for Nuclear Research

The "regularity" exhibited by the intermediate levels excitation energies of the most intense two-step cascades has been shown to be most clearly manifested in the intensity distributions of the cascades [1] between the compound state of ^{174}Yb and its first excited level (Fig.1). In the correspondig spectrum there are no less than four groups of intense cascades. The distances between these groups are practically constant. A similar equidistance can be revealed in practically all the cascade intensity distributions hitherto obtained for nuclei distinguished by such parameters as the neutron number parity or by their deformation. It should be noted, that at a quite definite distance from the intermediate level of the observed intense cascade there may appear not only another level of a single intense cascade, but also groups (multiplet) of intermediate levels of intense cascades.

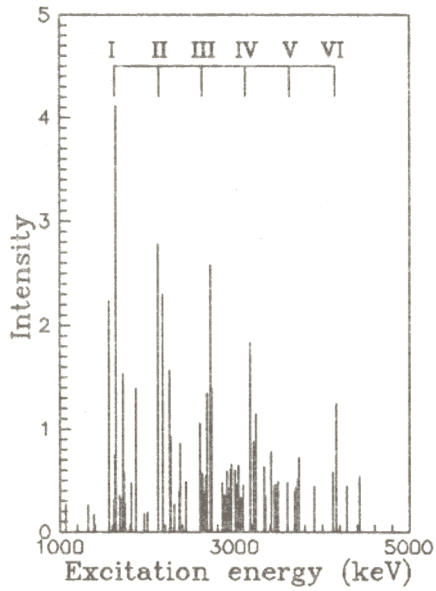

Fig.1. The dependence of the relative intensity of resolved intense two-step cascades to the first excited state of ^{174}Yb upon the excitation energy. The possible groups of equidistant states are marked by Roman numerals.

By now the cascades from two γ-transitions have been studied experimentally for more than 18 nuclei from the region $143 < A < 187$. These data allow us to perform an analysis in a broad range of nuclei.

It is now possible to single out one value for the equidistant interval T from our experimental data for many nuclei. In Fig. 2 the dependence is shown of the obtained equidistance period T as a function of the atomic weight of the nucleus under study.

It is seen from Fig. 2 that (in regard to errors of revealing the possible equidistant period) on the whole, regular dependence of equidistant period upon atomic weight is observed if one divides all studied nuclei into 4 groups differing by types of cascade transitions or by structure of decaying compound-state.

Obtained data allow one to suppose a presence of groups of vibration excitations with characteristic energy T≃500-800 keV.

Similar equidistant periods between intermediate levels of the most intense cascades were revealed also in nuclei ^{114}Cd and ^{124}Te.

For final proof of presence of pointed excitations it is necessary to search for two-step cascades in many neutron resonances.

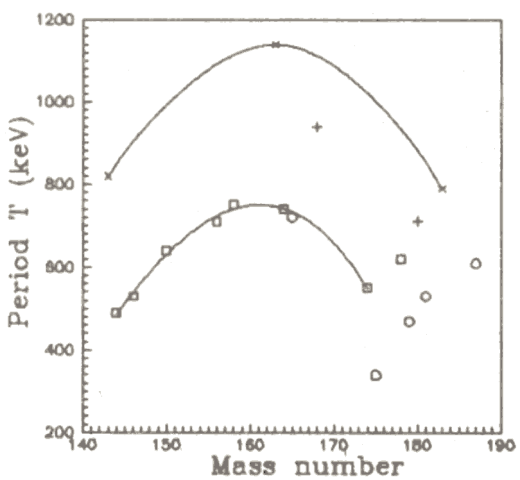

Fig.2. The dependence of the most probable equidistance period T on the mass number of the studied nuclei.

□ - even-even nuclei, cascades of E1+M1-transitions;

o - even-odd nuclei with $\Gamma_n^o / < \Gamma_n^o > > 1$;

×- even-odd nuclei with $\Gamma_n^o / < \Gamma_n^o > < 1$;

+ - nuclei ^{168}Er and ^{180}Hf, cascades of E1+E1-transitions.

The maximum and minimum values are connected by lines separately.

Boneva S.T. et al. Izv. Akad. Nauk SSSR, Ser. Fiz. V53, 2092 (1989)

The peculiarity of the high-lying states excitation of the even-even nuclei from the region $150 \leq A \leq 164$

V.A.Khitrov, A.M.Sukhovoj, A.V.Voinov

Frank Laboratory of Neutron Physics, Joint Institute for Nuclear Research

Performed by now investigations of the peculiarities of the heavy deformed nuclei states excitation and decay at the excitation energy region below neutron binding energy show that usually accepted notions of their neutron resonances γ-decay mechanism does not take into account some important features.

So, the single-particle transitions between the 4s and 3p neutron shells must influence essentially on the cascade γ-decay in the 4s-region of the neutron strength function. It is impossible to distinguish such transitions by traditional methods of nuclear spectroscopy due to the fragmentation process (well studied theoretically) of such states over many nuclear levels. At the same time, the method of the cascades γ-transitions analysis, summing by natural manner the strength of states over a given excitation interval, allows us to observe directly these single-particle transitions.

Their significant role in the neutron resonances γ-decay process was demonstrated by investigation of the even-odd nuclei [1]. Up to one half of the total intensity of all the primary transitions may be due to the neutron transitions between 4s and 3p shells.

Similar effects cannot be unobservable also in the even-even nuclei γ-decay. To reveal the role of similar transitions we studied [2] cascades of γ-transitions in the even-even compound-nuclei ^{150}Sm, $^{156,158}Gd$ and ^{164}Dy. According to theoretical calculations single-particle state [510]$\uparrow$, concentrating the strength of the 3p shell in deformed nuclear potential, lies by 2.5-3 MeV below neutron binding energy in this atomic weight region. This state must be excited intensively by the primary transitions with correspondent energy. It is seen from the figures that in all these nuclei at indicated primary transition energy it is really observed an enhancement of the cascades intensities relatively both model calculation (curve in figure) and cascades with some higher primary transition energy. Moreover, in some cases the experimental intensities exceed the model calculation by order of magnitude.

Hence, it is impossible to describe the neutron radiative capture process in heavy deformed nuclei [3] (including transuranium isotopes) without taking into account the shell effects of the similar kind.

1. Boneva S.T. et al., Particles and Nuclei, 1991, V.22, p.1433
2. Boneva S.T. et al., Z. Phys. A - Hadrons and Nuclei, 1991, V.338,. p.319
3. Beitins M.R. et al., Z. Phyz. A - Hadrons and Nuclei, 1992, V.A341, p.155

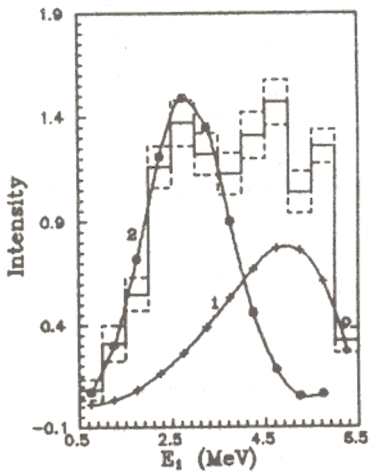

Fig.1. Sum intensity of cascades for the two low-lying levels in ^{150}Sm (% per decay) as a function of primary transition energy. Histograms represent the experimental data with ordinary statistical errors; curves 1 and 2 represent the BSFG and the Ignatyuk thermodynamical model predictions respectively.

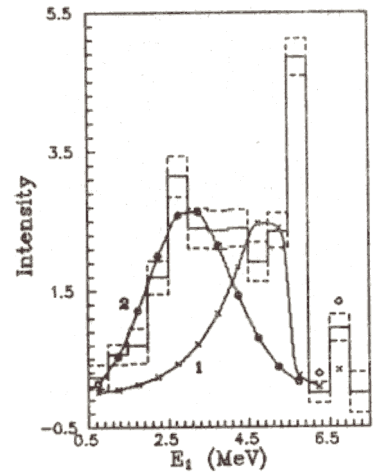

Fig.2. The same as in Fig.1 for cascades to the three low-lying levels in ^{164}Dy.

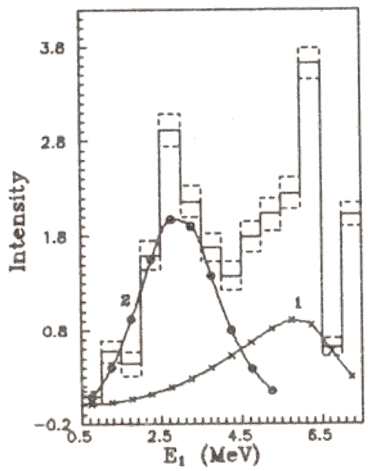

Fig.3. The same as in Fig.1 for cascades to the three low-lying levels in ^{156}Gd.

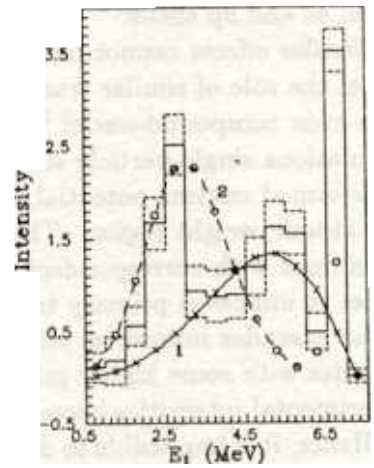

Fig.4. The same as in Fig.1 for cascades to the three low-lying levels in ^{158}Gd.

ON A NEW WAY OF COMPTON BACKGROUND SUBTRACTION IN INVESTIGATION OF γ γ-COINCIDENCES BY SUMMATION THE AMPLITUDES OF COINCIDING PULSES (SACP)

E.V.Vasilieva, A.V.Voinov, V.D.Kulik, Yu.P.Popov, A.M.Sukhovoi, V.A.Khitrov, Yu.V.Kholnov, V.N.Shilin

Frank Laboratory of Neutron Physics

The SACP method developed to study the γ-decay of compound states of nuclei [1] has been applied recently to investigate the decay of radioactive nuclei [2]. It is based on separation of two-quantum cascades with the same total energy, that is to say the cascades between two definite states of a nucleus. The work [3] (Fig.2) gives the SACP spectrum for the decay of $^{170}Lu \rightarrow ^{170}Yb$. It contains 70 peaks against a continuous Compton background. Each peak is for the sum of two-quantum cascades with the same total energy. Some of these total energies are indicated in this picture. To obtain spectra of γ-quanta which form the cascades, one must subtract the Compton background. Fig.1 demonstrates the applied method of subtraction of the Compton background [4]. It schematically shows two SACP peaks: the peak "i" which is under investigation, and the peak "j" at a larger energy. Both are located on the continuous spectrum of sums. Two bands are shown on both sides of the peak with the sum of their widths being equal to the background width under the peak. The spectrum composition for the hatched sections and the background under the curve is practically the same. Therefore the subtraction of the hatched sections is equivalent to the subtraction of the background itself. Fig.2a presents the differential spectrum of the cascades with the total energy $E_s = 2498\ keV$ which has been obtained in this way. There are two cascades in the spectrum, i.e. two pairs of lines which are symmetrical with respect to the spectrum center. The x-axis corresponds to the objective zero and if the data are close to the x-axis it means that the Compton background has been subtracted completely.

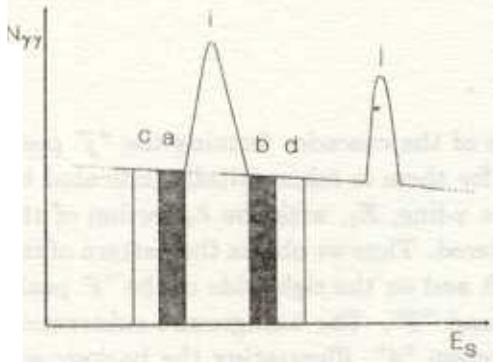

Fig.1. Schematic representation of a part of the SACP spectrum.

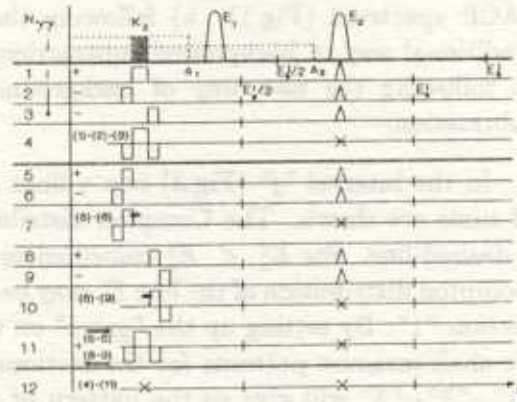

Fig.3. The way of subtracting the background in the SACP method.

However there is a background smooth component left in the form of structures of three peaks, one of them with a positive amplitude, two others with a negative one. These structures have no satellites in the other half of the spectrum. They appear following the background subtraction under the influence of the γ-lines forming the "j" peaks (Fig.1) of greater total energy. Fig.3 explains the nature of the false structures.

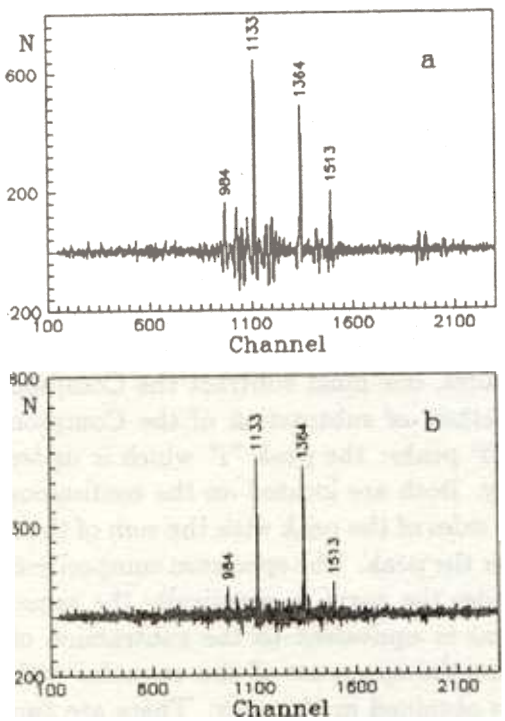

Fig.2. The γ-rays spectrum for the two-quantum cascades corresponding to the energy peak of $E_s = 2498\ keV$ in the SACP spectrum (Fig.1): a) following the traditional way of background subtraction; b) following the new way of background subtraction.

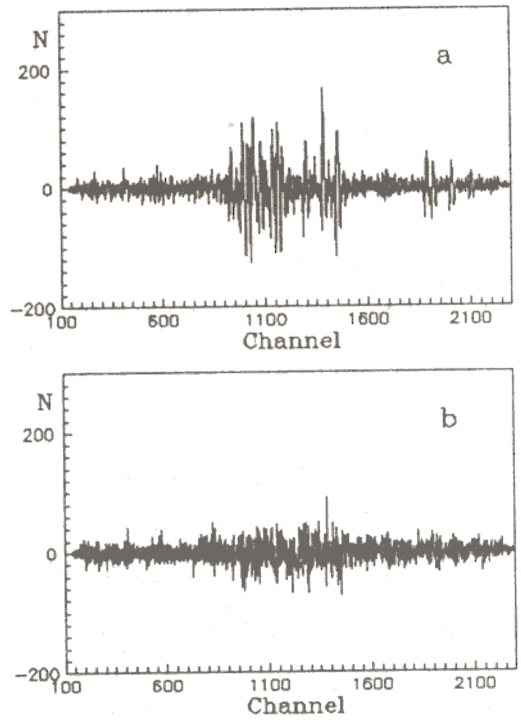

Fig.4. The same as in Fig.2 for the energy interval of the SACP spectrum of $2430 - 2443\ keV$.

In the interval "j" (Fig.3) two γ-lines of one of the cascades forming the "j" peak of sums are shown. The Compton distribution for them is schematically indicated by a dashed-line. For $E_s^i < E_s^j$ coincidences of the γ-line, E_2, with the k_2 section of the Compton distribution of the line E_1 may be registered. Thus we obtain the pattern of the section "1". By setting up the "gates" on the left and on the right side of the "i" peak, we shall measure patterns for the sections "2" and "3". The background subtraction "1"$-$"2"$-$"3" will give us the pattern of the section "4", illustrating the background structure in Fig.2a. The number of such structures increases rapidly with diminishing energy of the peak of sums under investigation, E_s^i. At $E_s < Q - 1\ MeV$ where Q is the energy of decay, measurements become practically impossible. A repeated background subtraction makes it possible to eliminate false structures.

Let us consider the "a" section (Fig.1) to be an effect and the "c" section — a background. The result of the above-mentioned operation will be the pattern of section 7 shifted to the left from the centre to a distance of "a" width. The same is true for the section 10 shifted to the right to a distance of "b" width.

If we shift both patterns as it was described above and add them together, as a result we shall have "11" identical to "4". The subtraction of "11" from "4" gives zero. The E_2 line turns out to be subtracted as well.

The shifts of "7" and "10" correspond to the move of the whole differential spectrum scale by a corresponding number of channels. Having performed the aforecited operations on the spectrum (Fig.2a) we obtained Fig.2b. All the background structures have disappeared completely.

The part of the spectrum of sums for the interval of $2430-2443\ keV$ is the best example in this respect. Fig.4a comprises more than 25 background structures. On applying this new method of background subtraction (Fig.4b) they are removed completely.

We have made use of this method to investigate the complicated scheme of the decay of $^{146}Eu \rightarrow ^{146}Sm$ [5]. The measurement has been taken for the whole energy interval. The method can be successfully applied to the study of the $(n, 2\gamma)$ reaction. It is dealt with in more detail in [6].

References

[1] Bogdzel A.A. et al., JINR, P15-82-706, Dubna, 1982

[2] Vasilieva E.V. et al., Izv. AS USSR, ser. phys. 1991, V.56, p.2, JINR, P6-91-568, Dubna, 1991

[3] Vasilieva E.V. et al., see the current report, p.

[4] Boneva S.T. et al., Izv. AS USSR, ser.phys., 1987, V.51, p.1882 JINR, P6-87-98 Dubna, 1987

[5] Vasilieva E.V. et al., The programme and abstracts of 43d International workshop on nuclear spectroscopy and the structure of a nucleus. Publishing house of PINP, St.-Petersburg, 1993

[6] Vasilieva E.V. et al., Izv. RAS, ser.phys., 1993, V.57, p.77; JINR,P6-92-148, Dubna, 1992

ON APPLICATION OF THE $\gamma\gamma$- COINCIDENCE METHOD INCLUDING SUMMATION OF THE AMPLITUDES OF COINCIDING PULSES (SACP) TO INVESTIGATION OF NUCLEAR RADIOACTIVE DECAY SCHEMES

E.V.Vasilieva, V.D.Kulik, E.V.Kulikov*, N.A.Lebedev* Le Hong Khjem, A.F.Novgorodov*, Yu.P.Popov, A.M.Sukhovoi, Fam Dinh Khang, V.A.Khitrov, Yu.V.Kholnov

Frank Laboratory of Neutron Physics
**-Laboratory of Nuclear Problems*

The decay of compound states of nuclei, produced by the capture of thermal neutrons, has been successfully investigated by the SACP method [1] for more than 10 years. The work [2] shows that the field of application of this method could be extended to investigation of complicated radioactive decay.

The gist of the method consists in successive measurement of the spectral composition of the two-quantum cascade groups with the same sum energy, E_s. After the decay of a compound state (Fig.1a), it will be groups of cascades between the compound state, (B_n), and different low levels of a nucleus, E_f; following the decay of a nucleus (Fig.1b) — between numerous levels populated by β-(α)- decay and low-lying levels.

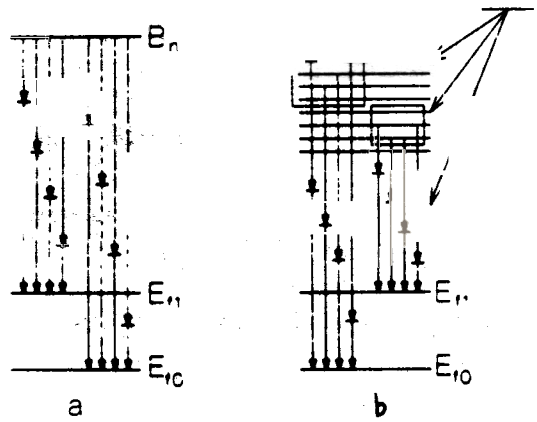

Fig.1 Two types of decay schemes for nuclei: compound states (a) and β- (α)- decay (b).

The energy of cascades (Fig.1a) is known beforehand. In the case of 1b it was not clear whether there would be some lines in the SACP spectrum.

The measured SACP spectrum for the $^{170}Lu \rightarrow ^{170}Yb$ ($Q = 3.5\ MeV$) decay is given in Fig.2. It contains 70 peaks (there are usually only a few of them for the reaction $(n, 2\gamma)$). They correspond to the cascades between pairs of levels (combinations of ≈ 80 levels). Thus, the whole γ-spectrum ($\geq$ 600 transitions) falls into 70 spectra of two-quantum cascades. One of them with $E_s = 3081\ keV$ is shown in Fig.3. The pairs of lines, which are symmetric about the spectrum center, form cascades each of those determines the position of three levels of a nucleus. 497 cascades have been detected, and their characteristics are presented in the tables [2]. 413 γ-transitions are engaged in them. 129 new cascades, 133 new γ-transitions, and 17 new levels (3298, 3273, 3206, 3180, 3114, 3111, 3092, 3055, 3014, 3007, 2979, 2846, 2842, 2779, 2764, 2739 and 2657 keV) have been found.

It's surprising that such an abundance of new results have been obtained while investigating the scheme of the decay of ^{170}Lu, considered to be thoroughly explored at a high up-to-date level [3].

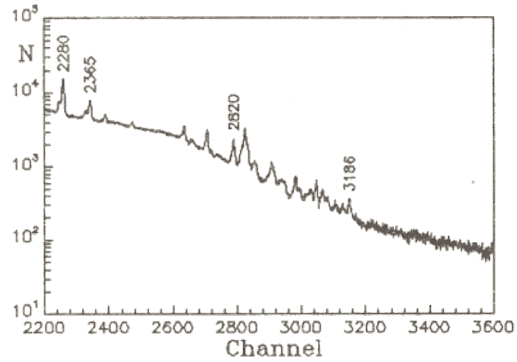

Fig.2 SACP spectrum for the decay of $^{170}Lu \rightarrow ^{170}Yb$.

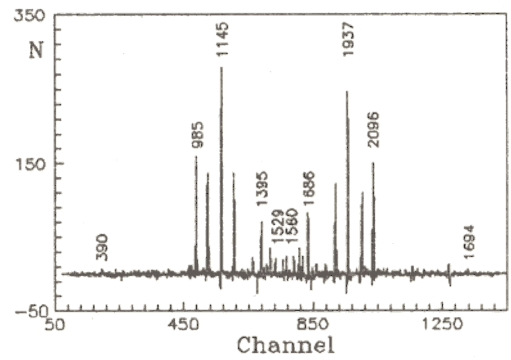

Fig.3 Distribution of intensities for the two-step cascades with the total energy $E_s = 3081\ keV$.

At the present time the construction of schemes of levels and transitions is based on the Ritz rule (the rule of sums and differences of transition energy values). In case of complicated decay schemes, when the total number of transitions $N > 100$, the number of accidental energy coincidences rises abruptly ($\approx N^2$), and application of these rules gives poor effect. For large N it is also difficult to interpret the results obtained with traditional method of coincidence with "gates".

To move further, it it necessary to increase considerably (by an order of magnitude) the measurement accuracy of transition energy or new methods should be found which either would not rely on the Ritz rules at all or would use them only to a certain extent. The present work has shown that the SACP method is one of such methods due to its following characteristics:

1. The possibility of dividing a complicated spectrum into a large number of sections, the rarefaction of spectra, and identification of weak components.
2. Weak degree of dependence on the Ritz rules.
3. The possibility of a complete subtraction of the Compton background.
4. The possibility of separating transition multiplets regardless of the component's energy value difference. It can be illustrated [2] by duplets 1514.26 - 1514.47 (2.6 - 61), 1674.11 - 1674.22 (15.6 - 2.73) and 1700.76 - 1700.80 (8.4 - 8.9) (in brackets the intensities are given per 10^{-4} decays)
5. The results can be easily interpreted.

References

[1] Boneva S.T. et al, Particles and Nuclei, 1991, V.22, p.479; V.22, p.1433

[2] Vasiljeva E.V. et al, Izv. RAS, V.57(9), p.77; JINR, P6-92-148, Dubna, 1992

[3] Dzhelepov B.S. et al, The properties of atomic nuclei. I.26 Schemes of a decay of radioactive nuclei. A = 169,170. 1988, L., Science, p.104-192

ON THE INDEPENDENT FRAGMENT YIELDS IN THE FISSION OF ^{239}Pu INDUCED BY RESONANCE NEUTRONS

N.A.Gundorin, A.B.Popov, Dao Ahn Minh, L.V.Michailov

Frank Laboratory of Neutron Physics, Joint Institute for Nuclear Research

The analises of gamma-spectrum from the resonance neutron induced fission of ^{239}Pu at 0.2 eV to 230 eV were developed [1].

The refined independent yields of some fragments as well as the time of life of some isomers were obtained /Table1 and Table2/.On the base of the comparison of our experimental results with those obtained for thermal neutron induced fission we may conclude that the variations in the mass distribution don't exceed 25 % for the fragments identified.

The relative yields of some fragments to the 11-th resonance with spin 1^+ were obtained for all identified fragments. The weighed mean values for 18 light and heavy fragments were calculated from these data as a function of E_n and $1/\Gamma_f$ /Fig.1 and Fig.2 /.

We have not seen the fluctuations from one resonance to other more than 5 % within the error of measurements.

The decrease of relative yields from the resonance with small Γ_f due to the competition between the (n,f) reaction and the (n,γ f) process is in qualitative agreement with the Cowan et al. data [2] on the P/V ratio /Fig.3/ as well as with the experimental [3] and calculated data [4] on the total energy of fission gamma-rays /Fig.4/. But no quantitative estimate in favour of this observation is possible to be made from these measurements due to considerable experimental errors.

So higher precision measurements of independent yields from the resonance neutron induced fission of ^{239}Pu are necessary.

References

1. N.A.Gundorin et al., Proceedings of the Second International Simposium on Nuclear Excited States, Łòdż, June 22-26, 1992.
2. G.A.Cowan et al., Phys.Rev., 144, no.3 (1966).
3. O.A.Scherbakov, Phys. Elem. Part and Atom. Nucl. 21, 419 (1990).
4. U.Gohs, Proceedings of International Conference on Nuclear Data for Science and Technology, Jülich, 1991.

Table 1.Independent yields of fission fragments from the resonanace neutron induced fission of ^{239}Pu in comparison with those from thermal neutron induced fission.

Z-Fr-A	Gamma energy E_γ keV	Preliminary results/9/ $Y_{res}\pm\Delta Y$ %	Refined results $Y_{res}\pm\Delta Y$ %	A.C.Wahl /8/ $Y_{th}\pm\Delta Y$ %	J.Kaufmann /10/ $Y_{th}\pm\Delta Y$ %
36-Kr-88	775	0.77±0.23		0.79±0.03	
90	707	1.58±0.27	1.00±0.20	1.18±0.05	1.25±0.03
38-Sr-92	814.7		0.60±0.24	1.00±0.06	
94	837.4	2.65±0.33	3.32±0.42[a]	3.14±0.16	3.30±0.05
96	815		1.40±0.56	1.90±0.10	1.75±0.04
40-Zr-98	1223	2.78±0.29	2.4±0.36	2.85±0.14	2.83±0.05
100	212.4	3.95±0.20	4.08±0.21	4.76±0.24	4.40±0.06
102	152	0.99±0.14		1.19±0.12	0.54±0.02
42-Mo-102	296		2.00±0.20	1.70±0.12	
104	192	4.02±0.20	5.07±0.21	4.12±0.21	5.19±0.06
106	171.7	1.48±0.21	2.20±0.24	2.06±0.10	2.05±0.04
52-Te-132	974	1.79±0.23	2.00±0.40	2.36±0.07	
134	1279.8	2.70±0.28[b]	4.50±0.81[c]	4.71±0.51	
54-Xe-136	1313	1.83±0.17[b]		3.02±0.36	
138	589	3.56±0.28	4.06±0.34	4.08±0.33	
140	376.8		1.30±0.27	1.50±0.09	
56-Ba-142	359.7	3.49±0.32	3.11±0.24	3.27±0.26	
144	199.4	2.51±0.15	2.32±0.19	2.05±0.23	
58-Ce-146	259	1.13±0.18		0.95±0.01	
148	159	1.70±0.16		1.09±0.12	

a-This value has been evaluated due to the large interference caused by the ^{72}Ge (n,n'γ) broad neutron inelastic scattering peak.

c(b)-This value has (not) been corrected for the cascade isomeric transition.

Table 2.Cascade delay γ-rays observed in the experiment.

Gamma energy keV	Z-Fr-A	Intensity $Y_\gamma\pm\Delta Y$ %	$T_{1/2}$ ns
115		1.60±0.16	162/5/[a]
297	52-Te-134	2.90±0.26	165±18
1280		3.20±0.32	154±15
161	40-Zr-97	0.80±0.16	104/11/[a]
1103		1.50±0.30	76±11
314		0.90±0.18	10.0±1.0
400	54-Xe-137	1.10±0.20	7.0±1.0
1221		0.80±0.16	9.0±1.4
204	38-Sr-95	2.40±0.15	22.0±1.5
352		2.40±0.12	18.0±1.1

a-This value was taken from /Ref./ and used as input.

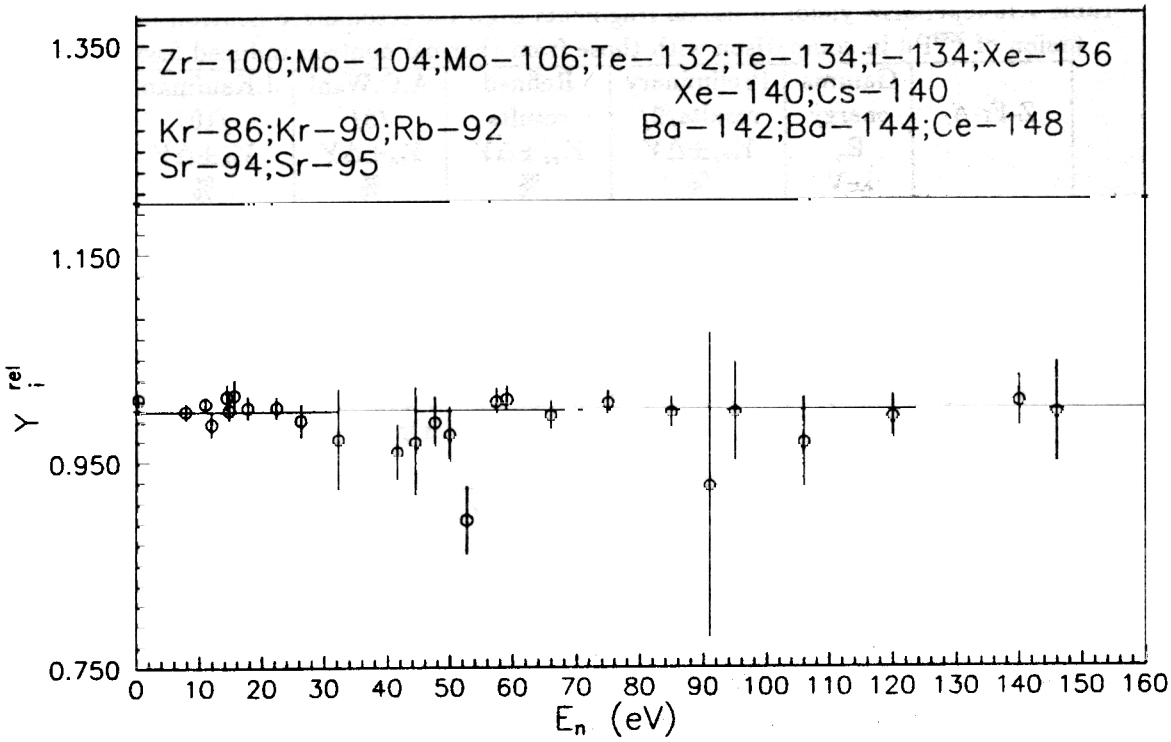

Fig.1 : The weiged mean value of relative yields for 18 fragments vrs neutron energy.

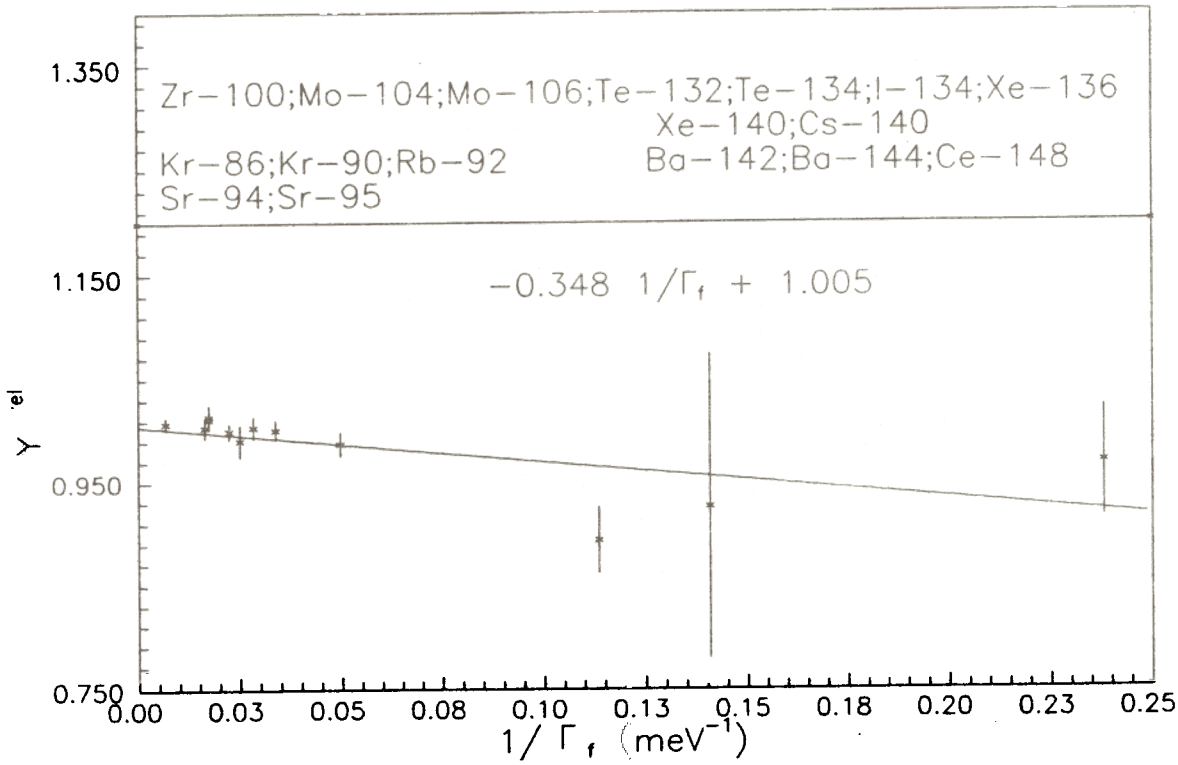

Fig.2 The weighed mean values of relative yields for 18 fragments vrs $1/\Gamma_f$ resonance.

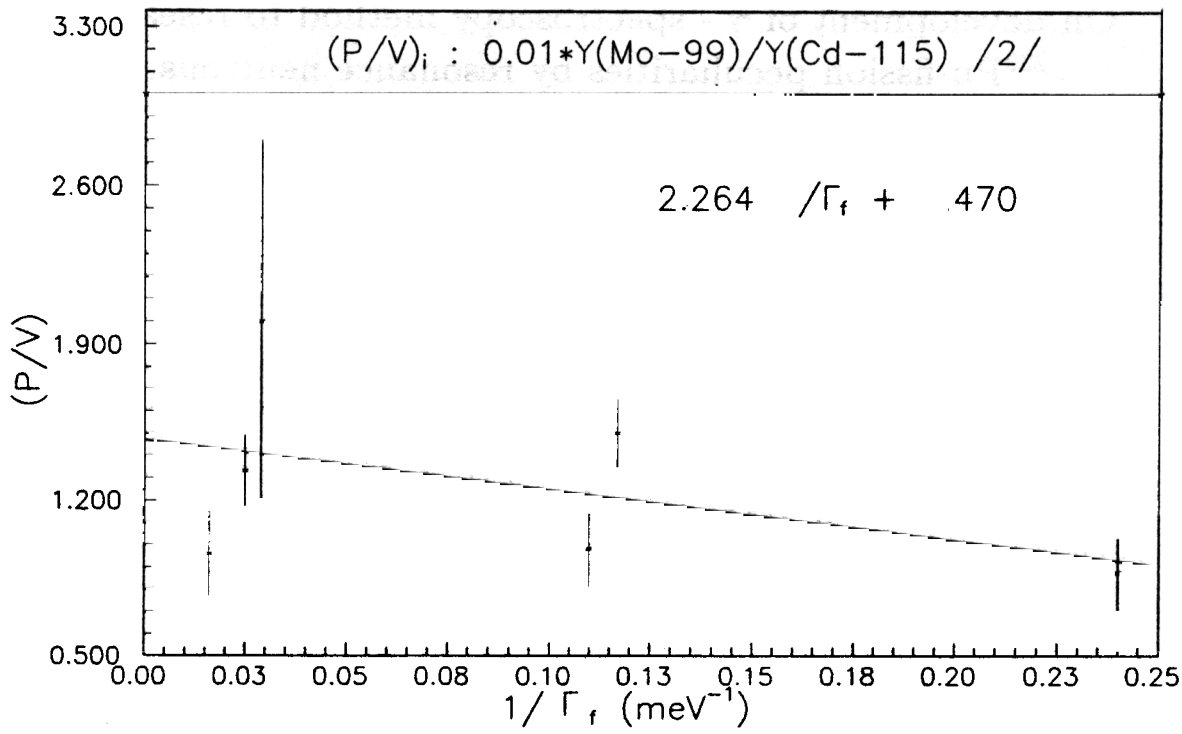

Fig.3 :The relative value P/V from the data of Cowan, et al. /2/ vrs $1/\Gamma_f$ resonance.

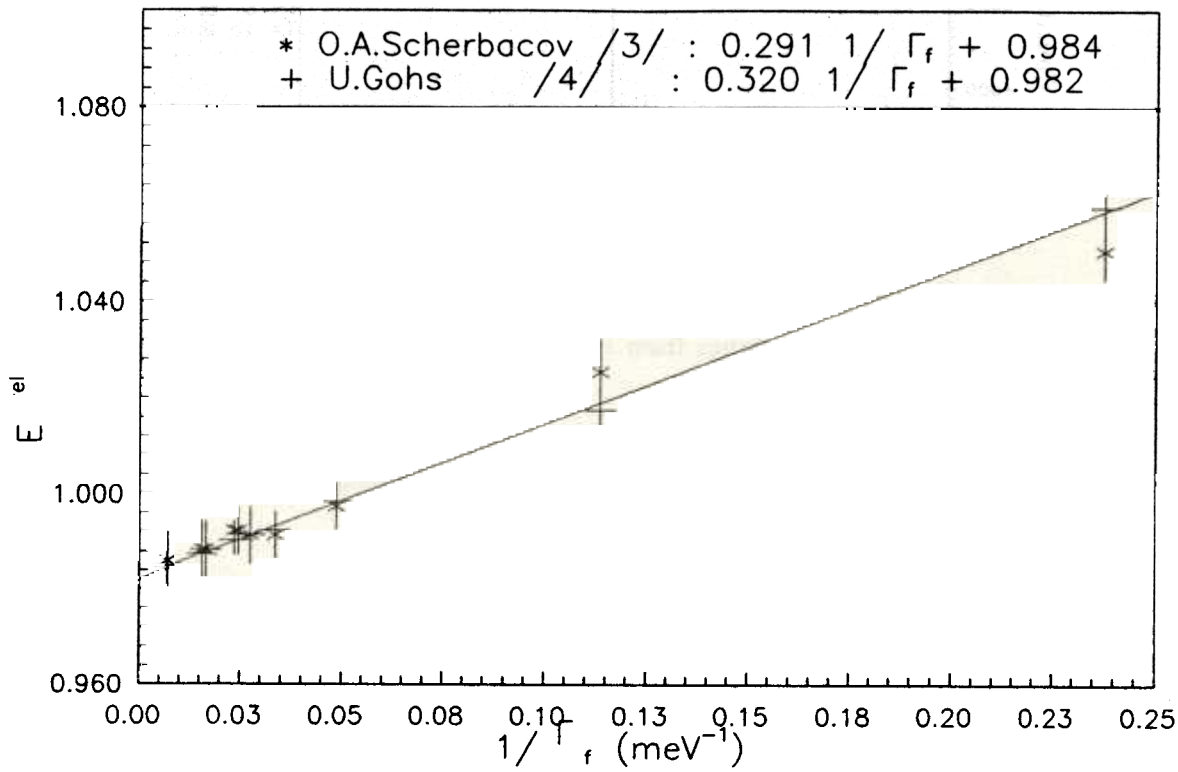

Fig.4 :The relative energy of gamma-rays from the $(n,\gamma f)$ process vrs $1/\Gamma_f$ resonance.

On development of γ - spectroscopy method to research ^{239}Pu fission peculiarities by resonance neutrons.

N.A.Gundorin

Frank Laboratory of Neutron Physics, Joint Institute for Nuclear Research,

The measurements of independent fission fragment yields by means of gamma - spectroscopic method was demonstrated during the investigation of spontaneous fission of ^{252}Cf [1],[2]. This method was used in the investigation of gamma - rays from fission fragments of ^{235}U induced by resonance neutrons [3]. Further developments of the gamma - spectroscopy method were in conjunction with the research of peculiarities in the fission of ^{239}Pu [4].

Neutron spectroscopy is carried out using the time - of - flight method with the IBR - 30 as a neutron source. The fission chamber is employed as the target and as the fast detector of fission events. The semiconducting Ge detector is used to measure the gamma - ray spectrum. The basic characteristics of the gamma - spectrometer are shown in Table 1. The time-of-flight spectrum from the fission chamber (fig.1) demonstrates insufficient energy resolution, especially for the range (40 - 230)eV.

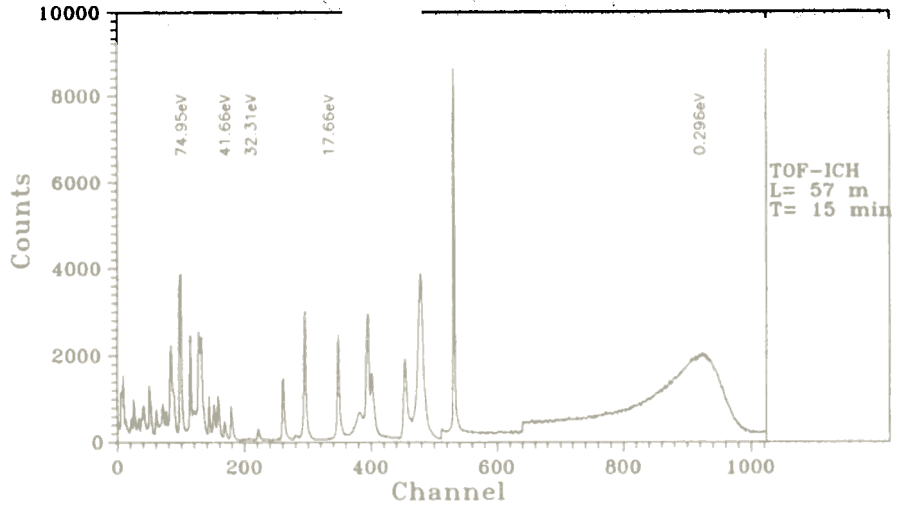

Figure 1: Time-of-flight spectrum from the fission chamber for energy region (0.2 230)eV.

For increased resolution it is necessary to use a source with shorter neutron pulse duration. It will be possible after reconstruction of the neutron source in Dubna according to the IREN project [5].

Table 1: Basic characteristics of fission gamma - spectrometer.

Parameters of Fission Gamma - Spectrometer		
Neutron spectrometer	IBR - 30 1992y.	IREN project
Distance of neutron flight (m)	57 - 60	57 - 60
Neutron flux (n/cm^2 s eV)	$2 \times 10^3 E^{-0.9}$	$3 \times 10^3 E^{-0.9}$
Energy resolution (eV)	$1.9 \times 10^{-3} E^{3/2}$	$1.9 \times 10^{-4} E^{3/2}$
Recycling energy (eV)	0.17	0.17
Fission chamber (IFC)	^{239}Pu	
Fission material (g)	1.6	
Number of targets	19	
Density (mg/cm^2)	1.0	
Target diameter (cm)	7.5	
Enriched (%)	99.9	
Efficiency (%)	60	
Time resolution (ns)	2.6	
Number of sections	19	
Ge - detector	DGDK-110	GR3019
Efficiency (%)	12	30
Energy resolution (keV)		
122 keV	1.4	0.9
1332 keV	2.3	1.9
Peak/Compton	24	48
Distance IFC - Ge (cm)	28 - 31	14
Raddition - resistance fluence (n/cm^2)	10^9	$\geq 10^{10}$
Price (in 1989y.)	30×10^3 rouble	48.5×10^3 $ USA
Counting rate in spectroscopy channel (s^{-1})	$(3-4) \times 10^3$	6×10^4

The gamma - spectrum, measured by the spectrometer with Ge detector DGDK - 110 (fig.2), has a few "bumps" and a small ratio between gamma - lines and the underlayer due to insufficient quality of the Ge detector and the high neutron induced γ-background.

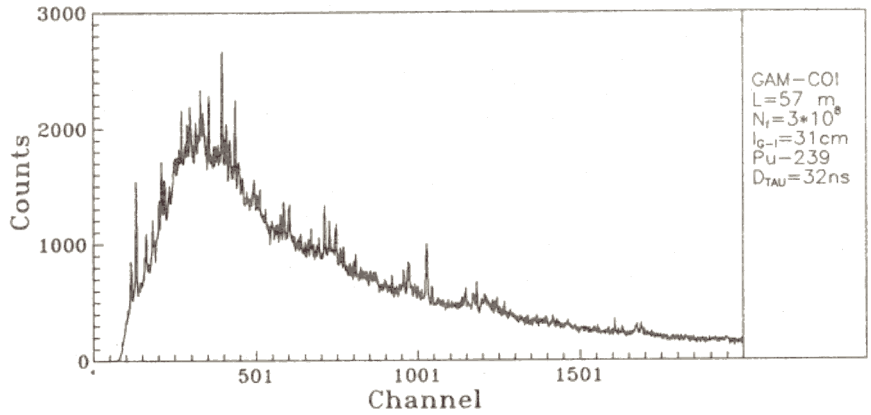

Figure 2: Coincidence gamma - spectrum for the energy region (100 - 1000)keV.

Efficiency of the gamma-spectroscopy method in investigating nuclear fission depends on the parameters of a spectrometer and the quality of a measured spectrum. Perfection of spectrum by reducing the Compton-underlay with the help of an "active" shielding of the Ge detector is doubtful due to unfavorable background conditions of the neutron beam. Nevertheless, that way of spectrum improvement was tested with a model spectrometer with incomplete "active" and complex "passive" shielding. An incomplete "active" shielding consisted of three plastic scintillators $20 \times 20 \times 40 cm^3$ and one NaI(Tl) crystal - 15cm×10cm (fig.3). A complex "passive" shielding - 5cm of ^{10}B - CH and 5cm of Pb - was used to decrease the gamma counts connected with a high neutron background.

The efficiency estimation of the Compton-underlayer reduction was defined to compare the ratio peak/underlayer for gamma - lines in the energy region (100 - 400)keV between two fragments gamma - ray spectrum: without (A) and with "active" shielding (B) (fig.4). The mean value of the reduced coefficient is $K_{red} = 2.6 \pm 0.2$. If the condition of incomplete shielding - nearly $(0.65 - 0.7) \times 4\pi$ - is taken into account, with the spectrometer's size and construction being optimized the reduction could be over 90%. As far as the main part of the experimental error is connected with the large spectrum's underlayer, after it is reduced 10 times, the precision of the data may be more than 3 times greater. The statistical error may be reduced more than 3 times using a quality n-HP Ge detector (GR3019), a fast electronic system and to reducing the distance between it and the IFC (Table 1).

As a result the summary experimental error could be improved by nearly one order of magnitude compared to the preceeding data [6]. Modification of the spectrometer by using a high quality n-HP Ge detector and a fast electronic system, will allow measurement of much more gamma-lines with the intensity precision of (1-3)%. Thus the efficiency of gamma-spectroscopy method will be increased essentially.

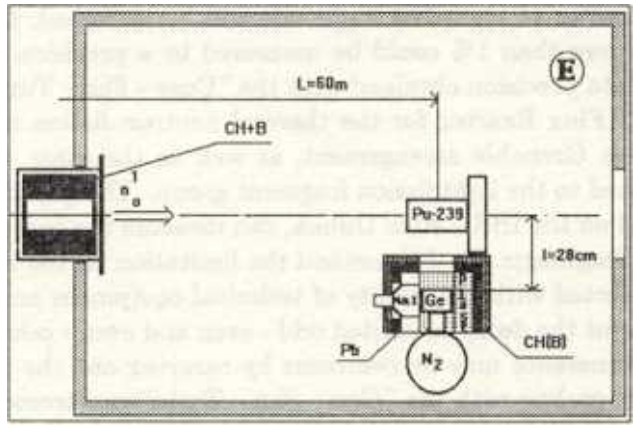

Figure 3: Scheme of gamma - spectrometer with incomplete "active" shielding on IBR - 30.

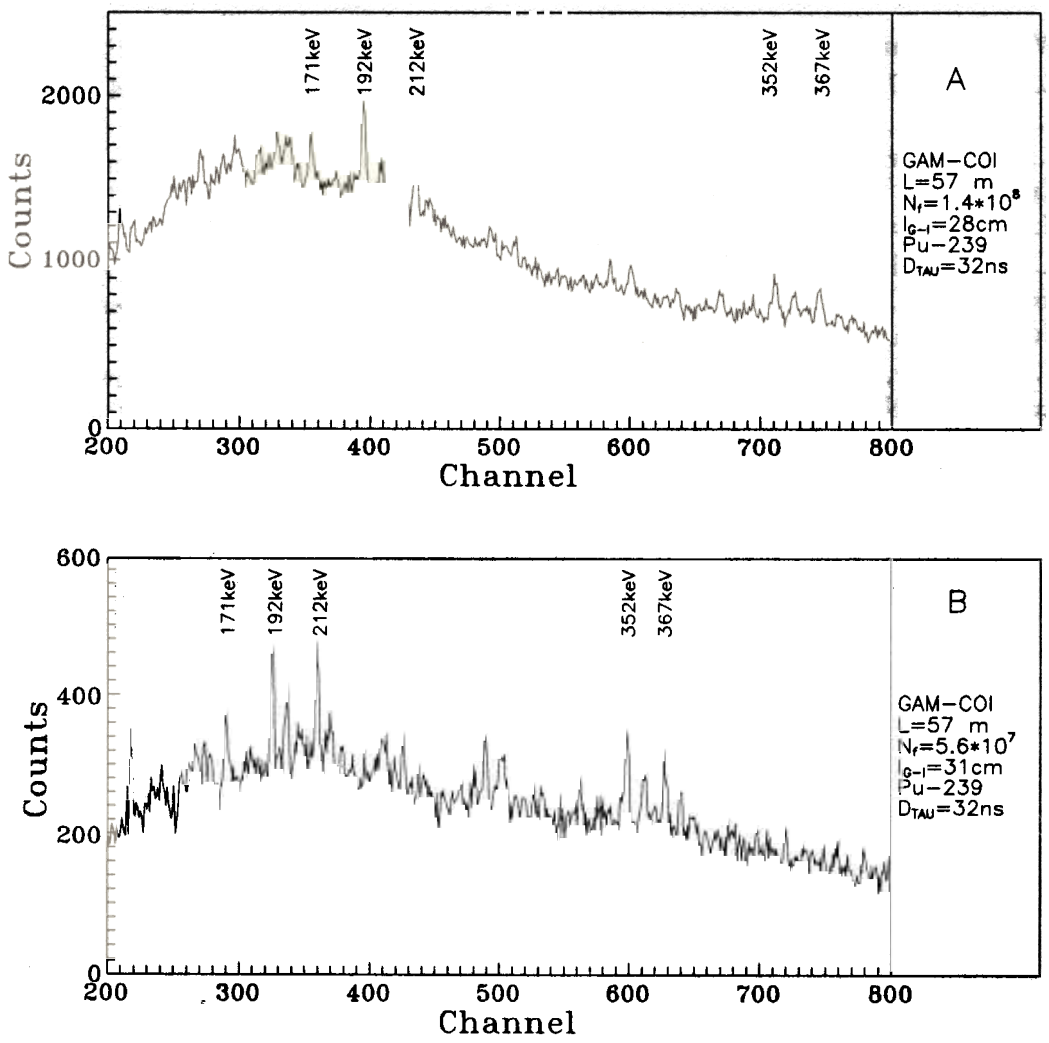

Figure 4: Coincidence gamma - ray spectrum without (A) and with "active" shielding (B) for the energy region (100 - 400)keV.

In this way the number of identified fragments will be increased; for those with independent yields of more than 1% could be measured to a precision of 1 - 3%. This value is close to the data precision obtained with the "Cosy - Fan - Tutte" spectrometer at the Grenoble High Flux Reactor for the thermal neutron fission of ^{239}Pu [7]. But the possibilities of this Grenoble arrangement, as well as the mass - separator "LOHENGRIN", are limited to the light fission fragment group. The gamma - spectroscopy method, which is used on the IBR - 30 in Dubna, can measure the independent yields of both light and heavy fragments. In this method the limitation on the number of identified fragments is connected with the quality of technical equipment and the incomplete spectroscopic data about the decay of excited odd - even and even - odd fission fragment states. This last circumstance may be overcome by carrying out the fission fragments gamma - spectroscopy on-line with the "Cosi - Fan - Tutte" spectrometer or any other similar arrangement at a high flux neutron source.

References

[1] W. John, Frank W. Guy and J.J. Wesolowski, Phys. Rev. C2, 1970, p. 1451.

[2] E. Cheifetz, J.B. Wilhelmy, R.C. Jard and S.G. Thompson., Phys. Rev. C4, 1971, p. 1913.

[3] S.A. Antonov, A.A. Bogdzel, N.A. Gundorin, À. Duka - Zòlyǫmi, J. Kliman, D. Krjistec, A.I. Ostrovnoi, T.M. Ostrovnaia, A.B. Popov, B. Prespirin, V.G. Tishin, N.U. Shirikova, Communication of JINR 13-85-701, 1985, Dubna.

[4] A.A. Bogdzel, N.A. Gundorin, U. Gohs, À. Duka - Zolyòmi, J. Kliman, V. Polgorski, A.B. Popov, Dao Anh Minh, Proceedings of International Conference on Nuclear Data for Science and Technology, Jülich, 1991, pp. 150-152.

[5] V.L. Aksenov, N.A. Dikansky, V.L. Lomidze, A.V. Novokhatsky, Yu.P. Popov, V.T. Rudenko, A.N. Skrinsky, W.I. Furman, Communication of JINR E-3-92-110, 1992, Dubna.

[6] N.A. Gundorin, A.B. Popov, Dao Anh Minh, J. Kliman, V. Polgorski, À. Duka - Zolyòmi, U. Gohs, Proceedings of the Second International Symposium on Nuclear Excited States, Łòdż, 1992, p. 181.

[7] J. Kaufmann, Physikalisches Institut, Univ. Tübingen, private communication (1991).

THE FISSION CROSS SECTION AND RESONANCE PARAMETERS OF ^{237}Np IN THE SUB-BARRIER REGION ($E_n \leq 500eV$)

E.Dermendjiev, I.Ruskov, Yu.S.Zamyatnin

Frank Laboratory of Neutron Physics, JINR, 141980 Dubna, Moscow Reg. Russia

A.A.Goverdovsky

Institute of Physics and Power Engineering, 249020 Obninsk, Kaluga Reg., Russia

The reported work sought to achieve more precise values for the fission cross section, $\sigma_f(E_n)$, and the resonance parameters, $\sigma_o\Gamma_f$ and Γ_f for ^{237}Np in the sub-barrier range of neutron energies, where there is a considerable discrepancy (about three times) between σ_f values of American and Japan groups [1], [2] and the Saclay results.

It should be added that these neutron data on ^{237}Np are of important significance for simulating the processes going in high burnup reactors and for the transmutation of long-lived radioactive wastes.

The experiment was performed using the neutron time-of-flight method on beam 3 at the IBR-30 pulsed booster at JINR. The flight path of 58.5 m, the neutron pulse frequency of 100 Hz, and the pulse width of ≈ 4 μs were used.

A relative method of measurement was applied and the multilayer ionization fission chamber comprising 12 targets from ^{237}Np with the overall weight of 132 mg and one target from ^{235}U weighing 8.5 mg were used. The measuring time amounted to 1042 hours.

The cross section dependence $\sigma_f(\Delta E_n)$ was measured over the neutron energy interval from 3 to 500 eV.

The results, compared with other authors' data, are shown in Fig.1.

One can see that our data in resonance cluster range are in good agreement with both the American results obtained using neutrons from an underground nuclear explosion [1] and the Japan ones in a lead cube [2], but about three times larger than the Saclay data [3].

At the same time the inter-cluster cross section values are closer to those measured at Saclay [3] which can be attributed to the difference in resolution power of the measuring methods.

The resonance parameters, $\sigma_o\Gamma_f$ and Γ_f, obtained in Dubna recently and those that had been measured earlier [4] are given in Table 2. Also shown are the Saclay [3] and Geel [5] results. One can see that the Dubna data are systematically by several times higher than the data of the French group.

A conclusion is made that the new values of neutron constants for ^{237}Np measured in Dubna and Kyoto, and also at Los Alamos [6], although showing quite good agreement, still require correction and re-evaluation of the ENDF/B-VI and YENDL-3 values, relying on the measurements reported in the work [3].

References

[1] M.Hoffman et al., Bul.Amer.Phys.Soc. **21**, 655 (1976).

[2] I.Kimura et al., Report, Int.Sem. on Neutron Physics, Dubna, April 1992.

[3] S.Plattard et al., Nucl.Sci.Eng., **61**, 477 (1976).

[4] K.A.Gavrilov et al., Atom.Energy, **28**, 362 (1970).

[5] W.Kollar et al., Z.Physik, **248**, 355 (1971).

[6] A.D.Carlson et al., Report, *Measurements of the ^{237}Np cross section*, Reactor Dosimetry ASTM STP 1228, Amer.Soc. for Testing and Materials, Philadelphia, 1994.

[7] "Neutron Cross Sections", **1B**, Editor S.F.Mughabghab, BNL, Academic Press Inc., (1984), New York, USA.

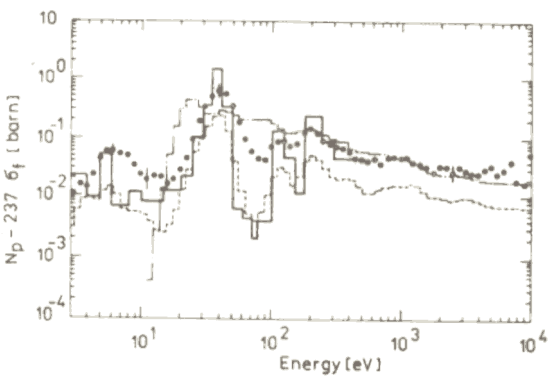

Fig.1 Comparison of σ_f values for ^{237}Np measured at Saclay [2], using neutrons from an underground nuclear explosion [3], in a lead cube of Kyoto University [5] and given in the present work.
– – – [2]; · - · - · [3]; · · · · · [5]; —— the present work.

Table 1. The cross section of ^{237}Np averaged by resonance neutrons in the energy interval from 3 eV to 500 eV.

Energy interval, (eV)	Averaged cross section $<\sigma_f>$ (barn)	Energy interval, (eV)	Averaged cross section $<\sigma_f>$ (barn)
3 – 4	0,022 ± 0,006	50 – 60	0,006 ± 0,002
4 – 5	0,009 ± 0,003	60 – 70	0,005 ± 0,002
5 – 6	0,055 ± 0,010	70 – 80	0,002 ± 0,001
6 – 8	0,006 ± 0,002	80 – 90	0,004 ± 0,002
8 – 10	0,012 ± 0,003	90 – 100	0,004 ± 0,002
10 – 15	0,008 ± 0,003	100 – 110	0,016 ± 0,004
15 – 20	0,014 ± 0,004	110 – 130	0,16 ± 0,03
20 – 25	0,023 ± 0,006	130 – 150	0,050 ± 0,009
25 – 30	0,11 ± 0,02	150 – 180	0,013 ± 0,003
30 – 35	0,35 ± 0,06	180 – 240	0,22 ± 0,04
35 – 40	1,64 ± 0,26	240 – 300	0,091 ± 0,017
40 – 50	0,34 ± 0,06	300 – 500	0,046 ± 0,012

Table 2. Resonance area ($\sigma_o\Gamma_j^I$) for ^{237}Np in the neutron energy interval from 0.5 eV to 50 eV

E, (eV)	Γ_j^I[ĈÝó]		
	Pikelner et al.[4] $\sigma_o\Gamma_j^I$, (barn.eV).10^{-3}	Plattard et al.[3] $\sigma_o\Gamma_j^I$, (barn.eV).10^{-3}	The present work $\sigma_o\Gamma_j^I$, (barn.eV).10^{-3}
0.489	2.9 ± 0.7		
1.321	3.8 ± 1.0		
1.479	3.5 ± 1.0		
1.969	1.9 ± 1.0		
3.865	16 ± 4	6 ± 0.9	12 ± 2
4.26		0.4 ± 0.3	1.3 ± 0.2
4.86		0.1 ± 0.1	1.0 ± 0.2
5.78	46 ± 9	1.6 ± 1.8	35 ± 6
7.42	12 ± 6	2.7 ± 0.6	6.6 ± 1.1
8.30		0.9 ± 0.5	3.5 ± 0.6
8.97		4.1 ± 0.5	12 ± 2
10.68		2.5 ± 0.4	10 ± 2
10.84		1.8 ± 0.6	3.0 ± 0.5
11.10		1.0 ± 0.3	2.6 ± 0.5
24.98		17.8 ± 1.8	43 ± 7
26.19		11 ± 4	44 ± 7
26.56		70.7 ± 5.5	170 ± 30
29.49		0.6 ± 0.2	23 ± 4
30.41		308 ± 12	850 ± 140
30.75		1.3 ± 0.6	5.2 ± 1
31.30		2.2 ± 0.7	1.5 ± 0.3
37.15		147.3 ± 12	440 ± 70
38.18		7.7 ± 2.2	82 ± 13
38.92		288 ± 24	890 ± 140
39.24		153.2 ± 12	530 ± 80
39.79		69.4 ± 22	190 ± 30
39.93		891.8 ± 44.5	2900 ± 470
41.35		389 ± 27	1230 ± 200
42.81		21.3 ± 7	95 ± 15
46.04		130.2 ± 7	400 ± 60
50.34		111.7 ± 13	370 ± 60

Table 3. Fission widths, Γ_f^I, of ^{237}Np resonances in the energy interval from 0.5 eV to 50 eV

E, (eV)	Γ_f^I[Ýó]			
	Recommended values [7]	Pikelner et al. [4]	Plattard et al. [3]	The present work
	1.24 ± 0.26	1.3		
	8.7 ± 0.5	4.1		
	1.33 ± 0.14	1.1		
	4.2 ± 0.3	8.4		
	7.0 ± 0.7	7.8	3 ± 0.5	5.8 ± 1.0
	0.34 ± 0.20		0.2 ± 0.2	6.4 ± 1.2
	7.9 ± 0.2		0.07 ± 0.07	4.4 ± 0.9
	12.6 ± 0.5	13	5 ± 0.5	11 ± 2
	9.5 ± 0.9	19	4.2 ± 1.0	10 ± 2
	670 ± 2		2.1 ± 0.6	8.7 ± 1.6
	24.0 ± 1.2		8.8 ± 1.2	26 ± 5
	5.4 ± 0.4		1.5 ± 0.3	6.4 ± 1.1
	0.8 ± 0.3		0.8 ± 0.3	1.3 ± 0.2
	3.4 ± 0.3		0.4 ± 0.1	1.2 ± 0.2
		Kollar et al. [5]		
24.98	8.5 ± 0.6	40.8 ± 3.4	3.6 ± 0.5	8.2 ± 1.5
26.19	85 ± 5	71.6 ± 24	30.6 ± 8.5	160 ± 30
26.56	63 ± 2	64.2 ± 7.3	22.5 ± 3.2	57 ± 10
29.49	62 ± 46	–	9.9 ± 6.1	300 ± 50
30.41	270 ± 8	109 ± 13	79.8 ± 10.2	250 ± 40
30.75	6.6 ± 6.6	132 ± 40	5.1 ± 2.7	18 ± 3
31.30	17 ± 3	44.3 ± 23	6.9 ± 2.4	5 ± 1
37.15	340 ± 10	232 ± 46	142.3 ± 28.5	360 ± 60
38.18	20 ± 2	68.5 ± 21	8.6 ± 3.0	72 ± 13
38.92	1000 ± 200	710 ± 180	380.2 ± 84.0	970 ± 170
39.24	840 ± 12	533 ± 160	333.1 ± 105.8	1100 ± 190
39.79	21 ± 21	–	1686.9 ± 800.0	1500 ± 260
39.93	7720 ± 66	5500 ± 970	864.7 ± 122.7	6400 ± 1100
41.35	700 ± 20	275 ± 48	216.7 ± 32.5	720 ± 130
42.81	1000 ± 100	307 ± 88	236.8 ± 153.4	1100 ± 200
46.04	700 ± 40	550 ± 110	276.1 ± 139.8	820 ± 140
50.34	57 ± 70	57.2 ± 8.4	23.2 ± 5.9	310 ± 50

AN EXPERIMENT TO MEASURE DELAYED NEUTRON YIELD AND TO SEARCH FOR SHORT-LIVED GROUPS OF DELAYED NEUTRONS ($T < 0.5\ s$).

E.Dermendziev, Ju.S.Zamjatin, V.M.Nazarov, I.Ruskov

Frank Laboratory of Neutron Physics

1. A setup to investigate delayed neutron yields has been constructed and tested at the IBR-2 pulsed reactor. It includes a neutron chopper, a collimation system and a neutron detector. The setup is placed on beam 11 of the IBR-2 reactor.

The neutron chopper is synchronised with reactor pulses and has an adjustable phase shift and a variable rotation frequency. The measuring interval for delayed neutrons is $50 - 200\ \mu s$ at a neutron pulse frequency of 5 Hz, and up to 1 s, at a chopper frequency of 1 Hz.

Test measurements have been made to study the setup capabilities and characteristics in different modes of operation (at a chopper frequency of 5 and 2.5 Hz and different phase shifts).

The results of the preliminary measurements with ^{235}U and Pb samples inside the detector have shown that for the measuring time of 400 μs the number of delayed neutrons in the groups with the known periods falls by 15% (See Figure 1). The new groups with shorter periods over the background level have not been detected yet. The ways of reducing the background by means of neutron beam filtration and decreasing the number of fast neutrons have been outlined.

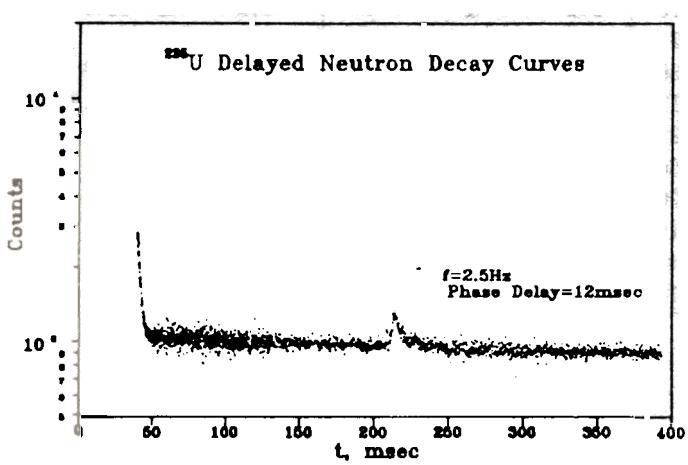

Fig.1.

INVESTIGATIONS OF THE ^{235}U NUCLEI FISSION INDUCED BY RESONANCE NEUTRONS

N.N. Gonin, L.K. Kozlovskiy, D.I. Tambovtsev
IPPE, Obninsk

A.A. Bogdzel, N.A. Gundorin, L.V. Mikhailov, A.B. Popov, W.I. Furman
Frank Laboratory of Neutron Physics
Joint Institute for Nuclear Research, Dubna, Russia

The measurements of the angular distribution of fragments from the resonance neutrons induced fission of aligned ^{235}U nuclei have been started at the 5th beam of the booster at the IBR-30 reactor on the 30 m flight path.

The purpose of these investigations is an independent evaluation of the $A_2(E_n)$ anisotropy factors for the resonance neutrons in the interval of 0.3 to 50 eV as well as the analysis of the angular-dependent part of the fission cross-section within the frames of the multilevel and multichannel model of fission.

The nuclei alignment is attained by cooling the rubidium uranyl nitrate (RUN) single crystals down to 0.15K in the $^3He - ^4He$ dilution refrigerator (Fig. 1). Two sets of the single crystal targets with the area of 20 and 24 cm^2 are attached back-to-back to the each side of the copper plate which is in thermal contact with the refrigerator dilution chamber. The fission fragments from each sample side are registered by the silicon detectors of 2 x 5 area at 0°, 45°, and 90° with reference to the c-axis of the single crystals (the c-axes of all the crystals are directed along the neutron beam).

By now, only the preliminary measurements have been carried out. Low content of the uranium nuclei in the samples ($\sim 10^{20} cm^{-2}$) leads to the necessity of the long-time measurements. Certain problems in using the surface-barrier superconductor detectors have arisen. At the helium temperatures, the contacts sometimes give trouble, the noise arises, and other instabilities take place.

Fig. 2 shows the example of the effect observed in the time-of-flight spectrum caused by alignment of ^{235}U nuclei. The spectrum has been registered by the detector positioned at θ=90°. One can see relative changes of the resonance areas when comparing the "warm" and the "cold" spectra

The first estimations show that the mean value of A_2 within the interval of 0.3 to 50 eV is colse to $< A_2 >$ value obtained by Pattenden and Postma (1971) in the similar experiment which has been the only one up to now.

This experiment is the first and preparatory step towards the future experiments at the IREN installation which will have more perfect parameters.

The experiment is intended to be performed in cooperation with Delft and Darmstadt.

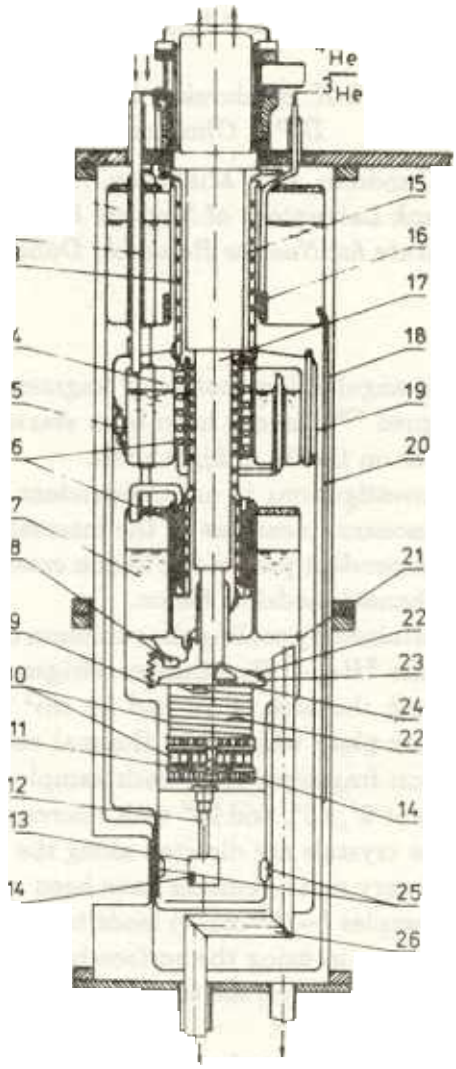
4He
3He
15
16
17
18
19
20
21
22
23
24
22
14
25
26
4
5
6
7
8
9
10
11
12
13
14

Fig.

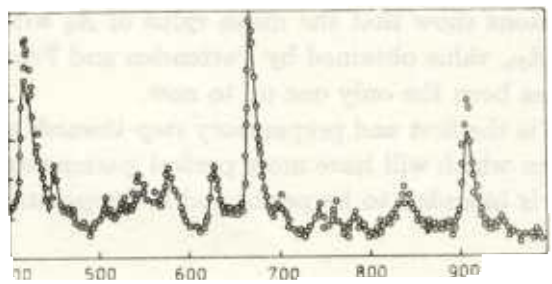
500
600
700
800
900

ig.2.

^{36}Cl(n,p)^{36}S cross section from 25 meV to 800 keV and the nucleosynthesis of rare isotope ^{36}S

P.E.Koehler, S.M.Graaf, H.A.O'Brien
Los Alamos National Laboratory, Los Alamos, New Mexico 87545, USA
Yu.M.Gledenov, Yu.P.Popov
Frank Laboratory of Neutron Physics, JINR, Dubna

The ^{36}Cl(n,p)^{36}S reaction can play a critical role in the production of the rare isotope ^{36}S in explosive nucleosynthesis and s-process calculations. We have measured the ^{36}Cl(n,p)^{36}S cross section from thermal energy to approximately 800 keV. The main measuremens were performed at the moderated "white" neutron source of LANSCE (Los Alamos). Protons and α- particles from this reaction were detected with a silicon surface-barrier detector. Measurements were also made with a dual-gridded ion chamber. The result from the latter detector were limited to energies below a few keV, however it give us possibility to separate of the alpha-particles from the protons for the E_0=902.6 eV and 1297.3 eV resonances.

Our value for the thermal cross section 46.2± 0.4 mb is in good agreement with value of 46± 2 mb [1], but disagree with the value reported in [2]. Additional measurements of thermal cross section were performed by us at the WWR-M reactor in Gatchina.

In a multilevel analysis of our data we determinated parameters for eight resonances in the energy range from 900 eV to 70 keV instead three in [3]. The ^{36}Cl(n,p)^{36}S cross section for energies between 500 eV and 800 keV from our measurements is shown in Fig.1.

At astrophysically relevant temperatures the reaction rate, $N_A\langle\sigma\ v\rangle$, calculated from our data is about a factor 2 times smaller than the theoretical rate used early. The new rate should help to reduce the overproduction of ^{36}S from explosive nucleosynthesis calculations and may significantly reduce the amount of ^{36}S calcalated to be synthesized in the s-process.

Results are presented in Ref.[4,5].

References

1. S.Druyts et al. Ann.Geophys.**9**(Suppl.), 336 (1991)
2. J.Andrzejewski et al. JINR Communication, P3-87-319, Dubna (1987)
3. Yu.M.Gledenov et al. Z.Phys.**A322**, 685 (1985)
4. P.E.Koehler et al. Phys.Rev.**C47**, 2107(1993)
5. P.E.Koehler et al.In: 8th Intern.Symp. on Capture Gamma-Ray Spectroscopy and Related Topics, p.65, Fribourg (1993)

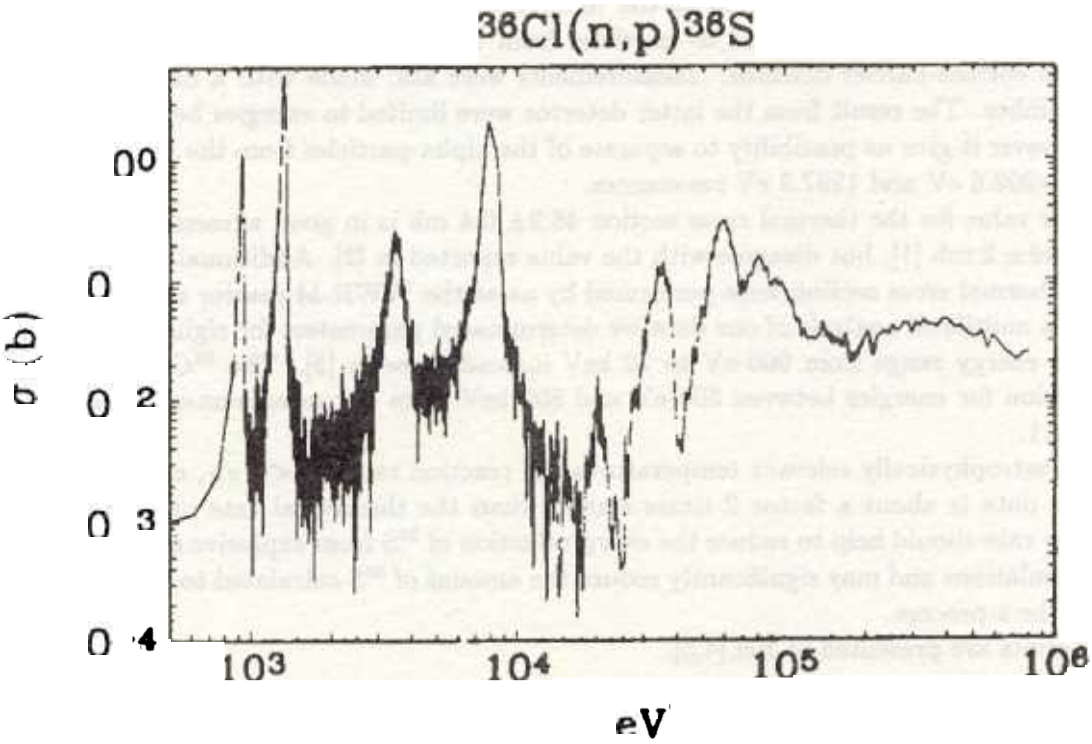

ig.

$^{14}N(n,p)^{14}C$ Reaction Cross Section at Thermal, 24.5 keV, 53.5 keV and 144 keV Neutron Energy

Yu.M.Gledenov, V.I.Salatski, P.V.Sedyshev, M.V.Sedysheva, Li Ho Bom
Frank Laboratory of Neutron Physics, Joint Institute for Nuclear Research, 141980 Dubna, Moscow region, Russia
V.A.Pshenichnyj
Institute for Nuclear Research, Academy of Science of Ukraine, 25028 Kiev, Ukraine
J.Andrzejewski
Department of Nuclear Physics, University of Lodz, 90131 Lodz, Poland

Depending on the $^{14}N(n,p)^{14}C$ reaction cross section, ^{14}N isotope may exhibit essential influence on the neutron balance and the formation of certain elements at the stage of stellar nucleosynthesis. Our measurements were carried out on the IBR-30 pulsed booster of the Frank Laboratory of Neutron Physics in Dubna and on the beam of filtered neutrons from the VVR-M reactor of Institute for Nuclear Research in Kiev. The ionization chamber served as the detector of charged particles. Solid adenine targets were used. Fig.1 presents the experimental spectrum read out during the measurement in Kiev on the neutron filter for the 53.5 keV neutrons. The peak A is the protons from the $^{14}N(n,p)^{14}C$ reaction on the 53.5 keV neutrons. The proton peaks B and C from the same reaction appear due to 0.49 MeV and 0.65 MeV neutron resonances of the ^{14}N, because the filter transmits about 1% of the neutrons of such energies. The cross sections were found to be 1.83±0.07 b, 2.02±0.16 mb, 2.08±0.23 mb and 2.07±0.27 mb for thermal, 24.5 keV, 53.5 keV and 144 keV neutron energy, respectively.

Our results are in a good agreement with earlier estimations [1,2] and with experimental data which were obtained by Koehler et.al. in Los Alamos [3], but about a factor of 2 larger than the results [4] by Brehm et.al. According to the our data the ^{14}N isotope may act as a strong neutron "poison" in s-process during the operation of the chain of reaction involving the $^{13}C(a,n)^{16}O$ neutron source. Also, ^{14}N may play a crucial role in the nucleosynthesis of ^{19}F. Our results have been presented in [5,6,7].

1. N.A.Bahcall and W.A.Fowler. Astrophys.J. **157**, 659 (1969).
2. F.Ajzenberg-Selov. Nucl.Phys. **A449**, 1 (1986).
3. P.E.Koehler and H.A.O'Brien. Phys.Rev.**C39**, 1655 (1989).
4. K.Brehm et.al. Z.Phys. A **330**, 167 (1988).
5. J.Andrzejewski et.al. In "Nuclei in Cosmos". Int.Symp. on Nucl. Astrophys., Karlsruhe, Germany, 6-10 July 1992.
6. Yu.M.Gledenov et.al. Z.Phys. A **346**, 307 (1993).
7. Yu.M.Gledenov et.al. 8th Int.Symp. on Capt. Gamma-Ray Spect. 20-24 Sept. 1993.

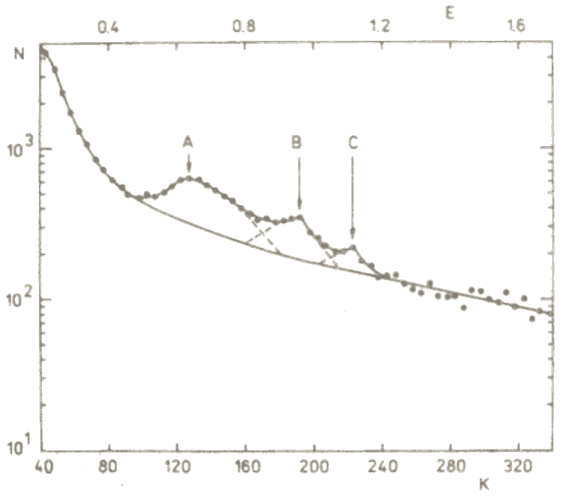

Fig.1. Spectrum of the protons from the $^{14}N(n.p)^{14}C$ reaction when the majority of neutrons have the energy 54 keV.

^{26}Al(n,p)^{26}Mg and ^{26}Al(n,a)^{23}Na Cross Section from Thermal Energy to Approximately 50 keV

Yu.M.Gledenov, Yu.P.Popov
Frank Laboratory of Neutron Physics , Joint Institute for nuclear Research, Dubna, Russia
P.E.Koehler, H.A.O'Brien
Los Alamos National Laboratory, Los Alamos, NM, USA.
S.M.Graff
9413 Stitt Rd., Whitehouse, Ohio, USA
J.A.Harvey, N.V.Hill
Oak Ridge National Laboratory, Oak Ridge, TN, USA
R.W.Kavanagh
Caltech, Pasadena, CA, USA
R.B.Vogelaar
Princeton University, Princeton, NJ, USA
M.Wiescher
University of Notre Dame, Notre Dame, IN, USA
F.Kappeler, H.Schatz
Kernforschungszentrum Karlsruhe, Karlsruhe, Germany
H.-P.Trautvetter
Ruhr-Universitat Bochum, Germany

At our participation preliminary measurements on ^{26}Al isotope were carried out within neutron energy region from thermal up to 50 keV. Most of this energy range has not been explored by previous measurements. Understanding the origin of ^{26}Al is important because it is one of the few radioactive products of stellar nucleosynthesis to be observed directly by γ-ray telescopes or indirectly as a ^{26}Mg anomaly in some meteorites. The ^{26}Al(n,p) and ^{26}Al(n,α) reaction are thought to be major means for the destruction of ^{26}Al in some astrophysical enviroments.

The measurements were made at the white neutron source of the Manuel Luian, Jr. Neutron Scattering Center (LANSCE) using a ΔE-E semiconductor detector telescope. Several resonances were observed. The preliminary results for the (n,α_0) channel are in a good agreement with data obtained from the investigation of reversal reaction [1] , but for the (n,p_1) channel they are about a factor of 2 larger than previous measurements [2]. Thus, our measurements indicate that the destruction of ^{26}Al in neutron enviroments is even greater than previously thought.

1.R.T.Skelton and R.W.Kavanagh, Phys.Rev. C **35**, 45 (1987).
2.H.-P.Trautvetter et.al. Z.Phys. A **523**, 1 (1986).
3.P.E.Koehler et.al. April Meeting of Am.Phys.Soc. 12-15 April, 1993.
4.P.E.Koehler et.al. 8th Int.Sym.Capture Gamma-Ray Spec. 20-24 Sept., 1993.

Measurement of P-odd asymmetry in the $^{10}B(n,\alpha)^{7}Li$ reaction

V.A.Vesna[1], Yu.M.Gledenov[1], I.S.Okunev[2], S.S.Parzhitskii,[1]
Yu.P.Popov[1], E.V.Shul'gina[2]

[1] Frank Laboratory of Neutron Physics, JINR, Dubna
[2] Petersburg Nuclear Physics Institute, Gatchina

On the high flux beam of the polarized cold neutrons of the WWR-M reactor at the PINP (Gatchina) in frame of collaboration was performed the measurements of asymmetry of the emission of α-particles in the $^{10}B(n,\alpha)^{7}Li$ reaction. Asymmetry of the type: $W \sim 1 + \alpha_{pN}(\vec{\sigma}_n \cdot \vec{k}_\alpha)$ was measured where $\vec{\sigma}_n$, $\vec{k}_\alpha$ are the neutron spin and the unit vector of α-particle emission direction, respectively .

The measuring conditions was following

neutron intensity	$N = 3 \cdot 10^{10}$ n/s
mean wavelength	$\lambda = 4.5$ A
polarization	$P = 80$ %

For the detection of the charged particles was used an assambly of twenty four identical double proportional chambers (layout of the experimental apparatus on the reactor lid presented in Fig 1) operating in ionization current mode /1/. The conditions of a detector work (geometry, the insensetive gas-filled gap, the gas pressure) was selected such to not detect the ions ^{7}Li in the reaction and mean cosine of the detected α-particles with respect to the target plane was equal ~0.8. With selection of gas work pressure mixture it was possible not to detect α_1-particles from a α-decay in the first excited state of the daughter nucleus ^{7}Li also.

As a target was used the layers of a amorphous ^{10}B of the 50-150 μg/cm^2 thickness with enrichment ~90% sprayed on an aluminium foil of the thickness d = 20 μm. Thanks to the experimental geometry chosen in which $\vec{\sigma}_n$, $\vec{k}_n$, $\vec{k}_\alpha$ vectors are collinear a suppression factor of the left-right hand asymmetry ($\vec{\sigma}\,[\vec{k}_n\,\vec{k}_\alpha]$) was achieved to be not worse than 10^{-4}, what allowed the exclusion of the possible contribution of this asymmetry into the effect to a level of ~ 10^{-8}.

The measurements performed gave the following values for the coefficients of P-odd asymmetry /2,3/

$$\alpha_{0pN} = (3.4 + 6.7)\ 10^{-7}$$
for α_0-line $E_{\alpha 0} = 1780$ keV

$$\alpha_{1pN} = -(2.5 + 1.6)\ 10^{-7}$$
for α_1-line $E_{\alpha 1} = 1479$ keV

The obtained values improve essential the values of the coefficients P-odd asymmetry measured in works /4,5/.

1. Vesna V.A. et al. Preprint PNPI N 1694 , S.-Petersburg, 1991.

2. Vesna V.A. et al. Annotations of the projects of experiments in field of the fundamental particles physics and nuclear science proposed in 1991-1995, S.-Petersburg, 1991, p.92.

3. Vesna V.A. et al. Proceedings of 111 International Symposium on Weak and Electromagnetic Interactions in Nuclei (WEIN'92).Ed.by T.D.Vylov, World Scientific, p.419.

4. Vesna V.A. et al. Pisma ZhETF, v.38, 1983, p.265.

5. Ermakov O.N. et al. in book: Neutron Physics Proceed.of the

6. Conference on Neutron Physics, Kiev, 1983, M.: CNII-atominform, 1984, v.3, p.403.

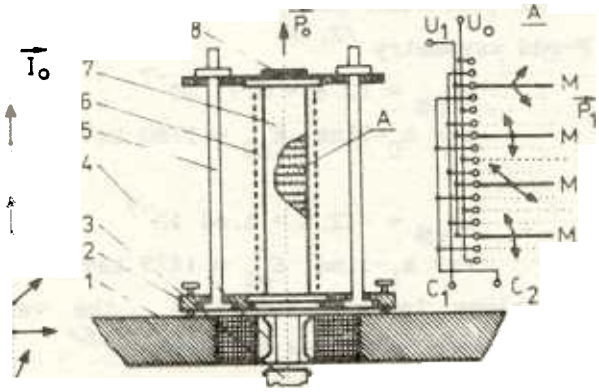

Fig. 1. Layout of experimental apparatus on the reactor lid. 1 - the lid of the reactor, 2 - table for proportional chamber , 3 - polarizing neutron guide, 4 - radio-frequency flipper, 6 - magnetic field guiding the neutron spin, 7 - proportional chamber, 8 - ^{6}LiF neutron absorber. The cross section "A" shows one chamber module. I_0 - is the neutron spin, P_0 - is the neutron momentum, P_i - is the momentum of the detected alpha-particle. C_1, C_2 - are the outputs from signal grids of the "forward" signal (U_f) and the "backward" signal (U_1). $U_{o,1}$ - the potential supply the block grid and the target, respectively.

Investigation of Charged Particles Emission Reaction Induced by Fast Neutrons

Yu.M.Gledenov, G.Khuukhenkhuu, Yu.P.Popov
Frank Laboratory of Neutron Physics, JINR, Dubna

Bao Shanglian, Tang Guoyou, Cao Wentian, Qu Decheng
Peking University, Beijing, China

Chen Zemin, Chen Yingtang, Qi Huiquan
Tsinghua University, Beijing, China

Experiments carried out on the D+D neutrons using the Van de Graaff accelerator at the Institute of Heavy Ion Physics, Peking University, China. Charged particles emitted in the investigated reactions were detected with a double-grid, parallel-plate, twin ionization chamber with a common cathode, which was manufactured at the Frank Laboratory of Neutron Physics, JINR. Argon mixed with 5% carbon-dioxide was utilized to fill the chamber. The first section of the twin ionization chamber contained studied target. The second section was empty and was used for background measurements.

Two dimensional energy spectra of signals from the anode and cathode were obtained for emitted charged particles from neutron induced reactions with the help of a measuring system based on the IBM PC AT-386 computer. Measured angular distributions of α- particles emitted in the $^{40}Ca(n,\alpha_0)^{37}Ar$ reaction at E_n= 4 and 5MeV are nearly symmetrical with respect to ϑ=90° (Figs.1 and 2). This fact shows that the compound nucleus mechanism predominates in the energy range E_n= 4-5 MeV for the double magic target nucleus ^{40}Ca. Cross section of the $^{40}Ca(n,\alpha_0)^{37}Ar$ reaction at a neutron energy of 5 MeV was found to be $\sigma(n,\alpha_0)$=234±23 mb. Measurements also carried out on natural zink and ^{64}Zn at E_n=2.7 and 5 MeV. Alpha-peaks from the $^{64}Zn(n,\alpha)^{61}Ni$ reaction were observed. Additionally to those of the investigated reactions there were observed alpha-peaks from $^{36}Ar(n,\alpha)$ ^{33}S as a background.

References

1. Tang Guoyou et al.Communication of nuclear data progress, No.8, p.7-15 (1992)

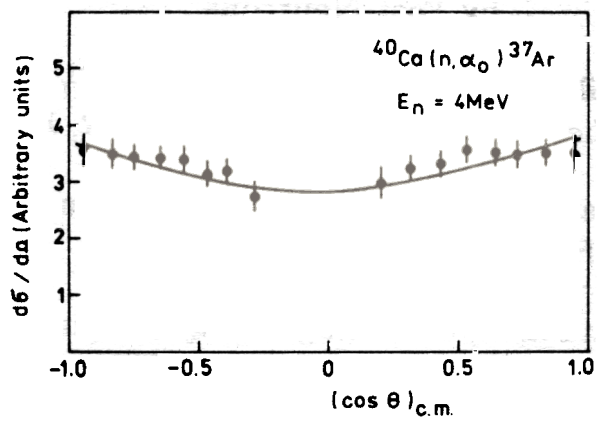

Fig.1. The angular distribution of α - particles from the $^{40}Ca(n,\alpha_0)^{37}Ar$ reaction at E_n=4 MeV. The solid curve is only an eye-guide.

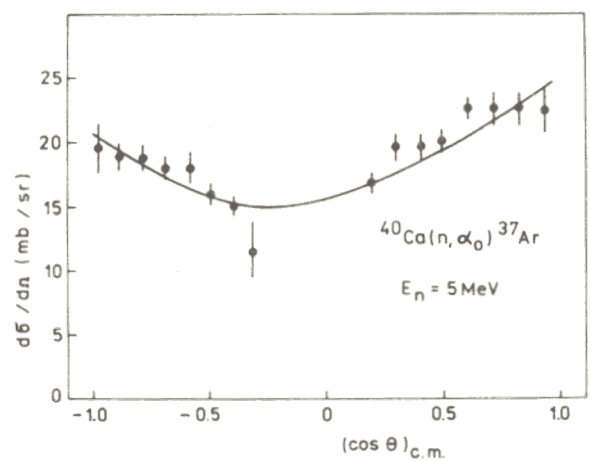

Fig.2. The same as in Fig.1 at E_n=5 MeV.

INTERACTION OF POLARIZED NEUTRONS WITH A POLARIZED LANTHANUM TARGET AND STRUCTURE OF THE NEUTRON CROSS SECTION UP TO 20 eV

V.P.Alfimenkov, Yu.D.Mareev, V.V.Novitsky, L.B.Pikelner, V.R.Skoy
Joint Institute for Nuclear Research, Dubna, Russia

Interest in the neutron cross section of lanthanum is connected with the discovery of a very strong parity nonconservation effect in the p-wave resonance of ^{139}La at 0.74 eV. This stimulated a theoretical search for the possibility of a T-noninvariance test in lanthanum. A principal part of the neutron cross section of La at low energy is connected with a negative resonance. It influences the parity violation in the p-wave resonance and must be studied in more detail.

All of these circumstances have stimulated our measurement of the total cross section in vicinity of the 0.74 eV resonance up to 20 eV, and our research of the polarization property of La in an experiment with polarized neutrons and a polarized La target.

The interaction of polarized neutrons with a polarized La target was measured on a neutron beam of the IBR-30 by use the POLYANA installation. Neutrons were polarized by transmission through a polarized proton target, and polarization of the metallic La sample was achieved by cooling it to about 0.1 K in a magnetic field of 1.5 T. The neutron time-of-flight spectra for two directions of neutron polarization were measured and the dependence of the transmission effect,

$$\varepsilon = \frac{N_+ - N_-}{N_+ + N_-} = f_n th(f_N n \sigma_{pol})$$

on neutron energy in the 0.5-20 eV interval was obtained. The value of the polarization cross section σ_{pol}, which was measured with polarized neutrons and nuclei was found to be in good agreement with the results of our total cross section measurement.

All data were described very well by the negative ^{139}La resonance with the parameters of $E_0 = -28\ eV$, $\Gamma_n^0 = 60\ meV, \Gamma_\gamma = 50\ meV, J = 4, \sigma_{pot} = 5b$. Spin of the 3.0 eV resonance of ^{138}La was identified as $I + 1/2 = 11/2$.

STUDY OF THE DEPOLARIZATION OF RESONANCE NEUTRONS IN AN EXPERIMENT TO SEARCH FOR THE T-NONINVARIANCE

V.P.Alfimenkov, Yu.D.Mareev, V.V.Novitsky, L.B.Pikelner, V.R.Skoy
Joint Institute for Nuclear Research, Dubna, Russia
C.R.Gould, D.G.Haase, N.R.Roberson
TUNL, North Carolina, USA

Experiments on the measurement of the five-fold correlation for time reversal test have been discussed in recent years. In these experiments the transmission of polarized resonance neutrons through aligned nuclear targets must be measured. The effect which is under investigation consists of a change in the total neutron cross section of the change of the sign of the $\vec{s}[\vec{I}\times\vec{k}](\vec{I}\cdot\vec{k})$ term. Here $\vec{s}$ and $\vec{I}$ are the spins of the neutron and nucleus, respectively, and $\vec{k}$ is the neutron momentum. The experiment is very complicated technically because the effect is very small and is easily masked by additional false effects. All of them must be investigated and taken into account.

One of these effects is the depolarization of polarized neutrons at their transmission through a monocrystal sample with aligned nuclei. The value of the depolarization strongly depend on the crystal orientation and neutron energy.

Now an experiment to investigate this depolarization is ready and preliminary results have been obtained. Measurement with a *Ho* monocrystal was carried out at the POLYANA installation on a neutron beam of the IBR-30 system. A strong angle dependence of the depolarization was observed. Measurements were made for angles between the *c*-axis and the direction of neutron polarization, from $-\pi/2$ to $+\pi/2$.

Sample temperatures were 4, 80 and 300 K. The values of the depolarization at helium temperature are very large and reach up factor 3-4. We intend to develop these investigations which are of additional interest in the study of the magnetic properties of matter.

MULTIPLICITY OF GAMMA-RAYS IN NEUTRON RESONANCES OF ^{176}Hf AND ^{179}Hf

G.P.Georgiev, Yu.V.Grigoryev, G.V.Muradyan, N.B.Yaneva

Neutron time-of-flight spectroscopy measurements were made on the samples of Hafnium isotopes at the pulsed neutron booster IBR-30 of the Joint Institute for Nuclear Research in Dubna. A preliminary results are presented of an investigation of the radiative capture of resonance neutrons by ^{176}Hf and ^{179}Hf isotopes in the region of resolved resonances making use of the method of multiplicity spectrometry. The choice of the indicated isotopes for studies was due to the data on their spins and radiation widths being incomplete [1]. The cross section of radiative capture by Hafnium isotopes in the region of resonance neutron energies is interesting from the points of view of understanding nucleosynthesis and of reactor construction.

A multisection 4π- "Daisy-type" scintillation detector (Fig.1) located at the 500-metre-long time-of-flight base of the IBR-30 pulsed neutron booster of the JINR FlNP was used for measurements [2] . The detector consisted of 16 independent NaJ(Tl) crystal sections with a total volume of 36 litres and geometric efficiency of 80% . A ^{176}Hf target 2.88 x 10^{-4} nuclei/barn thick and a ^{179}Hf target 2.14 x 10^{-4} nuclei/barn thick were used in the measurements. The neutron time -of- flight and the coincidence multiplicity of gamma-quanta were determined for each interaction event. In parallel with the gamma-quanta from radiative capture in the target, single 480 keV gamma-quanta produced in the ^{10}B(n, $\alpha\gamma$) reaction caused by neutrons scattered in the target and occurring in the thin Bohr converter surrounding it were detected. Thus, the same detector registered events of radiative capture and of neutron scattering in the target simultaneously and in identical conditions.

The experimental gamma - quantum multiplicity spectrum $P(k) = S_\gamma(k)/\sum S_\gamma(k)$ was obtained, and the mean gamma-quantum multplicity $\langle k \rangle = \sum kP(k)$ determined. It turned out to be that

<k>=2.50 for the even-even ^{176}Hf isotope, while in the case of the even-odd ^{179}Hf isotope the <k> values concentrated about two points: <k>=2.78 and <k>=2.91. Thus, in the range of energies up to 200 eV, 18 spin 4^+ resonances and 19 spin 5^+ resonances were successfully identified for ^{179}Hf. The multiplicity distribution P(ν) (Fig.2) for gamma quanta emitted by the nucleus was computed from the gamma-quantum multiplicity distribution P(k) observed experimentally for ^{179}Hf. This was done making use of the gamma-cascade model, of the theoretical description of the strength function and of available data on the lower energy levels of the composite nucleus. Monte -Carlo simulation was performed of the propagation of gamma-quanta through the detector and the shielding. For determining the parameters of the resonances a program was written which made possible computation of the expected time-of-flight radiative capture and scattering spectra and fitting them to the respective measured spectra by varying the resonance parameters and fitting the parameters of the neutron spectrometer. The radiation width Γ_γ was fitted with the aid of the ratio of the partial areas A_γ and A_S under the respective resonance peaks in the radiative capture and scattering spectra, of the known neutron width Γ_n [1] and of the distribution function obtained. In the fit, that value of Γ_γ was determined for which the computed A_γ/A_S ratio was in agreement with its experimental value.

Besides the levels indicated in ref. [1], 17 new levels were observed for ^{176}Hf in the energy range up to 1500eV. The values of D_o = 37 +/- 7 eV and $\langle\Gamma_\gamma\rangle$ = 45 +/- 15 meV were obtained.

We obtained $\langle\Gamma_\gamma\rangle$ = 47+/-6 for ^{179}Hf. The strength function was calculated , with the aid of the spins determined , in the range up to 200 eV : $S_o = (1.8^{+1.0}_{-0.7}).10^{-4}$ and $S_o = (2.4^{+1.2}_{-0.8}).10^{-4}$ for the $J^\pi = 4^+$ and $J^\pi = 5^+$ set of resonances respectively , meaning that they are identical within the experimental errors .

References

1. S.F.Mughabghab, Neutron cross Section 1, Part B (Academik Press, New York, 1984) .
2. N.B.Yaneva, G.P.Georgiev et al., Nuclear Instruments and Methods in Physics Research A313 (1992), p.266 .

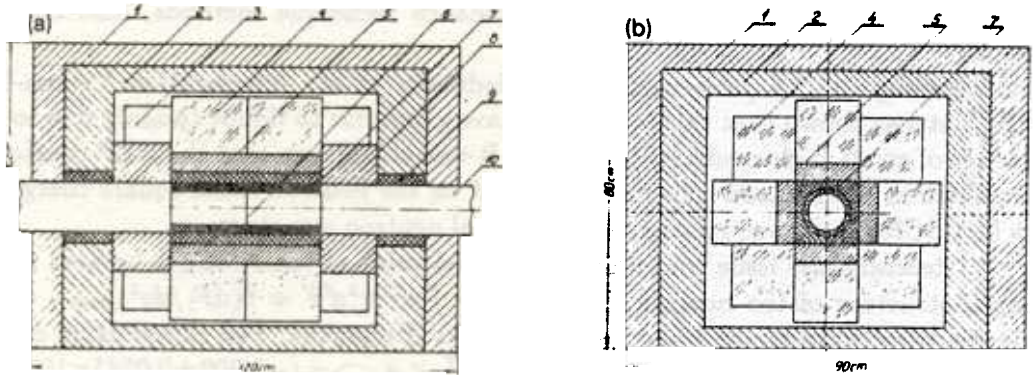

Fig. 1. Side - (a) and rear - (b) view of the detector . 1,5,8 - shield made of paraffin and boron carbide; 2 - lead shield; 3 - photomultiplier; 4 - NaI(Tl) crystal; 6 - sample; 7,9 - shield made of polyethylene and boron carbide; 10 - evacuated tube.

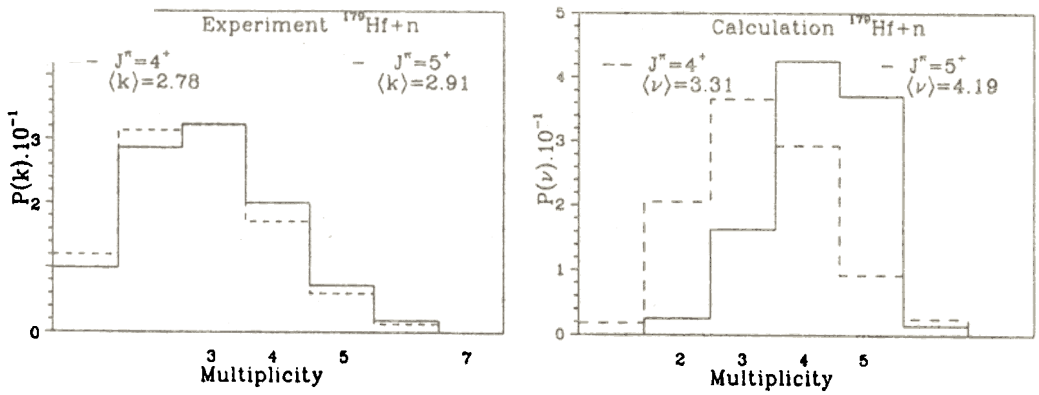

Fig. 2. Experimental P(k) and calculated P(ν) distributions of the gamma-quanta multiplicity of the ^{179}Hf (n,γ) reaction.

Situation in Study of Electric Polarizability and Mean Square Charge Radius of the Neutron

Yu.A.Alexandrov
Frank Laboratory of Neutron Physics, JINR, 141980 Dubna, Moscow Region, Russia

The concept of neutron electric polarizability (NEP) was introduced in 1955-56 in connection with studies of neutron scattering by the Coulomb fields of nuclei[1] . The best result for the NEP coefficient $< 0.7 \times 10^{-3} fm^3$ was obtained in Dubna-Garching cooperation (time-of-flight and neutron resonance technique methods, lead-208 and bismuth)[2-4] .

Concerning the job performed by Schmiedmayer et al. (cooperation Vienna-Oak Ridge)[5] it was shown that this job should have given rise to doubt (mainly due to the influence of small angle neutron scattering). It was also shown that the NEP coefficient determined in the neutron transmition depend on the neutron mean square charge radius (NMSCR) $< r_{in}^2 >_N$, related to the internal neutron structure.

Recently, the issue concerning the actual value of the NMSCR, related to the internal structure of the neutron, ($< r_{in}^2 >_N = \int \rho(\vec{r}) r^2 d^3\vec{r} = 6(dF_1/dq^2)_{q^2=0}$, where F_1 is the Dirac form factor) has been also under discussion. The experiments can be divided into two groups (see table): the results[6-7] $< a_{ne} > = (-1.309 \pm 0.024) \times 10^{-3} fm$, which lead to $< r_{in}^2 >_N > 0$ in contradiction with modern theory , and[2,8,9] $< a_{ne} > = (-1.577 \pm 0.034) \times 10^{-3} fm$ to lead to $< r_{in}^2 >_N < 0$ in confirmation of modern theory. It is shown that the most probable reason for the discrepancy between the results of the Garching and Dubna determination of the a_{ne} for bismuth is the difference in the method of accounting for the influence of negative energy resonances on the measurable a_{ne} . It is also shown that introduction into σ_{tot} of energy independent inter-resonance interference terms does not affect the result on a_{ne} obtained in Dubna.

1. Yu.A.Alexandrov and I.I.Bondarenko. *Zh.Eksp.Teor.Fiz.* **31**, 726 (1956).
2. Yu.A.Alexandrov et al. *Sov.J.Nucl.Phys.* **44**, 900 (1986).
3. Yu.A.Alexandrov et al. *JINR Rapid.Comm.* No.6[45]-90 (1990).
4. Yu.A.Alexandrov et al. *Intern.Semin. on Interaction of Neutr. with Nuclei*, E3-92-128, p.19, Dubna (1992).
5. J.Schmiedmayer et al. *Phys.Rev.Lett.* **66**, 1015 (1991).
6. V.Krohn and G.Ringo. *Phys.Rev.* **D8**, 1305 (1979).
7. L.Koester et al. *Z.Phys.* **A329**, 229 (1988).
8. E.Melkonian et al. *Phys.Rev.* **114**, 1571 (1959).
9. Yu.A.Alexandrov et al. *Yad.Fiz.* **20**, 1190 (1974); *Zh.Eksp.Teor.Fiz.* **89**, 34 (1985).

Table

Authors, year	Method	Magnitude of effect, ne/tot	$-a_{ne} \times (10^3) fm$	Ref.
P.Dee, 1932	Recoil electrons in cloud chamber		<1000	
E.Fermi, L.Marschall, 1947	Neutron scattering on noble gases	$\Delta\sigma/\sigma \cong 0.5\%$	100 ± 1800	
W.Havens, et al., 1947-51	Total neutron cross section on lead and bismuth	$\Delta\sigma/\sigma \cong 1.5\%$	1.91 ± 0.36	
D.Hughes et al., 1952-53	Neutron total reflection from $O_2 - Bi$ mirror	$\Delta\Theta/\Theta \cong 50\%$	1.39 ± 0.13	
M.Hamermesh et al., 1952	Neutron scattering on noble gases	$\Delta\sigma/\sigma \cong 0.5\%$	1.5 ± 0.4	
M.Crouch et al., 1956	Neutron scattering on noble gases	$\Delta\sigma/\sigma \cong 0.5\%$	1.43 ± 0.30	
E.Melkonian et al., 1959	Total neutron cross section on bismuth	$\Delta\sigma/\sigma \cong 1.5\%$	1.56 ± 0.05*	[8]
V.Krohn, G.Ringo, 1966-73	Neutron scattering on noble gases	$\Delta\sigma/\sigma \cong 0.5\%$	1.30 ± 0.03	[6]
L.Koester et al., 1970-88	Total neutron cross section and atomic scattering length on bismuth and lead	$\Delta\sigma/\sigma \cong 1.2\%$	1.32 ± 0.04	[7]
Yu.Alexandrov et al., 1974-85	Neutron diffraction on a tungsten-186 single crystal	$\Delta\sigma/\sigma \cong 20\%$	1.60 ± 0.05	[9]
Yu.Alexandrov et al., 1985	Total neutron cross section on bismuth	$\Delta\sigma/\sigma \cong 1.2\%$	1.55 ± 0.11	[2]

Without correction for Schwinger scattering and resonance scattering.

ON THE ELECTRIC POLARIZABILITY OF THE NEUTRON

Yu.A.Alexandrov*), L.Koester**), L.V.Mitsyna*), P.Prokofiev***), G.S.Samosvat*), J.Tambergs***), W.Waschkowski**)

*) Joint Institute for Nuclear Research, Dubna, Russia
**) Technical University Munich, Garching, Germany
***) Nuclear Research Centre, Salaspils, Latvia

Precise measurements of the total neutron cross sections were performed for samples of lead enriched up to 98, 83 92% by 208,207 and 206 isotopes accordingly. The quasi-monochromatic neutrons were used with energies 1.26, 5.19 and 1970 eV which were got on Munich Technical University FRM reactor by means of corresponding neutron resonances [1]. The obtained cross sections in barns are shown in the table.

Sample	1.26 eV	5.19 eV	1970 eV
208	11.4388(31)	11.4718(35)	11.4635(26)
207	11.1510(120)	11.1320(130)	11.0520(120)
206	10.7988(51)	10.8270(70)	10.8030(60)

Two different methods developed in Garching and Dubna were used to extract the neutron polarizability coefficient α_n; they both gave practically the same α_n values. The total results depends on accepted value of the $n-e$ scattering length b_{ne} and looks as

$$\alpha_n = \begin{cases} (-0.3 \pm 0.5) \cdot 10^{-3} fm^3, & if \quad b_{ne} = (-1.32 \pm 0.04) \cdot 10^{-3} fm, \\ -1.3 \pm 0.5) \cdot 10^{-3} fm^3, & if \quad b_{ne} = (-1.59 \pm 0.04) \cdot 10^{-3} fm. \end{cases}$$

So there is only one meaning result [2] $\alpha_n = (1.20 \pm 0.15 \pm 0.20) \cdot 10^{-3} fm^3$ by which teoretists are "satisfyed",it is possibly to confirm that present result intensifies the problem of reliable experimental value of not only α_n, but b_{ne} too.

References

1.Koester L.,Waschkowski W.,Meier J.Z.Phys.A,1988, v.329, p.229.
2.Schmiedmayer J.,Riehs P.,Harvey J.A.,Hill N.W. Phys. Rev. Lett., 1991, v.66, p.1015.

UCN High Density Pulse Source at the BIGR Reactor (Arzamas-16) and Neutron Lifetime Experiment.

A.V.Strelkov, V.N.Shvetsov
FLNP, JINR
A.D.Stoica
IFTM, P.O. Box MG52, Bucharest, Romania

Abstract. The method of dynamic ultracold neutrons (UCN) converter, using high flux pulse reactor BIGR (Arzamas-16) is proposed. Different types of converters have been compared and estimations of maximal UCN density were obtained ($n \approx 7 \times 10^5 n/cm^3$). The possible experiment on neutron lifetime (τ_β) determination is discussed (the accuracy 0.5% for τ_β per one reactor pulse can be achieved).

1. Introduction

Ultracold neutrons (UCN) - neutrons with extremely low energy $\sim 7 \times 10^7$ev (V $\sim$ 5 m/s)[1]. They have an unique property of total reflection from substance surface and so can be stored in evacuated material traps for a long time. UCN are very useful for experiments on studying of fundamental neutron properties:neutron lifetime, electric dipole moment an so on.

UCN can be produced from thermal neutrons for one impact. The probability of such process is very small($\sim 10^{-11}$) and flux density of UCN is: $F_{ucn} = \frac{1}{8} F_{th} \left[\frac{V_{lim}}{V_{th}} \right]^4 \frac{\sigma^{\ominus}_{ie}}{\sigma^{\oplus}_{ie} + \sigma_a}$ (1), $\frac{F_{ucn}}{F_{th}} \propto 10^{-12}$,

where F_{th} - flux density of thermal neutrons , V_{lim} - limiting velocity of the trap walls $\sim$(3-6)m/s, V_{th}= 2200 m/s - thermal neutron's velocity, $\sigma^{\ominus}_{ie}$ and $\sigma^{\oplus}_{ie}$ - inelastic cross-sections of cooling and heating, σ_a-capture cross-section .

The first experiments with UCN have been carried out with UCN density $\sim 5 \times 10^{-6}$ n/cm^3 [2,3]. In modern times the highest UCN density is $\sim 10^2$ n/cm^3 [4]. The possibilities of significance increasing F_{th} for stationary reactors are exhausted now, so further increasing of the UCN density may be done using pulse reactors only, where pulse flux densities are many times larger than at stationary ones.

2. Dynamical converter method

2.1 Constant density of the converter

UCN density inside the converter in nonstationary case described with differential equation:

$$\frac{dn(t)}{dt} = F_{th}(t)\bar{\Sigma}^{\theta}_{in} - \frac{n(t)}{\tau(t)} \qquad (2), \quad \bar{\Sigma}^{\theta}_{in} = N(t)\bar{\sigma}^{\theta}_{in},$$

where n(t) - UCN density, N(t) - number of converter's molecules in cm^3, $\tau(t)$ - UCN lifetime in converter: $\tau(t)^{-1} = N(t)V(\sigma^{\theta}_{in} + \sigma_a)$, V-UCN velocity.

For the Gaussian form of thermal neutrons flux and BIGR characteristics (fluence 10^{15} n/cm^3, s=1ms):

$$F_{th}(t) \propto \exp(-\frac{t^2}{2\sigma^2}) \qquad (3),$$

the equation (2) has been solved numerically. The values of n_{max} - maximal UCN density inside the converter - are: $1.8x10^5$ n/cm^3 for polyethylene converter, $2.5x10^5$ n/cm^3 for Be and $9x10^5$ n/cm^3 for parahydrogen ones. If N(t) value stays constant, the UCN density decreases for a short time due for a large value of losses cross-sections, and it becomes difficult to realize the isolation of UCN from converter. To provide the fast isolation of UCN cloud from converter without significant decreasing of it's density the method of dynamical converters is proposed.

2.2 Gaseous expanding converter

Sharp fall of pressure in gaseous converter in a time of reactor pulse, when thermal neutron flux reaches it's maximal value, leads to decreasing of UCN losses. The calculation of n(t) has been made using (2), and the time of the expansion beginning coincides with the time of maximal flux of thermal neutrons. Calculation shows that for real times of gas expansion one can store UCN cloud some times longer then without expansion.

UCN density $\approx 7x10^5$ n/cm^3 can be obtained with parahydrogen (30 atm.) converter.

2.3 Moving solid converter

The fast removing of the converter after reactor pulse can be realized also by mechanical movement of the converter. In this case the speed of UCN, unmovable in a lab frame, relatively converter will be V - the converter speed and the losses cross-section will be reduced by factor 1/V.

During the passing of converter in a field of the thermal neutrons, the veil of UCN is producing behind the converter. The UCN density subordinates for dependency similar that described with (2). Calculations for Be and polyethylene converters has been made to select the converter for preliminary experiment on method examination. It was found that it's possible to obtain UCN density up to 10^5 n/cm^3, using polyethylene converter about 10 mm thick with velocity $\approx$50 m/s. Be converter has to be about 100 mm thick at the same speed and the value of density will be $\approx 3x10^4$ n/cm^3.

3. Possible experiment on neutron lifetime determination

The cloud of UCN, produced with expanding gaseous or moving converter can be enclosed in a trap,transported out of reactor hall and placed into detector system, including thermal neutron counter and electron counter. The UCN density in a trap will be:

$$n(t) = n_0 \exp\left(-\frac{t}{\tau_\beta} - (\eta_{ie} + \eta_a)\int_0^t \gamma(t')dt'\right) \qquad (4),$$

where η_{ie}, η_a, $\gamma(t)$ - certain parameters, depending from neutron spectra and trap properties. Then, count rates for neutron and electrondetectors will be consequently: $J_{ie} = \varepsilon_{ie}\eta_{ie}\gamma(t)n(t)$ and $J_\beta = \varepsilon_\beta\eta_{ie}\frac{1}{\tau_\beta}n(t)$, where ε_{ie} and ε_β- detector's efficiencies. Therefore, one can obtain:

$$-\frac{d}{dt}\left[\ln(J_\beta)\right] = \frac{1}{\tau_\beta}\left[1 + \frac{\eta_{ie} + \eta_a}{\eta_{ie}}\frac{\varepsilon_\beta}{\varepsilon_{ie}}\frac{J_{ie}}{J_\beta}\right] \qquad (5)$$

Equation (5) shows, that neutron lifetime can be extracted with linear extrapolation of experimental data down to zero value of $\frac{J_{ie}}{J_\beta}$. The mathematical simulation of the UCN behavior in a trap has been carried out to obtain the evaluation of the neutron lifetime determination accuracy. It was found, that accuracy =0.5% can be achieved per one pulse of the reactor.

4. Conclusion

It's necessary to emphasize that dynamical converter method does not increase the initial UCN density in converter. Initial density determines only by the thermal neutron flux value and converter's properties. This method let us to extract UCN from significantly large area of the converter than for stationary converter.

To understand the advantages of the new UCN source one can turn to existing UCN sources and experiments. In experiment on neutron lifetime measurements [5] (that has been made at the best after Grenoble UCN source) the accuracy 0.3% has been achieved. The number of neutrons "used" in experiment at 2.5 months of the "reactor" time were $\approx 10^8$,that is the same order of magnitude as in proposing experiment for one pulse of BIGR reactor.

References

[1] Golub R. and Pendlebury J. M. 1979 Rep.Prog.Phys. 42 439-501
[2] Shapiro F. e.a. 1969 JETP Letters 9 40
[3] Steyerl A. 1969 Phys.Lett. 1969 29 33
[4] Steyerl A. e.a. 1986 Phys.Lett. A116 347
[5] Alfimenkov V P e.a. 1990 JETP Letters 52 984-989

A MOVING CONVERTER AS A POSSIBLE TOOL FOR PRODUCING ULTRACOLD NEUTRONS AT PULSED NEUTRON SOURCES

Yu.N.Pokotilovski
Frank Laboratory of Neutron Physics,
Joint Institute for Nuclear Research, Dubna, Russia

A method for producing ultracold neutrons (UCN) at aperiodic pulsed neutron sources is proposed. The method exploits an UCN converter that moves fast near a pulsed neutron source. The motion of the converter is synchronized with the pulse of the neutron source for the converter to cross the region of maximum neutron flux exactly at the moment of the pulse. The UCN born in the converter during the neutron pulse form a cloud in the region which the converter has occupied during the time of the pulse. Immediately after the pulse the UCN cloud is caught in a trap instantaneously (within a few miliseconds) moved into the region now occupied by UCN. Then the trap is slowly moved off to a region at some distance from the reactor for carrying out experiments with trapped UCN.

Estimates show that this method, if used with powerful aperiodic pulsed reactors of the TRIGA or BIGR type at a pulse fluence of 10^{15} n/cm^2, would allow having an UCN density of 10^5 UCN/cm^3 in a volume of $1-2$ *liters*. At present FLNP and the Institute for Applied Physics do preparatory work for realization of this method at the BIGR reactor (Arzamas-16).

1.Yu.N.Pokotilovski, Nucl.Instr.Meth., 1992, A334, 561.
2. Yu.N.Pokotilovski, Pis'ma ZhTF, 1980, 6, 1300 (in Russian).

ON EXPERIMENTAL VERIFICATION OF THE SKOBELTSYN-BALDIN HYPOTHESIS OF EMISSION OF A NONSTABLE PARTICLE FOLLOWING THE DECAY OF ^{214}Bi

Yu.N.Pokotilovski, G.G.Takhtamyshev
Joint Institute for Nuclear Research, Dubna, Russia

Interpretation of Darmstadt effect consisting in observation of narrow positron-electron pairs following collision of very heavy ions with the energy near the Coulomb barrier has been a serious problem for about ten recent years [1].

None of a few dozen hypotheses that have been advanced explains the observed phenomena. A.M.Baldin [2] assumed some relation of this effect with the experimental results of Skobeltsyn [3] who, investigating the scattering of β−rays with a Wilson chamber placed in a magnetic field, had observed anomalously large β−ray scattering by ^{214}Bi at large angles which exceeded that calculated after the Mott formula by a factor of a few tens. In these experiments he also observed numerous events of inelastic β−scattering with a considerable (by several times) loss of energy. Later Skobeltsyn [4] interpreted his observations as a birth with a probability of $7-12$ % following β-decay and a decay while flying of a particle with a mass ofabout 3 m_e and the lifetime of $(2-5)\times 10^{-10}$ *sec*. Independent calculations [5] in the frame of a quasipotential approach performed for a system of two fermions had yielded a conclusion about existence of a rich spectrum of relativistic Coulomb levels. These levels merged in continuum must exist in e^+e^-, (pp), and (e^-e^-) systems, and probably in a number of other systems which also include composed neutral particles. The calculations of [5] found confirmation in [6] where the $J=0$, $L=1$, $S=1$ resonances in the (ee) system were obtained by solving under different approximations three different relativistic equations following from quantum electrodynamics. The hypothesis of [2] consists in actualization of Skobeltsyn's assumption [4] that the unstable particle observed in experiments [3] is a quasicoupled complex, $(e^+e^-e^-)$, which decays into an electron and a γ-quantum.

Under conditions close to those of Skobeltsyn's experiment we tested the possibility for a $(e^+e^-e^-)$ complex, decaying into an electron and γ-quantum, to be formed following the decay of ^{214}Bi. A ^{226}Ra source was positioned in a vacuum chamber. Decay events of $(e^+e^-e^-)$ hypothetical particles were sought for along a decay base by measuring electron spectra in coincidence from an electron and a γ-detector. To compare experimental data with the tested hypothesis we simulated numerically the events of emission from the source and decay of a hypothetical particle into an electron and a γ-quantum over the mass and the lifetime range of the $(e^+e^-e^-)$ complex from 1.5 to 2.0 MeV/c^2, and from 5×10^{-11} to 10^{-9} s, respectively. The limit for the probablity of $e^+e^-e^-$ complex emission is 10^{-3} in accordance with the hypothesis in [1,3] 10^{-3}.

Reports on the work have been published in JINR Rapid Communications No. 2(53)-92, p.29, and in Yad.Fiz. 1992, 55, 2017 in Russian.

1. H.Bokemeyer, W.Koenig. Preprint GSI-91-45 (1991).

2. A.M.Baldin. JINR Rapid Comm., N3(42)-90, Dubna, 1990, p.4 (in Russian); Lebedev Phys.Inst. Rapid Communications on Physics, 190, N6, 42 (in Russian).

3. D.V.Skobeltsyn. Izv. AN SSR, ser.fiz., 1938, N1-2, p.75 (in Russian); Doklady AN SSSR, 1938, 21, 435 (in Russian).

4. D.V.Skobeltsyn. In: "To the Memory of S.I.Vavilov", M., 1952, p.292 (in Russian).

5. B.A.Arbuzov et al. Pis'ma Zh.Exp.Teor.Fiz., 1952, **50** 236 (in Russian); Mod.Phys.Lett. 1990, **A5**, 1441; Phys.Lett., 19990 **240B**, 477.

6. J.R.Spence, I.V.Vary. Phys.Lett., 1991, **254B**, 1; **271B**, 1

MÖSSBAUER EFFECT BASED EXPERIMENTS TO SEARCH FOR NEW LIGHT BOSONS

Yu.N.Pokotilovski
Joint Institute for Nuclear Research, Dubna, Russia

Feasibility of an experiment on the basis of Mössbauer effect to search for new light bosons with the mass less than a few tens keV is discussed. The idea consists in using a pulsed neutron source for obtaining a large number of excited isomeric states after the capture of neutrons by nuclei:

$$n + (Z,N) \rightarrow (Z,N+1)^{**} \rightarrow (Z,N+1)^{*}, \qquad (\textit{the isomeric state}),$$

and a resonance detector containing the (Z,N+1) nuclei.

In such experiment a new light boson instead a γ-quantum could be emitted with a low probability during an isomeric transition, and then absorbed in the detector exciting the initial isomeric state. Estimates show that with a TRIGA type reactor and a detector with the volume of tungsten-scintillator of 10 l the sensitivity to boson emission of $\sim 10^{-10}$ would be achieved. For a pseudoscalar particle that value corresponds to the level of several hundred TeV in the scale of violation of Peccei-Quinn symmetry and is over two orders of magnitude higher than the level achieved in the most high sensitivity accelerator-based experiments.

1. Yu.N.Pokotilovski. Proc. of III Int. Symp. on Weak and Electromagn. Int. in Nuclei, Dubna, June, 1992, p.878; Ts. Vylov (Ed.), World Scientific, Singapore, 1993.

2. Yu.N.Pokotilovski. Pis'ma Zh.Exp.Teor.Fiz., 1983, **37**, 51 (In Russian); JETP Lett, 1983, **37**, 60.

Some aspects of estimation of n,e-amplitude and neutron polarizability

V.G.Nikolenko, A.B.Popov
Frank Laboratory of Neutron Physics, JINR, Dubna

1. The physical importance of the n,e-amplitude b_{ne} consists in the fact that it allows determination of the neutron mean square charge radius that is proportional to $(b_{ne} - a_F)$, where the Foldy term $a_F = -1.468$ mfm.

It is important to note that, in spite of the many year investigation, the problem of b_{ne} estimation has not been solved. All known precise results fall into two groups: one near $-1.55(5)$ mfm [1-3] and the other near $-1.32(4)$ mfm in the range critical for sign assignment to the neutron mean square charge radius .

So, the obtained in [2] value of b_{ne} differs from the estimates of refs [4,5] by nearly 10 errors and, as we have shown [6], this is connected with different mathematical descriptions of the measured effects. But the difference between the values $-1.49(5)$ [1], $-1.55(2)$ [3] and $-1.31(4)$ [4,5] has not found any explanation up to now. And so, estimates of b_{ne} from [5] depend on the reliability and precision of the rich set of coherent amplitude b_{coh} values (for Bi) obtained in different years on the gravitational spectrometer and (in the last time) on the interferometer and lie essentially beyond error limits. These b_{coh} lead to the values of b_{ne} from -1.32(3) to -1.43(3).

Such uncertainty evokes the necessity of analysis of the measurement and data processing methods. Here one more approach to n,e-amplitude estimation is proposed. The nuclear scattering cross section $\sigma_s(0) = 4\pi R'^2(0)$ is calculated by extrapolation of known scattering cross sections from the energy region of tens or hundreds eV to $E \Rightarrow 0$. The values of b_{ne} are obtained from a comparison of $\sigma_s(0)$ and $4\pi b_{coh}$ with $b_{coh} = R'(0) + b_{ne}Z$. The authors discuss also the discrepancy between the existing b_{ne} estimates and conclude that it is yet impossible to reliably determine the neutron mean square charge radius. The obtained "nonmodel" estimates of b_{ne} agree nicely with the results [5].

Method	Bi	Pb
$R'_0 = const$ [5]	-1.30 ± 0.06	-1.32 ± 0.04
$R'_0 = const$ [6]	-1.30 ± 0.04	-1.32 ± 0.03
Extrapolation $\sigma_s \Rightarrow 0$	-1.33 ± 0.03	-1.32 ± 0.03

2. A reliable estimate of the neutron polarizability (α_n) depends on the accuracy of theoretical description of the neutron- nucleus interaction and the choice of corrections to be made in data processing. The experimental data relative precision must be of about 10^{-4} and higher.

In refs.[7,8] the α_n value was estimated with the statistical error $\Delta\alpha_n$ of about 3 and 5 for Bi and Pb, respectively. Schmiedmayer and colleagues [10] reported on the new value for $\alpha_n = 1.20 \pm 0.15 \pm 0.20$ that was obtained just by formal extraction of a proportional to k term (responsible for polarizability scattering contribution) from the energy dependence of σ_s expansion into a power series of the wave number k.

To pursue the aim of the reliable estimation of α_n one has to critically examine the analysis method and the different factors that affect the accuracy of calculated α_n values. The difficalty of the neutron polarizability coeffitient determination is connected

with the smallness of its contribution into σ_s. So for $\alpha_n = 1$ (in 10^{-3} fm^3 , by analogy with measured proton polarizability) this contribution makes from 10^{-3} to 10^{-2} .

Our analysis of the two methods of α_n estimation and the description we made of σ_s by using the nuclear physical parameters have shown that the exactness of α_n estimate depends on variations of the resonance corrections which are of about the same order of $10^{-3} - 10^{-2}$. By using the neutron scattering cross section data for Bi, Pb and ^{208}Pb from refs [7,10] we investigated stability of the neutron polarizability α_n estimate to different corrections and data processing methods .

The α_n reestimated values [9,6] from data for Bi, Pb [7,8] and ^{208}Pb [10] turn out to be sensitive to account of resonance contribution uncertaincy and to accepted values of nuclear s- and p- scattering radii. That is why we conclude that to the existing α_n estimates (from Bi and Pb cross sections) not the statistical errors must be attributed, but some 5-10 times higher uncertainties. It is shown that the result [10] should be interpreted as $\alpha_n \leq 2$.

References

1.Melkonian, E., et.al.: Phys. Rev. 1959,**114**,p.1471.
2.Alexandrov, Y., et.al.: Sov. J. Nucl. Phys., 1986,**44**,p.900.
3.Alexandrov, Yu., et.al.: Yadernaya Fisika, 1974,**20**, p.1190.
4.Krohn, V., Ringo, G.:Phys.Rev., 1973,**D8**, p.1305.
5.Koester, L., et.al.: Z. Phys. A , 1988,**329**, p.229
6.Nikolenko, V., Popov, A.: Z. Phys. A - Hadrons and Nuclei,1992,**341**,p.365
7.Koester L. et.al.: Physica, **329**,229(1988)
8.Alexandrov Yu. et. al.: Sov.J.Nucl.Phys., **44**,900(1986)
9.Nikolenko V.,Popov A.:JINR, R3-90-568, Dubna, (1990)
10.Schmiedmayer J. et. al.: Phys.Rev.Lett.,**66**,1015(1991)

Properties of ρ- and ω-mesons in dense and hot nuclear matter near the critical pion mode softening

G.G. Bunatian[1], B. Kämpfer[2]

Forschungszentrum Rossendorf e.V., Inst. für Kern- und Hadronenphysik
O-8051 Dresden, PF 19, Germany

Abtract:

The propagators of ρ- and ω-mesons in nuclear matter are analyzed. Due to the strong coupling to pions in $\rho\pi\pi$, $\omega\pi\pi\pi$, $\rho\rho\pi\pi$ etc. vertices, the ρ,ω-meson properties depend sensitively on the behaviour of the pionic mode. Relying on previous investigations of the pion propagator in nuclear matter, we elucidate the main features of the ρ- and ω-meson behaviour in dense and hot nuclear matter in the asymptotic case near the critical pion mode softening. We find that under such conditions the ρ-meson mode becomes stiffer, while the ω-meson mode softens. The widths of both the ρ,ω-mesons increase significantly and become essentially greater than the ones of free mesons.

[1]permanent address: JINR Dubna, Lab. Neutron Physics, Head Post Office, P.O.B. 79, 101000 Moscow, Russia

[2]also: Inst. Theor. Phys. (KAI e.V.), Tech. Univ. Dresden, Mommsenstr. 13, O-8027 Dresden, Germany

Quasi-particle description of a strongly interacting pion gas

G.G. Bunatian[1], B. Kämpfer[2]

Forschungszentrum Rossendorf e.V., Inst. für Kern- und Hadronenphysik

O-8051 Dresden, PF 19, Germany

Abtract:

The pions system at nonzero temperature T, $m_\pi \sim T \ll m_{\rho,\sigma}, M_N$, is studied, the pion-pion interaction being described by underlying Weinberg Lagrangian. In the framework of Hartree approximation, the pion self-energy part and propagator are obtained. The modification of the pion spectrum proves consisting in the replacement of the free pion mass m_π by the effective one $\tilde{m}_\pi(T)$, depending on temperature and increasing with the temperature growth. The calculated thermodynamical quantities (the density of pion excitations, energy, entropy and pressure) of considering system come out to be smaller than ones of the free pions system.

[1]permanent address: JINR Dubna, Lab. Neutron Physics, Head Post Office, P.O.B. 79, 101000 Moscow, Russia

[2]also: Inst. Theor. Phys. (KAI e.V.), Tech. Univ. Dresden, Mommsenstr. 13, O-8027 Dresden, Germany

Quantum Phenomena at Fast Modulation of a Neutron Wave

D.V.Amandzolova, A.I.Frank, V.G.Nosov †

†Institute of General and Nuclear Physics RRC "Kurchatov Institute", Moscow

In a number of papers quantum phenomena are considered that are related to a fast periodic influence exerted on a neutron beam. Periodical chopping of neutron beam is the simplest case. The following wave function is found in [1],[2] for a periodic chopper:

$$\psi(x,t) = \frac{1}{2}e^{i(kx-\omega t)} + \frac{i}{\pi}\sum_{s=-\infty}^{\infty}\frac{e^{i(k_s x-\omega_s t)}}{2s-1}, \qquad \Omega = 2\pi/T, \tag{1}$$

where $\omega_s = \omega + \Omega(2s-1), k_s = k\left[1+(2s-1)\gamma\right]^{1/2}, \gamma = \Omega/\omega \ll 1$. Thus, the state in the semi-space to the right represents a non-stationary superposition of waves, each of which has an energy $\hbar\omega_n$ and a corresponding wave number k_n.

To obtain a state with a discrete energy spectrum it is not necessary to chop the neutron beam simultaneously over the whole of its cross section. Periodic chopping at each point of the beam cross section, even changing the moment of chopping from point to point, will do the job quite well. In this way we come to the problem of the motion of a periodic structure, a grating, across a beam [2],[3].

The wave function of the difracted neutron in the laboratory reference system is found by subsequent application of the Galilean transformation to the neutron wave function in a moving reference system connected with the grating. In the limit, when the grating has a high velocity and its period, one readily arrives at the formula (1), given above. In the same way was a solution found, also, for the phase grating.

It has been shown in [5],[4] that the problem can be solved without invoking the precise solution of the Schrödinger equation with the corresponding time-dependent potential. If the action of some device located at $x = 0$ being a periodic variation of the amplitude or phase of the initial plane wave then as was obtained for $x > 0$:

$$\psi(x,t) = \sum_{n=-\infty}^{\infty} C_n e^{i(k_n x-\omega_n t)} \qquad \omega_n = \omega + n\Omega, \qquad k_n = k(1+n\gamma)^{1/2} \tag{2}$$

where C_n are the Fourier coefficients of the modulation function $f(t)$.

It was found in [2],[4] that the transmitted wave exhibits a structure characteristic of space beats with a large-scale period of $L = (vT)^2/\pi\lambda$.

In the case of phase modulation it is possible to reconstruct the initial monoenergetic state with the aid of a second modulator. Here modulators act like a coherent splitter and combiner of neutron waves. The possibility is considered of creating a neutron interferometer with beams coinciding in space and based on this idea.

The above arguments make it easy to obtain a solution of the problem for neutrons reflected from an oscillating (magnetic, for example) potential barrier. In the stationary case, the amplitude r of the wave reflected from a potential U is given by the usual solution of the stationary Schrödinger equation. In the case of a time-dependent potential the amplitude $r(t)$ is also readily found by formal substitution of the quantity $U(t)$ into the corresponding expression for the amplitude. The state characterizing the reflected wave is a superposition of coherent waves, the amplitudes of which are the Fourier coefficients of the function $r(t)$. Consequently, reflected waves corresponding to various satellites will exhibit different reflection angles and energies. The picture that arises can be illustrated by Fig.1.

Figure 1: Quantum reflection

It was estimated, that angular distribution of reflected waves may be quite within the range of resolutions exhibited by ordinary reflectormeters.

A number of experiments is proposed and now in a preparation for testing the theory.

References

[1] V.G.Nosov, A.I.Frank. VI Int. School in Neutron Phys. (Alushta, 1990), **1**, 313.

[2] A.I.Frank,V.G.Nosov. *Quasi-energy of Ultracold Neutrons* JINR, E4-92-457.

[3] A.I.Frank and V.G.Nosov. Phys.Lett. A (1994) (in print)

[4] A.I.Frank and V.G.Nosov. Yadernaya Fizika (1994) (in print). (1994).

[5] A.I.Frank, V.G.Nosov *Quasi-Energy of Cold Neutrons and Neutron Time Interferometry.* To be published in: F.De Martini, A.Zeilinger (Eds.) **Quantum Interferometry,** World Scientific, Singapore, 1993.

[6] A.I.Frank, D.B.Amandzolova. *Neutron Quantum Refraction,* JINR E3-93-418.

INTERACTION OF WAVES AND PARTICLES WITH LAYERED MEDIA
(all media can be considered to be layered)

V.K.Ignatovich
Joint Institute for Nuclear Research, Dubna, Russia

The results presented here are related to two topics: 1)interaction of particles with a periodic potential and 2)a model of the ball lightning.

Periodic potential

Usually to solve one-dimensional Shrödinger equation with an arbitrary potential u means to find the reflection and transmission amplitudes. It is shown in [1, 2], that the physical problem is not changed if the potential is split by an infinitesimal gap in two parts at any point. But the reflection R_{12} and transmission T_{12} amplitudes of the whole potential are now represented through the amplitudes of its parts:

$$R_{12} = R_1 + \frac{T_1^2 R_2}{1 - R_1 R_2}, \qquad T_{12} = \frac{T_1 T_2}{1 - R_1 R_2} \tag{1}$$

The equations (1) are very useful when we consider semi infinite periodic potential. Here we can cut off one period from remaining part (fig.1),

fig.1

and if the reflection, r, and transmission, t, of a single period are known, then the reflection R_∞ of the whole potential is represented by the solution of the algebraic equation:

$$R_\infty = r + tR_\infty(1 - rR_\infty)^{-1}t. \tag{2}$$

For a scalar wave propagation the solution of (2) is

$$R_\infty = \frac{\sqrt{(1+r)^2 - t^2} - \sqrt{(1-r)^2 - t^2}}{\sqrt{(1+r)^2 - t^2} + \sqrt{(1-r)^2 - t^2}}; \tag{3}$$

which contains all the features related to the Bragg structure of the reflection spectrum.

It is not difficult to obtain also the Bloch phase factor

$$\exp(iql) = \frac{\sqrt{(1+t)^2 - r^2} - \sqrt{(1-t)^2 - r^2}}{\sqrt{(1+t)^2 - r^2} + \sqrt{(1-t)^2 - r^2}},$$

where l is the length of the period and q is the Bloch wave number.

To get the reflection and transmission amplitudes for a periodic potential with a finite number of periods it is necessary to note that the potential with a period l is periodic also with the period $L = nl$. The result is

$$T_n = \frac{(1 - R_\infty^2)\exp(iqL)}{1 - R_\infty \exp(iqL) R_\infty \exp(iqL)}, \qquad R_n = \frac{R_\infty - \exp(iqL) R_\infty \exp(iqL)}{1 - R_\infty \exp(iqL) R_\infty \exp(iqL)} \tag{4}$$

The equation (1) is applicable also to vector fields of any dimension. This gives a way for generalization to 3-dimensional space. In particular, it is possible to get a new method for the dynamical diffraction of waves on three-dimensional single crystals [1].

The same approach is applicable to any linear equation of mathematical physics of second order (see, for example, [3, 4]).

The ball lightning

The model for ball lightning was constructed during consideration of ultracold neutrons interaction with matter. This interaction is described by the potential $u_0 = 4\pi N_0 b$, where N_0 is atomic density and $b > 0$ is coherent scattering amplitude. If $b < 0$ the potential is attractive. So the substance is represented by a potential well, where bound levels for neutrons are possible.

It is important to notice that not only the well holds the particle, but the particle also holds the well, i.e. it compresses the substance as is illustrated in fig. 2.

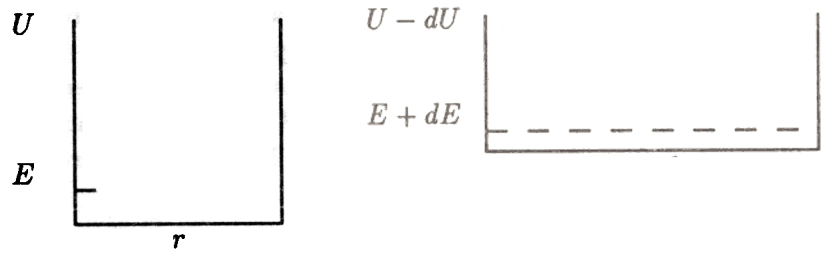

fig.2

The compression force can be very important in neutron stars. But the most interesting is to consider an analogy with γ-quanta. They are Bose particles, can be accumulated on a single level in any number and their compression force can be arbitrary high.

This leads to a model of the ball lightning [5]. It can be visualizer as a shock wave of a point explosion in an excited gas with a laser discharge at its front. The discharge photons with their electrostrictive force may stop the shock wave. So the ball lightning is a frozen spherical thin skin filled with a great number of photons.

References

[1] V.K.Ignatovich. Multiwave Algebraic Darwin Method In Dynamic Theory Of Diffraction. Kristallografiya 37(5):1100-1112, 1992. (see Sov. Phys. Crystallography)

[2] V.K.Ignatovich. An Algebraic approach to the propagation of waves and particles in layered media. Physica B 175(1-3):33-38, 1992.

[3] V.K.Ignatovich. Propagation of Acoustic Waves in Layered Elastic Media. Acoustic Journal 38(1):70-78, 1992. (see Sov. Physics Acoustics-USSR 38(1):34-39, 1992.)

[4] V.V.Golikov, V.K.Ignatovich, E.N.Kulagin. Measurement of the loss coefficient of UCN in Beryllium powder. Yad.Fiz 55(3):608-616, 1992. (see Sov. J. Nucl. Phys.-USSR 55(3):337-341, 1992.)

[5] V.K.Ignatovich. The Ball Lightning. Laser Physics v. 2, n. 6, p. 991-6, 1992.

PROMISING AND CRUCIAL EXAMPLES OF CLUSTER RADIOACTIVITY PROCESSES

S.G.Kadmensky
Voronezh State University, Russia
W.I.Furman
Frank Laboratory of Neutron Physics, JINR, Dubna
Yu.M.Tchuvil'sky
Moscow State University

The general problems of the cluster radioactivity study: an adiabatic or nonadiabatic character of the process, its connection with fission and α-decay, even-odd effects, the fine structure, heavy and light cluster mass limits etc., are discussed. Special attention is paid to the experiments, that might help finding an optimal theoretical approach to the description of the above characteristics of the process. The wide-scale search for the new examples of such experiments was carried out using our theoretical scheme[1]. Not many cases of cluster decay in the traditional $A > 208$ parent nucleus mass region are the prospective objects of a crucial experiment. Most of them are presented in the table.

No.	Decay	$log(T^{theor}_{1/2x}(sec)$	$-log(\Gamma_x/\Gamma_\alpha$	Note
	$^{220}Ra \rightarrow ^{12} C$	11.1	≥ 12.7	$T_{1/2\alpha} \geq 1sec$
2	$^{221}Ra \rightarrow ^{13} C$	14.7	13.2	short-lived*(sl)*
3	$^{221}Fr \rightarrow ^{14} C$	16.2	13.7	sl
4	$^{223}Ac \rightarrow ^{14} C$	14.3	12.2	sl
5	$^{224}Ac \rightarrow ^{14} C$	17.4	12.4	$\frac{\Gamma_{\beta(\epsilon)}}{\Gamma_\alpha} \approx 10.2sl$
6	$^{224}Th \rightarrow ^{14} C$	12.8	12.8	$T_{1/2x} \approx 1sec$
7	$^{226}Th \rightarrow ^{14} C$	17.5	14.2	
8	$^{226}Th \rightarrow ^{18} O$	18.5	15.2	
9	$^{230}U \rightarrow ^{22} Ne$	19.6	13.3	
10	$^{232}Th \rightarrow ^{26} Ne$	30.1	12.5	long-lived *(ll)*
11	$^{235}U \rightarrow ^{25} Ne$	30.1	13.8	1. and other clusters 2.*ll*
12	$^{236}U \rightarrow ^{30} Mg$	29.1	14.4	*ll*
13	$^{237}Np \rightarrow ^{30} Mg$	29.3	15.5	*ll*
14	$^{234}Pu \rightarrow ^{26} Mg$	21.1	15.4	$\frac{\Gamma_{\beta(\epsilon)}}{\Gamma_\alpha} \approx 17$
15	$^{236}Np \rightarrow ^{28} Mg$	28.7	14.7	*ll*
16	$^{240}Cm \rightarrow ^{32} Si$	21.3	14.9	

Even the listed above cases are difficult to be measured. To achieve the goal it is necessary to measure the cluster decay of a short - (No. 2-5), a very short - (No. 1,6), and a long-lived (No. 10-13) isotope. Sometimes (No. 5,15), the β-decay influence is strong. In some cases it is difficult to have the parent nucleus obtained. Thus one may hope to have data measured for a few cases only. The most interesting of them are Nos. 1, 2, 8, 9-14 — where the new clusters are emitted, including the lightest (1, 2) and the heaviest (16) ones, as well as (5, 15), the cases of the decay of odd-odd nuclei.

In spite of the difficulty of performing measurements with other parent nuclei some of them are worth the effort of experimentalists. Even obtaining of the upper limit of the branching ratio for the emission of a very light cluster $^{8}Be(-log(\Gamma_x^{theor}/\Gamma_\alpha) = 14.3)$ from ^{218}Ra, or a very heavy cluster ^{34}Si from $^{240}Pu(17.6),^{241}Am(19.2),^{242}Cm(18.7)$ and a superheavy cluster ^{48}Ca from ^{249}Cf ($\sim$ 30 in accordance with our estimations) will give some indications of the cluster mass dependence of the branching ratios and will be an additional test of the known theoretical approaches.

Due to the difficulty of real measurements in the discussed mass area, it is useful to look for new regions of cluster radioactivity. The one, first indicated in [2], was confirmed by our approach. This region includes the processes with the daughter nuclei, close to ^{100}Sn, and relatively light clusters $^{12}C,^{16}O$, etc. The folding procedure of the cluster-nucleus potential evaluation was used. The initial potential was the same as we used for the $A > 208$ region [1].

The obtained results are strongly different from those for the $A > 208$ region. For example, in the case of the $^{114}Ba \rightarrow^{12} C +^{102} Sn$ decay the branching ratio is $log(\Gamma_x/\Gamma_\alpha) = -0.4$. The half-life of the ^{12}C-decay, $T_{1/2x} = 6 \times 10^3$ sec, and the ratio, $(\Gamma_x/\Gamma_{tot}) \approx 10^{-4}$, make this decay observable. The characteristics of another example, $^{118}Ce \rightarrow^{16} O +^{102} Sn, log(\Gamma_x/\Gamma_\alpha) = +3.7, T_{1/2x} = 8.8 \times 10^2, (\Gamma_x/\Gamma_{tot}) \approx 10^{-3} \div 10^{-4}$, are as good as previous ones. Other variants of cluster decay in this region do not have such good characteristics but may be preferred as giving the possibility of obtaining the parent nucleus.

It is interesting to note that other theoretical approaches [3,4] give the width values for the emission of the ^{12}C and ^{16}O clusters many (respectively $4 \div 8$ and $8 \div 12$) orders of magnitude lower than our calculation does. So, further experiments should be performed to test different theoretical approaches.

References

1. Zamyatnin Yu.S. et al. Sov. J. Part. Nucl., 1990, v.21(2), p.537.
2. Price P.B. Nucl.Phys., 1989, v.A502, p.41.
3. Poenaru D.N. et al. Atomic Data and Nucl. Data Tables, 1986, v.34, p.423.
4. Blendowske R. and Walliser H. Phys. Rev.Lett., 1988, v.61, p.1930.